INTERFACIAL FRICTION IN FABRIC MECHANICS.

by

Farshad Motamedi

A dissertation submitted to the University of London for the degree of Doctor of Philosophy.

Department of Chemical Engineering and Chemical Technology

Imperial College of Science, Technology and Medicine

London SW7 2BY.

April 1989.

PREFACE

This dissertation is a description of the work carried out in the department of Chemical Enginnering and Chemical Technology, Imperial College, London between October 1985 and October 1988. Except where acknowleged, the material is the original work of the author and includes nothing which is the outcome of work in collaboration, and no part of it has been submitted for a degree at any other University.

I would like to convey my gratitude to the following people;
First and foremost I would like to sincerely thank Dr. B.J.Briscoe for his enormous help and guidance throughout the past 4 years (both MSc and PhD). I believe that without his supervision and support this work may never have seen the light of day. I am also deeply indepted to Professor A.I.Bailey for her generous moral and financial support and to Professor D.Tabor for his useful and stimulating comments throughout this work.

My thanks are also due to the members of the technical staff at the department of chemical engineering particularly those at the student services and the electronic workshop namely M. Dix, D. Wood.

I would also like to thank all my fellow members of the Particle Technology and the Interface Science groups in particular D.Liatsis, P.Tweedale, B.Chaudhary, S.Zakaria, M.B.Khan, D.Williams, I.Blazquez, M.Kamyab and K.Galvin. Without their pleasant company and help the work would have been less enjoyable.

I am also grateful to Mrs. J.E.Burberry for her care and dedication in the typing of this dissertation.

Finally my thanks and love go to my darling wife, Banafsheh, who has always been there for me. Her unfailing belief and support through some rough times is dearly cherished.

Farshad Motamedi

April 1989.

To my late father,

my wife Banafsheh and my son Ashkan.

ABSTRACT

This thesis describes the results of an experimental and theoretical study of the in plane and the out of plane deformation of two simple fabrics constructed from a cotton staple yarn and a continuous filament aramid yarn. The theme has been to account for the deformation characteristics observed in a number of special geometries.

Three particular deformation cases have been analysed namely the fabric indentation experiments, the ballistic experiments and the yarn pull-out experiments. The observed microscopic behaviour in the latter case has been used to predict the macroscopic response of the system. This has involved separately investigating the friction and extension properties of isolated yarns and the visual examination and quantification of the local deformation fields. The major conclusion of this particular study has been that it is possible to use simple models and assumptions to generate realistic models for the deformation of fabrics on the basis of the operation of tensile forces only. Amongst the range of variables adopted have been the introduction of lubricants which are believed to modify the tensile properties of the yarns by interfilament lubrication and the behaviour of the cross-overs by cross-over contact lubrication.

The deformation characteristics of the fabrics (semi-pyramidal) during the indentation experiments were found to resemble those in the pull-out process. The force-displacement profile of this system was predicted using a standard constrained coherent plate deformation model. The conclusion of this work was that the behaviour of this system may be reasonably interpreted using an effective modulus which arises largely through the propagation and the interaction of mostly tensile forces and hence the operation of a tensile rather than a bending modulus.

Finally the plate deformation theory was used to interpret the ballistic capture

performance of aramid fabrics possessing various surface characteristics. The influence of surface modifications in the ballistic experiments was in keeping with those observed in the indentation experiments.

The main overall conclusion is that the transmission of tensile forces dominates the out of plane deformation of these fabrics and that lubrication affects both the stress fields in the yarns by modifying fibre-fibre interactions and also the manner in which force transmission occurs between the yarns into the fabric as a whole.

CONTENTS

FIGURE LEGENDS

Chapter 1

1.1 A schematic representation of the deformation geometries; a) the pull-out experiment, b) the "hardness experiment and c) the ballistic experiment.

1.2 A block diagram representing a summary of the various elements in the thesis.

Chapter 2

2.1 Glucose rings linked together.

2.2 A schematic drawing of a cotton fibre illustrating the layered structure. Reproduced from Duckett (1979).

2.3 The morphology of Kevlar 49 fibre. Reproduced from Pruneda *et al* (1981).

2.4 Comparison of Hailwood & Horrobin's equation with experimental results for cotton and wool.

2.5 The effect of relative humidity on the equilibrium moisture regain and regain rate of 380 denier yarn of Kevlar 49. Reproduced from Kevlar 49 Data Manual, E.I. du Pont & Co.

2.6 A four element model representing the extension, primary and secondary creep and stress relaxation of a fibre.

2.7 Eyring's three element model.

Chapter 3

3.1 The idealised helical geometry of a yarn, due to Hearle (1965).

3.2 Comparison of typical stress-strain curves of a staple and a continuous filament yarn.

3.3 A schematic representation of an extended yarn based on the ideal helical geometry.

3.4 Contact between a rough solid and smooth rigid plane showing only a few asperities touching the surface.

3.5 Schematic diagram of deformation friction due to viscoelastic hysteresis

losses within the bulk of the specimen either during rolling or well lubricated sliding.

3.6 A force diagram for the capstan theory of friction.

3.7 Schematic representation of the stick-slip phenomenon showing the effect of imposed sliding velocity.

3.8 Schematic diagram of the geometric theory of the differential friction effect. The scales on the fibre interlock or catch against asperities on another surface.

3.9 General behaviour of liquid-lubricated textile yarns showing the three regimes of lubrication and the regions at which they become operative.

Chapter 4

4.1 Schematic diagram of Pierce's model of a simple plain weave.

4.2 An alternative "race-track" shape for the yarn cross section. Here the race-track geometry has been extended by the straight portion z. In this way the problem of non-plain fabric geometry can be converted into plain fabric geometry.

4.3 The load extension curve for a fabric showing three distinct sections representing initial high modulus, a relatively lower modulus and ultimately a rise in modulus.

4.4 Schematic diagram of a cross-over point in a fabric showing the bent character of the yarn within the weave.

4.5 Equilibrium absorption from CTAB solutions by purified cotton at room temperature. Reproduced from Sexsmith & White (1959).

4.6 Kim and Vaughn's (1979) graphical representation of fabric hand; fabric C, 50/50 polyester/cotton batsice; fabric Q, 50/50 polyester/cotton denim; fabric S, 50/50 polyester/cotton gabardine.

4.7 A schematic representation of the configuration of a yarn impacted transversely.

4.8 The effect of fibre modulus on the proportion of the transverse wave being either transmitted along the original fibre or be diverted to the second fibre at a cross-over point.

4.9 The effect of friction at a cross-over on the coefficient of reflection of the transverse wave front.

4.10 The effect of friction on the coefficient of wave diversion.

4.11 The influence of friction at the cross-over on the transmission of the

transverse wave front.

4.12 Factors which may influence the ballistic performance of aramid fabrics.

Chapter 5

5.1 A microscopic photograph of the cotton weave.

5.2 Schematic drawing (plan) of the upper part of the force measuring device.

5.3 Point contact frictional character of two orthogonal cotton yarns. The yarns were untreated and dry (RH ≈ 40%).

5.4 Photograph of the hanging fibre-friction apparatus.

5.5 Schematic diagram of the hanging fibre arrangement showing the directions of motion and the yarns in contact.

5.6 Variation of friction force with load in the hanging fibre experiment. The dead load W_d was 10 g. The normal load on the contact was a component of W_d through angle θ which changed during the course of the experiment. The gradient is the mean coefficient of friction.

5.7 Variation of friction force with angle θ in the hanging fibre experiments. Increasing the angle has the same effect as decreasing the load, hence the force decreases. W_d = 10 g.

5.8 Variation of coefficient of friction with normal load for untreated cotton yarns in the hanging fibre experiments. μ was calculated for each point as = F/W. The values for W_d = 5 and 10 g are included.

5.9 Variation of μ with W for untreated Aramid 1 (Kevlar 49) yarns in the hanging fibre experiments. W_d = 5, 10 and 20 g.

5.10 Force-extension profiles for untreated cotton yarns of varying gauge lengths. The yarns were taken to the point of rupture in the tensile experiment. Instron cross-head speed = 2 mm/min.

5.11 Force-strain character of untreated cotton yarns of different lengths. The extension data in Figure 5.10 was divided by the corresponding yarn length to obtain the strain. However, the position of the profiles have reversed here from that of Figure 5.10.

5.12 Variation of the point to point tensile modulus (force/strain) of untreated cotton yarns with strain and the rate of strain.

5.13 Comparison of the force-strain character of treated cotton yarns. The water and tetradecane treated yarns were wet during the experiment while the rest were dry. Average yarn length = 20± 2mm. Rate of strain = 10% per minute.

5.14 Force-strain character of as received Aramid (Kevlar 29 and 49) yarns. The experiment was taken beyond the point of failure. Yarn length = 20 ± 2mm, strain rate = 10% per minute.

5.15 Photograph of the "hardness" experiment apparatus.

5.16 Photograph of the high speed gas gun.

5.17 Schematic diagram of the high speed impact arrangement showing the gas gun and the steel protective chamber together with the associated velocity measuring and photography equipment.

5.18 Projectile velocity in the ballistic experiments as a function of gas pressure in the gas gun.

5.19 Photograph of the apparatus used in the pull-out experiments including the enclosed chamber containing the force measuring device, and the video recording measurement facilities.

5.20 Photograph of the force measuring device showing the clamped fabric, in the movable stage, the hook, the phosphur bronze springs and the linear displacement transducer.

5.21 Schematic diagram of the set-up used to measure the force (stage 1) and video record of the deformation of the fabric matrix (stage 2) during the pull-out experiment.

Chapter 6

6.1 Typical force-vertical displacement profiles for untreated cotton fabrics during the "hardness" experiment. The effect of weft yarn tension is seen to be negligible; (120° conical indentor, 100 mm holder diameter).

6.2 Variation of force with area of indentation for untreated cotton fabrics. The values for different weft yarn tensions fall on the same line.

6.3 Schematic diagram of the deformations produced during fabric indentation. For cotton the deformation zone was asymmetric about the warp and weft directions, while for the Aramid fabrics the deformation zone was symmetrical.

6.4 Comparison of the response of untreated cotton fabrics to indentors of differing angles in the "hardness" experiments (100 mm holder).

6.5 Force and area of deformation of untreated cotton fabrics as a function of the angle of the indentor.

6.6 The response of untreated cotton fabrics of different diameters to indentation by 60° and 120° conical indentors. The fabric with the larger diameter is seen to be more compliant.

6.7 The effect of fabric holder diameter on the deformation zone area of untreated cotton fabrics using 60° conical indentors.

6.8 Force and area of deformation of untreated cotton fabrics as a function of fabric holder size using 120° conical indentor.

6.9 A plot of the hardness value again tan β where

$$\beta = (\frac{\pi-\theta}{2}) ,$$

θ being the indentor angle.

6.10 Indentation of an elastic-plastic half space by spheres and cones. Small dashed line - elastic: A cone, B sphere. Solid line - finite elements. Chain line - cavity model: F cone, G sphere. Large dashed line - rigid-plastic. Reproduced from Johnson (1985).

6.11 The response of as received Aramid (Kevlar 49) fabric to indentation by indentors possessing different angles. Holder size = 100 mm.

6.12 Variation of the ratio h/y with vertical displacement for different cone angles and fabric holder sizes.

6.13 The comparison of the experimental data and the ideal response of a very stiff system during fabric indentation processes.

6.14 Comparison of the "hardness" experimental data and the response of a very compliant (in bending) system to indentation for various cone angles and fabric holder sizes. The figure represents the extent to which the cotton fabric under study was bent or stretched during the indentation process.

6.15 Comparison of the response of untreated and 5% PDMS treated cotton fabrics to the indentation process. (60° conical indentor, 100 mm holder).

6.16 Comparison of the responses of untreated and 5% PDMS treated cotton fabrics in the "hardness" experiment using 120° indentor and 100 mm holder.

6.17 Comparison of the response of untreated cotton fabric to that treated with different concentrations of CTAB solution using 120° indentor and 100 mm holder.

6.18 Comparison of the response of Aramid (Kevlar 49) fabrics possessing different surface characteristics (clean [soxlet extracted], as received and 5% PDMS treated) to the indentation process. (120° indentor, 100 mm holder).

6.19 The response of untreated cotton fabrics to small diameter indentors as a function of the indentor angle. (100 mm holder).

Chapter 7

7.1 High speed photograph of the impact process. Projectile velocity=113 m/s, as received aramid 1 fabric, time interval between frames=40 μs.

7.2 Same as figure 7.1 for the 5% PDMS treated aramid 1 fabric.

7.3 Same as figure 7.1 for the soxlet extracted aramid 1 fabric.

7.4 The effect of impact velocity and surface treatment of Aramid (kevlar 49) fabrics as the projectile residual velocity.

7.5 The effect of surface treatment on the energy absorbing efficiency of aramid (Kevlar 49) fabrics at different impact velocities.

Chapter 8

8.1 General form of the force-displacement profile obtained in the yarn pull-out process showing the four regions of response.

8.2 Variation of the pull-out profile and the associated parameters of untreated cotton fabric with imposed side tension.

8.3 The gradient of elastic part of the pull-out profile (Region II) G, as a function of side tension for untreated cotton fabrics.

8.4 Junction rupture force (JRF) as a function of imposed side tension for untreated cotton.

8.5 Sliding friction force per cross-over (Region IV) as a function of side tension for untreated cotton fabrics.

8.6 Measured pull-out force (Region IV) as a function of the number of cross-overs remaining for untreated cotton fabric under zero side tension.

8.7 Ratio G/JRF as a function of side tension showing JRF to be a stronger function of tension.

8.8 Extension of the pull-out yarn against plate displacement at particular values of the pull-out force. The diagram compares each portion of the extension profiles to a particular region in the pull-out profile.

8.9 Measured force before JRF (Region II), as a function of the extension of the portion of the pull-out yarn between cross-overs 1-20.

8.10 Tensile extension of discrete elements of the pulled yarn between cross-overs corrected for the out of plane displacements as a function of cross-over number. The averaged increasing trend is depicted by the solid line.

8.11 Displacement of cross-overs 1 and 20 with side tension. The solid lines

represent the least square fits to the data.

8.12 Schematic representation of the out of plane vertical displacement of the weave during the pull-out process, the displacements increasing towards the hook.

8.13 Out of plane micro displacements for the weave as a function of cross-over number for three different force levels on the pulled yarn.

8.14 The effect of the number of cross-over points at the same force level (0.1 N) on the vertical displacements of the weave.

8.15 Schematic diagram of the vertical micro displacement of a section of the weave, used to correct the displacement of the cross-overs and the extension of the elements of the pulled yarn.

8.16 Experimental values of the cross-over displacements for untreated cotton fabric at zero side tension as a function of cross-over number. Both the corrected and the uncorrected data are shown, the correction becoming more significant at higher cross-over numbers.

8.17 Experimental values of the distance between the top of the cross-over or pulled yarn and the surface of the weave with increasing junction number. The yarns orthogonal and crossing over the pulled yarn were displaced upward more than the adjacent portions of the pulled yarn and this is depicted in the line named "difference".

8.18 The "difference" line in Figure 8.17 depicted for two different force levels. The figure shows the influence of the force on the pulled yarn on the level of yarn migrations.

8.19 The pull-out profiles for two untreated Aramid (kevlar 29 and 49) fabrics. Side tension = 0.

8.20 Variation of JRF with side tension for the Aramid 1 (kevlar 49) fabric.

8.21 Variation of the sliding friction force per junction (Region IV) with imposed side tension for untreated aramid 1 fabrics.

Chapter 9

9.1 Comparison of the pull-out profiles of dry untreated cotton fabric with that of a cotton fabric submerged under water for 30 minutes prior to pull-out. Side tension = 0.

9.2 The effect of the time of submergence on the value of the gradient G of the linear portion of the pull-out profile (Region II).

9.3 Values of junction rupture force (JRF) for submerged cotton fabrics as a function of the time submerged.

10.12 Comparison of the experimental fabric indentation force-displacement profile with that produced using the plate model. The data are for cotton fabric with 120° conical indentor and 100 mm fabric holder.

10.13 Experimental against plate model data for the indentation of cotton fabrics with a 120° conical indentor, fabric holder size=180mm.

10.14 Experimental vs. plate model profiles for the indentation of untreated (as received) aramid 1 fabric using 120° cone and 100 mm fabric holder.

10.15 Same as figure 10.14 for 5% PDMS treated aramid 1 fabric.

10.16 A schematic representation of the indentation and the ballistic processes showing their respective deformation patterns. In the quasi-static case, the hinge is at the clamp while for the ballistic case it is variable.

10.17 A block diagram showing the path taken to calculate the integral work done W_I in the ballistic process from information produced in the quasi-static analyses.

10.18 Quasi-statically based values of integral work done for the ballistic impact process at increasing transverse fabric displacements (depths).

10.19 Normalised absorbed energy as a function of the fabric surface characteristics. Energies were calculated at 15% nominal strain.

LIST OF SYMBOLS

Chapter 2

A	area, fibre cross-sectional area
E	Young's modulus
E'	fibre tensile modulus
E_f	tensile modulus of crystalline fibre
H	relative humidity
k, k_1 & k_2	constants
k_s	capillary water transport constant
K	bulk modulus
l	length
L	distance
m,n	constants
M	molecular weight of polymer unit
N	number of twists
r	regain
r_e	effective radius of capillary
r_b	radius of curvature
s	horizontal distance travelled by liquid
S	fibre length
t	time

T_b	fibre linear density
u	constant
v	volume
α	constant
ε	strain
ε'	modulus of rigidity
γ	liquid surface tension
η	liquid viscosity
η_S	shape factor
δ	fibre density
σ	stress
υ	Poisson's ratio
θ	helix angle
θ_A'	apparent advancing contact angle
θ_c	convolution angle

Chapter 3

a', b, c_1	constants
A	real area of contact

c	crimp ratio = h/L
D	cylinder diameter
E	Young's modulus
E_f,E_y	fibre and yarn modulus
F	yarn tension, yarn strength or friction force
F_d	the grooving force
F_1,F_2	yarn strengths
g	transverse stress distribution
G	transverse compressive stress
h	length of yarn
H	indentation hardness
K	friction factor
l	length of filament at distance r from axis
L	length of filament at the yarn surface
n	load index
p	ploughing component of friction
P	nominal pressure
r	radial position in yarn
R,R_o	radius of yarn or sphere
s	shear strength
t_1 & t_2	times
T	linear density or fibre tension
v	velocity

v_y	yarn specific volume
W	normal load
w_f	work done in extension
W_y	total elastic energy stored
X	tensile stress
Y	specific stress
α	twist angle or material parameter
α'	constant
$\varepsilon_f, \varepsilon_y$	filament and yarn extensions
μ	coefficient of friction
υ	Poisson's ratio
ϕ	elastic work done per unit length
ρ_o	materials flow stress
η	lubricant viscosity
σ	work done in extension
σ_1	axial Poisson's ratio
σ_y	lateral contraction ratio of yarn
τ	interfacial shear strength

θ'	subtended angle in a capstan geometry

Chapter 4

c	crimp ratio, sonic velocity
D	sum of diameters of yarns in warp and weft directions
E	Young's modulus
f	lead on a single yarn
F	total load on fabric
h	crimp height
k	constant
l	yarn length
m	mass per unit length of unstrained filament
n	number of yarns
p	thread spacing
t	time
T_p	maximum tension
u	transverse wave velocity
v_o	projectile impact velocity
ε	strain
ε_p	maximum strain
ρ	material density
σ	stress

θ	weave angle
subscripts1 & 2	warp and weft directions respectively

Chapter 5

F	force
n	load index
w	normal load
w_d	dead load
μ	coefficient of friction

Chapter 6

a & b	distances in pyramidal deformation zone
A, B, C	constants
A', B', C'	constants
E	Young's modulus
F	force
h	height to which fabric contacts the indentor
k_1 & k_2	constants
P	concentrated centre load
q	unit load
r	plate radius
R_c	radius of conical indentor
R_h	radius of fabric holder

t	plate thickness
y	vertical displacement
υ	Poisson's ratio
θ	angle of conical indentor

Chapter 7

E_d	dissipated energy
m	mass of projectile
v_i	impact velocity
v_r	residual velocity

Chapter 8

a	number of digitised position / mm
d	cross-over displacement
d_o	initial cross-over displacement
d_c	corrected cross-over displacement
D	displacement of stage
G	gradient of elastic region of pull-out profile
JRF	junction adhesive force
L	correction length or distance
x	digitised position of cross-over

Chapter 10

a & b	constants
d_o	half width of fabric
d_N	cross-over displacement
E	plate Young's modulus
E_m	global cross-over spring constant
E_y	tensile yarn spring constant
f, F	force
fc	force along cross-over yarns
fy	force along tensile yarns
f_s	tension on a single cross-over yarn.
f_o	friction force at zero load
F_s	total side tension
JRF	junction adhesive force
N	number of cross-overs
p	vertical component of side tension on one cross-over yarn
r	plate radius
t	plate thickness
v	sonic velocity
W_I	integral work done in deformation
y	vertical displacement
α & ϕ	angles

δ	extension of cross-over yarns
ε_N	tensile yarn extensions
μ	coefficient of friction
ρ	material density
ω	$\alpha + \phi$
θ_c	propagation angle at penetration
θ_N	weave angle
θ_w	stress wave propagation angle

CHAPTER ONE

INTRODUCTION

Treloar (1964) in his Mather lecture almost a quarter of a century ago outlined a general strategy for the analysis of the mechanics of complex structures. He said " In a typical engineering problem, it is required to calculate the response of a structure when a given set of stresses is applied to it. For the solution of such a problem, the engineer must have first a complete specification of the description of the components, ie. of the geometry of the structure. Secondly he must have a knowledge of the mechanical properties of the materials used in these components, and finally, he must have at his disposal a method of analysis that will enable him, on the basis of these pieces of information, to arrive at a mathematical solution to his problem". This is very much applicable to textile structures.

This thesis describes a number of experiments which have been designed to probe the behaviour of fabrics when they are deformed in a particular configuration. The deformation geometry is sketched in figure 1.1. It corresponds to the generation of an out of plane deformation produced by a force which has a component normal to the plane of a constrained fabric. In practice three geometries of deformation have been studied. Figure 1.1 shows these geometries in a schematic way.

Figure 1.1(a) is a yarn pull-out experiment where a single yarn is withdrawn from a fabric. The configuration in figure 1.1(b) represents a quasi-static indentation experiment and 1.1(c) a transverse ballistic experiment. The three configurations produce a pyramidal (or partially pyramidal) distortion. Each experimental configuration was designed to facilitate the study of a particular facet of fabric

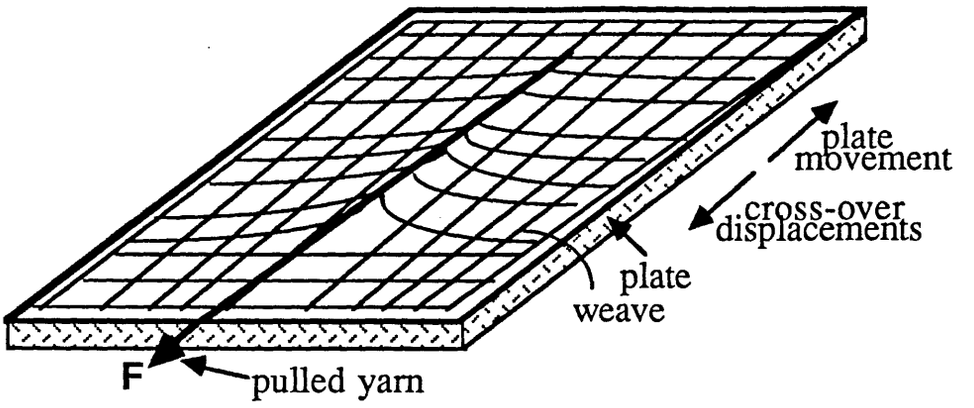

(a)

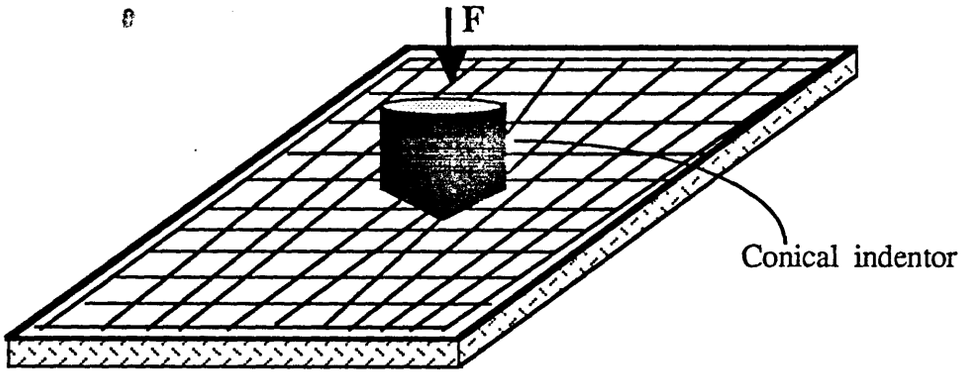

(b)

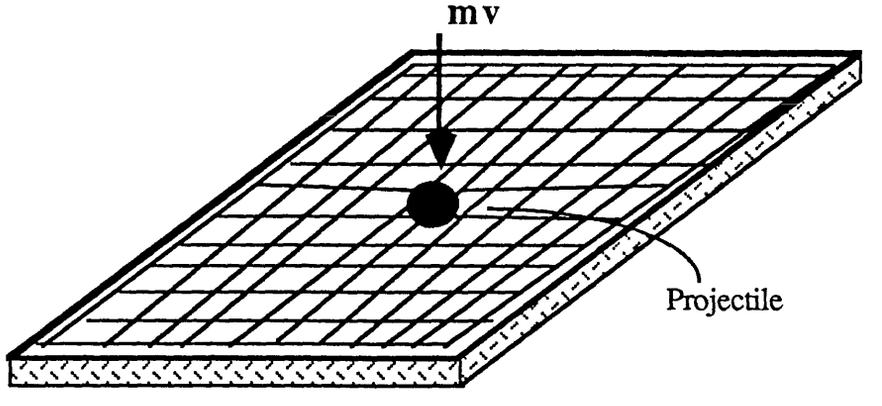

(c)

Figure 1.1 A schematic representation of the deformation geometries; a) the pull-out experiment, b) the "hardness experiment and c) the ballistic experiment.

mechanics. However. it will be shown that in each case, at low strains at least, the major governing factor controlling the response of the system was dictated by the tensile characteristics of the constituent yarns and to a lesser extent by the bending character and the properties of the yarn-yarn junctions. At higher strains the yarn-yarn interactions become important but at this level of stress the tensile properties of the yarns themselves are also of consequence.

A major theme in the present thesis is the way in which the tensile characteristics of the yarns and also the frictional properties of the yarn-yarn junctions influence the behaviour of fabrics in this mode of deformation. The study has sought to alter these two properties by the use of lubricants. It will be shown that the lubricants change the yarn-yarn frictional forces required to both to initiate and to maintain steady motion. The same lubricants also appear to modify the tensile properties of yarns by reducing the filament-filament frictional forces in the yarn. The thesis describes a number of aspects of the influence of lubricants on the yarn tensile and inter yarn frictional properties.

This study was undertaken for two rather separate and distinct technical reasons both of which are related to the influence of yarn mechanics on the performance of fabrics. The choice of fabrics studied, a cotton fabric and an aramid fabric reflects these technical bases. The cotton systems are of commercial interest because of the common belief that fabric mechanics is a key aspect of the group of attributes which convey sensual or tactile appreciation of fabrics. It is of course common practice to modify this property by the use of fabric conditioners. The way in which these species act is still unclear and the thesis addresses this problem. The thesis does not however attempt to correlate mechanical or deformation properties with subjective handle assessment of the fabrics. The latter type of characterisation was considered inappropriate since it enters the realms of psychophysics. In the context of tactile appraisal the thesis addresses a number of the main features of the mechanical

properties of fabrics and provides a basis for data analysis. A major conclusion is that the influence of fabric conditioners may be interpreted in terms of their influence on the tensile properties of their constituent yarns and the monofilaments.

The adoption of aramid fibres focuses upon a different area of fabric mechanics; and that is the energy dissipation characteristics of fibres in ballistic impacts. Here the mechanical property of these fabrics is a critical factor in defining the energy dissipation characteristics and again it is argued that a prime mechanism for energy dissipation involves the tensile extension of the constituent yarns. Quasi-static simulations of the ballistic process were also performed. The energy was found to be dissipated through mainly a tensile extension mechanism and to a lesser extent through bending of the fabric. The trends of the response of the system to surface modifications were in keeping with those found for the ballistics experiments where they were seen to reduce the energy absorption characteristics at low strains and also the work done at high strains.

It should be pointed out that the deformations in the three systems outlined above are similar in shape, figure 1.1 and that the elasticity of the matrix in the hardness and the ballistic experiments are seen to originate from the microscopic processes responsible for the elasticity of the weave observed in the pull-out process.

The general layout of the thesis is as follows; chapters 2, 3 and 4 are review chapters dealing with various properties of fibres, yarns and fabrics respectively that are relevant to the current study. It was seen to be appropriate to divide the reviews into these three chapters because each system has it's own particular characteristics. Although the single filament conveys certain properties to the assembly system through the influence on yarn characteristics, the assembly possesses it's own characteristics, mainly due to the geometric arrangement of the yarns.

Chapter 2 is a detailed review of single filament properties. It begins by outlining the structure of cotton and aramid fibres. It then describes the dimensional

and water absorption (swelling) properties of these fibres. The tensile properties of single filaments are described in more detail and included are references to previous work by other researchers. Bending and twisting of fibres are briefly reviewed at the end of the chapter.

Chapter 3 contains a detailed survey of the properties of single yarns made of staple fibre and continuous filaments. The structure of the yarns and, in particular the so called "fibre migration" process, is described. The tensile behaviour of both types of yarns, continuous and staple forms, and the related theories based on single filament properties are outlined. Chapter 3 also includes a fairly comprehensive section on the relevant theories of the origins of the frictional processes for both general cases and those specific to fibres and yarns. This section also includes brief reviews of the stick-slip process, the differential friction effect and the influence of lubrication.

Chapter 4 presents a detailed review of some of the properties of fabrics and the studies undertaken previously that are most relevant to the current study. It begins by describing the geometrical properties of woven fabrics. The tensile and bending properties are also briefly outlined. The way in which chemicals may modify the surface characteristics of fabrics in relation to a fabrics' tactile and frictional properties are also included. The final major section of this chapter deals with the subject of the ballistic impact of yarns and fabrics and presents some of the theories that will be utilised in later chapters of this thesis.

Chapter 5 provides details of all the materials and experimental techniques used in this study. In addition there are sections dealing with the experimental procedures and the results of various friction and tensile experiments carried out on the chosen cotton and aramid yarns.

Chapter 6 presents the results of the so called "hardness" experiments, dealing with the influence of the side force, the fabric holder size, the indentor shape and size and the influence of various surface modification procedures. The chapter also

discusses the observations and the results in relation to some of the properties described in chapters 2, 3 and 4.

Chapter 7 describes the data obtained in the ballistic impact experiments. It includes mainly a description of the high speed photographic data obtained during the impact process together with the observed projectile velocity data.

In chapter 8 the results of the pull-out experiment on untreated dry fabrics are introduced. This chapter includes the described micro-displacements of the weave both in the plane and out of plane of the fabric and the influence of weft yarn tension on parameters specific to these experiments. Chapter 9 deals with the influence of chemical treatments on the specific fabric properties as measured in the pull-out experiments. The influence of the "treating" agents such as water, tetradecane, stearic acid, CTAB (Cetyl trimethyl ammonium bromide), and PDMS (Poly dimethyl siloxane) are described. The changes in fabric properties brought about by these treatments are discussed in terms of the mechanical properties of the constituent yarns and filaments.

Chapter 10 is occupied with the analysis and discussion of all the separate experiments. It begins by presenting two models which have been found useful to describe the fabric matrix shear processes and the effect of side force in the pull-out experiments. Inherent in these analyses is the attempt to quantify the effect of the surface treatments adopted. The chapter then discusses some of the results of the indentation experiments in terms of a continuum plate model. The last section deals with the results of the ballistic experiments and in particular the way in which a quasi-static model derived from the "hardness" experiments may be satisfactorily used to explain some of the observations of the ballistic impact process; in particular the influence of surface treatments.

The main features of these chapters are summarised and restated in chapter 11 as general conclusions. A diagramatic summary of the various elements of the thesis

and their interrelationships is given in figure 1.2.

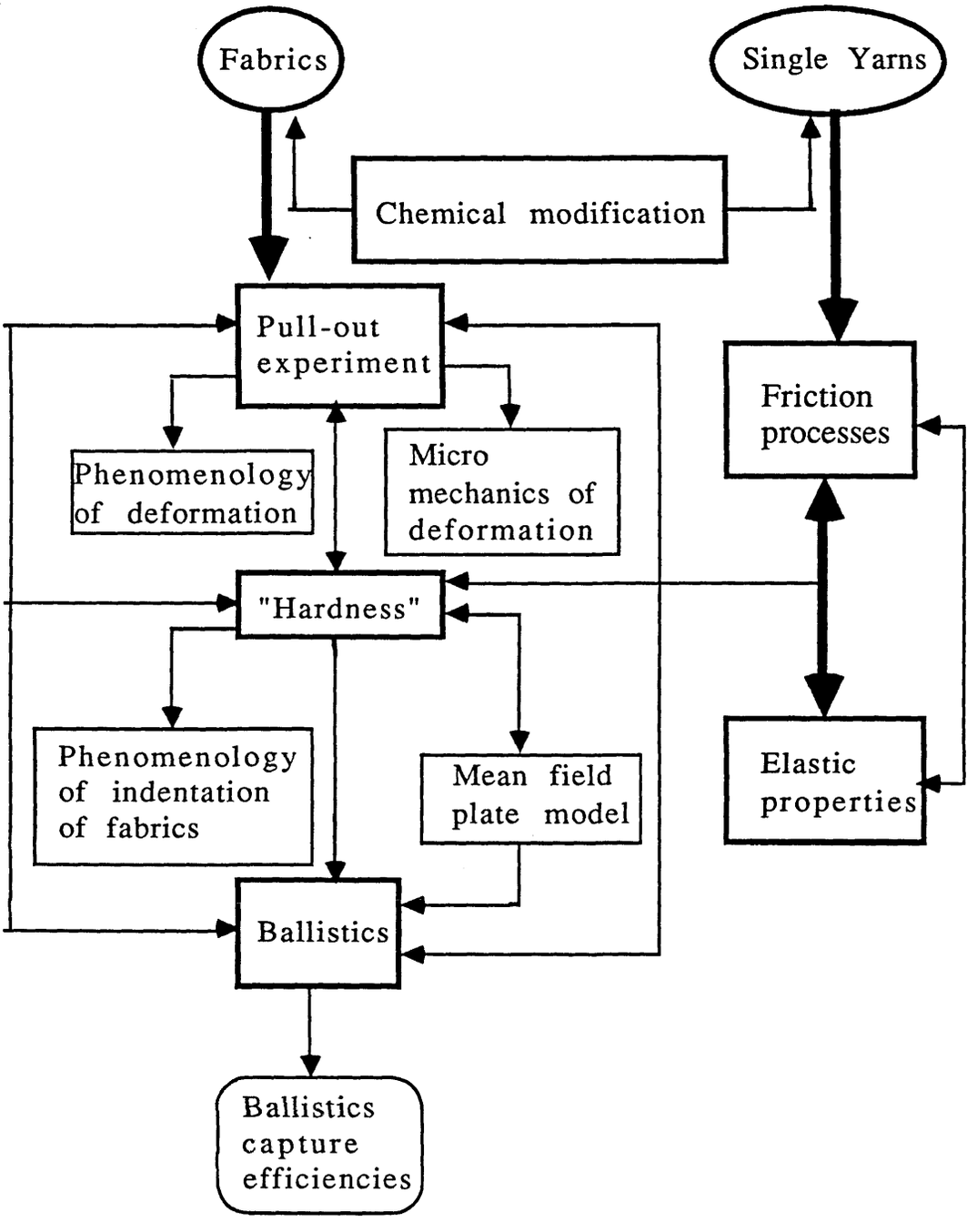

Figure 1.2 A block diagram representing a summary of the various elements in the thesis.

CHAPTER TWO

A REVIEW OF SINGLE FIBRE PROPERTIES

2.1 Introduction

In later chapters, the tensile, frictional and deformation properties of yarns and fabrics are reviewed and examined in different experimental environments. Yarns and subsequently fabrics are assemblies of fibres. Fibres in spun yarns are arranged in a special geometry which is discussed later. The mechanical properties of yarns and hence fabrics are controlled by the properties of the constituent fibres and the geometrical arrangement mentioned above. Although this thesis is not concerned with single fibres or filaments in a direct way, it is appropriate to review some of the fibre characteristics that affect assembly properties. The main purpose of the chapter is to introduce in a general way what are regarded as the main areas of established wisdom and indicate the very complex nature of fibre systems.

The chapter is divided into several sections. It begins by outlining the structure of the cotton and the aramid fibres investigated in this thesis. Then, the dimensional properties of these fibres will be reviewed. The subject of the absorption of moisture by these fibres, in particular cotton, is described briefly. The tensile, bending and twisting of fibres are discussed and some of the available theoretical treatments which have been developed are presented. Since the availability of aramid fibres is a fairly recent development, the literature on their properties is not as widespread as that for cotton. Thus, most of the qualitative information in this chapter relates to cotton, although the theoretical parts are applicable to both cotton (staple fibre) and aramid (continuous filament) yarns (see Section 3.1).

2.2 The Structure of Fibres

2.2.1 Cotton fibres

Cotton is a natural cellulose fibre. A fairly comprehensive review has been produced describing the structure and surface properties of cotton by Duckett (1975). Table 2.1, reproduced from that review, illustrates the chemical composition of a typical cotton fibre and the so called "primary" wall.

Table 2.1 Chemical composition of typical Cotton Fibre and Primary Wall.

Constituent	Percent of dry weight	
	Fibre	Primary wall
Cellulose	94.0	54
Protein	1.3	14
Pectic substance	1.2	9
Wax (alcoholic solubles)	0.6	8
Ash	1.2	3
Other	---	4

The cellulose molecule consists of a series of linked glucose rings, Figure 2.1. They may also bond to other chains by hydrogen bonds at the protruding hydroxyl groups. The complete chain is about 5μm long and 8×10^{-4} μm wide. The ratio of length to width is about the same as that of a typical cotton fibre.

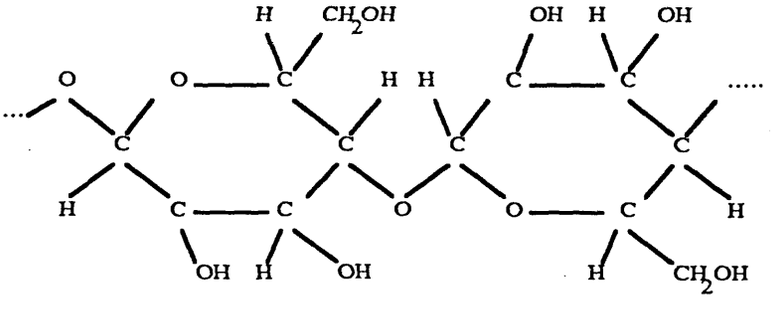

Figure 2.1 Glucose rings linked together.

As far as the fine structure of cotton is concerned, X-ray diffraction patterns have shown that the structure is a mixture of large crystalline regions and large amorphous regions in the ratio of ca. 2:1. The cotton fibre is a long irregular, twisted and flattened tube, possessing convolutions along its length. Figure 2.2 shows a schematic representation of the various layers of which the fibre is composed.

The fibre morphology can be summarised as follows. There are six distinct regions. The cuticle exists as a separate outer boundary and consists of a layer of wax and pectin materials that appear to be structureless. The primary wall consists mainly of a network of cellulose fibrils which are long, thin crystalline structures of cellulose molecules. The diameters of the crystallites is approximately 10 nm.

Beneath the primary wall is the thin layer of the secondary wall (less than 0.1μm thick) which is built up of closely packed parallel-ordered fibrils with a spiral winding angle of 25-35° to the longitudinal fibre axis. Below this thin layer is a thicker secondary wall (several micrometers thick) which contains the majority of the cellulose in the fibre. The fibrils spiral the axis at angles up to 25° and the spiral direction periodically reverses itself in this layer. A thin third layer of the secondary wall is distinguished, impregnated with non-cellulose substances. The lumen, the inner most region, contains the remains of the cell contents.

Among other important structural features of the cotton fibre are the surface waxes which act as interfibre lubricants. These materials comprise of a system of roughly parallel ridges and grooves on raw cotton fibre, spiralling about the fibre axis at angles varying between 20-30°. Also important are the fibre crimp and convolutions, the latter being a corkscrew-like twist in the structure of the fibre. Convolutions frequently alternate in the directions of their rotation and also vary in their pitch. They are not present during the initial growth, but are formed as a result of

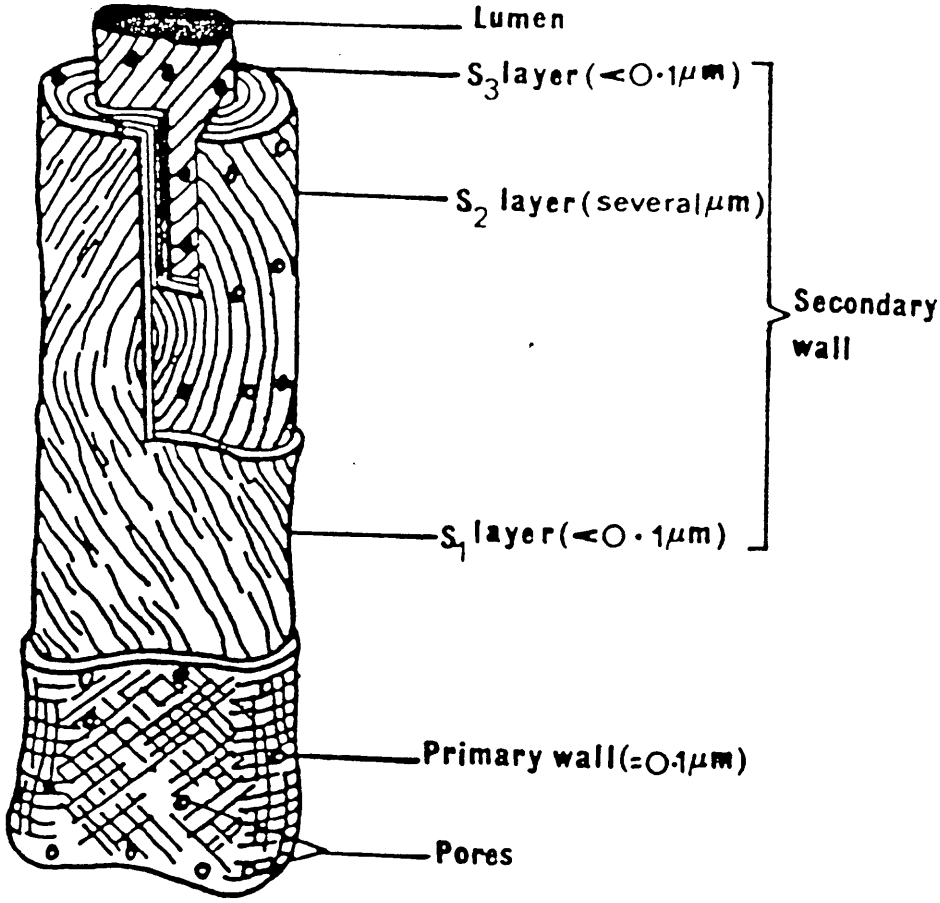

Figure 2.2 A schematic drawing of a cotton fibre illustrating the layered structure. (reproduced from Duckett)

fibre dessication after boll opening. Convolution generation is ultimately related to the spiral arrangement of the micro fibrils, which reverses in the direction of rotation periodically along the length of the fibre. The convolutions correlate negatively with such physical measurements as bundle tenacity, and their role may be extremely important in determining such mechanical properties as strength, extension and modulus of elasticity (Meredith, 1975).

Berkley and Woodward (1948) have attempted to correlate the strength of bundles of cotton fibres with the average angle of the molecular orientation. Meredith sought to correlate single fibre strength measurements with optical measurements of the convolution angle. It was found that the spiral angle of the crystallites in all cottons in the original unconvoluted fibre is the same and approximately 21°. The following equation has been produced to relate the convolution angle to fibre strength:

$$S_o = S_k \, e^{-k \sin^2 \theta_c} \qquad (2.1)$$

where S = fibre strength and θ_c = convolution angle.

In summary, the cotton fibres are extremely complex in their chemistry, morphology and gross structure. Their surfaces are also chemically and topographically very complex.

2.2.2 Aramid Fibres

The aramid fibre investigated was a commercial material called "Kevlar", developed by E.I. du Pont Co., and was a high strength, high stiffness organic fibre. It has become very popular for a variety of applications ranging from body armour to

aircraft structural parts. Aramids are often selected as fabrics or composite matrices because of their attractive properties such as chemical stability, light weight and high strength. Aramids have been identified by chemical analysis, X-ray crystallography and infrared spectroscopy as a poly (p-phenylene terephthalamide) (PPTA). The polymer, aramid fibre, is made by polymerising the acid chloride of terephthalic acid with p-phenylene diamine in a suitable solvent. The polymer is dissolved in sulphuric acid, and is formed into fibre filaments with a dry-jet wet spinning process. The filaments are subsequently washed with a solution of sodium carbonate to neutralise the excess sulphuric acid, Penn and Larson (1979). This process yields an extended chain polymer which is highly crystalline. The molecular and supra molecular structure of aramids have been investigated by many workers, Dobb *et al* (1979), Mogat (1980), Simmens and Hearle (1980). The aromatic polyamide fibres are characterised by - CONH - links in the para position between aromatic rings giving a fairly rigid chain.

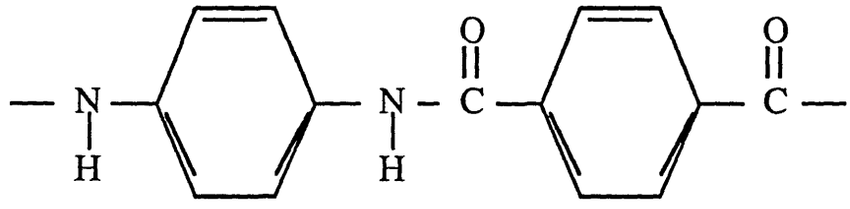

This feature, together with a large number of hydrogen bonds per unit volume between the CO and the NH functional groups on adjacent chains, contributes significantly to the high strength and relatively large axial modulus of elasticity in the oriented direction.

Pruneda *et al* (1981) have reported on the relation between the structure and the properties of aramid fibres. They proposed a morphological model for aramids as illustrated in Figure 2.3. A physical model was suggested in which there is an

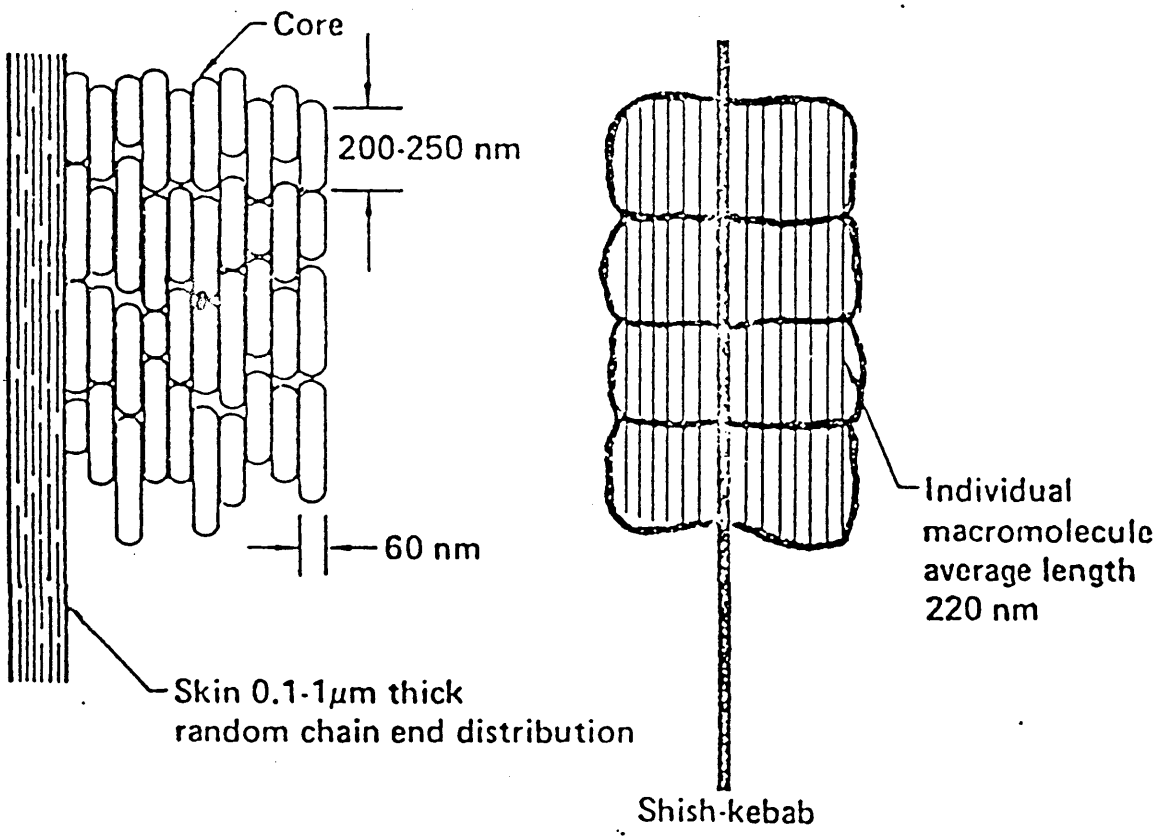

Figure 2.3 Morphology of Kevlar 49 fibre.
(reproduced from Pruneda etal)

amorphous skin and a crystalline core. The core was reported to consist of periodic transverse defect planes spaced about 200nm along the fibre. Chain ends were assumed to cluster within the vicinity of these planes. The non-crystalline skin, in which chain ends are arranged essentially randomly relative to one another, was not thought to contain such transverse weak planes. They argued that one of the most critical physical structural parameters that controls the deformation and failure processes is the chain end distribution within the fibre.

Northolt (1980) has investigated the tensile deformation of PPTA fibres. He derived functional relationships between stress, crystalline orientation distribution, dynamic modulus and strain from an analysis of the deformational behaviour of a simple mechanical series model consisting of a linear arrangement of crystallites. He showed that the deformation of these fibres is probably largely due to the elastic strain and irreversible rotation of the crystallites.

2.3 Fibre Dimensions

The fibre length is an important parameter, both with regards to the physical characterisations of the resulting fibre and the characteristics of the fibre processing operations. The fibre length, for natural textile raw materials, like most of their physical properties, varies greatly and the coefficient of length variation from sample to sample for cotton is about 40%. For wool it is 50-60%, while for man-made staple fibres the coefficient is approximately 10%. The range of length of cotton fibres, produced around the world, is approximately 12.5-44.5 mm. The I ength is important in fibre processing operations since the machines are designed to operate efficiently only on a comparatively narrow range of staple lengths and it is desirable to maintain

optimum processing conditions and avoid repeated and costly alterations. Fibre length measurement can be performed in one of two ways, either individually or in a group. The individual fibre methods are rather laborious and at best semi-automatic, involving measurement of a single fibre on a scale. For group measurements there are several methods available. These include the Comb sorter method, the Balls sledge sorter, the scanning methods and cutting and weighing methods.

The characteristic transverse dimensions of a fibre includes the parameters; diameter, width, perimeter, area of cross-section, specific surface, linear density, wall thickness and, for natural fibres, maturity. It is these parameters that affect the physical properties such as fibre fineness, stiffness, handle, torsional rigidity, absorption of liquids and vapours and many other yarn properties. Amongst the aforementioned properties, only fibre fineness and its' relation to other properties will be discussed here and the remainder are discussed later. Fineness which is related to the transverse dimensions of fibres can be measured using various methods; micrometric measurements, gravimetric measurements, air-flow methods and the vibroscope method.

Fibre fineness is an extremely critical parameter in determining the quality and commercial value of fibres. Length and fineness are strongly correlated. The correlation is negative with wools and positive with cottons. In cotton fibres fineness is also associated with variety and maturity. Also, all other conditions being equal, the finer the fibre the stronger and more uniform is the resulting yarn (Rusca and Sands 1968). Fineness is also seen as the dominating factor in determining the limiting count to which a raw material can be spun. Fineness also affects the flexural and torsional rigidities of the fibre, with the finer fibres possessing lower values. This is an important property in controlling the handle and the draping quality of fabrics.

The mean linear density (mass per unit length) is the most convenient way of comparing different samples. In natural fibres, there are significant variations in the mean linear density between samples and even along the length of the stapled material. This variation is less pronounced in man-made fibres. For example, Turner (1929) working on cotton found the mean linear density to change from 215 to 318 mtex in adjacent 6.4mm lengths.

Crimp is an important characteristic. It is generally defined as the waviness of a fibre and may be measured in terms of either the number of crimps or waves per unit length or percentage increase in length of fibre on removal of the crimp.

Brown and Onions (1961) have investigated the bilateral structure of wool and its crimp and used the classical treatment for the bimetallic strip to predict the crimp-forming tendency of wool fibres. Holdaway (1956) proposed a helical spring model to represent the load-extension behaviour of a wool fibre in uncrimping and found the model to be in good agreement with experiments at low and high decrimping loads. Shiloh and Litav (1965) studied the recovery of crimp for cotton fibres after successive loadings. They concluded that cotton crimp includes three components; a component which recovers immediately after initial extension; a component which recovers after a relaxation period and is responsible for the reversible deformation of crimp; and a third component which does not recover at all.

2.4 Sorption and Swelling of Fibres

When fibres absorb water, their dimensions increase both transversely and axially. The extent of swelling can be expressed in terms of diameter, area, length or volume. This effect has technical consequences as it results in a shrinkage of twisted

or interlaced structures. It also means that in closely woven fabrics, the pores will be completely blocked and the fabric becomes impermeable to water. Between dryness and saturation cotton fibres typically swell from 0-2% axially and 0-40% in area.

In cotton, although the glucose and cellulose groups are chemically similar, glucose dissolves in water while cellulose swells only to a limited extent. Water can penetrate into the non-crystalline regions of cellulose or between fibrils and dissolve these regions but it cannot penetrate the crystalline regions where the active groups are cross-linked. For aramid fibre "Kevlar 49" it is reported(Kevlar 49 data manual, E.I.du Pont CO.) that the moisture regain of the yarns at 55% RH is 3.5-4% after extended periods of time (typically over 10 hours).

Several theories exist to account for the moisture absorption of fibres. These include the early theories where molecules are directly and indirectly attached, the multilayer adsorption theory (the BET equation), Langmuir (1918) and solution theories. Perhaps the most interesting model is the treatment proposed by Hailwood and Horrobin (1946). They considered that some of the water is present as hydrates formed with definite units of the polymer molecule and that the rest form an ideal solid solution in the polymer. They derived a general equation which relates the amount of water absorbed to the relative humidity and allows for a variety of different hydrates to be formed. The equation is:-

$$\frac{Mr}{1800} = \frac{kH}{1-kH} + \frac{k\,k_1\,H}{1+k\,k_1 H} \qquad (2.2)$$

where M_r= molecular weight of polymer unit, k_1 and k are constants and H = relative humidity. Figure 2.4 reproduced from Morton and Hearle (1975) gives a comparison of observed and calculated results for cotton and wool at 25°C and shows how water

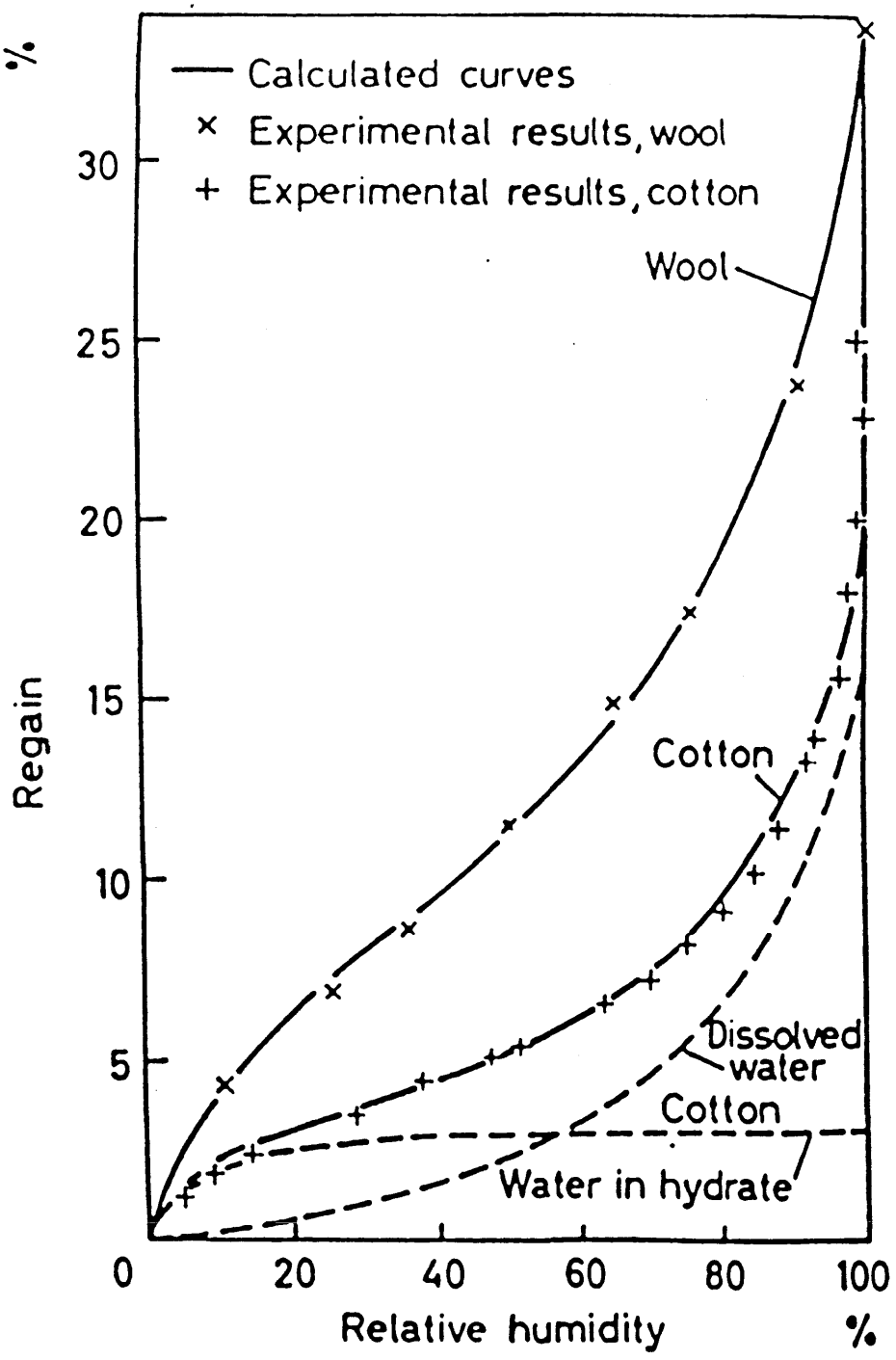

Figure 2.4 Comparison of Hailwood and Horrobin's equation with experimental results for wool and cotton.

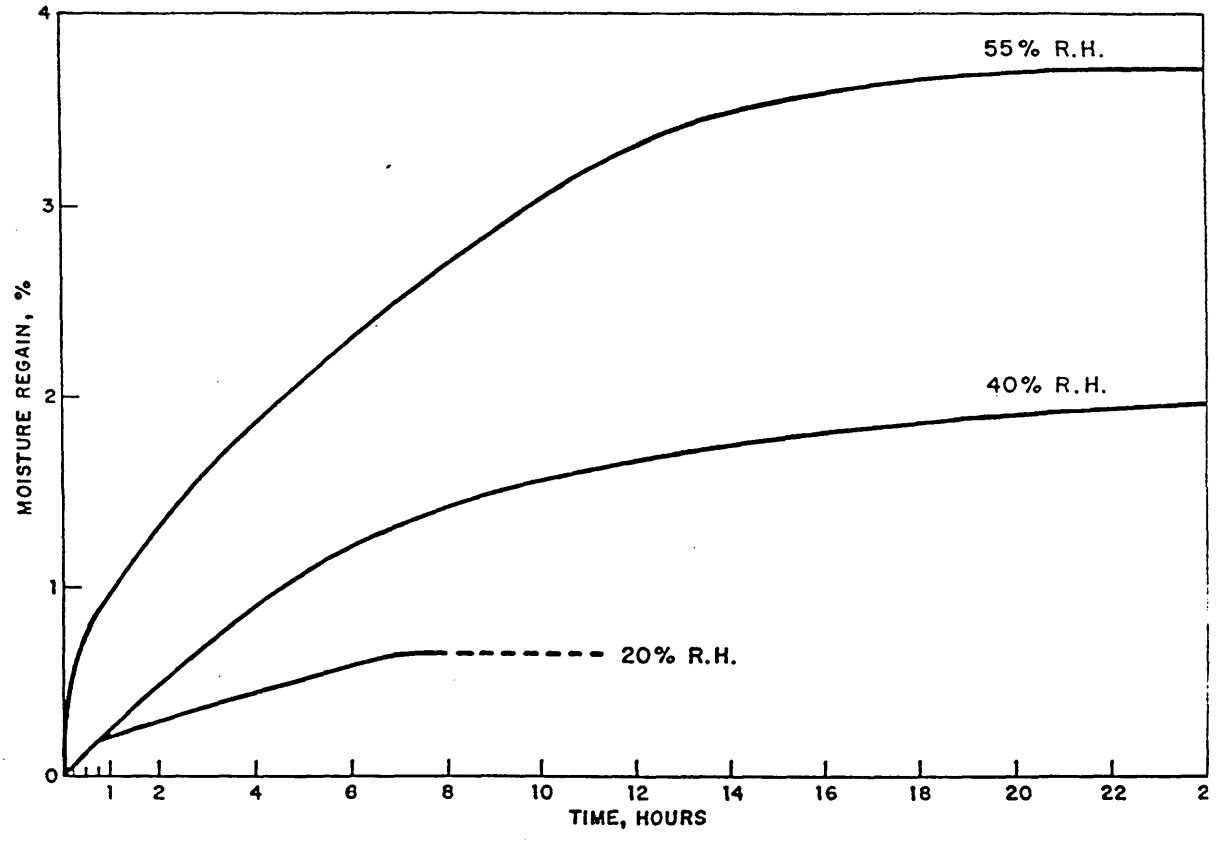

Figure 2.5 The effect of relative humidity on the equilibrium moisture regain and regain rate of 380 denier aramid 1 yarn.

in cotton is taken up between the hydrate and the solution. Figure 2.5 shows the effect of time and relative humidity on the moisture regain of Aramid fibre 1 yarn.

The sorption of water and other liquids in fibrous assemblies, namely yarns and fabrics, is also of considerable practical interest. Hollies *et al* (1956) studied the effect of various yarn construction features such as twist, diameter, crimp, fibre arrangement and the denier of yarns of cotton, nylon, Dacron and wool, on the transport of water through these yarns. They concluded that water transport occurs essentially by capillary motion and all the aforementioned features affect the rate of water transport insofar as they control the size of the interfibre capillaries. Large capillaries in general produce higher rates of transport. They also measured contact angles on yarns and fibres and showed that water migration in yarns is directly related to the apparent advancing contact angle of water on the yarn and only indirectly to the surface properties of the fibre material. They developed an equation based on the laws of hydrodynamic flow through capillaries ;

$$s^2 = \frac{\gamma \cos \theta_A^1}{2\eta} r_e t = k_s t \qquad (2.3)$$

where s = horizontal distance travelled by liquid, γ = liquid surface tension, η = liquid viscosity, t = time, r_e = effective radius of capillary, θ_A^1 = apparent advancing contact angle and k_s = rate of water transport. Later Minor *et al* (1959) expanded this work to include liquids other than water and other yarns.

If a yarn or fabric is totally immersed under a liquid, then the liquid displaces the air in the capillary spaces. Fowkes (1953) has shown that the sinking time of a cotton yarn in an aqueous solution of surfactants is a function of the adsorption of

surfactant and the cosine of the advancing contact angle of the solution on the fibres. For sorption of liquids by fabrics, from an unlimited reservoir of liquid, the distance L covered in a time t by liquid flowing under capillary pressure is given by:

$$L = \left(\frac{r\gamma t}{2\eta} \cos \theta_A^1\right)^{\frac{1}{2}} \qquad (2.4)$$

The spreading process of a liquid drop placed on a fabric may be divided into two parts, (Gillespie ,1958). Some of the liquid remains on the surface and when the liquid is completely contained within the substrate.

For two-dimensional circular spreading in textiles during phase II, Kisa (1981) developed Gillespie's equation to propose the following result:

$$A = k(\gamma/\eta)^u v^m t^n \qquad (2.5)$$

where u, m and n are constants, v = volume penetrating the substrate and A = area covered by spreading liquid. The exponent n = 0.3 for n-alkanes on cotton fabrics. Also, the above equation only holds for fibres that are impermeable to liquids.

Kawase *et al* (1986) have investigated the capillary spreading of liquids (including water) on fabrics (including cotton). They found that during phase I, the exponent n in Equation (2.5) is equal to 0.5 while when diffusion of liquid into fibres must be considered n decreases (as low as 0.1 for water on cotton), m increases and u remains constant. Minor *et al* (1959) also examined the behaviour of small single droplets of organic liquids on a variety of textile fibres. The liquids did not penetrate, react or swell the fibre. They measured the contact angle and contact angle hysteresis and discussed the observed behaviour in terms of capillary theory.

2.5 Tensile Properties of Fibres

The responses of fibres to applied forces and imposed deformations are perhaps their most important mechanical properties and have been widely studied. The behaviour of a fibre under an increasing applied load may be expressed by a load-elongation curve. However, the characteristics of such a curve depends on a number of parameters, the condition of the material, the arrangement and dimensions of the specimen, and the testing period. The load-elongation curve can be transformed into a stress-strain curve where stress = load/area of cross-section and strain = elongation/unit length. However, in textiles it is more convenient to use quantities based on the mass rather than volume and hence one generally uses specific stress = load/linear density where linear density = mass/unit length.

There are several important features apparent in a typical stress-strain curve; the initial modulus, the tensile modulus, the breaking load (specific strength or tenacity), breaking extension, the work of rupture and the yield point. The load elongation curve can be obtained by one of two methods, at constant rate of elongation or at constant rate of loading. The most commonly used method of fibre testing adopts a constant rate of elongation based on instruments such as an Instron tensiometer.

There has been numerous studies of the tensile properties of fibres. Meredith (1945) made one of the best early comprehensive sets of measurements of this kind. Using several fibres, he measured their fineness, strength, extensibility, yield stress and strain, work of rupture and variation in a given sample. He measured the *weight* of a 2cm long fibre on a microbalance to provide an estimate of the fineness and used a Cliff load-elongation recorder to obtain the load-elongation character of the fibres. The following results for three varieties of cotton were, Table 2.2:

TABLE 2.2

Cotton	Tenacity N/tex	Breaking Extension %	Work of rupture (mN/tex)	Initial mod. (N/tex)
St. Vincent	0.45	6.8	14.9	7.3
Upper	0.32	7.1	10.7	5.0
Bengals	0.19	5.6	5.1	3.9

The stress-strain curve for cotton is very slightly convex to the extension axis and there is no obvious yield point.

In his experiments, Meredith (1945) only used the results from experiments where the fibre rupture occurred away from the grips. 24% of his fibres ruptured at the grips. He explained this effect in terms of three possibilities: damage at the grip (heat tendering, skew mounting, etc.), naturally occurring weak sites and the weakening of a very regular fibre by the restraining action of the grips. Finer cottons show higher values of tenacity and initial modulus. The breaking extension was observed to occur between 5-10%. For Kevlar 49 yarns the elongation to break is reported to be around 2.5% (Kevlar 49 data manual, E.I du Pont &Co.). Table 2.3 from Farrow (1956) shows the effect of moisture on various tensile characteristics of cotton.

TABLE 2.3

Ratio of Values wet/65% RH

	Tenacity	Breaking extension	Work of Rupture	Initial modulus
Cotton (uppers)	1.11	1.11	0.92	0.33

It is important to note that the modulus, i.e. stress/strain, changes during the

load-elongation test. This is because when fibres are extended, their diameters contract and hence the true stress increases more rapidly than the apparent value.

Various mechanically based models have been proposed. The elasticity theory assumes that for small stresses and strains, the effect of each stress is independent and that the total effect of a complex stress situation is the product of the sum of all the stresses. For instance, the initial modulus of a fibre would be unaffected by slight twisting. However, this is not the case for larger strains. Dent and Hearle (1960) have studied the tensile properties of twisted single fibres. Their experiments were performed with a constant length during twisting and constant low tension during twisting. They measured the variation with twist in the tenacity, the breaking extension, the modulus and the contraction or contractive stress. With constant length twisting, for an increase in twist, the start of the stress-strain curve was shifted up the stress axis. The initial modulus was traversed and the breaking load and extension were decreased.

Meredith (1951), in an investigation of the tensile strength of cotton fibres in relation to their X-ray orientation, found a correlation between initial modulus and orientation. Meredith also found that the coarse fibres had a higher breaking load but not in proportion to their area of cross-section. Morlier *et al* (1951) noted that the tenacity and the breaking extension increased with the increasing length of their cotton fibres. Meredith (1951) correlated tensile strength of single raw cotton fibres with the orientation of the crystallites and found correlation coefficients ranging from 0.77-0.84. Molecular orientation is closely related to the spiral angle in cotton fibres, but since the spiral angle is found to be rather constant in cotton fibres (20-23°), the difference seems to be due to the effect of the convolutions. Also, wet cotton was found to be stronger than dry cotton and the probable reason suggested was that in

the wet cotton the shear stresses that can occur by the untwisting and the unbending of the fibre, which can lead to rupture, have been relieved. Hearle and Sparrow (1971) investigated the fracture of dry, wet and mercerised cotton fibres using scanning electron microscopy. They found that the tensile fracture occurred adjacent to a reversal zone and not through it. Splitting between fibres occurs due to the untwisting effect. Fibres broken in the dry or cross-linked state result in the fracture running across the fibre with little splitting. In wet cotton, due to the weaker attraction between fibrils, they give a long break.

According to Meredith, the mean measured tenacity decreased with length as shown in Table 2.4.

TABLE 2.4 The effect of length on tenacity.

	Tenacity(N/tex)		
	1 cm	1 mm	0.1 mm
Cotton	0.81	0.43	0.59
Nylon	0.47	0.50	0.54

Table 2.5 shows the variability within a sample of cotton fibres (after Meredith).

TABLE 2.5

Coefficient of Variation %

Fineness	Breaking Load	Tenacity	Breaking XTN
24	46	43	40

The above variation can be explained in terms of the weak link effect which can be applied to both fibres and yarns. The weak link effect described by Morton and

Hearle (1975) has the following results:

(a) the mean measured strength of a specimen decreases as the test length increases;

(b) for more irregular fibres, this decrease is more rapid;

(c) the order of ranking of specimen strengths may alter if the test length is changed.

Attempts have been made to produce a mathematical analysis to estimate the strength that would be obtained at some greater test length than that actually used. The analyses of Pierce (1926) and Spencer-Smith (1947) are such examples but neither method gives satisfactory results. The weak link effect also influences the stress and strain characteristics in a tensile test, as well as breaking extension. The latter decreases as the specimen length increases. The effect of the variability on the shape of the stress-strain curve of dry and wet wool fibres has been investigated by Collins and Chaikin (1969). The elastic recovery of a fibre is of great technical importance. It will not be discussed in detail here, since it is not directly related to this work. Elastic recovery is the ratio of elastic extension to total extension.

On a molecular level, elastic deformation is due to the stretching of inter-molecular or inter-atomic bonds, while plastic deformation occurs when bonds break. There are many parameters that can affect recovery, including, time, rate of extension, humidity, temperature, etc. Compared to other fibres, the elastic recovery of cotton is only moderate. For a given strain, recovery is independent of variety, but the recovery is less in coarse cottons since they possess lower moduli. Table 2.6 indicates the extent of the recovery in cotton and nylon fibres, after Beste and Hoffman (1950).

TABLE 2.6

Elastic Recovery

	1% extension		5% extension	
	60% RH	90% RH	60% RH	90% RH
Cotton	91	83	52	59
Nylon	90	92	89	90

The analysis of the mechanics of cotton and other plant fibres is somewhat similar to that of the twisted yarn mechanics (due to their fibrillar structure), Hearle *et al* (1969). Hearle (1967) has analysed the mechanics of fibres using a minimum energy method and considered both the extension of the crystalline fibrils and the possible reduction in volume. For an assembly with a constant helix angle at all radii, he obtained the following result:

$$E' = E_f (\cos^2\theta - \upsilon \sin^2\theta)^2 + K(1-2\upsilon)^2 \qquad (2.6)$$

$$\upsilon = (E_f \cos^2\theta \sin^2\theta + 2K)/(E_f \sin^4\theta + 4K) \qquad (2.7)$$

where E'=fibre tensile modulus, θ=helix angle, E_f=tensile modulus of crystalline fibre, υ = Poisson's ratio and K=bulk modulus. In ordinary cotton fibres, there are other features such as variation in the helix angle, the collapsed shape of the fibre, helix reversals and convolutions that can lead to further extensions.

It is important to recognise that the mechanical properties of fibres are viscoelastic and this is why most fibres exhibit characteristics of yield point and creep. Cotton is somewhat different in that it does not possess a yield point and it's

stress-strain behaviour is rather Hookian, i.e. stress $\sigma = E'\varepsilon$ for relatively small strains where ε = strain.

One way of analysing viscoelastic properties of any material is to use models based on ideal elastic springs and viscous dashpots. However, in the case of fibres, this would require a very complex arrangement of elements to represent all the characteristic behaviours of fibres. One of the simplest models that shows qualitatively the form features of instantaneous extension, primary and secondary creep and stress relaxation is shown in Figure 2.6.

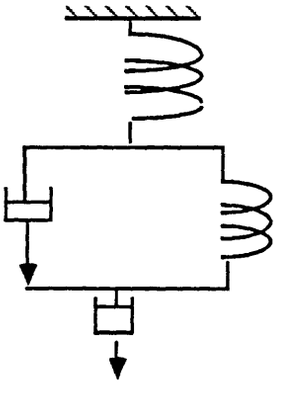

Figure 2.6 A four element model representing the extension, primary and secondary creep and stress relaxation of a fibre.

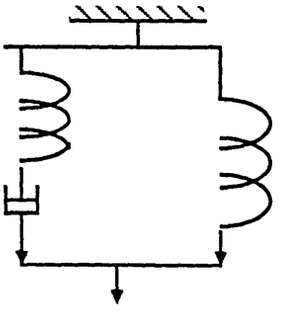

Figure 2.7 Eyring's three element model.

However, the most successful model, proposed by Eyring *et al* (1941) is the three element system, Figure 2.7 and its behaviour is represented by equation 2.8:

$$\frac{d\varepsilon}{dt} = k \sinh \alpha \sigma \qquad (2.8)$$

where k and α are constants.

The material discussed so far on the tensile properties of fibres refers to these properties at low speeds of testing (rates of strain). At higher speeds (ballistic rates) other methods and analyses must be adopted.

2.6 Bending and Twisting of Fibres

2.6.1 Introduction

The bending and twisting characteristics of fibres are of great practical significance. They affect the behaviour of bulked-yarn filaments and the handle and drape of fabrics and play an important role in the arrangement of fibres in yarns. The bending properties also influence fabric properties such as flexibility, crease retention and wrinkle-recovery. Bending strength and shear strength may be important in wear. In this section, the bending and torsional properties of fibres are briefly discussed in relation to some of the theories developed in the literature

.

2.6.2. Bending

Compared to the tensile properties of fibres, bending properties have received little attention, although Guthrie (1954) has emphasised that bending properties

of single fibres may be more important in practical textile applications. The objective measure of the intuitive concept of bending stiffness is known as the bending or flexural rigidity of the specimen and is defined as the couple required to bend the fibre to unit curvature and in this way the direct effect of length is eliminated.

Theory of Bending

For a specimen of length l, bent through an angle θ_b to a radius of curvature r, the outer layer will be extended, while the inner layer is compressed. But there will be a plane in the centre, known as the neutral plane, whose length will be unchanged.

Then

$$\text{Total internal couple} = \frac{E A k_b^2}{r} \qquad (2.9)$$

where E = Young's modulus and A = Area of cross-section

k_b is analogous to a radius of gyration

$$k_b^2 = \frac{1}{4\pi}\eta_s A$$

and $A = T/\rho$ and $E = \rho / y$

η_s is a shape factor. We obtain

$$\text{total couple } M = \frac{1}{4\pi}\frac{\eta_s y T_b^2}{r\rho} \qquad (2.10)$$

where T_b = linear density of filament and ρ = density

$$\text{and flexural rigidity} = \frac{1}{4\pi}\frac{\eta_s E T_b^2}{\rho} \qquad (2.11)$$

Flexural rigidity may be measured statically or dynamically. Four main types of methods have been used in the study of single fibre bending.

1. Cantilever loaded at one end
2. Loaded loop
3. Searle's double pendulum
4. Vibrating rod.

Owen (1965) used Searle's single and double pendulum methods to measure the flexural and the torsional rigidity of single fibres. According to the author, both these properties are closely related to the fibre linear density within a sample and hence he also measured the length of his specimens. He tested a large variety of fibres. For cotton he obtained a value of 0.53 mN mm^2/tex^2 for the specific flexural rigidity, this being the flexural rigidity over square of linear density.

Guthrie (1954) used static and dynamic methods to measure bending rigidities and their relation to tensile measurements and found that at similar rates of loading for acrylic, polyamide and polyester fibres, the dynamic bending modulus was higher than the static bending moduli. In most cases, the measured tensile modulus lay between the dynamic and static bending moduli.

The above analysis and investigations have been performed at bending strains <0.5% where the bending and tensile stress-strain curves are virtually coincidental. Chapman (1971, 1973) studied the viscoelastic properties of single fibre in pure bending up to strains as high as 20%. He presented his results as bending stress-strain curves; defining the bending strain as b/n where b is half the thickness in the plane of bending, provided the neutral plane is in the middle. He found that in all

the man-made fibres, the bending stress-strain curve lay below the tensile curve indicating that yield in bending (on the compressive side) occurred more readily than yield in tension. However, in horsehair (and wool) the situation was reversed. Chapman also investigated the influence of temperature and relative humidity on bending modulus and found the modulus to decrease with increasing temperature and humidity.

Buckley (1979) performed a theoretical study of the effect of environmental conditions on the mechanical properties of fibres including bending and twisting and presented equations relating the changes to variations in fibre properties.

2.6.3. Twisting

The torsional rigidity or resistance to twisting of a fibre is defined as the couple required to introduce a unit twist, i.e. unit angular deflection between the ends of a specimen of unit length. The torsional rigidity can be obtained in terms of the shear modulus, defined as the ratio of shear stress to shear strain, the shear strain being in radians. When torsional rigidity is defined as torque necessary to produce unit twist in radians it will equal $\varepsilon' n T^2/2\pi\rho$. The expression shows the effect of the modulus of rigidity, fineness, shape and density.

Pierce (1923) has investigated the torsional rigidity of cotton fibres and found a mean value for the modulus of rigidity to be 2.3×10^9 Pa. He also found the torsional rigidity to halve for every 10% increase in moisture regain and the modulus of rigidity to halve for every 7.2% increase in moisture. Later Clayton & Peirce (1929) found that in the range 20-40°C, the torsional rigidity decreased by 1.2% of its value at 20° for each degree increase in temperature at 7% moisture regain.

Meredith (1954) studied the initial torsional rigidity of single fibres using the torsion pendulum method for twists less than half a turn per cm. For cotton he obtained a value of $522 \pm 92 \times 10^{-5}$ Pa for the torsional rigidity and 2.51×10^{9} Pa for the modulus of rigidity. He also produced relationships to estimate the shape factor of various shaped fibres. Studying the effect of tension on torsional rigidity he concluded that if tension is kept below 0.2 g/tex, the positive correlation will be negligible.

Guthrie et al (1954) have also used the torsion pendulum method to study the torsional rigidity of fibres and found that for various diameters of fibres, the torsional rigidity was proportional to $(\text{tex})^{1.9}$ (cf. theoretically $(\text{tex})^2$) and accounted for this by the difference of shape in fibres of different fineness.

Owen (1965) has studied the torsional rigidities of fibres dynamically. He found values for the specific torsional rigidity and shear modulus of fibres [specific torsional modulus is torsional rigidity of a specimen of unit linear density = $\varepsilon' n / \rho$, the value for cotton being 0.16 mN mm^2/tex^2.

In torsion, one is concerned with forces at right angles to the fibre axis, in other words, they act between the molecules and not along their length as is the case when a fibre is stretched. Deformation through twist is easier and hence one expects the shear modulus to be less than the tensile modulus. This is indeed the case, the difference being greatest for the most highly oriented fibres such as aramids. The ratio of the tensile to shear moduli gives a rough measure of the anisotropy of the fibre as far as its cohesion lengthwise and laterally is concerned. The value for cotton is found to be ca. 3.7 while the value for a typical nylon is 5.8.

2.7 Summary

This review has ranged through a number of physical characteristics of fibres. It has focused mainly upon structure, dimension, mechanical properties and environmental sensitivity. Cotton fibres are seen to be of a complex chemistry, morphology and dimension whilst the aramid fibres are comparatively simple species. Both fibres show a pronounced sensitivity to water although these effects for cotton are more pronounced. The mechanical properties have been reviewed under three headings; tension, torsion and bending and while the intrinsic behaviour in each mode is different the deformation characteristics exhibited in the three modes show some similarity at a first order level. This is particularly so with respect to the environmental changes discussed.

CHAPTER THREE

SINGLE YARN PROPERTIES

3.1 Introduction

A major part of this thesis is concerned with the tensile and frictional properties of staple and continuous filament yarns and this chapter reviews these properties and the models which have been developed to account for these characteristics. The extensile behaviour of yarns arises from a complicated interaction of the intrinsic deformation behaviour of the single filaments or fibres, the interfilament friction and the relative geometry of the filaments in the yarn. The tensile and bending behaviour of the single filaments were discussed in Chapter 2. In this chapter, the manner in which the yarn structure influences the tensile extension of yarns is introduced. The chapter reviews the various analyses that have been developed to account for the behaviour of yarns using filament and interfilament characteristics. The chapter also reviews a number of aspects of the friction and lubrication of fibres and yarns and the way in which these processes affect the bundle strength and tensile behaviour of yarns.

Because of the important role which filament friction plays in affecting the mechanical properties of yarns and also fabrics, the subjects of friction and lubrication, both generally and in the context of fibres and yarns and to some extent fabrics, are reviewed in this chapter.

Yarns are complex structures. They comprise a rather isotropic or oriented collection of filaments. If the filaments (sometimes called fibres or monofilaments) are long, say one hundred times the diameter of the yarn, the yarn is called a continuous spun yarn. Where the filaments are only a few times the yarn diameter in length, the

yarns are called staple or discontinuous yarns. This chapter will describe the behaviour of both of these classes. Natural yarns are usually discontinuous and comprise short filaments. Cotton yarns are an example. Many synthetic yarns are constructed from continuous filaments. The aramid yarns investigated in this thesis fall into this category.

The yarns produced by both routes usually have characteristically similar structures in order to produce particular properties. These properties are discussed later. The main similarity is that the yarns are invariably spun and hence they compose of more or less extended helically wound filaments. This structure is responsible for many of the observed properties and most importantly the yarn coherence. The cotton yarns studied in this thesis possessed such a spun structure. The structure of the aramid yarns were rather different to those of the cottons. The aramid yarns were composed of filaments lying adjacent to each other with relatively little spin or migration. Thus, the properties of the yarn and in particular the extensile properties of the yarns are affected to a lesser extent by the geometry of the yarn than in the case of the cotton yarns.

3.2 Structure of Yarns

Many of the early studies of yarn mechanical properties often adopted unrealistic models of the yarn structure to facilitate the modelling of their properties. Figure 3.1 depicts an ideal helical geometry due to Hearle *et al* (1965), often adopted in theoretical studies of the structural mechanics of yarns. It is assumed that the yarn is circular in cross-section and that the fibres are following helical paths around concentric cylinders of a constant radius. At a distance r from the axis, Figure 3.1, the fibre length is l; at the surface of the yarn with radius R, the fibre length is L. h denotes the filament length associated with one complete rotation of the filament about the yarn axis. This

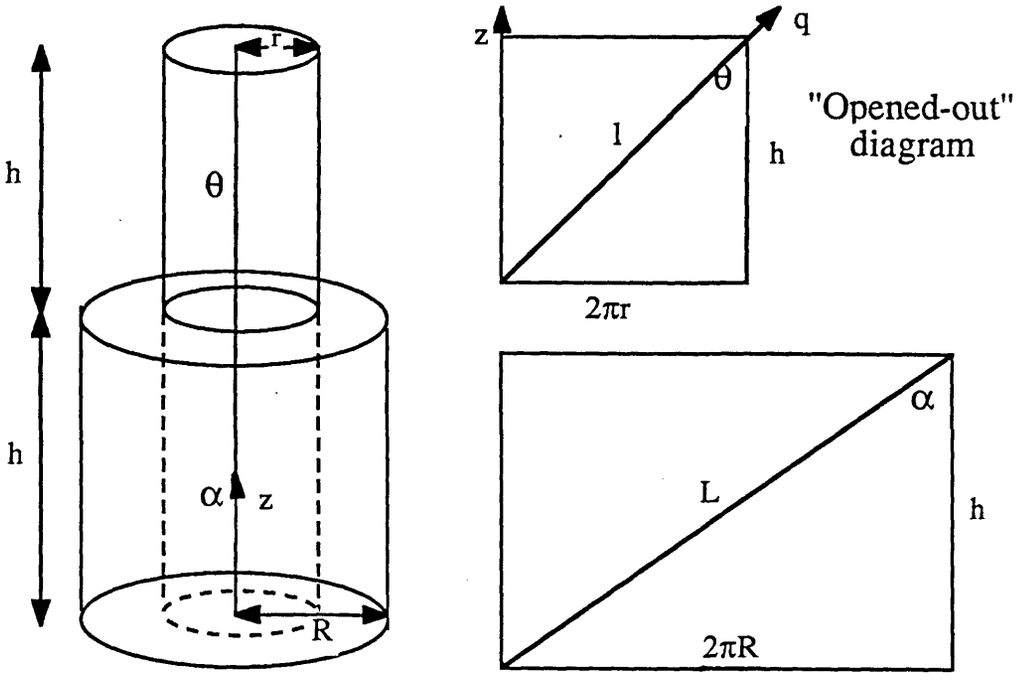

Figure 3.1 The idealised helical geometry of a yarn, due to Hearle (1965)

structure is however quite unrealistic. The actual position of a fibre in a yarn can be traced for example by the colour contrast fibre trace method of Morton and Yen (1952). It will then be seen that the fibres traverse back and forth across the imaginary cylindrical zones of the yarn body. Sometimes it is at or near the surface and sometimes at or near the core. This interchange of position produces a tangle of interconnected fibres. This type of behaviour was initially observed by Morton (1956). He termed the process "fibre migration" and the usage is still retained.

There are various factors that affect fibre position in the yarn, and these can be considered to belong to three groups: fibre factors, yarn factors and process factors. Fibre factors include properties such as length, fineness, shape, coefficient of friction, tensile modulus, flexural and torsional rigidities, extensibility and recovery. Among the yarn factors we can find properties such as yarn count and amount of twist, and process factors would include the tension during processing, the drafting system and the amount of draft, the position of fibre when delivered and the machine geometry and setting.

The theories or mechanisms proposed to account for fibre migration up to 1968 have been reviewed by El-behery (1968). Migration processes occur as a result of two different mechanisms described as the tension variation mechanism and the geometric mechanism. Morton (1956) postulated the tension variation mechanism of migration in the following way. Because the length of the fibre path as proposed by the simple helical model above, increases from the core to the surface, so also must the tension in the fibres. The fibres near the surface of the yarn are at a higher tension than those near the core. When the spinning tension is removed, the most likely nett result of the stress relaxation would be that the fibres at the surface would remain under a reduced tension and the fibres in the core will be buckled. Thus, in continuous spinning it is supposed that the taught filaments will attempt to release their strains by gradually migrating towards the centre, while the buckled ones will migrate to the surface. The

ultimate result of this process would be a yarn with component filaments all of the same length in a unit length of yarn.

Onions *et al* (1960) suggested that migration mechanisms are different for fibres of different lengths and diameter. The coarser and stiffer fibres tend to drift to the outside of the yarn as they store more elastic energy which can be dissipated by this process. In contrast, Hickie and Chaiken (1960) suggested that any migration is mainly a result of fibres moving towards the yarn axis. The twist insertion at the twist zone plus inter-fibre friction will cause the fibres to extend longitudinally and they will tend to move to the interior under forces acting radially. They also suggested that fibres under higher tension will migrate to the interior more rapidly than those with lower tensions.

Hearle and Merchant (1962) have introduced yet another migration theory based on a study of a seven-ply structure and argued that migration will only take place when the tension in the "central" ply has fallen to zero.

The geometric mechanism was first described by Hearle and Bose (1965) and they claimed that it may either combine with or replace the tension mechanisms. It is based on the fact that in practical twisting operations, it is probably more common for the yarn to be processed as a *ribbon* rather than a cylinder. In this mechanism, fibres on the outside would show a very marked migration while those originally near the centre would show little or no migration. Later Hearle *et al* (1965) concluded that the two migration mechanisms were not mutually exclusive.

There are basically two methods of investigating fibre migration in yarns. The tracer fibre technique first adopted by Morton and Yen (1952) and mentioned earlier and adopted by several other investigators such as Wray and Truong (1965), Riding (1964) and Hickie and Chaikin (1960) is simple in principle. The basic idea here is that the coloured tracer fibre can be mapped against the background of the body of the yarn to produce a trace line representing the projection in one plane of a helix. The

second technique involves the cross-sectioning of yarns. Several workers, Coplan & Bloch (1955), Hamilton (1958), Onions *et al* (1960) and Rudolph (1955) have used this technique. The basic principle is that cross-sections are cut from the yarn and are divided into a series of zones concentric with the axis and the fibres or blend composition is studied in each zone. In both cases the experiments are difficult and tedious to perform and only rather qualitative empirical data are obtained.

3.3 Mechanical Properties of Single Yarns

3.3.1 Introduction

The mechanical properties of yarns have been studied extensively by many workers. These properties, like those of fibres, can be divided into three groups; the extensile properties, the torsional properties and the bending properties. The thesis is primarily concerned with the tensile properties of yarns and hence this review of literature will only deal with the theories and the observations which relate to the tensile properties of yarns. Figure 3.2 shows the tensile characteristics of a staple fibre and a continuous filament yarn. Certain differences in the behaviour of the two types of yarn necessitates the adoption of rather different theoretical and analytical treatments. The first part of this section deals with experimental studies and the influence of a number of variables. The theoretical treatment of the mechanics of yarns has been approached from two directions, the classical treatment and the energy method of analysis. These techniques are briefly reviewed here.

3.3.2 The Tensile Mechanics of Continuous Filament Yarns

A general strategy for the analysis of the mechanics of yarns was outlined by Treloar (1964) in his Mather lecture almost a quarter of a century ago. The essence of

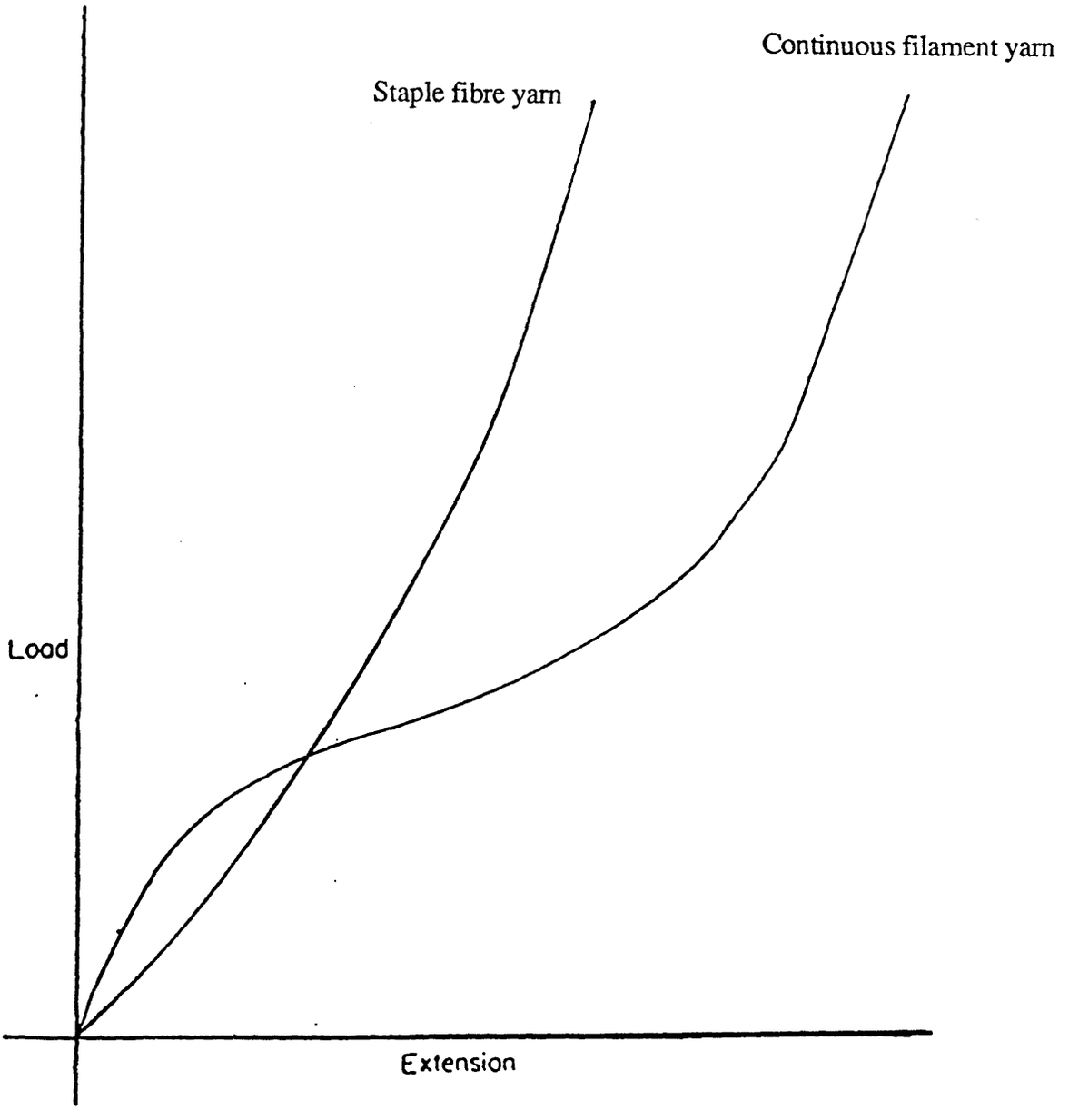

Figure 3.2 Comparison of typical stress-strain curves of a staple and a continuous filament yarn.

his argument was cited in the Introduction to this thesis.

Two methods of analysis exist in the literature. The classical method demands the calculation of the strains due to an imposed deformation and then a calculation of the stress distribution and the equilibrium of forces. The energy method first proposed by Treloar & Riding (1963) requires the calculation of energy as well as the strain due to the deformation. Both of these methods are reviewed here.

3.3.3 The Classical Analysis of Tensile Behaviour

The inherent helical geometry of twisted yarns has already been discussed in Section 3.2. The analysis reviewed here assumes that the yarn possesses such a geometry. The simplest first order treatment is to calculate the modulus of a continuous filament yarn in terms of the modulus of a filament, taking into account only tensile forces in the fibres and ignoring the effect of yarn contraction (Figure 3.3). The filament extension can thus be represented by:

$$\varepsilon_f = \varepsilon_y \,.\, \cos^2\theta \qquad (3.1)$$

where $\varepsilon_y = \delta h/h$, ε_f = filament extension, ε_y = yarn extension.

This equation shows that the filament extension falls from a value equal to the yarn extension for a straight filament at the centre of the yarn (θ=0) to a value $\varepsilon_y \cos^2\alpha$ at the yarn surface, where α is the twist angle. The specific stress in the filament and the yarn are respectively (Figure 3.3):

$$\text{specific stress}_f = E_f \varepsilon_f \qquad (3.2)$$

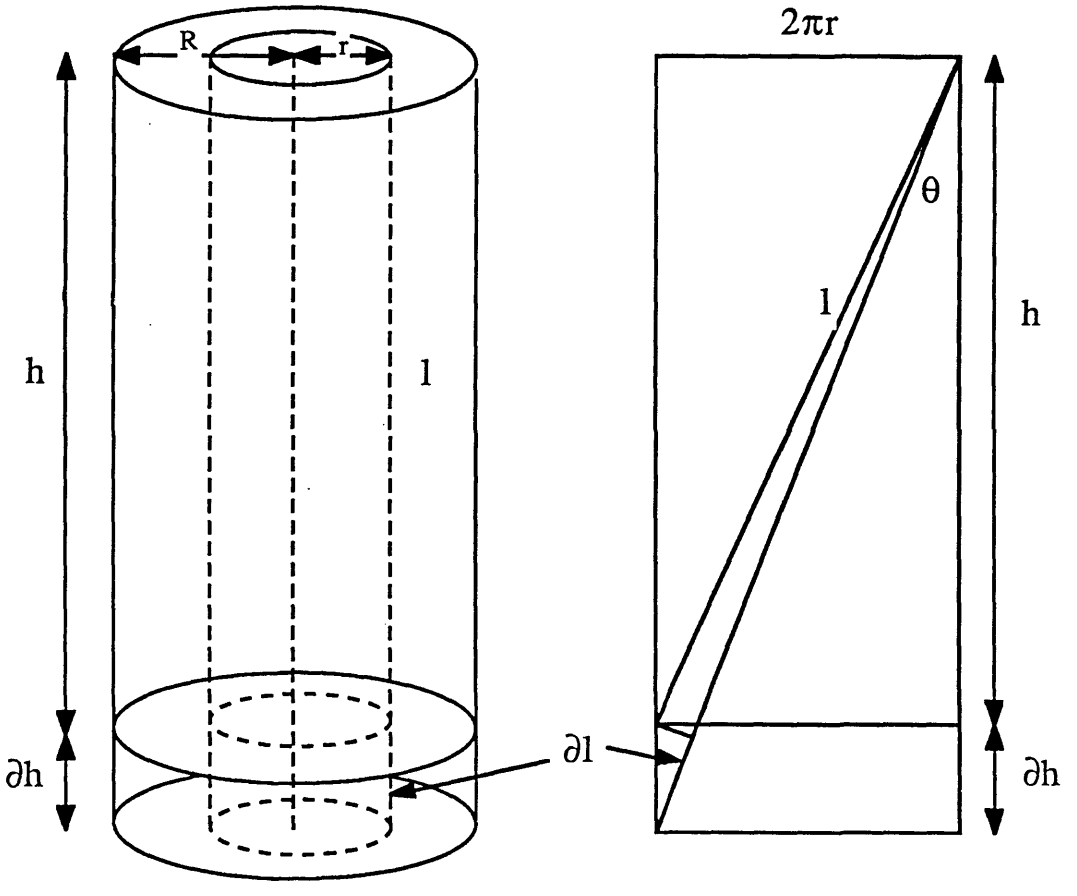

Figure 3.3 A schematic representation of an extended yarn based on the ideal helical geometry.

$$\text{specific stress}_y = E_f \varepsilon_y \cos^2\alpha \qquad (3.3)$$

and hence $$E_y = E_f \cos^2\alpha \qquad (3.4)$$

where E_y and E_f are yarn modulus and fibre modulus respectively. This simple treatment has two major defficiencies. It ignores the effect of the diametric yarn contraction and also the contributions of any transverse forces at right angles to the fibre axis are neglected.

Hearle, El-behery & Takur (1961) have presented a more comprehensive analysis which includes these factors. It was based on the following assumptions:

1. The yarn is a continuous filament yarn of circular cross-section, uniform along its length and having a constant specific volume.
2. All the filaments possess identical properties, are uniform along their length, perfectly elastic and possess a Hookian response.
3. The ratio of yarn to fibre diameter is large.
4. The fibres are assumed to lie on perfect helices, of constant radius and angle, possessing the same number of turns per unit length parallel to the axis of the helix.
5. The strains involved are small.
6. The transverse yarn contraction is assumed to be uniformly distributed across the yarn.
7. The stress distribution is uniform across that part of each face of a yarn element occupied by fibre material.
8. The stresses orthogonal to the fibre axis are assumed to be isotropic.
9. The shear forces and couples of the yarn are neglected.

The yarn geometry is defined by the following relations, see Figure 3.3.

$$l^2 = h^2 + 4\pi^2 r^2 \qquad (3.5)$$

$$\cos\theta = h / l = c / u \qquad (3.6)$$

$$\sin\theta = 2\pi r / l = (1 - c^2/u^2)^{1/2} \qquad (3.7)$$

where $u = l / L$ and $c = \cos\alpha = h / L$.

The variation of strain through the yarn is defined by the differential equation:

$$\frac{dl}{L} = \frac{h^2}{l^2}\frac{dh}{h} - \frac{4\pi^2 r^2}{l^2}\sigma_y \frac{dh}{h} \qquad (3.8)$$

where σ_y = lateral contraction ratio of yarns. This equation is only valid for small strains. The relation between the tensile stress X and compressive transverse stress G in a filament is defined by the equation:

$$X = E_f \varepsilon_y [c^2/u^2 - \sigma_y (1-c^2/u^2)] - 2\sigma_1 G \qquad (3.9)$$

where σ_1=axial Poisson's ratio. The term $E_f \varepsilon_y$ represents the stress in a single filament X_f when it is extended by the same amount as the yarn. Normalising equation 3.9 by X_f yields:

$$x = c^2/u^2 - \sigma_y (1-c^2/u^2) - 2\sigma_1 g \qquad (3.10)$$

The transverse and tensile stress distributions in the yarn are defined by the two following equations respectively.

$$g = \frac{1+\sigma_y}{(1+2\sigma_1)}\frac{c^2}{u^2}(1 - u^{1+\sigma_1}) - \sigma_y \frac{1-u^{2\sigma_1-1}}{(2\sigma_1-1)} \qquad (3.11)$$

$$x = \frac{(1+\sigma_y)c^2}{(1+2\sigma_1)u^2}(1 + 2\sigma_1 u^{1+2\sigma_1}) - \sigma_y \frac{1-2\sigma_1 u^{2\sigma_1-1}}{(2\sigma_1-1)} \qquad (3.12)$$

Using the above assumptions and equations, and for small strain, the equation for the mean normalised yarn stress can be obtained:

$$\text{mean normalised yarn stress} = \frac{2c}{(1+2\sigma_1)(1-c^2)}\{(1+\sigma_y[\ln c + \frac{2(1+\sigma_1)}{1+2\sigma_1}(1-c^{2\sigma_1+1}) - \frac{\sigma_y}{2}[\frac{3(1+2\sigma_1)}{2\sigma_1-1} - \frac{4(1+\sigma_1)}{2\sigma_1-1}c^{2\sigma_1-1} - \frac{1}{c^2}]]\} \qquad (3.13)$$

For large yarn strains two complications arise. First, equation 3.8 is no longer valid and second, filament deformation usually deviates from Hooke's law. Hearle *et al* (1969) have tabulated a series of equations derived for the load-extension behaviour of twisted yarns. This book also includes detailed derivations of the equations presented here.

The equations presented are an expression of the load-extension behaviour of twisted filament yarns. They can be used to predict the stresses in a yarn in terms of the parameters: yarn contraction ratio, twist angle and Poisson's ratio of the fibres.

3.3.4 The Analysis of Load-Extension Curve Using the Energy Method

The classical method of analysis is rather inadequate in cases where the stress-strain curve of the fibres is non-linear or where it is necessary to consider both large extensions and transverse forces. Treloar & Riding (1963) first devised the energy method as an alternative method of analysis. They analysed the mechanics of

an extended yarn by calculating the energy of deformation, and related the elastic energy stored in the deformed filament to the work done in extending the yarn. The energy method is much simpler than the micro strain model but it produces less information. It provides only the total yarn tension and not the distribution of stresses in the yarn. Treloar & Riding (1963) also point out that the effects of transverse forces are automatically taken into account. Treloar (1965) and Treloar & Riding (1965) extended this theory to take account of the migration of filaments in a yarn and the apparent variation of twist with radial position. They made the following assumptions:

1. The unstrained yarn takes the idealised helical geometry with uniform density of packing.

2. The filaments deform without change of volume, i.e. it is assumed that they are compressible under hydrostatic pressure. This means that the energy stored is a function only of the axial strain and not the axial and lateral strains.

3. The yarn also deforms without change of volume. For small strains this is equivalent to the yarn lateral contraction ratio $\sigma_y = 0.5$.

4. The stress-strain properties of the filaments in the yarn are taken to be the same as the individual isolated filaments.

5. The fibres are perfectly elastic, i.e. all the work done is converted into stored elastic energy.

Regarding the third assumption, Hearle *et al* (1960) investigated the relative changes of yarn diameter during extension using a photographic technique. Their results show that there is a decrease in yarn volume with increasing extension. However, this decrease becomes smaller as the breaking point is approached.

The stress-strain relation of a filament of unit length can be given as:

$$X = \phi(\varepsilon_f) \qquad (3.14)$$

The work done in straining a filament of unit mass and length up to strain ε_f is:

$$w_f = \int_0^{\varepsilon_f} \phi(\varepsilon_f)\, d\varepsilon_f \qquad (3.15)$$

The elastic energy stored in an element of yarn of unit length, mass of $2\pi r_o dr_o/v_y$, specific volume v_y, lying between radii r_o and $r_o + dr_o$ is thus:

$$dW = (2\pi/v_y)\left[\int_o^{\varepsilon_f} \phi(\varepsilon_f)\, d\varepsilon_f\right] r_o\, dr_o \qquad (3.16)$$

By integrating Equation (3.16) over the whole yarn cross-section, the total elastic energy stored, W_y can be obtained as:

$$W_y = (2\pi/v_y)\int_o^{R_o}\left[\int_o^{\varepsilon_f} \phi(\varepsilon_f)\, d\varepsilon_f\right] r_o dr_o \qquad (3.17)$$

where R_o = yarn radius in unstrained state. By differentiation of W_y with respect to ε_y, the yarn tension F can be obtained. The specific stress Y in the yarn is thus:

$$Y = \frac{F}{(v_y/\pi R_o^2)} = \frac{2}{R_o^2}\int_o^{R_o} \phi(\varepsilon_f)\frac{\partial \varepsilon_f}{\partial \varepsilon_y} r_o\, dr_o \qquad (3.18)$$

However, in order to evaluate Y, it is necessary to know, first, the form of the fibre stress-strain relation and second, the way the filament strain ε_f varies with yarn strain ε_y and yarn radi al position r_o. $\phi(\varepsilon_f)$ can be represented by an appropriate

mathematical formula. $\partial\varepsilon_f/\partial\varepsilon_y$ can be shown to be represented by the formula:

$$\frac{\partial\varepsilon_f}{\partial\varepsilon_y} = \frac{1-\frac{1}{2}(1+\varepsilon_y)^{-3}\psi}{\{[1+\psi][1+(+\varepsilon_y)^{-3}\psi]\}^{1/2}} \qquad (3.19)$$

where $\psi = Y\pi^2 r_o^2 T^2$. The exact derivation of this formula is given in the book by Hearle *et al* (1969). Treloar (1965) has used this theory to derive the stress-strain properties of multiply cords.

More recently, Hearle & Sakai (1978) proposed a new extended theory of the tensile properties of continuous filament yarns. They introduced the idea of a distribution function for fibre angles and derived a general equation that enables the prediction of the stress-strain relations of twisted filament yarns from those of the constituent single fibres.

Komori, Makishima and Itoh (1980) have outlined an extended theory on the mechanics of twisted homogeneous-filament yarns at large deformations. They used a different description of the distribution of fibre orientation and included an estimate of the change in fibre orientation due to the deformation. By estimating the actual orientation distribution of yarns of different twist and using the tensile properties of constituent fibres, they calculated the load-strain relations of the yarns. They found the results to agree quite well with experiments although there was a certain amount of discrepancy for large strain and/or high twist.

3.3.5 Summary

The geometrical character of yarns known as migration has a pronounced effect on the properties of yarns. The mathematical treatment of the tensile behaviour of yarns has been analysed using two different models known as the microscopic velocity vector model (classical method) and the continuum model (energy method). Equations have been presented using these methods that enable the prediction of the tensile behaviour of yarns using filament parameters. In the proceeding chapters the principle of these analyses will be used to explain some of the phenomena observed in this thesis. It is notable however that in spite of the complexity and apparent successes, these models are still rather crude descriptions of the microscopic processes involved. For example the models donot specifically include realistic interfilament force contributions such as friction and adhesion. The models do however have the virtue that they address, all beit in a first order way, the micro-structural aspects of yarn mechanics.

3.3.6 The Mechanics of Staple Fibre Yarns

The analysis of the mechanics of staple fibre yarns is naturally less tractable than for the case of twisted continuous filament yarns. The constituent fibres are discontinuous and the short filaments may readily slip over each other. Twist and fibre migration are also more important in staple fibre yarns since these phenomena largely hold the assembly of short fibres together as a yarn. However, the approach is similar to that analysed for continuous filament yarns.

The analysis outlined here follows the work of Hearle *et al* (1965) on the mechanics of continuous filament yarns discussed in Section 3.3.3. The full analysis will not be discussed here. A brief review of how the analysis is approached is given. The analysis is based on the classical method and contains many assumptions. Some

of the assumptions are that the idealised staple fibre yarn is assumed to consist of a very large number of fibres of limited length packed in a uniform circular yarn. The fibres follow an idealised migration pattern, i.e. a helical path. The fibres are perfectly elastic, possess identical dimensions and properties and follow Hooke's and Amonton's laws. The strains experienced are small and transverse stresses between fibres are isotropic.

The steps needed to analyse the mechanics of such an assembly are outlined by Hearle (1969) and will not be included here. However, the steps are similar to those taken in Equations (3.5) through (3.13) inclusive. The modulus of staple fibre yarns can be obtained directly using an alternative method which makes gross approximations. It is rather a crude method which considers the yarns as a continuous filament yarn, taking the simplest relation between modulus with twist, Equation (3.4). Again, the procedure for this approximate treatment and the basic assumptions made are outlined in detail by Hearle *et al* (1969).

3.3.7 Extension and Breakage of Yarns

The mechanical properties and strength of staple fibre spun yarns vary greatly because there are invariably fluctuations in the linear density, the twist and the composition along their length. The variation is particularly severe in the case of the strength because the breakage condition is determined by the "weakest link" in the specimen.

Numerous studies have been carried out on the effect of twist on the extension and strength of staple fibre yarns including cotton. Amongst the earlier workers were Balls (1928) and Oxley (1922). For example, Platt (1950) undertook a theoretical investigation of the influence of yarn twist on the modulus of elasticity. He concluded that the modulus decreases with increasing twist and that this decrease was related to

the stress distribution arising as a result of the yarn geometry. Gregory (1953) conducted a series of studies on cotton yarn structures. He found that the breaking length increased to a plateau and then decreased as yarn twist was increased. He also investigated the effect of the yarn structure on the maximum breaking length of different varieties of cotton.

Iyengar and Gupta (1974) have investigated the proportion of the cotton fibre strength "utilised" in a single yarn spun by different systems. They found that greater length and fineness increases the proportion of fibre strength utilised. Nachane and Iyer (1980) developed a theory to predict the strength of a bundle consisting of a large number of filaments if the average breaking load and the breaking elongation of the elements were known. They used data for cotton fibres to demonstrate the usefulness of their theory.

The rate of strain in a tensile test affects the yarn tenacity. Higher breaking loads are observed at higher rates of strain. Meredith (1950) studied the variation of cotton yarn strength with time to break and established the following empirical equation:

$$F_2 = 0.09\, F_1 \log_{10} \frac{t_2}{t_1} \qquad (3.20)$$

where F_2 and F_1 are yarn strengths and t_1 and t_2 are the corresponding times to rupture.

Balasubramanian and Salhotra (1985) studied the effect of strain rate on cotton yarn tenacity. They found yarn tenacity to increase to a maximum at about 0.005 m/s and then decrease slowly. This trend was found to hold regardless of the cotton type, the yarn type and the twist factor. They explained the trend by the fact that the main factors that contribute to yarn tenacity are the realignment of fibres which results in a higher contribution to the yarn breaking load and the percentage of fibre rupture. At

very high strain rates (0.017 m/s) there may not be sufficient time for the fibres to realign causing a drop in tenacity that could not be offset by an increase in tenacity due to a higher percentage of fibre rupture. At lower strain rates (0.003 m/s) the time for realignment is sufficient causing an increase in yarn tenacity.

3.4 Interface Phenomena

3.4.1 Introduction

In the previous section the tensile properties of yarns were discussed in terms of the constituent tensile characteristics of single filaments. The filaments are of course in contact with each other and hence substantial adhesive forces operate. These forces contribute to the cohesion of the yarn and indeed without these forces the yarn would probably disintegrate under gravitational forces. The migration will also naturally require the sliding of the filaments over one another and the basic constraint or lack of constraint will involve interfacial friction processes. Friction and adhesion are therefore major factors which control the structure of yarns (and indeed fabrics). Similarly, these processes will invariably affect the deformation properties of the yarns and fabrics constructed from these yarns.

There is *no* systematic work recorded in the literature on the influence of adhesion and friction between filaments on the mechanical properties or indeed the structure of yarns. One can see in principle how these phenomena would influence the mechanical, say extensile, properties by constraining filament migration during deformation. The earlier models (section 3.3) which considered tensile deformation without radial contraction may correspond to high friction cases whilst low friction would favour diametric reduction. Alternatively, the radial stresses may be modified to account for the frictional restraint on migration. However, the real problem is that the extremely complex structure of the yarn and the individual filament cannot be

described with any realism. Hence, the role of the friction at the contacts cannot be quantified with any confidence. It will be shown later in this thesis that lubrication of the filaments in the yarns significantly reduces the modulus of the yarn and hence the effect is real. Thus while the effects of lubrication cannot be precisely specified in a yarn or indeed in a fabric the overall trends may be rationalised as will be demonstrated in later chapters.

By way of introduction, therefore, a brief account of friction and lubrication is therefore appropriate and the remainder of this chapter deals with these processes, particularly in the context of fibres and yarns. The general features are introduced first. General descriptions are then given of the associated stick-slip phenomena, the differential friction effect (DFE), the laws of friction and some of the models that have been developed to quantify the phenomenon of friction.

3.4.2 Friction, Historical Note

If two bodies are placed in contact under a normal load, W, a finite force is required to initiate or maintain sliding: this is the force of friction. Although Leonardo de Vinci and Newton had indicated the nature of the "laws of friction", it was not until sometime later in 1699 that Amonton rediscovered the two forgotten laws of friction and it is his name they now bear. These laws are entirely empirical and although valid for most situations, exceptions exist. The first law was that friction is independent of the area of contact and the second was that friction force is directly proportional to the normal load. Amonton recognised that the surfaces he worked with were not smooth. He thought friction arose from the work done in lifting one surface over the roughness on the other or from bending the roughnesses down or breaking off the roughnesses. There is also a third law of friction, due to Coulomb, which is of much more limited validity than the first two laws and can be stated as either, that dynamic friction is

independent of sliding velocity (Halling, 1976), or that dynamic friction is about one-third of the normal load (Tabor, 1972).

Coulomb, in his classical studies on friction, also recognised that most of the surfaces he worked with were not smooth. He favoured a mechanism for the contact of two surfaces resembling the interlocking of asperities. He appreciated that natural adhesion between solids may also contribute to the frictional work, but rejected it as the main cause. He felt friction was due to the surface roughnesses and frictional work was done by the dissipation of potential energy against the applied load as the asperities were 'lifted' over each other. This mechanism as a means of energy dissipation was largely discounted by his successors, due to the absence of apparent nett vertical motion. However the picture drawn by Coulomb and his mechanism describe quite well the kind of process that may occur in fibre contacts.

3.4.3 Generally Accepted Mechanism of Friction at the Present Time

Friction is an energy dissipation mechanism and this dissipation is thought of as occurring through two separate mechanisms involving adhesion between surfaces and subsurface deformation. Bowden and Tabor (1964) have contributed immensely to our present understanding of frictional processes, especially those between metallic systems. They postulated that friction between unlubricated surfaces arises from two main factors: the adhesion and rupture of adhesive junctions and ploughing or deformation which occurred between the two bodies. The adhesion model of friction arises from the fact that all surfaces are rough at the microscopic level with undulating asperities of varying heights, Archard (1951). Figure 3.4 is a diagram of a rough solid in contact with a smooth rigid plane. When two clean bodies are brought together, the attraction component of surface forces produces adhesive junctions. As the normal load is increased, the proportion of asperities in contact, yielding the real

area of contact, will increase, and the asperities deform initially elastically and finally plastically. The real area of contact will then be directly proportional to the normal load W if the asperities are in incipient plastic flow.

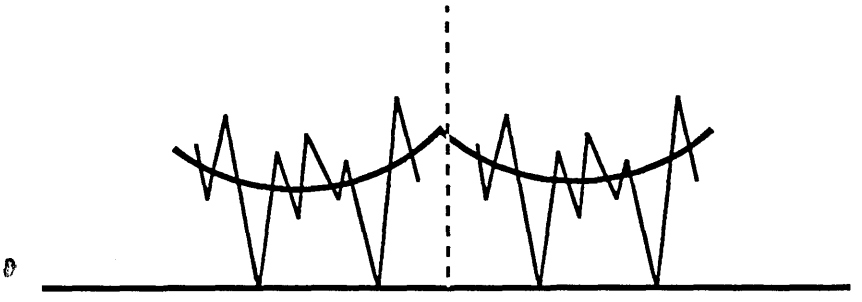

Figure 3.4 Contact between a rough solid and smooth rigid plane showing only a few asperities touching the surface.

The real area of contact A is then given approximately by:

$$A = \frac{W}{H} \qquad (3.21)$$

where H is the indentation hardness of the materials defined as load/surface area of contact. If the contacts deform in an elastic manner(see later), $A=KW^n$ where $1> n > 2/3$. If, for these contacts, the sliding friction is F, then it is common to write:

$$F = kW^n \qquad (3.22)$$

where k is termed the friction factor ($\mu(W)$) and n the load index. The values of n are generally found to be in the range 2/3 to 1. In order for sliding to occur, the junctions must be sheared. The amount of work done in shearing the junctions can be expressed by:

$$F = \tau A \qquad (3.23)$$

where τ is the interfacial shear strength, which generally depends on the contact

pressure (W/A) in the following way:

$$\tau = \tau_o + \alpha P_o \qquad (3.24)$$

where τ_o and α are material parameters. The quantity τ may be regarded as the work done per unit sliding distance per unit of real contact area A. It therefore describes the energy dissipation characteristics of the sliding contact. The calculation of A which was introduced earlier is rather problematic. For most solid bodies, the surfaces are sufficiently rough to ensure that the real area of contact is significantly less than the apparent values. It is therefore possible to distinguish from general cases which arise from permutations of elastic or plastic contact deformation on a rough or smooth substrate. If the pressure at the contacting asperities exceeds the elastic limit, plastic flow occurs in which case the contact area is proportional to a flow stress P_o as:

$$A = W/P_o \qquad (3.25)$$

However, for a smooth sphere on a smooth flat surface where the deformation is elastic, the contact area can be obtained from the Hertz solution. Thus:

$$A = \pi(E'R)^{\frac{2}{3}} W^{\frac{2}{3}} \quad (3.26) : E' = \frac{3}{4}[1-\upsilon_1^2)/E_1 + (1-\upsilon_2^2)/E_2]$$

where R is the radius of the sphere and E and υ are the Young's modulus and Poisson's ratio respectively for substrates 1 and 2.

By the combination of Equations (3.3) to (3.26) inclusive, we get:

$$F = \tau_o \pi (E' R)^{\frac{2}{3}} W^{\frac{2}{3}} + \alpha W \qquad (3.27)$$

which may be written in the form:

$$F = cW^{\frac{2}{3}}(1+aW^{\frac{1}{3}}) \quad (3.28) : a = \alpha/c : c = \tau_o \pi (E'R)^{\frac{2}{3}}$$

Dividing Equation (3.28) by the normal load gives the coefficient of friction as:

$$\mu = cW^{\frac{-1}{3}} + \alpha \qquad (3.29)$$

Alternatively $\mu = \tau / P + \alpha$ and if $P=P_0$ then $\mu = \tau_0 / P_0 + \alpha$. The latter equation follows the classical law that μ is not a function of load.

The above analysis deals mainly with the adhesion component of friction through real areas of contact. Equation (3.29) will be used in subsequent chapters to model some of the phenomena observed.

For contacting bodies with different hardness, description of the sliding friction force requires the inclusion of an additional term to account for the asperities of the harder material ploughing through the softer material. This is called the ploughing component of friction, denoted as P and involves a significantly larger volume of material during sliding than the adhesion induced dissipation processes. In the simple two term model, where there is negligible interaction between these two processes, we may add them as:

$$F = \tau A + P \qquad (3.30)$$

The ploughing component of friction is usually dominant in rolling contacts and sliding friction where there is efficient lubrication. If adhesion between the two surfaces is negligible, then the ploughing force may be easily calculated. These forces can arise from plastic flow and/or elastic or viscoelastic displacement. As the hard indentor traverses the surface of the softer substrate, energy is fed into the substrate ahead of the indentor and some of it is restored to the rear of the indentor because of

elastic recovery and urges it forward, Figure 3.5. The available analyses consider the work done on the system per unit distance traversed. Many studies of this process have been reported by workers such as Bowden and Tabor (1950), Briscoe (1981) and Dowson (1979). If the elastic work done on the contact per unit length is ϕ, the energy dissipated will be some fraction of this, i.e. $F_d = b\phi$. Using a contact mechanical approach for a sphere of radius R on an elastic body, Greenwood and Tabor (1958) arrived at the expression:

$$\phi = 0.17\, W^{\frac{1}{3}} R^{-\frac{2}{3}} (1-\upsilon^2)^{\frac{1}{3}} E^{-\frac{1}{3}} \qquad (3.31)$$

This enables the grooving force F_d to be calculated. For the case of a conical indentor, a relationship can be obtained to calculate the deformation losses. It is found that, for this case, if the semi-apical angle is θ, then ϕ is written as:

$$\phi = \frac{W}{\pi} \cot \theta \qquad (3.32)$$

3.4.4 Friction of Fibres

3.4.4.1 General features of fibre friction

The models described in the last section have been developed to interpret the frictional behaviour of gross contacts. This section will consider the special characteristics of fibres which arise from their particular geometric and surface features. A major consideration in studying friction of fibrous systems is their obvious importance in the textile industry. Here we shall review briefly the theory and

experimental methods and major trends of the results obtained in previous studies. As discussed earlier, there appears to be three mechanisms responsible for fibre friction; surface roughness, adhesion and ploughing. The surface roughness results primarily from asperities, surface cracking, convolutions and crimp and the important point is that the scale of these roughnesses is often comparable with the fibre dimensions.

The available experimental literature on single fibre friction, as classified by Tabor *et al* (1959) falls into two categories. The 'point contact' methods such as one fibre rubbing over another fibre at right angles or one fibre rubbing against a sharp slider such as a razor blade and the 'extended line contact' method, where a length of fibre is always in contact with either another fibre or fibres, or a cylindrical surface of a bulk material. One example of the extended line contact method is the early work of Morrow (1931) where he measured the frictional properties of cotton and rayon staple fibres by withdrawing a tuft of fibres from between two fibre pads of the same material. He lists values for the coefficients of friction for raw dry cotton around 0.25. Mercer and Makinson (1947) used crossed cotton fibres to determine the coefficient of friction. They used Amonton's law, i.e. $\mu = F/W$ to calculate their coefficients. They obtained a coefficient of 0.29 between cotton fibres taken from sewing thread and 0.57 between raw cotton fibres. The value for the coefficient of friction of aramid 1 yarn is reported to be 0.46 (Kevlar 49 data manual).

It is well accepted that the coefficient of friction drops with increasing normal load and this has raised questions regarding the accuracy of Amonton's law when applied to fibres. The most successful fitting relationship has been:

$$F = kW^n \qquad (3.33)$$

where $\frac{2}{3} < n < 1$.

The magnitude of n, is determined by the degree of elasticity or plasticity of the contact and the microscopic features of the contact geometry (see earlier).

If we combine Equations (3.23) and (3.25) from Section 3.4.2., the Amonton's law is given by:

$$F = \left(\frac{\tau_o}{P_o}\right) \qquad (3.34)$$

It can be seen that Amonton's law is a special case of the more general Equation (3.22 or 3.33) holding when $n = 1$ and $K = \tau_o / P_o$ = constant.

The coefficient K is generally negatively correlated with n and both are dependent on the molecular cohesion of the fibrous material as well as possibly on the mechanical properties of the material and the nature of the deformation.

There are various mathematical relationships between F and W that have been proposed. Olofsson (1950) offered the equation:

$$F = \mu_o W + \alpha' A \qquad (3.35)$$

where A = area of contact and α' = constant as a means of fitting a number of experimental results on fibre friction.

Gralen (1952) devised a method for measuring fibre friction in which he measured the friction in a twist of two fibres. His method was valuable for solving two experimental problems, (1) how to hold the fibres so that they can be rubbed together parallel to their axes, and (2) how to vary the area of apparent contact between them without changing the total load. He proposed the equation:

$$F = a'W + bW^c \qquad (3.36)$$

where $0 < a' < 1$ to fit his experimental data.

Many sliding systems show irregular motion and this behaviour has been termed 'stick-slip' (this is discussed in detail later). Belser & Taylor (1969) using the stick-slip process, studied the frictional properties of cotton fibres. They determined the static coefficient of friction by using the ten highest peaks from an analog plot and the kinetic coefficient by averaging the data plot over a selected length.

It was found that increases in temperature, in the case of cotton, results in only a slight increase in the coefficient of friction. Increasing the traversing velocity markedly increased the static friction but did not affect kinetic friction significantly. The coefficients of friction were highly sensitive to relative humidity, especially above 60%. The ratio μ_s/μ_k, however, remained reasonably constant. The next section discusses the stick-slip motion in more detail.

Intrinsic fibre characteristics also influence friction measurements. For example, the linear density and coefficient of friction are positively correlated. Pascoe & Tabor (1955), using crossed nylon cylinders, obtained the following relation:

$$\mu = c_1 s\, W^{-0.26} D^{0.52} \qquad (3.37)$$

where D= diameter of cylinder.

Basu *et al* (1978) studied the friction of cotton fibres using a device based on an earlier model, (Hepworth & Sikorski, 1976) which consisted of two brass cantilevers with a common axis, but oriented mutually at 90^o. They concluded that in the context of friction, four distinct features of cotton fibres must be considered, (a) the ribbon-like shape, with nearly elliptical transverse section, (b) convolutions, (c) the existence of folds on the surface of the fibres, and (d) the presence of reversals of fibullar texture on the fibre surface. They found a negative correlation between the coefficient of friction and the repeat distance between the convolutions.

Viswanathan (1973) has analysed the frictional interaction between fibre fringes,

with respect to raw cotton processing. He examined the friction of raw cotton, fibre blends, chemically treated fibres and friction during twisting. His measurements showed that the fibre characteristics of length, fineness and maturity have a decreasing influence on the frictional behaviour as the applied normal load increases. Also that interfibre friction increases significantly on wetting, bleaching or mercerisation. For a number of varieties of cotton, at 30g normal load, he obtained coefficients of friction ranging between 0.58-0.68.

The twisted fibres method of Gralen is an extended line contact method. Another method involves tension measurements over cylindrical surfaces (mainly capstans), Figure 3.6. When a fibre passes round a pulley, its tension must be increased by an amount to overcome the frictional resistance. Assuming the coefficient of friction is independent of load yields the classical capstan formula:

$$T = T_o e^{\mu\theta'} \qquad (3.38)$$

This experimental configuration has been used by many workers, and is considered to be a more rapid technique for evaluating frictional resistance than the point contact method, although it is generally agreed that Equation (3.38) is inadequate. A more complex equation was derived by Howell (1954):

$$T = T_o e^{\alpha\theta'(R/T_o)^{1-n}} \qquad (3.39)$$

He used the above equation in his study of the friction of nylon fibres against perspex and glass cylinders and the effect of radius of cylinder, R, Figure 3.6

Koza (1975) has studied the yarn to yarn friction of polyester, nylon and nylon 6.6 yarns removed from plain weave fabrics using a modified Instron tensile tester. He concluded that the frictional properties of polymer fibres vary with their elastic or plastic deformation properties.

Figure 3.5 Schematic diagram of deformation friction due to viscoelastic hysteresis losses within the bulk of the specimen either during rolling or well lubricated sliding.

Figure 3.6 A force diagram for the capstan theory of friction.

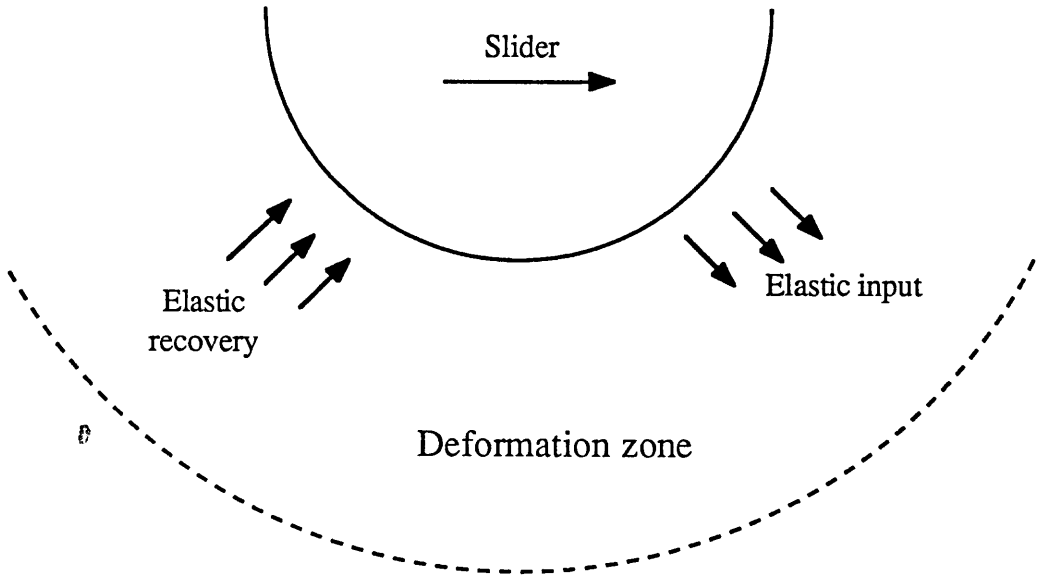
Slider
Elastic
recovery
Elastic input
Deformation zone

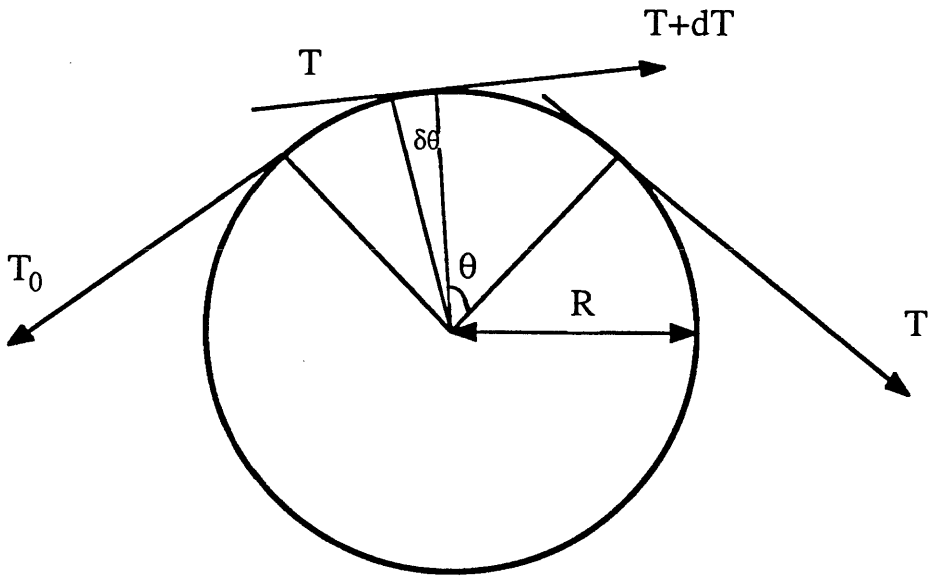
T+dT
T
δθ
θ
R
T_0
T

Galuszynski and Ellis (1983) and Galuszynski (1984) investigated the effect of yarn tension, contact angle, speed and linear density on the friction of yarns. Galuszynski (1984) studied these effects on wool, cotton, polyester and blended yarns. He found that increasing the yarn tension and contact angle increases the friction. An increase in yarn speed produced some fluctuations in the values of frictional force indicating that there are some changes from boundary to semi-boundary regions and *vice versa.*

3.4.4.2 Discontinuous motion

Stick-slip is the most pronounced form of discontinuous motion. It arises because the contacts between monofilaments appear to dissipate their frictional work in discrete packages which are separated by relatively long periods of time or imposed relative displacement. The dissipation process (the slip phase) occurs due to the generation of some threshold stress, after which the system relaxes. The stress is restored during the stick phase. The characteristic of these systems is that at low sliding velocities, the relative velocity between contacting surfaces is almost zero in the stick phase, and all the relative motion occurs in the very brief slip phase period. At higher imposed sliding velocities the velocity of the contact may fluctuate, but remains finite. Figure 3.7 depicts the effect of sliding velocity. It can be observed that the amplitude of the oscillation at low sliding velocities is greater than that at higher velocities.

The general requirement for the generation of stick-slip motion is that the static friction must exceed the dynamic friction. Bowden and Tabor (1964) have given a simple dynamic analysis of the stick-slip phenomenon where they assumed:
(a) the oscillation is free, i.e. no damping and (b) the dynamic frictional force is independent of the sliding velocity. Briscoe *et al* (1985) studied the friction generated

during intermittent sliding of polyethyleneterephthalate (PET) monofilaments. Winkler (1983) studied the stick phase of the stick-slip phenomenon at low sliding velocities using PET, glass and human hair monofilaments.

3.4.4.3 The Differential Friction Effect (DFE)

The friction generated by sliding synthetic fibres against one another is independent of the direction of sliding. However, the frictional characteristic of certain natural fibres such as wool and human hair depends on the direction in which it is pulled. In wool, the friction is greater if the fibre rubs against another surface in the direction from root to tip than when the direction is reversed. This anomalous behaviour is known as the differential friction effect (DFE). The occurrence of DFE has almost invariably been ascribed to the geometric form of the scales on the surface of wool or human hair. The simplest geometric theory is that the fibre acts as a ratchet, Figure 3.8, with the scales interlocking with one another or catching against asperities on another surface. Motion against the scales would be strongly resisted since it would involve rupture or deformation of the scales.

Seshan (1978) studied the frictional behaviour of root-tip aligned cotton fibre fringes under varying amounts of normal load. He observed that the coefficient of friction between the root points was higher than that between the tip points and called this the differential friction of cotton. He concluded that the surface area per unit length of the fibre increases gently from the root to the middle and decreases rapidly towards the tip of the fibres. He also found the convolution angle and absorptive capacity of the fibres to decrease from the root to the tip.

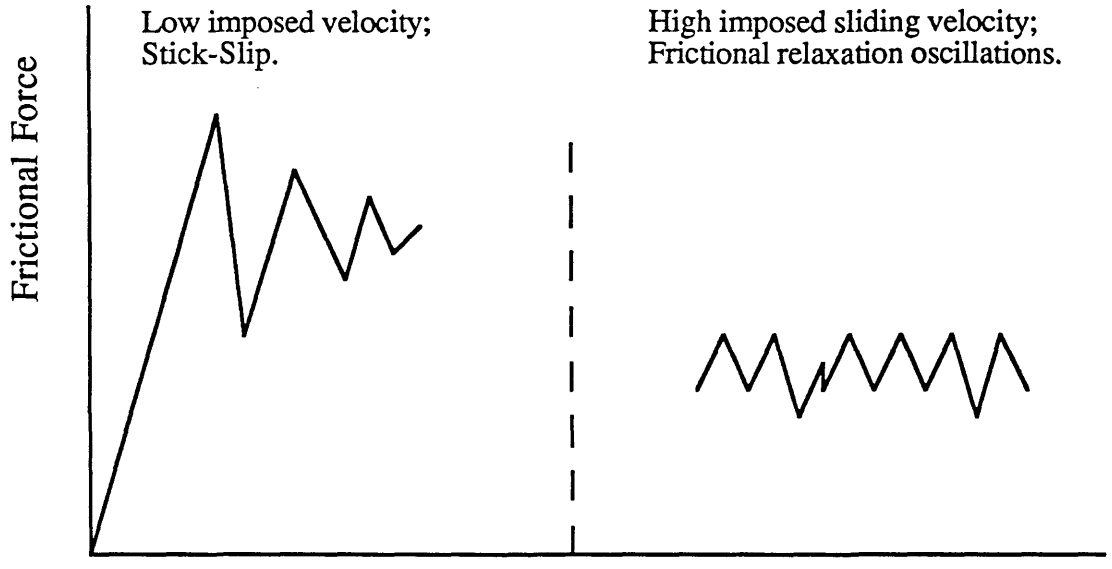

Figure 3.7 Schematic representation of the stick-slip phenomenon showing the effect of imposed sliding velocity.

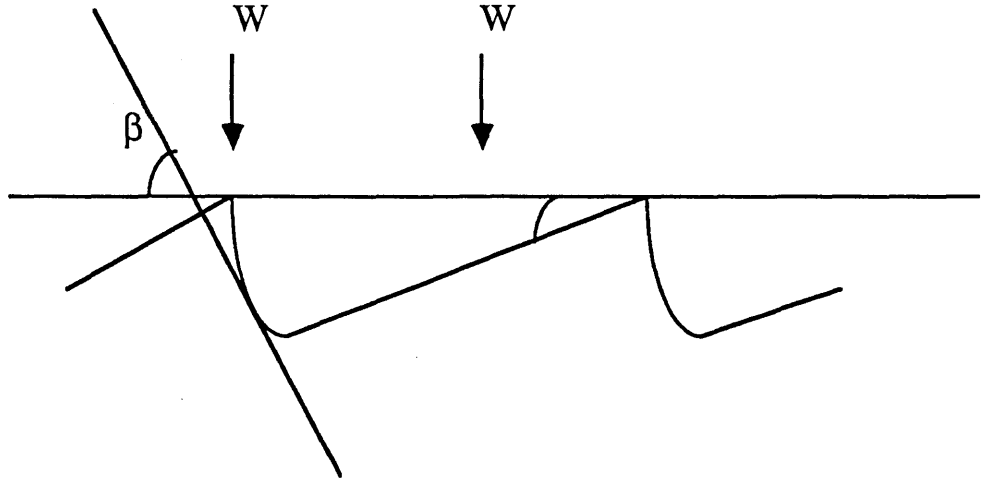

Figure **3.8** Schematic diagram of the geometric theory of the differential friction effect. The scales on the fibre interlock or catch against asperities on another surface.

3.4.4.4 Auto Adhesion and Contact Geometry of Fibres

Fibres possess surface geometric irregularities where size is comparable with their radii. This has two consequences in the context of friction modelling which are briefly reviewed. In many cases it appears the the contact area generated at the contact between two fibres may comprise of one, or only a few, asperity contacts. This condition, if it truely exists, greatly facilitates the modelling of the contact area (section 3.4.3). Briscoe *et al* (1982) have adopted this argument and their supposition that a point contact may occur between monofilaments is consistent with their experimental data. Their study also showed that the auto adhesion between fibres could produce a comparatively large normal force which could in some circumstances be comparable in magnitude to the applied loads. Thus some questions then arose as to whether the applied normal load should be used in say the adhesion model of friction. In their analysis they considered it sufficient to add the adhesive force to the normal applied load. These adhesive loads will be of consequence in fibre migration processes but probably not significant when large forces are introduced into yarns and fabrics.

3.4.4.5. Summary

The general models of friction, namely the adhesion model, the point contact and the extended line contact models are found to be applicable to friction in fibres and yarns. A knowledge of the force and normal load enables the calculation of the coefficient of friction μ and the load index n, representing the type of contact. On the whole the magnitude of μ for the yarn on yarn friction of cotton has been found to lie between 0.5-0.7 and for aramid fibre 1 to be 0.46 (Kevlar 49 data manual, E.I.duPont Co.). In the proceeding chapters the observations and results of friction experiments will be explained in the light of the information presented here. The mathematical treatments described here will be used to model some of the data obtained.

3.4.5 Lubrication

The term lubrication describes processes which reduce the friction and the wear generated at the interfaces between contacting bodies in relative motion. A lubricant is a mechanically weak material which is interposed at the interface between two stronger bodies. The purpose of this layer is to prevent extensive solid-solid contact and to form a weak interface layer in which all the relative motion is accommodated. According to Cameron (1971) and Tabor (1972) there are three basic forms of lubrication: (a) Hydrodynamic lubrication which was first studied by Osborne Reynolds in 1886. Hydrodynamic lubrication occurs under suitable conditions of the geometry of the contact, the entry conditions for the fluid, imposed normal load, the relative velocity and the viscosity of the fluid. The sliding surfaces can operate with a continuous film of lubricant between them. Hydrodynamic lubrication may be considered to be fully effective if it produces a separation of the two bodies in excess of typical asperity dimensions. Figure 3.9 illustrates the variation of the coefficient of friction with the dimensionless parameter $\eta v/p$ where η is the lubricant viscosity, v is the yarn speed and p is the nominal pressure, i.e. normal load/apparent area of contact. In hydrodynamic lubrication the overall pressures are low and the lubricant behaves as a Newtonian fluid.

(b) Elasto-hydrodynamic lubrication was introduced into the theory of lubricants about 30 years ago, Dowson (1979). It was recognised then that with real solids, as distinct from the ideal rigid solids assumed in classical hydrodynamic lubrication, appreciable elastic deformation of the surfaces or of the surface asperities could occur in the contact region. The behaviour is then determined by the flow of liquid between the elastically deformed geometry of the surfaces. The high contact pressures produce an enormous increase in the effective viscosity of the lubricant and convert it into a non-Newtonian fluid.

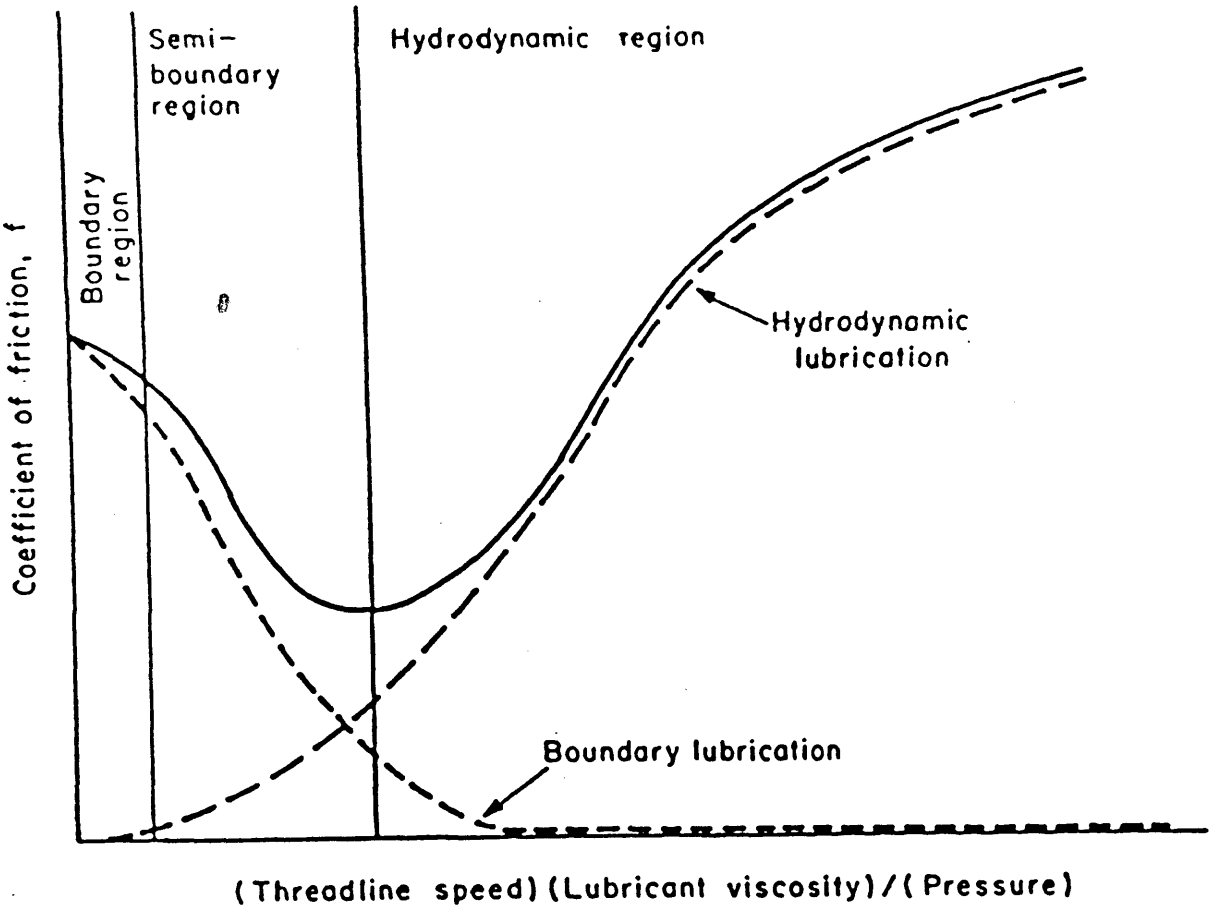

Figure 3.9 General behaviour of liquid-lubricated textile yarns showing the three regimes of lubrication and the regions at which they become operative.

(c) There are ambiguities in the definition of the regime of boundary lubrication. Sir William Hardy (1936) coined the phrase to describe what is considered to be lubrication by a mono-molecular layer. Boundary lubrication is provided by weak solid layers whose thickness is perhaps 100nm or less. The lubricant initially in the solid form responds to contact pressure in a manner resembling an elasto-hydrodynamic film.

An early study by Roder (1953) showed that the coefficient of friction increased with speed and interpreted this as being caused by a breakdown of the lubricant film and an increase in the amount of fibre-fibre contact. Lyne (1955), working with yarns, made similar observations and suggested that the friction may arise as a result of hydrodynamic lubrication. Hansen and Tabor (1957) followed up this suggestion and showed that the behaviour of a fibre passing over a cylindrical guide could be considered analogous to that of a journal bearing. For the case of monofilaments, the behaviour was not markedly dependent on lubricant viscosity, but when yarns were used, hydrodynamic factors were found to dominate. The frictional behaviour of liquid-lubricated yarns can thus be represented by a graph of the same form as in Figure 3.9.

Tabor (1959) stated that with yarns, the viscous factors are of great importance and that under hydrodynamic conditions the wetting angles of the yarn by the lubricant play some part. He pointed out that over a wide range of experimental conditions, the behaviour is dominated by hydrodynamic factors.

Olsen (1969) investigated the frictional properties of yarns under hydrodynamic and elasto-hydrodynamic conditions. He noted that where stick-slip behaviour was present, an increase in yarn speed produced a transition point where this behaviour disappeared. This point reflected the change from elasto-hydrodynamic to hydrodynamic lubrication.

Schick (1975), in a review of the friction and lubrication of synthetic fibres,

points to the same conclusions as Tabor. From lubrication studies on nylon 6.6, he concludes that lower friction reflects smaller contact angles and better wetting of the yarn.

Fort and Olsen (1961) studied the boundary friction of textile yarns. They found that stearic acid and n-octadecylamine reduced the boundary friction compared to that of the clean fibres. Hayes (1972) dealt with the subject of fibre and yarn lubrication from a textile processing viewpoint. He reviewed different types of yarns, suitable lubricants and the frictional effects produced.

In later chapters, the lubrication models described will be used to explain some of the experimental results. It will be proposed that the mechanical properties of yarns are influenced extensively by the filament friction behaviour and thus any modifications to the frictional behaviour modifies the yarn mechanics. Similarly interyarn friction influences the mechanical properties of fabrics.

CHAPTER FOUR

A REVIEW OF SOME PROPERTIES OF FABRICS

4.1 Introduction

This chapter is a review of some of the properties of fabrics that are relevant to the current work. It begins by outlining the basic features of the microgeometry of plain woven fabrics and presents equations that define this geometry. The major published studies of the tensile behaviour of woven fabrics, extended along the warp or weft directions but not at intermediate angles, will be reviewed. Empirical relationships derived by several investigators for the calculation of the fabric Poisson's ratio and tensile modulus in terms of structural parameters, such as crimp ratio and thread spacing, are presented. The bending behaviour of fabrics and the major published studies on this subject will also be reviewed. It should be pointed out that most of the studies on the above properties are rather dated and recent work on these subjects is surprisingly scarce and hence, much of the referenced material cited is over thirty years old. The material is no worse for its age but this situation reflects the level of interest in fabric mechanics in recent times.

The next section introduces the subject of the chemical modification of fabrics. It will discuss the effects of "surface" as against "bulk" modifiers with particular attention to cationic surface active agents. The problem of interrelationship between subjective and objective "hand" assessments will be introduced. A short description of the transverse ballistic behaviour of fabrics is included at the end of this chapter.

4.2 The Geometrical Properties of Woven Fabrics

4.2.1 A Model for The Woven Fabric Structure

This section is mainly concerned with the descriptive curvilinear shape of the yarn in the warp or weft normal cross-section of the fabric and the relationship between various structural or geometric parameters. In principle, a knowledge of this shape and it's development in chosen strain fields enables the calculation of the fabric mechanical deformations such as extension, bending or shear in terms of the intrinsic mechanical and surface properties of the fibres. The most elaborate early work was carried out by Pierce (1937). He showed that if one assumes the yarns to be circular in diametric section and that they possess negligible bending resistance, then a first order geometrical model of this type may be generated. Figure 4.1 shows Pierce's model of a simple plain weave. The basic geometric parameters consist of two values of yarn length l_i, two crimp heights h_i, two thread spacings p_i, and the sum of the diameter of the two yarns D. The suffixes 1 and 2 refer to the warp and weft yarns respectively. A knowledge of the form of these parameters allows the other three to be calculated. However, Pierce's analysis also uses additional parameters in the analysis such as c, the crimp ratio and θ, the weave angle, so that there are nine unknowns and actually five equations; 4.1 to 4.5 inclusive. The main equations are however 4.1 to 4.3 inclusive:

$$p = (l\text{-}D\theta)\cos\theta + D\sin\theta \qquad (4.1)$$

$$h = (l\text{-}D\theta)\sin\theta + D(1\text{-}\cos\theta) \qquad (4.2)$$

$$D = h_1 + h_2 \qquad (4.3)$$

The difficulties involved in solving these three simultaneous equations necessitated the

use of two approximate relationships, equations 4.4 and 4.5:

$$\frac{h}{p} = \frac{4}{3}\left(\frac{1}{p} - 1\right)^{\frac{1}{2}} \equiv \frac{4}{3}\sqrt{c} \qquad (4.4)$$

$$\theta = 106\sqrt{c} \qquad (4.5)$$

A basic difficulty in using Pierce's approach is the fact that the yarn cross-section, particularly during deformation, is often far from circular. Many attempts have been made to correct Pierce's original relationships by assuming various shapes for the yarn cross-section, such as elliptical and "race-track" shapes, Figure 4.2. Olofsson (1964) proposed that the yarn takes up the shape of an elastica. This assumes that the original yarn cross-section is so easily distorted that it can be ignored in determining the deformed shape. This approach gives similar values for some of the geometric parameters when they are compared with those obtained by Pierce. The Olofsson model actually gives a much closer fit for the value of the observed weave angle, θ. Nevertheless, the approximate relationships, Equations 4.4 and 4.5 (after Pierce) may still be used with considerable confidence. More recently, Leaf and Anandjiwala (1985) have used a more realistic approximation of yarn bending behaviour to develop a generalised model of plain woven fabrics. They proposed the following approximate formulae for calculating h/p and θ:-

$$\frac{h_1}{p_2} \approx 1.341\, c_1^{\frac{1}{2}} \qquad (4.6)$$

$$\theta_1 \approx 91.44\, c_1^{0.446} \qquad (4.7)$$

For more complex weaves, the race track (see Figure 4.2) or other simple geometries have been extended, using the principle of adding certain straight lengths to the plain geometry to allow for the "float". Figure 4.2 is the shape of a standard race track to which has been added the straight portion z. In this way, the problems of non-plain fabric geometry may be converted into plain fabric geometry.

4.2.2. Summary

The simple model originated by Pierce contains most of the essential geometric features of the simple microscopic weave structure. Its limitations have been explored and corrections suggested at the expense of more parameters, in particular those associated with non circular and stiff fibre bundles. Almost all of the published analysis of the tensile, bending, etc. behaviour of plain woven fabric uses Pierce's geometrical model as the microscopic weave structure. Some of these analyses and the subsequent results are presented in the later sections of this chapter.

4.3 Woven Fabric Tensile Mechanics

The tensile properties of woven fabrics, together with other mechanical properties, such as their behaviour in bending and shear, are of considerable importance in determining how the fabric will perform in use. It will be seen in chapter six that the tensile and to some extent the bending properties of fabrics play a substantial role in the deformation characteristics of the fabrics under study in this thesis. According to Grosberg (Hearle, Grosberg & Backer, 1969) the load-extension curve of a typical fabric shows three distinct sections, Figure 4.3. The initial high

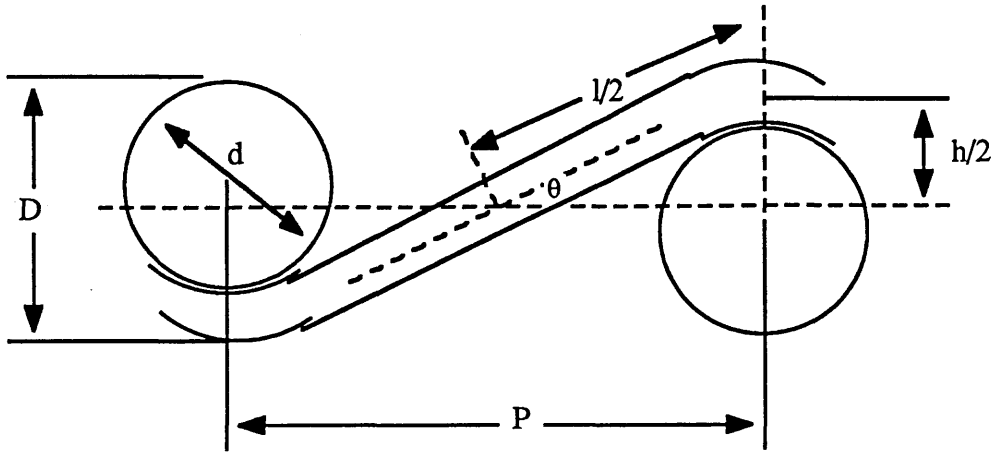

Figure 4.1 Schematic diagram of Pierce's model of a simple plain weave.

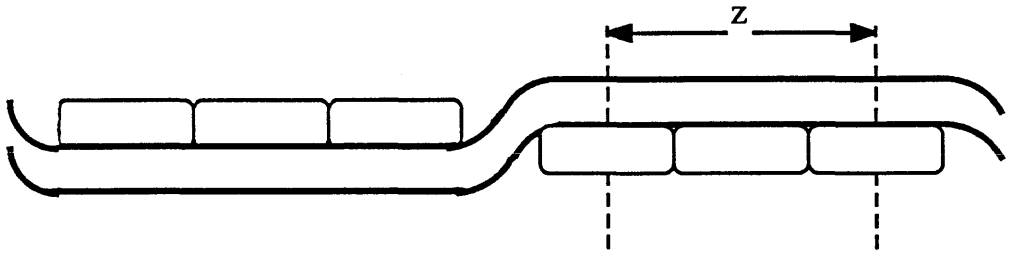

Figure 4.2 An alternative "race-track" shape for the yarn cross section. Here the race-track geometry has been extended by the straight portion z. In this way the problem of non-plain fabric geometry can be converted into plain fabric geometry.

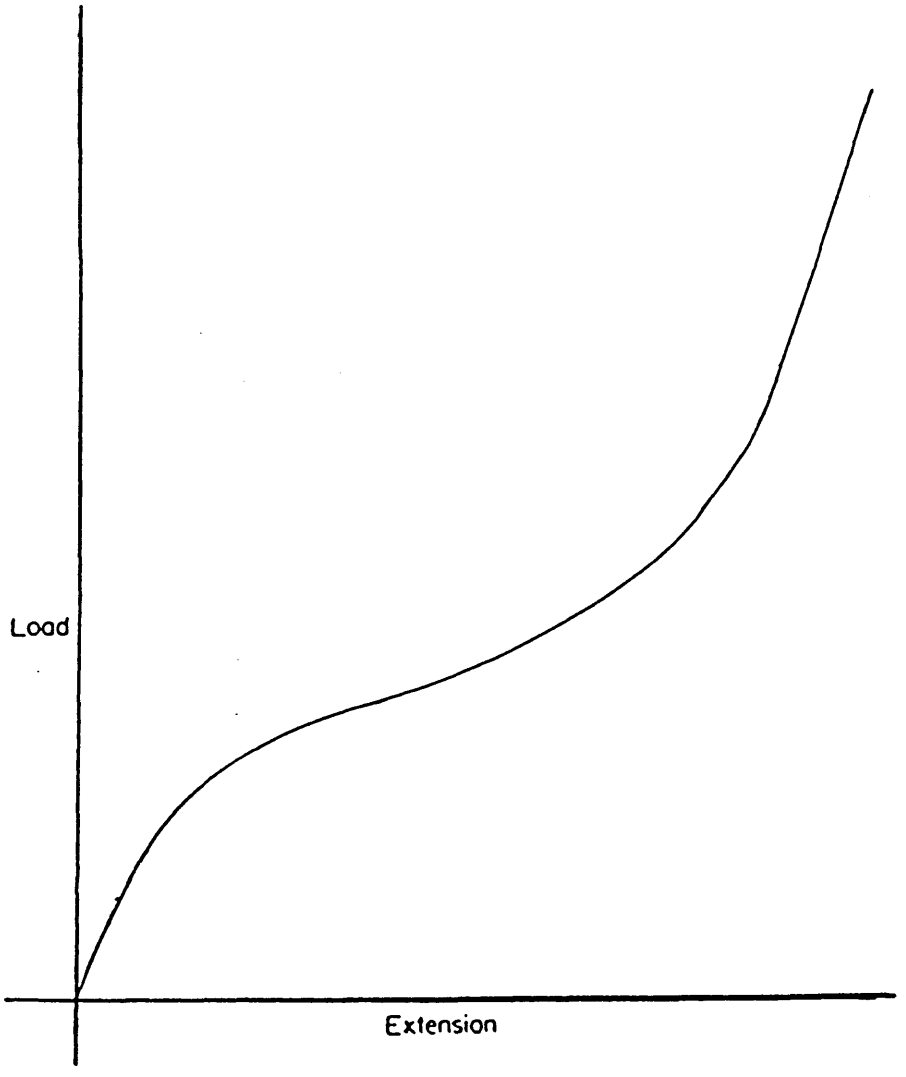

Figure 4.3 The load extension curve for a fabric showing three distinct sections representing initial high modulus, a relatively lower modulus and ultimately a rise in modulus.

modulus is probably due to a frictional resistance involved in the bending of the threads or fibres. The second region of relatively low modulus is mainly governed by the force *needed* to unbend the yarns in the direction of the force and bend those at right angles to the direction of the force. As the crimp is decreased, the fibres themselves begin to be extended, hence the ultimate rise in modulus. In the final region the load-extension properties of the fabric is almost totally governed by the load-extension properties of the yarns themselves. The above observations by Grosberg and also the information presented in this section on the tensile behaviour of woven fabrics only deal with extension along the warp or weft directions and not at any other intermediate angles which constitutes a shear of the fabric.

There are certain gross geometric changes that accompany the extension of fabrics. Under the restricted condition that the compression of the yarns and their extension are negligible the principles given in Section 4.2 may be applied. It is then possible to calculate the Poisson's ratio of the cloth. The basic relationships are given in Equations 4.4 and 4.8.

$$l = (1+c)p \qquad (4.8)$$

Assuming l, h_1 and h_2 are constants we have:

$$0 = d(h_1+h_2) = \frac{4}{3}\sqrt{c_1}\, dp_1 + \frac{2}{3}\frac{p_1}{\sqrt{c_1}} dc_1 + \frac{4}{3}\sqrt{c_2}\, dp_2 + \frac{2}{3}\frac{p_2}{\sqrt{c_2}} dc_2 \qquad (4.9)$$

since

$$dc = -\,(1+c)\frac{dp}{p} \qquad (4.10)$$

$$\frac{dp_2}{dp_1} = \frac{1 - c_1\sqrt{c_2}}{1 - c_2\sqrt{c_1}} \qquad (4.11)$$

This gives the Poisson's ratio of the fabric. If F_1 and F_2 and n_1 and n_2 are loads and number of yarns in the warp and weft directions respectively, then we have:

$$F_1 n_2 dp_1 = -F_2 n_1 dp_2 \qquad (4.12)$$

Since the extensions in the warp and weft directions are $n_2 dp_1$ and $n_1 dp_2$ we have:

$$\frac{f_1}{f_2} = \frac{(1 - c_1)}{(1 - c_2)} \frac{\sqrt{c_2}}{\sqrt{c_1}} \approx \frac{\tan\theta_2}{\tan\theta_1} \qquad (4.13)$$

where $f_i = \frac{F_i}{n_i}$

Assuming $\frac{f_1}{f_2} \approx \frac{\sqrt{c_2}}{\sqrt{c_1}}$ (4.14)

the modulus for the increase in f_1 at constant f_2 is:

$$(df_1)_{f_2 const} = f_2 \left[\frac{1}{2}(c_1 c_2)^{\frac{-1}{2}} dc_2 - \frac{1}{2}(c_1^{\frac{1}{2}} - c_1^{-\frac{2}{3}})\, dc_1\right] \qquad (4.15)$$

Defining the modulus as:

$$\text{modulus} = \frac{p_1}{p_2} \cdot \left(\frac{df_1}{dp_1}\right) \qquad (4.16)$$

gives:

$$\text{modulus} = \frac{f_2}{2c_1p_2}\left[(1+c_2)\left(\frac{p_1}{p_2}\right) + (1+c_1)\left(\frac{c_2}{c_1}\right)^{\frac{1}{2}}\right] \qquad (4.17)$$

This equation expresses the modulus of the fabric in terms of the load, the crimp ratio, and the thread spacings in the warp and weft yarns. Equations such as these can be obtained for other cases where the extensions and/or bending behaviour of yarns are taken into account. They provide a value for the modulus of the fabric extended along the warp or weft directions. Applied extensions at any other angle involve a consideration of the shear behaviour of the fabric. Grosberg and Kedia (1966) showed that the initial load extension modulus of woven fabrics (first 1% extension) is dependent upon the bending modulus of the yarn, the geometry it takes up in the fabric and the fabric history. They predicted the initial modulus of grey relaxed and finished cotton fabrics from the bending rigidity of their constituent yarns and found good agreement between the theoretical and the experimental values.

Grosberg (1977) sensibly attributed the energy loss which occurs during the cyclic deformation of fabrics to two separate causes. The first is the non-Hookian behaviour of the fibres themselves resulting from viscoelasticity, plasticity and creep effects. The second cause of hysteresis is the frictional restraint to interfibre and interyarn movements in the fabric during deformation. He also points out that the addition of lubricants or softening agents reduces the interfacial frictional hysteresis losses. The effect is, however, relatively small compared with such stress-relaxation techniques as heat or chemical setting treatments.

Leaf (1979) analysed the tensile behaviour of woven fabrics using three different approaches. He used a simple method based on Castigliano's theorem to analyse small strains. For larger strains he used a force equilibrium and an energy

approach.

4.3.1 Summary

In this section, the geometric principles discussed in Section 4.2 were used to arrive at an expression for the tensile modulus of a woven fabric extended in the warp direction in terms of the crimp ratio of warp and weft yarns, the ratio of the thread spacings and the load on the weft yarns. The bending modulus of the yarns, the geometry and the history of the fabric are seen to affect the tensile character of the fabric. It was also reported that interfibre and interyarn frictional restraint may contribute to the energy losses which occur during the cyclic deformation of fabrics.

4.4 The Bending of Woven Fabrics

The bending properties of woven fabrics, compared to their tensile properties, play a minor role in the deformation characteristics of the systems that were studied here (see chapters six and eight). The observed non-linear bending behaviour of a fabric can be separated into two components. A non-linear component due to friction and a linear component due to the bending resistance of the fibres or yarns lying in the direction of bending. The fibres in a woven fabric pass through two distinct regions. One region is the cross-over location between warp and weft and the other is between adjacent cross-overs, Figure 4.4. The bending of the fabric and hence the yarn will normally imply that the fibres on the "outside" will be in tension while those on the "inside" will be under a relatively lower tension. When the difference in tension between adjacent fibres exceeds the frictional resistance produced at cross-over regions

the outer fibres will slip. When all the fibres have slipped, as a result of the limiting frictional forces at all the fibre intersections, couples will be set up.

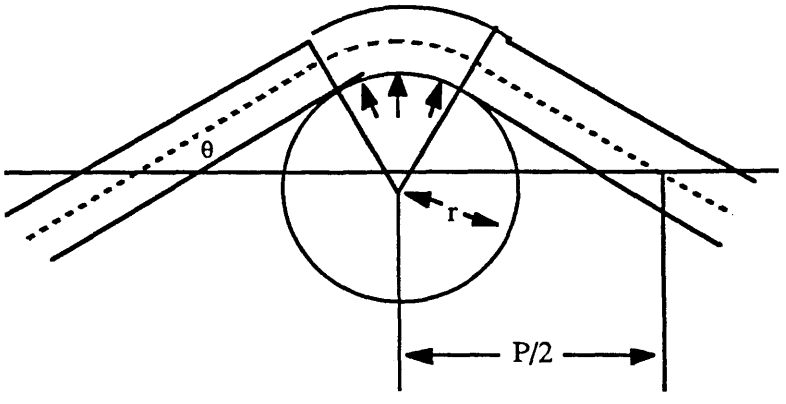

Figure 4.4 Schematic diagram of a cross-over point in a fabric showing the bent character of the yarn within the weave.

By considering the bending of a set of plates, Grosberg (1966) predicted the magnitude of these couples. He found the value of the bending resistance of the yarns to be greater than expected. Grosberg and Swani (1966) estimated the elastic bending rigidity and frictional restraint using the cantilever and the buckling tests on woven fabrics including cotton, worsted and blended worsted. They found good agreement between the values of the bending resistance represented by the flexural rigidity and frictional restraint represented by the coercive couple, produced from the two tests and concluded that the effect of frictional restraint cannot be ignored. Later, Abbott, Grosberg and Leaf (1971) refined Grosberg's theory and analysis on bending of fabrics and applied it to 75 plain weave fabrics including cottons, terylene and nylon constructed from yarns of different tex. Abbott *et al* (1972) analysed the elastic bending resistance of fabrics woven from circular and incompressible yarns.

However, their analysis did not compare favourably with the behaviour of normal fibres. They attributed this to the non-linear nature of the yarns.

Gibson and Postle (1978) studied the bending and shear properties of commercially-produced woven and knitted wool and wool-synthetic blended fabrics. They found that finishing has an enormous effect on the bending characteristics of fabrics. The influence of "finishing in this context is uncertain but fibre surface modification will undoubtedly modify the frictional characteristics.

4.5 Summary

The tensile and bending characteristics of woven fabrics were discussed in relation to the properties of the constituent yarns. The shear properties of the fabrics were not discussed because it is less relevant to this thesis. The available analyses of the shear behaviour are less well refined and not readily applicable to experimental data. The bending and extension of fabrics and yarns are not naturally exclusive since a significant proportion of these processes are controlled by interfibre and/or interyarn friction. The migration phenomenon and the way the yarn "holds together" is dependent upon interfibre friction. The energy losses both in tension and bending and represented by hysteresis effects are greatly affected by the friction. As will be seen in later chapters (chapters 6, 8 and 9) the observed tensile and bending behaviour of the fabrics under investigation will be discussed in terms of the inter fibre and inter yarn frictional processes.

4.6 Chemical Modification Processes

4.6.1 Introduction

In recent years, numerous fabric chemical treatments and finishing products such as softeners, lubricants, conditioners and crease resistant agents have been developed to provide specific functional properties. Improving the handle of fabrics remains one of the major requirements. Extensive efforts have been made to measure the handle of finished fabrics as perceived by the finisher or consumer. This research has established the fact that the "hand" of fabrics is influenced by or even correlatable to several physical and mechanical properties of the filaments, yarns and the fabric such as tensile properties, bending and shear properties, friction, compression, etc. It is the purpose of this section to discuss the relation between the "hand" of fabrics and the above properties and to consider how these properties are modified by the addition of the so-called softeners. The modifications of the "hand" of fabrics are brought about as a result of a complex interaction of surface and bulk effects. Both these effects will be discussed here in the context of fabric finishes. The modification of fabric "hand" is particularly relevant to the cotton fabrics while chemical modification processes with for example PDMS (poly dimethyl siloxane) will be seen to be important in the case of the aramid fabrics (chapters 7 and 10).

4.6.2 Chemical Finishing

Application of oils and fats for lubrication and softening of textiles began probably in prehistoric times and has continued until today. Advances in fat chemistry resulted in the use of fatty acids, fatty esters, sulphonated and sulphated fatty derivatives and, since the early thirties, cationic surface active agents have been used

extensively for this purpose.

Most chemical finishes are thought to mainly produce their effect by modifying the surface of the fibres. Such surface finishes may be called external finishes. When fabrics are treated with such agents as starches, resins or waxes, the peripheries of the fabric bond so well that the finish acts almost like an integral part of the fabric. Internal finishes also exist where the constituent molecules and perhaps small colloidal entities find their way into the internal structure of the filaments and may become affixed or cross-linked within the fibres. Even when chemical fixation does not occur, resins and metallic colloids can often be entrapped within the fibre walls. Speel and Schwartz (1957) have classified chemical finishes according to their location on or in a fibre as follows:-

1. Surface finishes
   (a) Softening agents
   (b) Film forming finishes
   (c) Corrective finishes
2. Internal finishes
   (a) Dimensional stabilisers
   (b) Crush inhibitors

Here we will only deal with softening agents. They not only improve the softness and handle of materials, but they also facilitate mechanical finishing. Mallinson (1974) defined softeners as "an auxiliary that when applied to textile materials, brings about an alteration in handle, resulting in the goods being more pleasing to the touch". However, softeners can perform other functions. They may contribute to the lubrication, abrasion resistance, antistatic properties and water absorbency of fabrics. The method of application of the softener can also greatly

affect softener efficiency. Modern fabric drying techniques have influenced the selection of softeners significantly. Valko *et al* (1966) studied the influence of the application conditions on the penetration, the ion-exchange and the oriented absorption. Hughes and Koch (1965) studied the adsorption and desorption of cationic softeners on cotton. Mallinson (1974) and Mooney (1980) classify softeners into the following categories:-

1. Cationics
   (a) Quaternary ammonium salts
   (b) Amino acids
   (c) Cyclic cationics
2. Anionics
   (a) Sulphates
   (b) Sulphonates
   (c) Sulpho-succinates
   (d) Sulphated fatty alcohols
3. Non-ionics
   (a) Ethoxylates
   (b) Esters
   (c) Polyethylene glycols
   (d) Silicones

The cationic surfactants dominate the field of commercial fabric softeners. Two of the most commonly used compounds in commercial formulations are:-

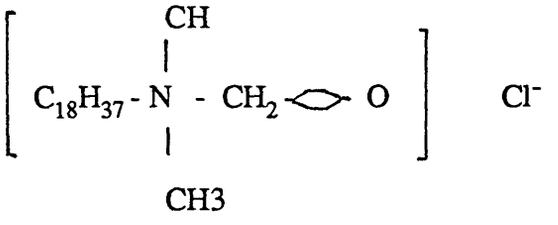

Octadecyldimethylbenzylammonium chloride

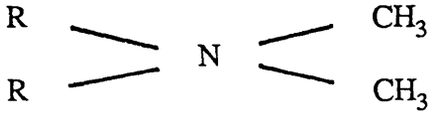

Dihardenedtallowdimethylammonium chloride

Evans (1969) has offered the following correlations between softening efficiency of cationics and their molecular structure:-

(a) softening depends markedly on the alkyl chain length with C16-C18 chains providing the best softening.

(b) two alkyl chains are preferred to one in a formulated finish.

(c) straight chain surfactants are better than branched ones.

(d) desaturation in the alkyl chain reduces the softening efficiency.

Many early workers have discussed the cause of the softness imparted to fabrics by softeners, including Sollenberger (1957) and DuBrow and Linfield (1957). The mechanism of softening appears to be largely a surface lubrication phenomenon. Although in the case of cellulosic fibres such as cotton, it is believed that, in addition to lubrication, there is a certain amount of plasticisation of the cellulose fibres by the softener molecules.

Since lubrication is believed to be the major cause of the imparted softness, only

those molecules which remain on the fibre surface are effective. In fact, the efficiency of a softener is therefore governed by its ability to be adsorbed and orientate in such a way as to project its long hydrophobic tail away from the cellulose substrate. This is the idea of classical lubrication. It is also considered to be important that the softener molecule is attached to the surface by strong chemical and physical bonds. The greater effectiveness of cationics in this respect is explained by their ability to interact chemically with cellulose by a cation exchange mechanism in addition to ion-pair adsorption. Sexsmith and White (1959) have studied the absorption of Cetyl trimethyl ammonium bromide (CTAB) by cotton fibres. They proposed that the absorption occurs by two major processes. Below the critical micelle concentration CMC (CMC for CTAB is 10^{-3}M) cation exchange is appreciable while in the vicinity of CMC, ion-pair absorption becomes important. Figure 4.5 reproduced from Sexsmith's paper shows the uptake of both cation and anion by a purified cotton at various equilibrium concentrations. The uptake increases with increasing ion concentration. The molarities of the CTAB solutions chosen in the current experiments fall both below and above the CMC of CTAB (see chapter 5). According to Sexsmith and White, the site of cation exchange is a carboxyl group. However, since pure cellulose does not possess any carboxyl groups, their presence in cellulose based fabrics indicates that textile processing and finishing treatments are responsible for their existence. This explains the difference in the level of softness imparted to nominally similar cellulose based textiles by the same cationic surfactant. The lubricating properties of CTAB were examined for the particular systems described in chapters six and nine, that is the "hardness" and the pull-out experiments.

The intrinsic lubricating property of commercial softeners is confirmed by the observations (Evans, 1969) that fabrics made of glass fibre are also softened by

cationic surfactants. However, unlike cotton, glass fibres are impervious to the softener molecules. Thus, the softening action here must involve a substantial amount of surface lubrication.

The second effect of cotton fabric softeners is believed to be their ability to induce filament plasticisation. Normally, plasticisers function by interposing themselves between the large polymer molecules and thus providing a greater freedom of motion which results in greater flexibility and a lower glass transition temperature. However, to be fully effective, the plasticiser has to be present in relatively large amounts, ca. 30% of weight of polymer. In the case of cotton, one can believe that the surfactant molecule (for C_{18} surfactant the nominal diameter is approx. 40 Å) applied from an aqueous solution may penetrate the pores of a fibre swollen with water (for a dry fibre pore size ≈ 5Å, for a swollen fibre pore size ≈ 20-100Å). The exact destination of the softener molecules is not known; however once inside they may lodge themselves between cellulose molecules or between the fibrils. Also, the amount of softener involved (nominally 0.1-0.2% weight of fabric) does not appear to be sufficient to provide substantial plasticisation. However, dynamic mechanical methods have yielded some evidence in favour of plasticisation. Pietikainen (1973) found that the logarithmic decrement, which is an indication of the internal friction, decreased for cotton treated with a cationic softener. Removal of the softener raised the loss value back to that of the untreated cotton.

Amongst the non-ionics, silicones are found to be good lubricants due to their low surface energy. These materials are now widely used in commercial softening packages either in an aqueous base or as neat fluids. In the current study solutions of PDMS are used for their lubricating properties (chapters 6, 7 and 9).

4.6.3. "Handle" as a Measurable Parameter

The definition of the term "handle" has been a subject for discussion for many years. Pierce (1930) described "hand" as being a judgment of the buyer which depends on time, place, season and personal preferences. In a series of technical investigations of textile finishing treatments, Schwarz (1939) defined fabric hand to be a property judged as a function of the feel of a material and states that sensations of stiffness or limpness, hardness or softeners, and roughness or smoothness constitute hand. He comments on the desirability of physical tests which would analyse and reflect the sensations felt and which would assign numerical values to these measurements.

The term handle has also been defined as "the subjective assessment of textile materials obtained from the sense of touch". Handle is thus a psychological phenomenon in that it is the ability of the fingers (or other parts of the human body) to make a sensitive and discriminating assessment, and of the mind to integrate and express the results in a single valued judgment. The psychology of handle has been reviewed extensively by Syed (1982).

In an attempt to relate the hand of a fabric to its physical properties, workers have defined hand in various ways. Elder (1978) has given references to lists of words which have been used to describe handle, and they run into hundreds.

Despite the confusion in the definition of handle, the need to quantify this sensation in terms of some measurable properties has always been recognised. The measurement of handle is carried out through two different approaches:

(a) Purely subjective approach

(b) Purely objective approach

(a) The concept of the purely subjective approach is that "hand" is genuinely a

subjective phenomenon evaluated by the hands of skilled finishers or consumers. There have been extensive studies on the subjective assessment of hand. Vaughn and Kim (1973) have summarised the techniques commonly used in early studies. These techniques can be put into two broad categories; the absolute method and the relative ranking method. These methods have been studied or used by various workers, including Binns (1934), Ginn *et al* (1965), Hoffman (1965), Lundgren (1969), Dawes and Owen (1971) and Kramer *et al* (1974).

(b) The purely objective approach to assess fabric handle is based on the idea that what ultimately contributes to differences in feel when handling fabrics originates from differences in the physical properties of the fabric. In this case, it is necessary to differentiate the physical parameters that influence hand from all other physical characteristics and to evaluate these "hand" physical parameters in numerical terms by instrumented measurements. In this context, four direct softness measuring machines have been patented by: Schwartz *et al* (1955), Plummer (1964), Flesher (1970) and Taylor (1972).

Pierce (1930) suggested that measurement of eight physical properties of fabrics related to their stiffness and friction would yield a direct evaluation of fabric hand. Skau *et al* (1958) and Honold and Grant (1961) studied the softness of cotton yarns by measuring the percent increase in yarn width when the yarn was subjected to lateral pressure between two parallel plane surfaces. Kakiage (1958), using a specially designed thickness gauge, expressed the hand of fabrics in terms of their compression and recovery under load. Dawes and Owen (1971) investigated the correlation between the results of the cloth-bending-hysteresis test, the shear hysteresis test and the cantilever stiffness test with subjective assessment of cloth stiffness and liveliness. They found the correlations to be highly significant.

Kim and Vaughn (1979) introduced a physical method to predict the hand of woven fabrics. Fourteen objectively measurable physical parameters were combined to calculate a hand value for a fabric in conjunction with a graph of logarithmic values of the hand parameters. Figure 4.6 is reproduced from Kim and Vaughn's paper. The objective hand parameters are:

G_o=Elastic flexural rigidity, C_o=Coercive couple, C=Single curvature bending rigidity, L_s=Multicurvature bending rigidity, ϕ=Drape coefficient, τ=Shearing stress, G_i=Initial shearing modulus, E_{xt}=Extensibility, E_i=Initial Young's modulus, R_t=Tensile recovery, T=Thickness, H=Hardness, R_c=Compressional recovery, and μ_k=Coefficient of kinetic friction

Elder *et al* (1981) investigated the relationship between the subjective assessment of the stiffness and the objective measurement of flexural rigidity and the subjective assessment of fabric "liveliness" and the objective measurement of coercive couple believed to represent the frictional characteristics of a fabric. They found strong linear relationships between them. More recently, Elder *at al* (1984) reported the results of subjective finger pressure assessment of fabric softness compared with objective measurements of compression. Good correlation was reported for a set of non-woven and a set of woven fabrics. They also reported on the relationship between touch, compressibility, weight, thickness, density and specific volume of these fabrics.

The most comprehensive and well known examination of the effect of basic mechanical properties of fabrics on fabric hand has been reported by Kawabata (1979, 1983). He uses the following objective hand judgement process:

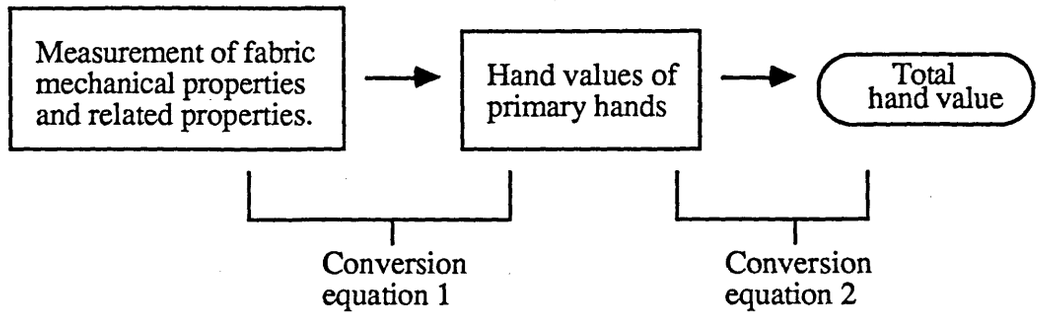

By using regression analysis and appropriate conversion equations, he has related the hand values of fabrics (actually only one fabric in a comprehensive way) based on the subjective sensations of stiffness (KOSHI), smoothness (NUMERI) and fullness and softness (FUKURAMI) to various mechanical properties of fabrics such as tensile, bending, shearing, compression, surface friction, weight and thickness.

4.6.4 Conclusion

Textile materials are invariably treated with certain chemicals during the finishing process to acquire the desired properties. Softeners and, in particular, cationic surfactants, are by far the most extensively used type of finishing treatment. They not only give a more pleasant feel to the fabrics but also ease their processing. Their effectiveness is thought to originate primarily from a lubricating process. They also affect other mechanical properties of fibres, yarns and fabrics. It had long been recognised that to correlate the objective measurement of the physical properties of fabrics to the subjective hand judgement would be a useful exercise. Much progress has been achieved in this objective, although there is still much work to be done.

Figure 4.5 Equilibrium absorption from CTAB solutions by purified cotton at room temperature. Reproduced from Sexsmith & White (1959).

Figure 4.6 Kim and Vaughn's (1979) graphical representation of fabric hand; fabric C, 50/50 polyester/cotton batsice; fabric Q, 50/50 polyester/cotton denim; fabric S, 50/50 polyester / cotton gabardine.

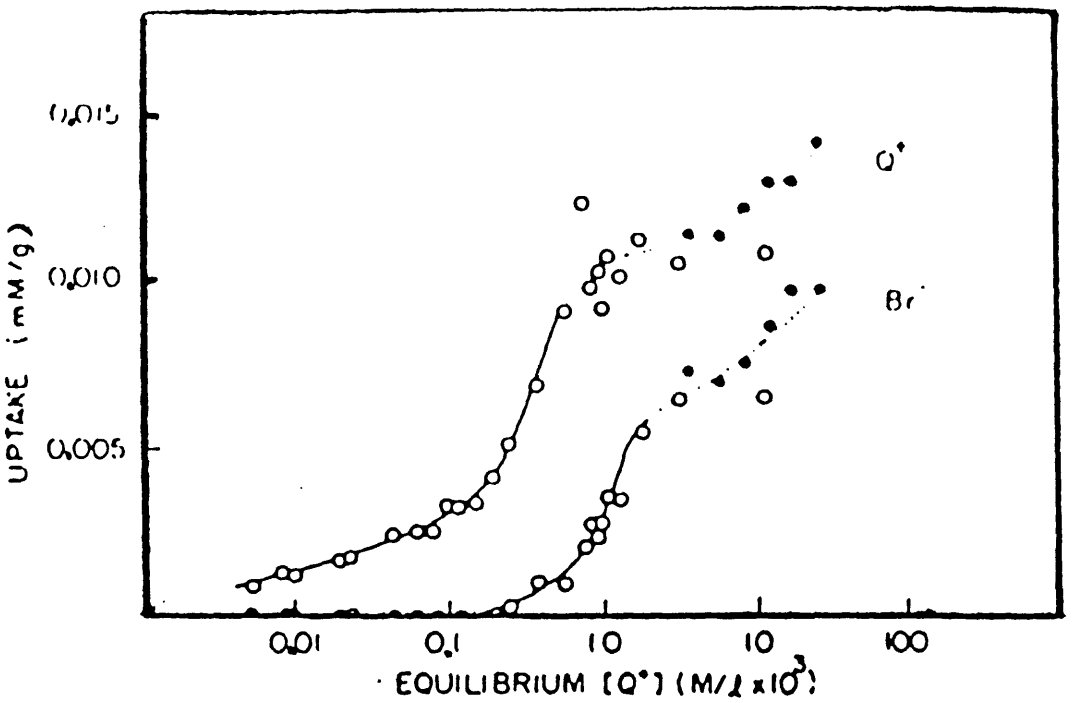
UPTAKE (mM/g)
0.015
0.010
0.005
Q°
Br
0.01
0.1
10
10
100
EQUILIBRIUM (Q°) (M/l x10³)

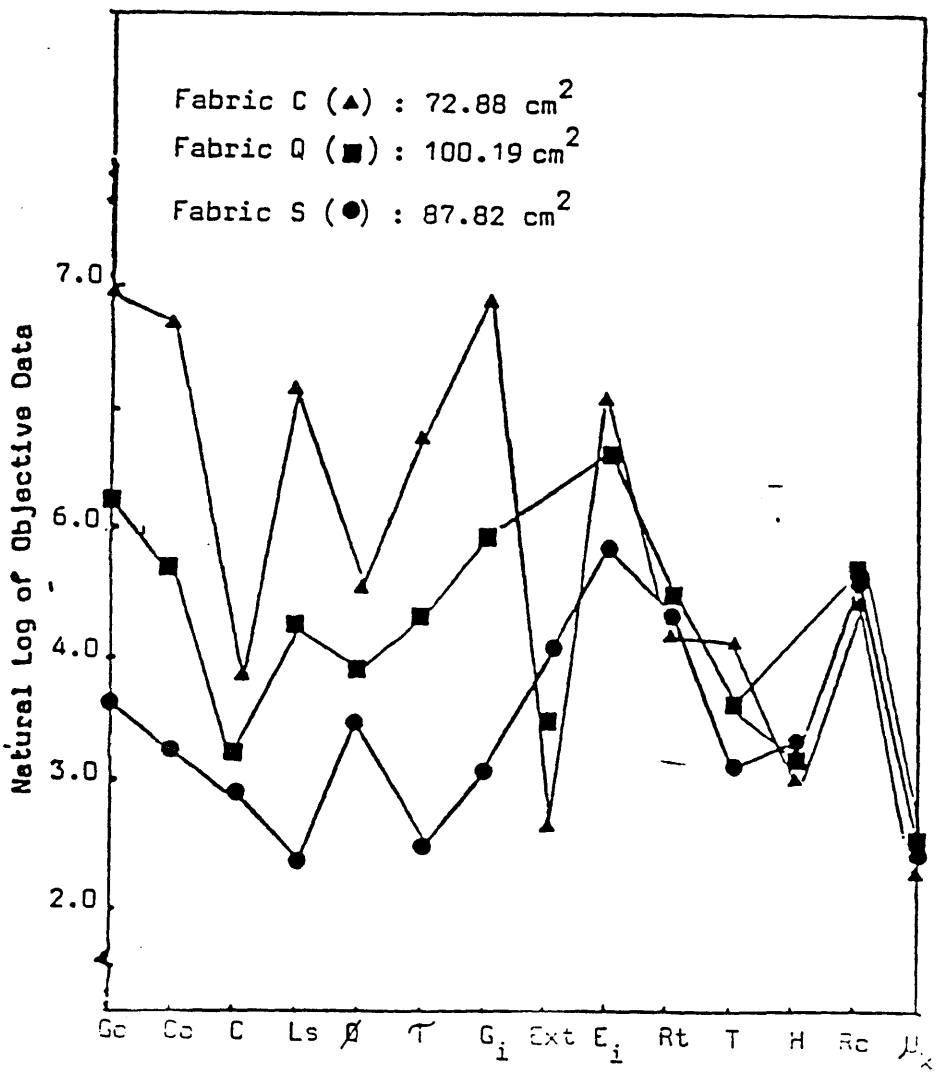
Fabric C (▲) : 72.88 cm²
Fabric Q (■) : 100.19 cm²
Fabric S (●) : 87.82 cm²
Natural Log of Objective Data
7.0
6.0
4.0
3.0
2.0
Gc
Co
C
Ls
Ø
T
Gi
Ext
Ei
Rt
T
H
Rc

4.7 Ballistic Impact of Fabrics

4.7.1 Introduction

This section is a review of some of the theoretical and practical aspects of the ballistic impact process. The review will include a brief description of the basic theory of longitudinal and transverse impact of fibres and yarns and the effect of cross-overs. It will also described some of the work of selected research groups on the transverse ballistic impact of fabrics.

4.7.2 Theoretical Aspects of Ballistic Impact of Yarns

An initial understanding of the tensile and transverse ballistic impact of yarns is essential before a theory can be developed for the ballistic impact of textile fabrics. Lyons (1963) has discussed the longitudinal impact of a rod in the context of textiles and has concluded that the familiar relationship for the propagation of a stress wave in an elastic medium, Equation 4.19, applies:

$$c = \sqrt{\frac{E}{\rho}} \qquad (4.19)$$

where c = sonic velocity, E = Young's modulus and ρ = material density. Equation (4.19) will be used in the analyses in chapter 10. This equation can be rewritten in conventional textile units as:

$$c = \sqrt{E_T} \qquad (4.20)$$

For non-linear materials, Equation 4.19 may be written as:

$$c = \sqrt{\frac{1}{\rho}\frac{\partial \sigma}{\partial \varepsilon}} \qquad (4.21)$$

where σ = stress and ε = strain. If the stress-strain curve of a non-Hookean material is concave to the stress axis, then in an impact situation the strain increments generated will overtake the original strain front and produce a shock wave, i.e. a sudden increase in the strain front velocity.

When the strain wave arrives at the boundary, it is reflected back along the yarn. Upon each reflection the strain is doubled and the direction of the wave front propagation is reversed. On subsequent arrival at the point of impact, the strain wave is again reflected. This process will continue until the breaking strain is exceeded, or a lower value of limiting strain is reached.

Roylance (1972, 1977) has studied the transverse ballistic impact of fibres and fabrics for many years. He suggested that for an infinite yarn or fibre at impact velocity v_0 and at a time t_0, assuming v_0 to be below the critical velocity, at some time t after impact, the yarn configuration will be as shown in Figure 4.7.

A longitudinal strain wave propagation away from the impact point is assumed to have reached point A in Figure 4.7. Following this wave and moving at a lower velocity is a transverse wave front. The longitudinal wave velocity is given by Equation 4.19. Smith *et al* (1958) derived an equation for the transverse wave velocity u in a Lagrangian co-ordinate system (co-ordinate system fixed to the yarn as opposed to the laboratory frame).

$$u = \sqrt{\frac{T_p}{m(1+\varepsilon_p)}} \qquad (4.22)$$

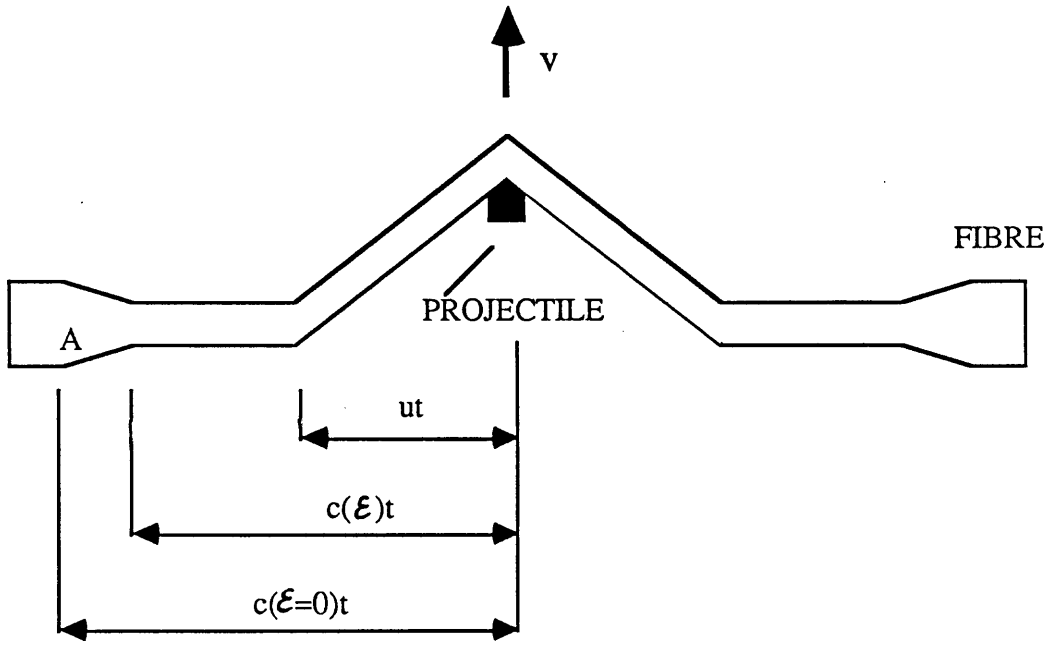

Figure 4.7 A schematic representation of the configuratin of a yarn impacted transverrsely

where u = transverse wave velocity, T_p = maximum tension, m = mass per unit length of unstrained filament and ε_p = maximum strain due to impact. Smith's analysis has shown that if the stress-strain relationship is linear then ε_p can be found from:

$$v_i = \sqrt{\varepsilon_p kE[2\sqrt{\varepsilon_p}(1+\varepsilon_p) - \varepsilon_p]} \qquad (4.23)$$

where v_i = impact velocity, E = tensile modulus and k = constant.

The important points of the above discussion are that the transverse and longitudinal wave velocities are both increased with increased material modulus and decreased linear density. Transverse waves absorb energy from the projectile in the form of kinetic energy. Therefore materials where the wave front propagates faster will have better energy absorbing characteristics.

4.7.3 The Effect of Cross-overs on the Stress Wave Propagation

When a yarn is woven into a fabric, the propagation of strain is modified by the presence of the cross-overs. Roylance (1980) has studied the effect of cross-overs using models that he developed to include the influence of fibre materials properties and fibre-fibre slip. At the cross-over some of the stress wave is transmitted along the primary fibre, some reflected and some diverted along the secondary fibre. The proportion of each of the above depends on the modulus of the fibre as well as the extent of fibre-fibre contact and slip. Figures 4.8 to 4.11

Figure 4.8 The effect of fibre modulus on the proportion of the transverse wave being either transmitted along the original fibre or be diverted to the second fibre at a cross-over point.

Figure 4.9 The effect of friction at a cross-over on the coefficient of reflection of the transverse wave front.

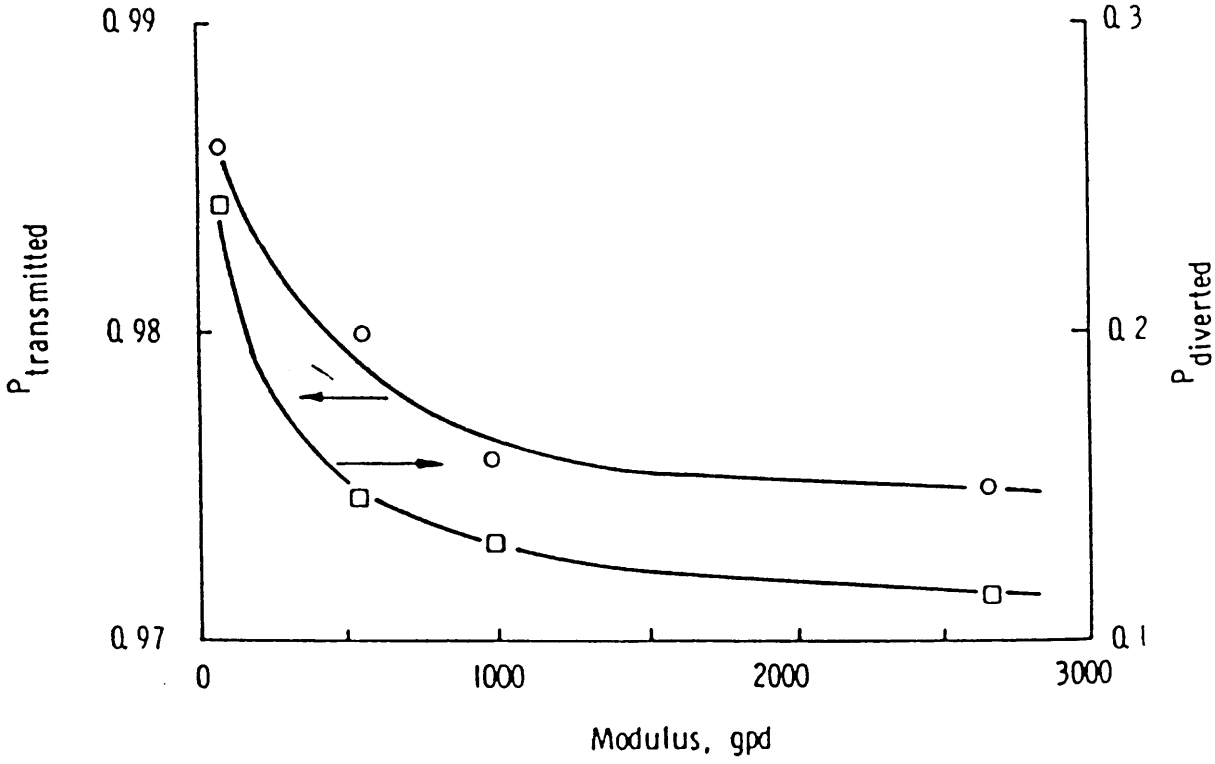
0.99
0.98
0.97
0.3
0.2
0.1
$P_{transmitted}$
$P_{diverted}$
0
1000
2000
3000
Modulus, gpd

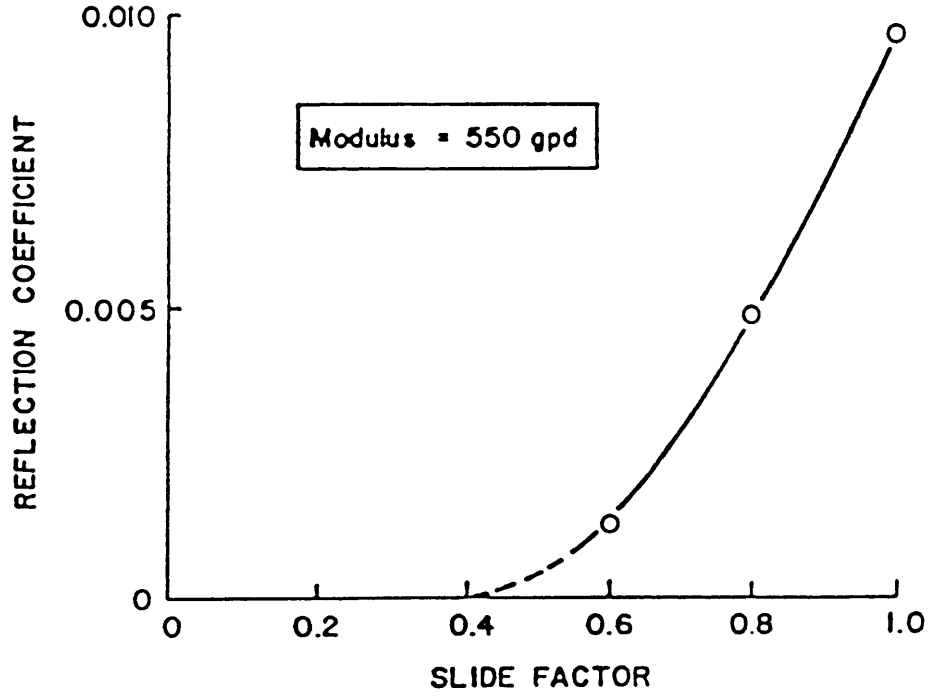
0.010
0.005
0
REFLECTION COEFFICIENT
Modulus = 550 gpd
0
0.2
0.4
0.6
0.8
1.0
SLIDE FACTOR

Figure 4.10 The effect of friction on the coefficient of wave diversion.

Figure 4.11 The influence of friction at the cross-over on the transmission of the transverse wave front.

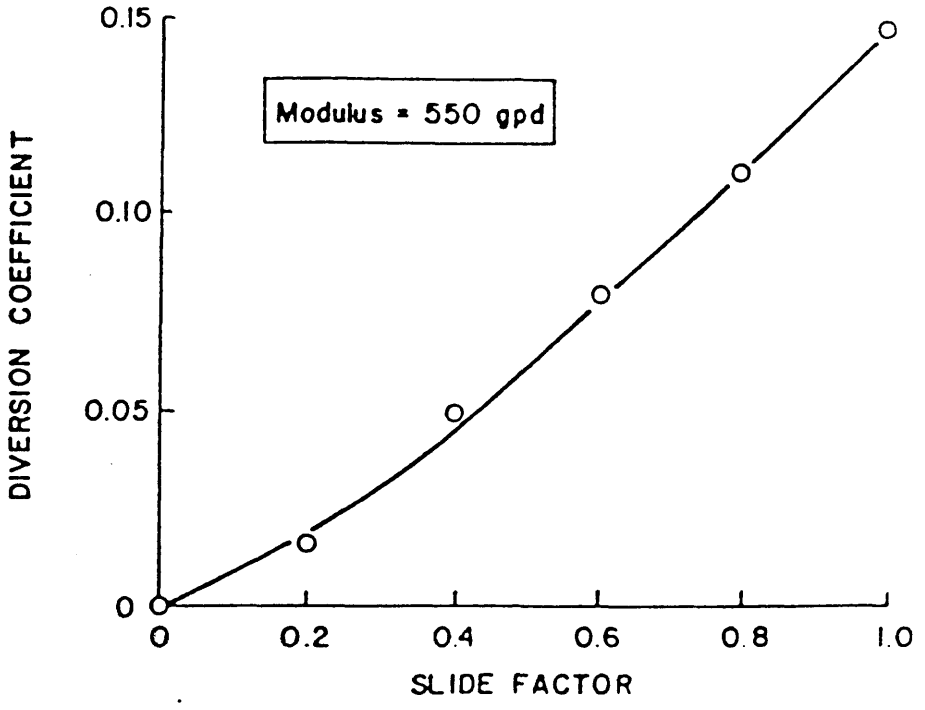
0.15
0.10
0.05
0
DIVERSION COEFFICIENT
Modulus = 550 gpd
0
0.2
0.4
0.6
0.8
1.0
SLIDE FACTOR

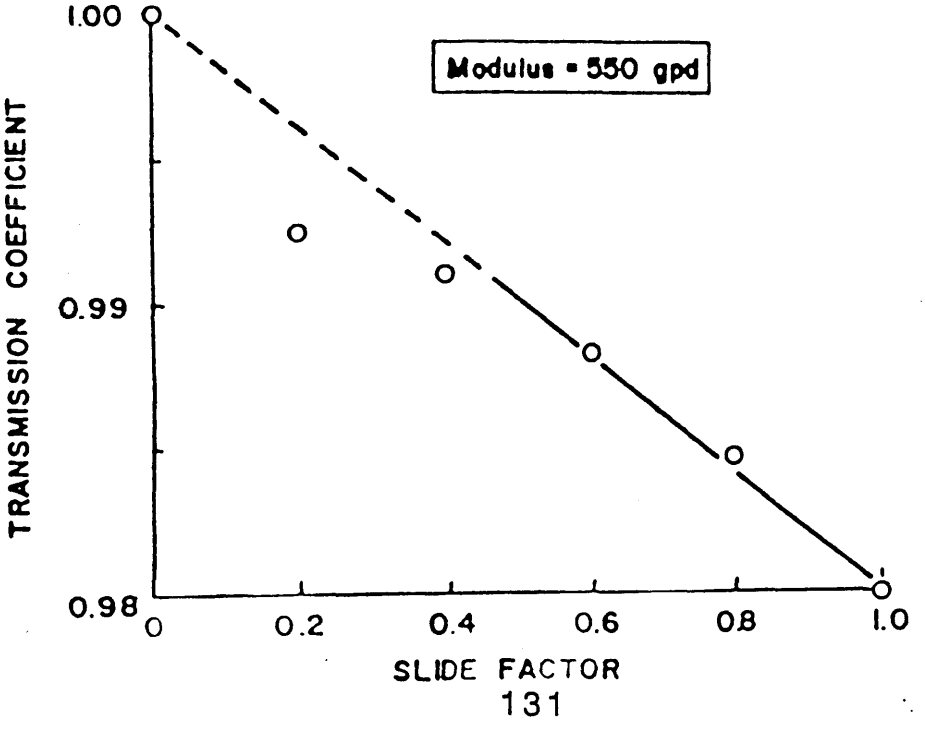
1.00
0.99
0.98
TRANSMISSION COEFFICIENT
Modulus = 550 gpd
0
0.2
0.4
0.6
0.8
1.0
SLIDE FACTOR

reproduced from Roylance's paper show the effect of the fibre modulus and slide factor on the proportion of the wave that may be transmitted, diverted or reflected. Cork (1983) has confirmed the above results.

4.7.4 The Ballistic Performance of Textile Structures

The most common approach that has been adopted for the testing of the ballistic resistance of textile structures is the "V_{50} limit" for a given area density of multi-layer fabric. The V_{50} limit is defined as the impact velocity at which 50% of the samples fail and 50% remain unpenetrated. Under real test conditions, however, for any chosen impact velocity, only a certain proportion of projectiles will penetrate the sample. This occurs partly due to differences between specimens, but mainly due to the exact location of the impact zone in relation to the cross-over points.

An alternative way of quantifying ballistic resistance is the ballistic performance indicator (BPI) developed by Figucia (1980). BPI is defined as the energy absorbed per unit increase in area density and corresponds to the slope of the energy vs. area density plot (the area density corresponds to the number of fabric layers). Figucia (1980) found that the energy absorbed and the area density were linearly related for Kevlar.

There are numerous parameters that influence the ballistic resistance of fabrics. Amongst workers such as Montgomery *et al* (1982) and Prosser (1988), Kruger (1987) has studied the ballistic performance of aramid fabrics. Figure 4.12 reproduced from that paper depicts the factors that may influence the ballistic efficiency of a textile structure. On the question of fabric finishing, which has a direct relevance to the current study, he found that non-finished wet aramid fabrics

lose up to 40% of their ballistic strength. Hence, he recommends careful fabric scouring followed by a suitable water repellent finish.

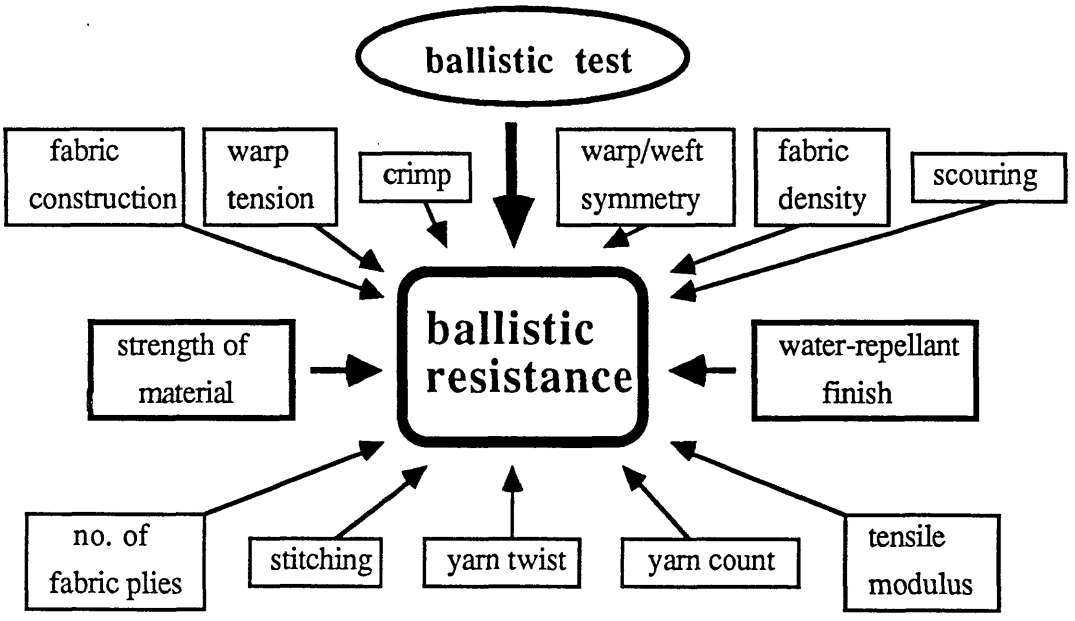

Figure 4.12 Factors that may influence the ballistic performance of aramid fabrics.

CHAPTER FIVE

MATERIALS AND EXPERIMENTAL TECHNIQUES

5.1 Introduction

This chapter provides details of all the materials and experimental techniques used in the current study. Included are descriptions of the preparation and characteristics of the materials investigated, the properties of the treating agents used, and the apparatus designed, developed or used in the evaluation of the properties of these materials. The chapter begins by describing the materials used. The next section describes the experimental methods followed and the results of the various friction and tensile experiments carried out on the cotton and the aramid yarns. Then the so called "hardness" experiments are described followed by an outline of the procedure adopted in the ballistic impact experiments. Next, the pull out experiments on untreated and treated fabrics are described and finally the micro-displacement measurements are outlined.

5.2 Selected Test Materials

Two kinds of fabrics were used in these studies, a 100% cotton fabric, commercially known as Sanfurised mull supplied by Proctor & Gamble Co., and two poly aramid fibre fabrics constructed from commercial yarns (Kevlar 49 and 29 denoted as aramid 1 and 2 respectively in this thesis) manufactured by E.I.duPont Co.

The cotton fabric possessed a plain weave structure and the average yarn diameter was 0.28 ± 0.04mm. The average yarn centre to centre spacing was 0.58 ± 0.09mm and the linear density was 22.4 ± 2mg/m. Figure 5.1 shows a typical microscopic photograph of this fabric. An SEM photograph of a single cotton yarn is

Figure 5.1 A microscopic photograph of the cotton weave.

shown in the Appendix 1.

Before each experiment or treatment, the cotton fabric was washed once with water only in a top loading washing machine (Hotpoint model 15790) and tumble dried (Indesit T2590 drier) at medium heat for about 40 minutes (hence totally dry). The aramid fabrics studied were a plain weave aramid 2 and a twill weave aramid 1. The aramid 2 fabric was several years old. The average yarn width for the warp yarns was 1.51mm and for the weft yarns was 1.26mm. The mean yarn thickness was 0.2mm and yarn spacing was virtually zero. The linear density was 0.164 mg/m. The aramid 1 fabric had an average yarn width of 1.42mm for the warp and 1.39mm for the weft yarns, an average yarn thickness of 0.15mm and a yarn spacing ranging from 0 to 0.25mm. The linear yarn density was 0.13 mg/m.

5.3 The frictional characteristics of the yarns

5.3.1 Introduction

This section describes the experimental apparatus and techniques used to measure the frictional character of single cotton and aramid yarns together with the results obtained. Two configurations were used, the point contact and the hanging fibre friction configurations. The point contact technique was only used with untreated cotton, aramid 1 and aramid 2 yarns, while the hanging fibre method was used with both untreated and treated cotton and aramid 1 yarns. The results are mostly presented as the calculated values of the coefficient of friction μ. The analysis described in section 3.4.3 has been applied to the results and found to describe the frictional character of yarns quite well.

5.3.2 Point contact friction measurements

The principle of this experiment was very similar to that of the Scruton point

contact friction machine described by Briscoe *et al* (1973). The force measuring device of the yarn pull-out machine to be described later was used as a force transducer. A single yarn of length ca.30mm was attached to a flat and horizontal piece of metal (A) which was directly connected to this transducer. Another yarn of similar length was attached to the movable stage directly underneath and at right angles to the first yarn. Figure 5.2 shows a schematic diagram of the force measuring device. The stage was set in motion and the dynamic frictional force associated with varying normal loads (0.01-0.1N) was measured.

Figure 5.3 shows a typical set of data obtained using the point contact method. The gradient of the line is a measure of the coefficient of friction μ. Table 5.1 presents the values of μ and the load index n (see section 3.4.3) for the three yarns tested.

Table 5.1

Type of yarn	Coefft. of friction μ	Load index n
Cotton	0.65	0.93
Aramid 1	0.25	0.92
Aramid 2	0.28	0.88

Aramids possess a much lower value of μ than cotton fibres. The load index n is an indication of the type of deformation the contact experienced during the frictional process. The numerical values obtained indicate that a multiple asperity elastic deformation is probably formed in each contact case.

5.3.3 The hanging fibre friction configuration

5.3.3.1 Experimental apparatus and procedure

The principle features of this apparatus were described by Howell (1954) and used later by Kremnitzer (1978) to measure the friction of PET fibres. The apparatus,

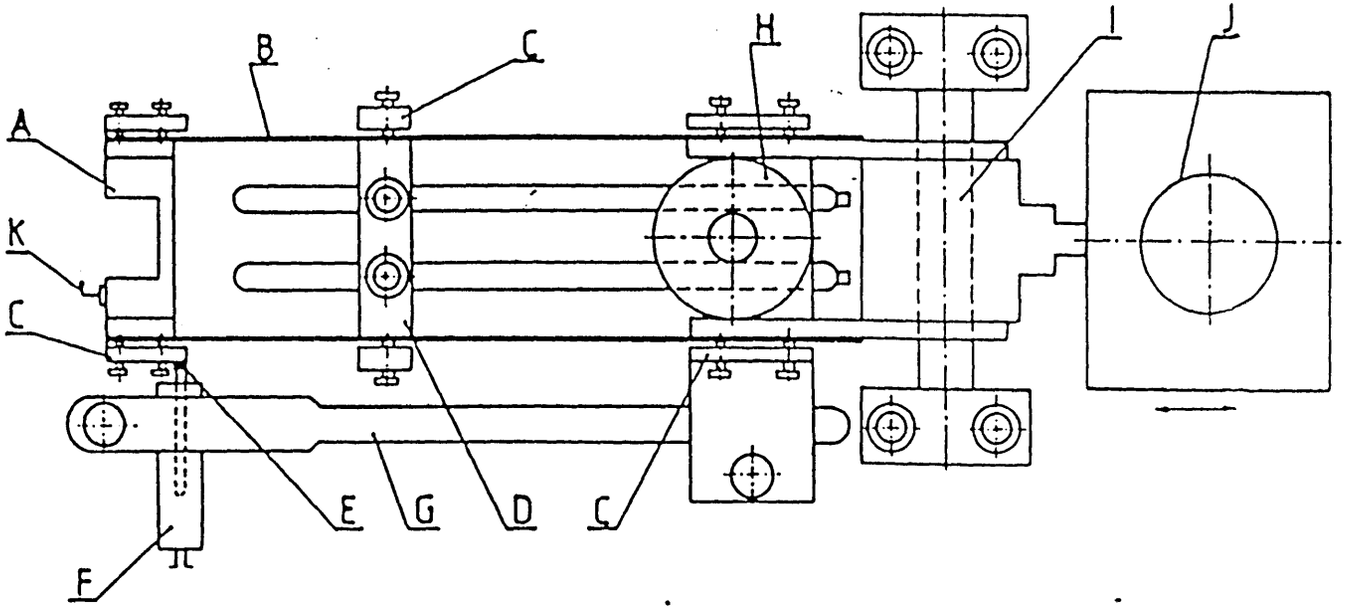

A - metal frame carrying the hook and springs

B - phosphor-bronze spring

C - clamps for holding the springs

D - moveable metal slider for adjusting the length of the springs

E - transducer inner-part

F - transducer outer part

G - holder for the transducer outer part

H - loading platform

I - pivot point

J - counterweight

K - hook to which the yarn is attached

Figure 5.2 Schematic drawing (plan) of the upper part of the force measuring device.

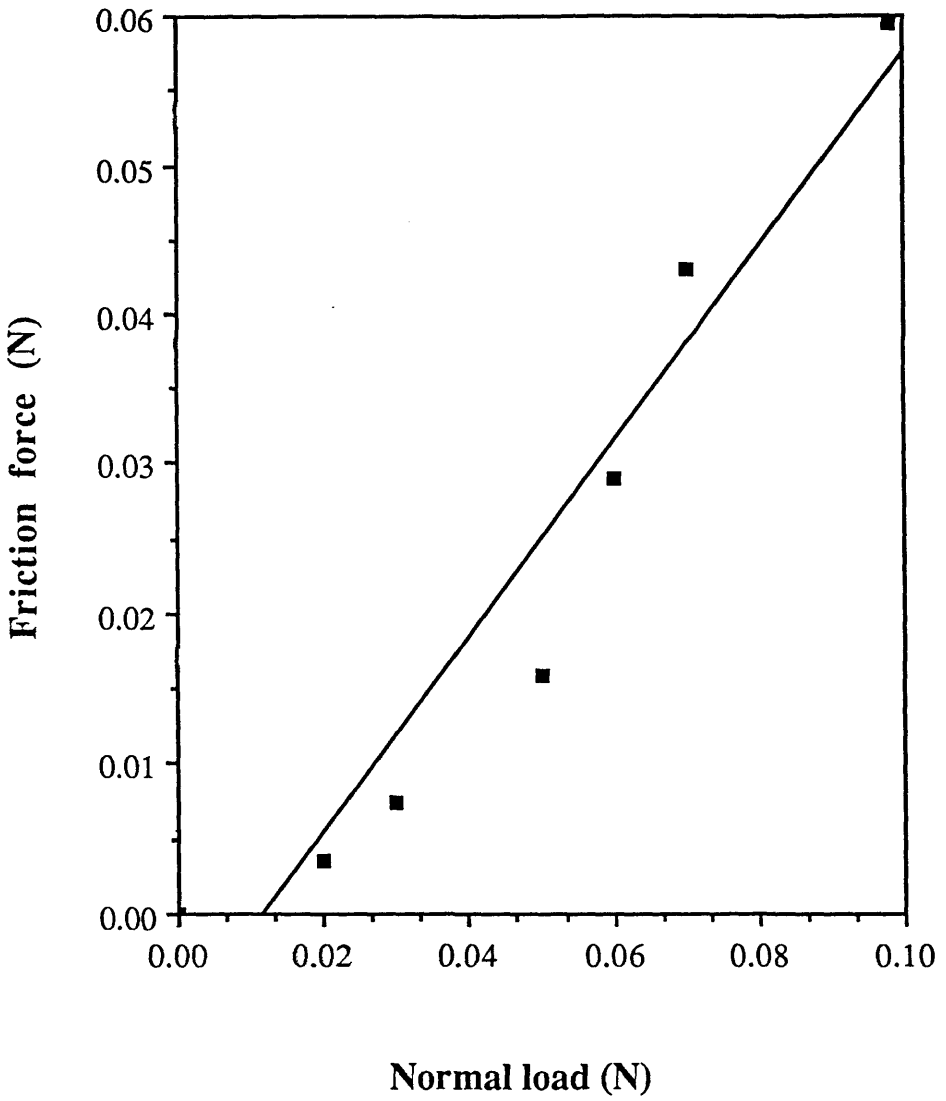

Figure 5.3 Point contact frictional character of two orthogonal cotton yarns
The yarns were untreated and dry (RH=40%)

depicted in Figure 5.4, consisted of a vertically suspended fibre, connected at the upper end to the hook of the force measuring device and at the lower end to a specified dead weight, W_d. A taut horizontal fibre was held in a holder under a specified pretension. The force measuring device was that used in the pull-out test, described in detail later, except that the measuring arm was tilted through 90^o to enable it to measure the force in the vertical direction. The signals from the linear displacement transducer were fed into a amplifier (Sangamo) and then into an A to D convertor. The digital signals were then recorded on a microcomputer (Apple Macintosh). Precalib ration enabled the signals to be converted into values of force.

The holder for the horizontal fibre was that used to hold the fabric in the pull-out apparatus and described in detail later. One end of the yarn was clamped, the other hung over a PTFE roller and connected to a weight, creating a specified tension in the yarn. The second end was then clamped. The measuring device and the suspended yarn were connected to the movable plate of an Instron tensile tester enabling the controlled vertical movements of the suspended yarn. The horizontal yarn holder was attached to the static bottom plate of the Instron. The hanging yarn was placed over the horizontal yarn. The distances d and h and hence the angle θ were measured, figure 5.5. The suspended fibre was moved up for a predetermined distance and then returned to its original position. In this way a dynamically varying normal load was produced as the upward and downward friction were being recorded. The compliance of the springs was 5 mm/N which was corrected for in the calculations.

The hanging fibre configuration was used to measure the friction between the following single yarns: untreated cotton, untreated aramid 1, 5% PDMS treated cotton, CTAB treated cotton, cleaned (soxlet extracted) aramid 1 and 5% PDMS treated aramid 1. The dead load W_d was varied and values of 0.05, 0.10 and 0.20N were adopted

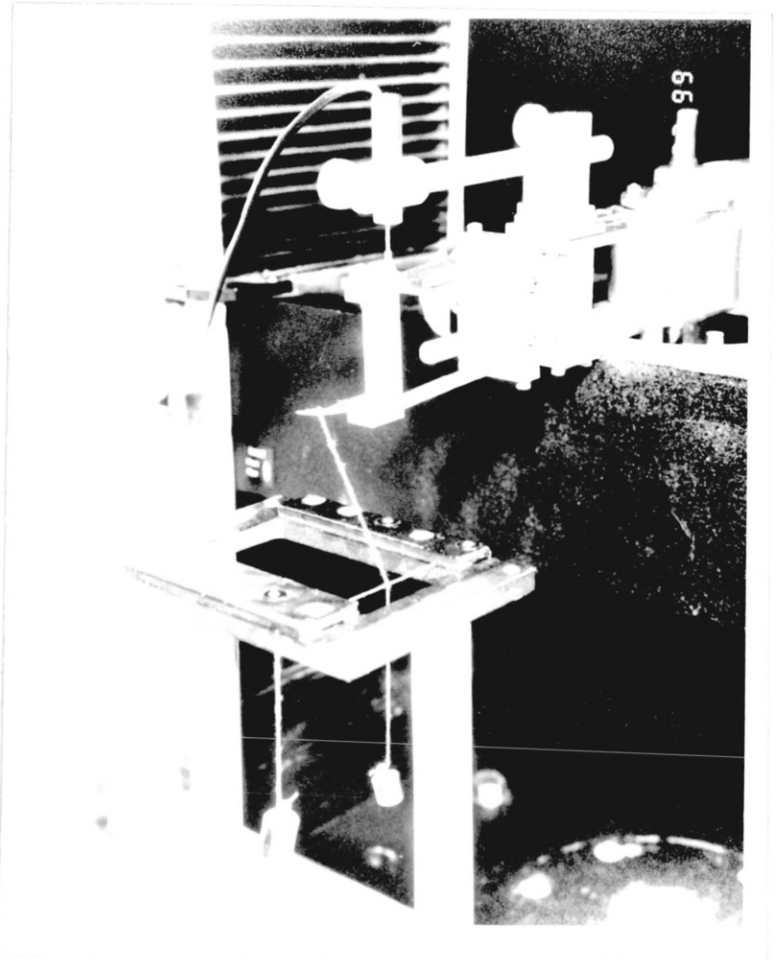

Figure 5.4 Photograph of the hanging fibre-friction apparatus.

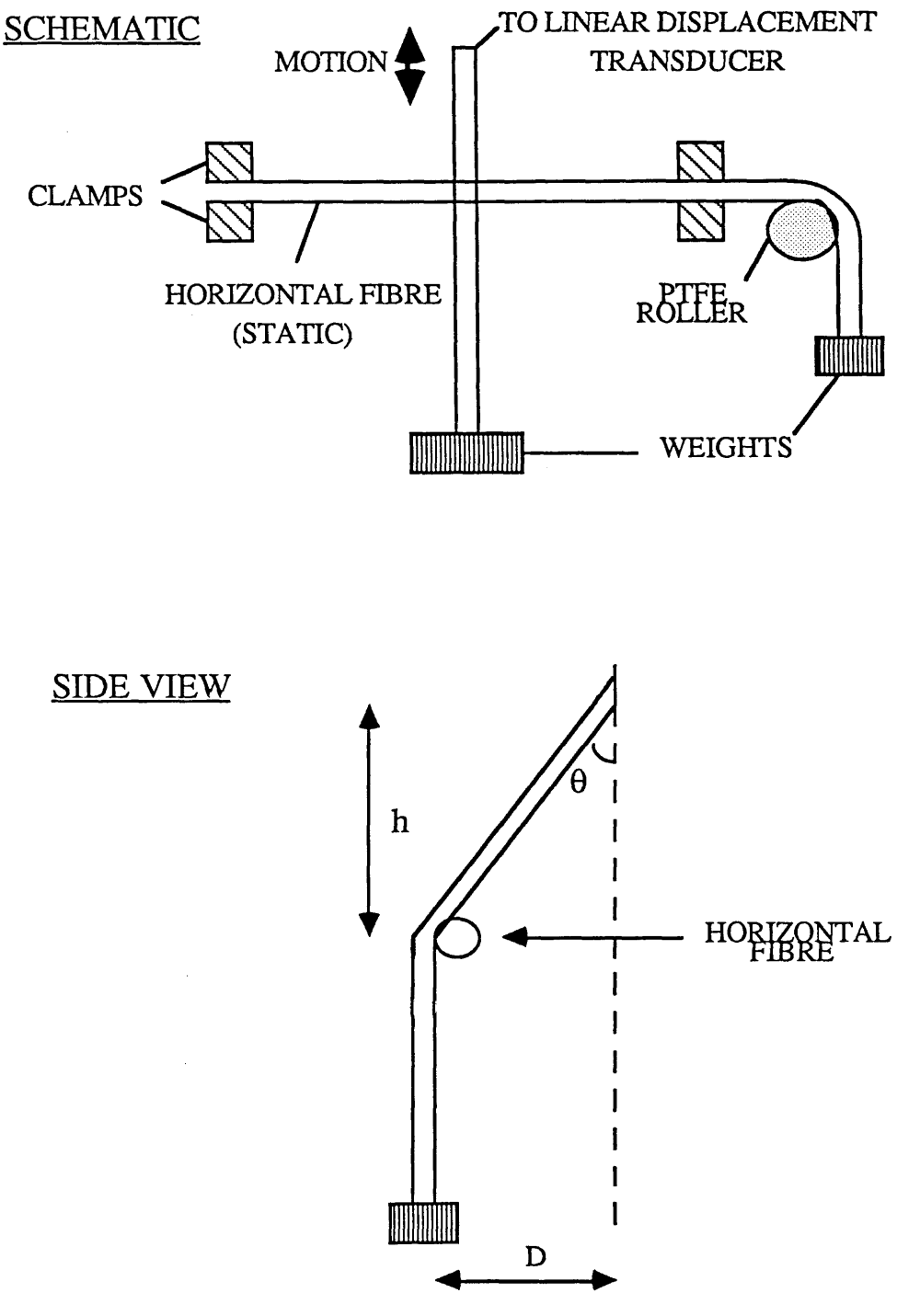

Figure 5.5 Schematic diagram of the hanging fibre arrangement showing the directions of motion and the yarns in contact

for systematic studies. The horizontal yarn pretension was 0.20 N.

5.3.3.2 The frictional character of yarns

Figure 5.6 shows a typical set of results obtained from the hanging fibre experiments. The force is calculated using the recorded data and the appropriate calibration curve (not included here) while the load was calculated as:

$$W = W_d * \cos\theta$$

where W_d is the dead load on the vertical yarn and θ the angle shown in figure 5.5. The effect of W_d on the measured values of force is eliminated by measuring the force both in the upward and downward directions of motion, subtracting the downward force from the upward and dividing by two. Typical data are shown in figure 5.6, table 5.2 presents the values of μ calculated as above for the cotton and aramid 1 yarns. The dead load W_d on the yarn for the results below was 0.10 N.

Table 5.2

Yarn Type	Ratio F/W
Cotton (untreated)	0.61
Cotton (5% PDMS)	0.39
Cotton ($1.4*10^{-3}$M CTAB)	0.52
Aramid 1 (as received)	0.27
Aramid 1 (5% PDMS)	0.16
Aramid 1 (soxlet extracted)	0.35

Figure 5.7 depicts the relation between the measured frictional force and the angle (figure 5.5) for cotton. It can be seen that as θ increases ie. decreasing load, the force

Figure 5.6 Variation of friction force with load in the hanging fibre experiment. The dead load W_d was 10 g. The normal load on the contact was a component of W_d through angle θ which changed during the course of the experiment. The gradient is the mean coefficient of friction.

Figure 5.7 Variation of friction force with angle θ in the hanging fibre experiments. Increasing the angle has the same effect as decreasing the load, hence the force decreases. $W_d = 10$ g.

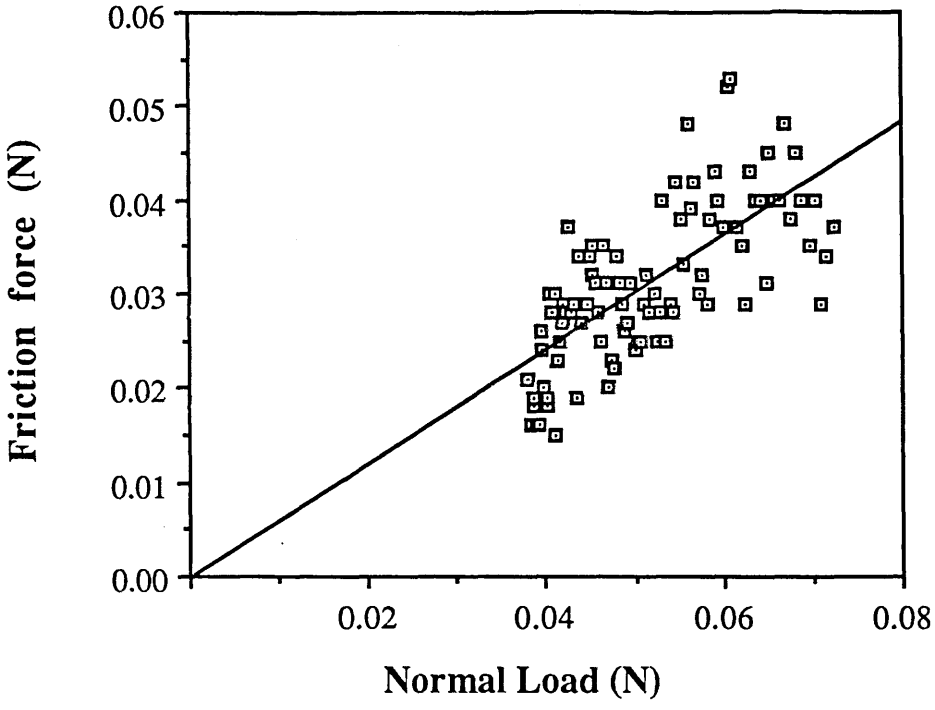
Friction force (N)
0.06
0.05
0.04
0.03
0.02
0.01
0.00
0.02
0.04
0.06
0.08
Normal Load (N)

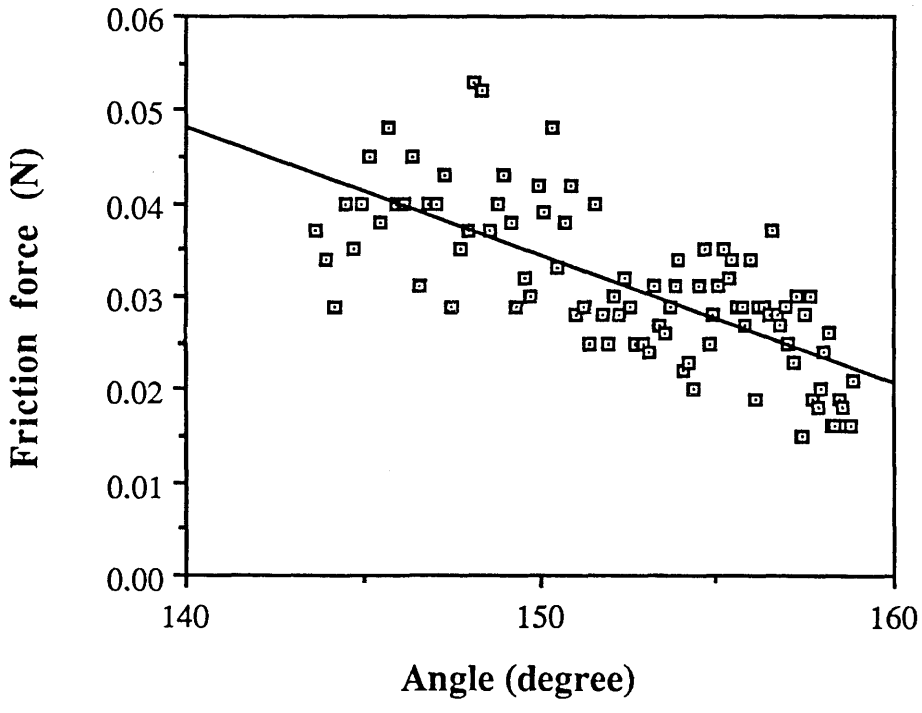
Friction force (N)
0.06
0.05
0.04
0.03
0.02
0.01
0.00
140
150
160
Angle (degree)

decreases accordingly.

On closer inspection of the values of μ, if one attempts to calculate μ, using the equation $F=\mu W$, for each and every point in figure 5.6, and plot μ against W, figure 5.8 is obtained. This figure is for untreated cotton at W_d=0.05, 0.10 and 0.20 N, while figure 5.9 is for untreated aramid 1 yarns at similar dead loads. It can be seen that the coefficient decreases with increasing load. This observation has been reported previously, for example Kremnitzer (1978) obtained similar trends for friction between PET fibres. The results of figures 5.8 and 5.9 are found to fit the analysis described in section 3.4.3, equation 3.29 quite well. The lines drawn through the data points in the two figures are represented by equations $\mu = 0.15 * W^{-1/3} + 0.1$ for untreated cotton and $\mu = 0.06 * W^{-1/3} + 0.08$ for as received aramid 1 yarns.

The fact that equation 3.29 describes the results of the hanging fibre experiments so well suggests that the geometry of contact in these experiments may be a point contact rather than an extended line contact geometry.

5.4 The Yarn Tensile Experiments

This section deals with the tensile characterisation experiments performed on both treated and untreated single yarns of cotton and aramid fibres. Both the experimental aspects and the results obtained will be presented. It is appropriate to do this here, because these studies were carried out so as to gain an insight into the characteristics of the yarns that went into constructing the fabric assemblies.

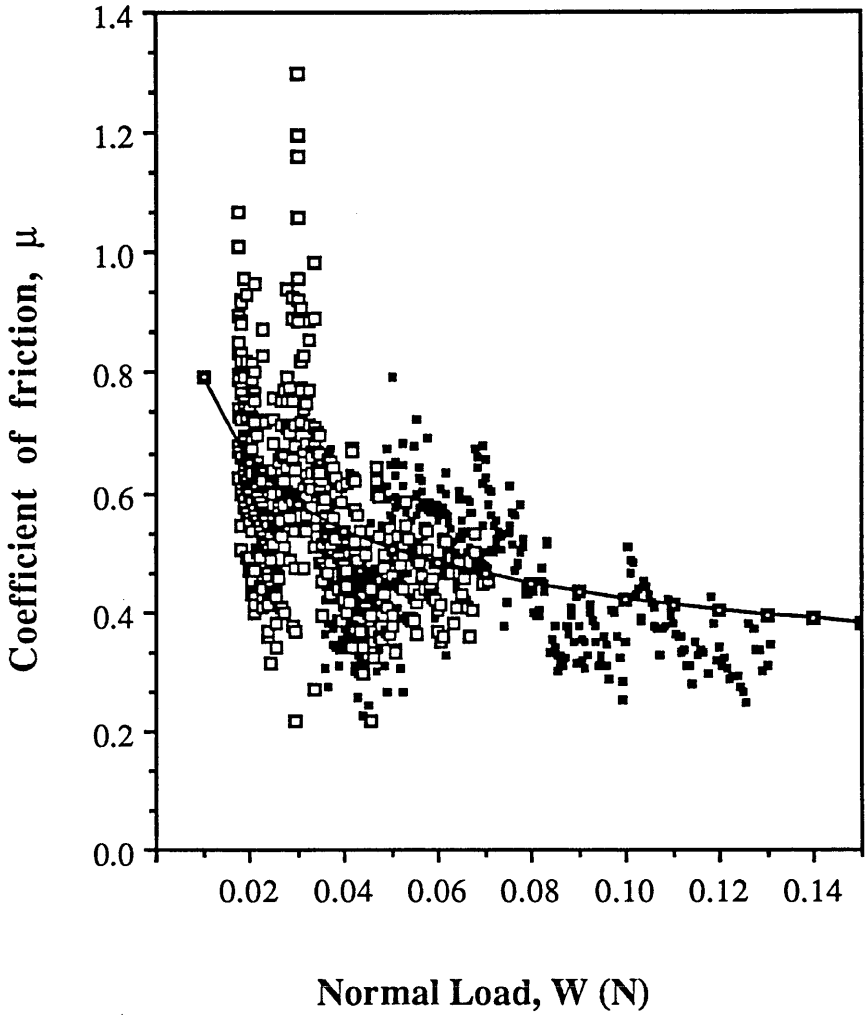

Figure 5.8 Variation of coefficient of friction with normal load for untreated cotton yarns in the hanging fibre experiments. μ was calculated for each point as $\mu = F/W$. The values for $W_d = 5$ and 10 g are included.

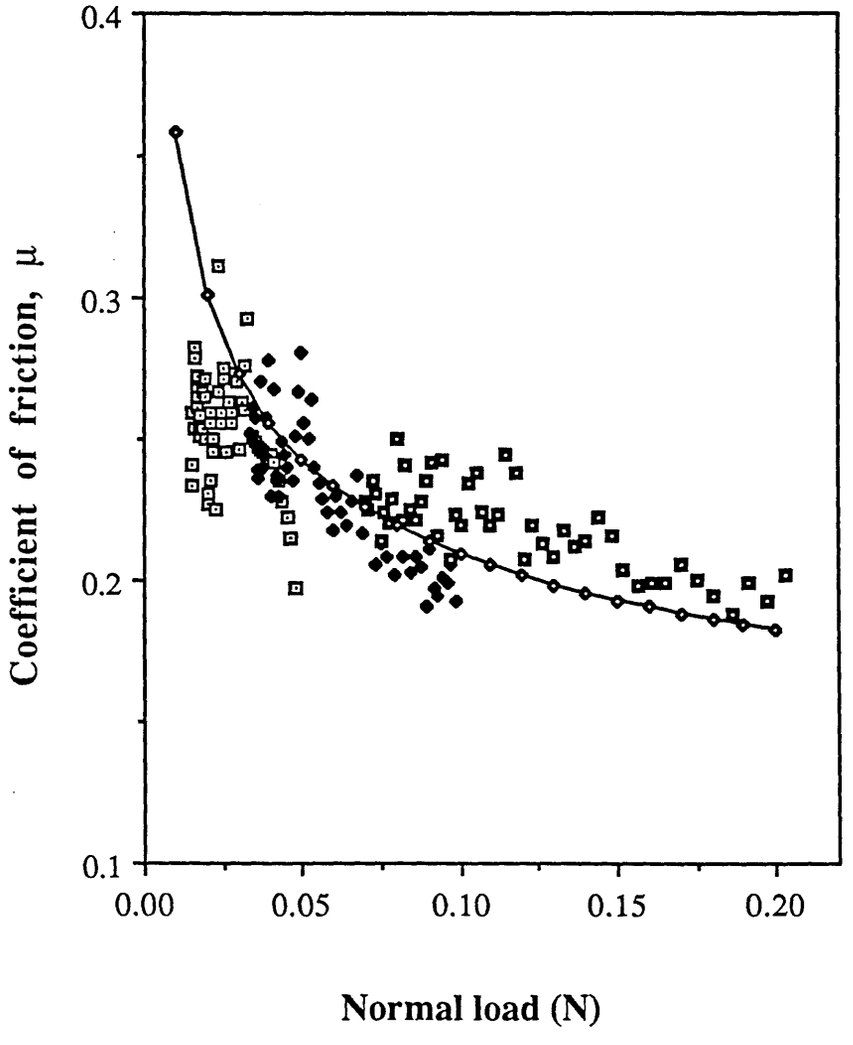

Figure 5.9 Variation of μ with W for untreated Aramid 1 (Kevlar 49) yarns in the hanging fibre experiments. W_d = 5, 10 and 20 g.

5.4.1 Experimental Set-up and Procedure

An Instron tensiometer (Model 1122) was used in these studies. The force measuring system comprised a Piezo-electric transducer (Kistler 9311A) of max. capacity 5 KN connected to a charge amplifier (Kistler, type 5007). The amplified signal went to an A to D convertor (3D Digital Design and Development Ltd.). The digital signal was then received by a micro computer (Apple Macintosh, 512K) where the force and corresponding times were recorded. The yarns were securely mounted between grips but not so tight as to excessively damage the yarn. The contacting faces of the grips were rubber and hence the yarn damage was minimised. The length of the yarn was measured and the upper grip was set in motion. With untreated cotton yarns, the variables investigated were lengths of yarn i.e. between 2 and 25mm, and cross-head speeds of 1, 2, 5 and 20mm/min. However, all other experiments on treated cotton and aramid yarns were performed at a yarn length of 20-25mm and a cross-head speed of 2mm/min.

Yarns with the following treatments were tested: cotton yarns (warp yarns only taken from untreated fabric randomly) were immersed in distilled water and pure tetradecane for 2 hours at 22 ± 2°C. They were then taken out of solution and tested wet before an appreciable amount of the liquid could drain away. Cotton yarns were also immersed in solutions of 1% w/w and 5% w/w PDMS (Poly dimethyl siloxane of viscosity 100cp) in petroleum spirit and 1.4×10^{-4} M and 1.4×10^{-3} M solutions of Cetyl trimethyl ammonium bromide (CTAB, mol.wt. 364.46, $[CH_3(CH_2)_{15}]$ (CH_3) NBr, min. assay 98%) in distilled water for 2 hours at 22 ± 2°C. They were then dried completely and tested in the tensiometer at approx. 20°C and 40% RH. Each experiment was repeated 3-5 times.

5.4.2 The Force-strain Characters of Yarns

Figure 5.10 shows the results of the tensile tests plotted as force vs. extension for various lengths of cotton yarns at a cross-head speed of 1mm/min. Firstly, it is important to note that, as described in chapter 2 for cotton fibres, the curves are, for most parts, quite linear and exhibit no yield point. The yarn break is a clear one and highest value on the force axis is the value of breaking load. As it can be seen, breakage for various yarn lengths occurs in a very close range of forces around 4 N. However, the breaking extension varies systematically with the yarn lengths and in fact the force-extension gradients for shorter yarns are steeper than those for longer yarns. This is acceptable since one would expect the longer yarns to be able to extend more. However, when the extension values are divided by the corresponding yarn lengths, the situation is totally reversed. Figure 5.11 illustrates the force-strain characteristics of untreated cotton yarns of varying lengths at a cross-head speed of 2mm/min. Here, the longer yarns possess the steeper gradients. This is in contradiction to the expectation that, the longer yarns should be able to accommodate more strain than the shorter yarns. This also means that the shorter yarns show less resistance to strain energy than the longer yarns. This systematic contradiction occurs in the force strain plots for all the different rates of extension examined in this study. The only reasonable explanation that can be given is that which also agrees with Professor Backer's observations. Backer (1987) proposed simply that there is a finite amount of strain experienced within the grip area and this amount becomes significant and can to some extent dominate with the smaller lengths of yarn. This would lead to lower gradients or moduli of the force-strain curves than one would expect. An appropriate correction factor would increase the moduli of the smaller lengths to more realistic values. In the proceeding sections, however, we shall only use the results of tensile experiments on specimens of gauge length 20-25mm, as recommended by BS 4029.

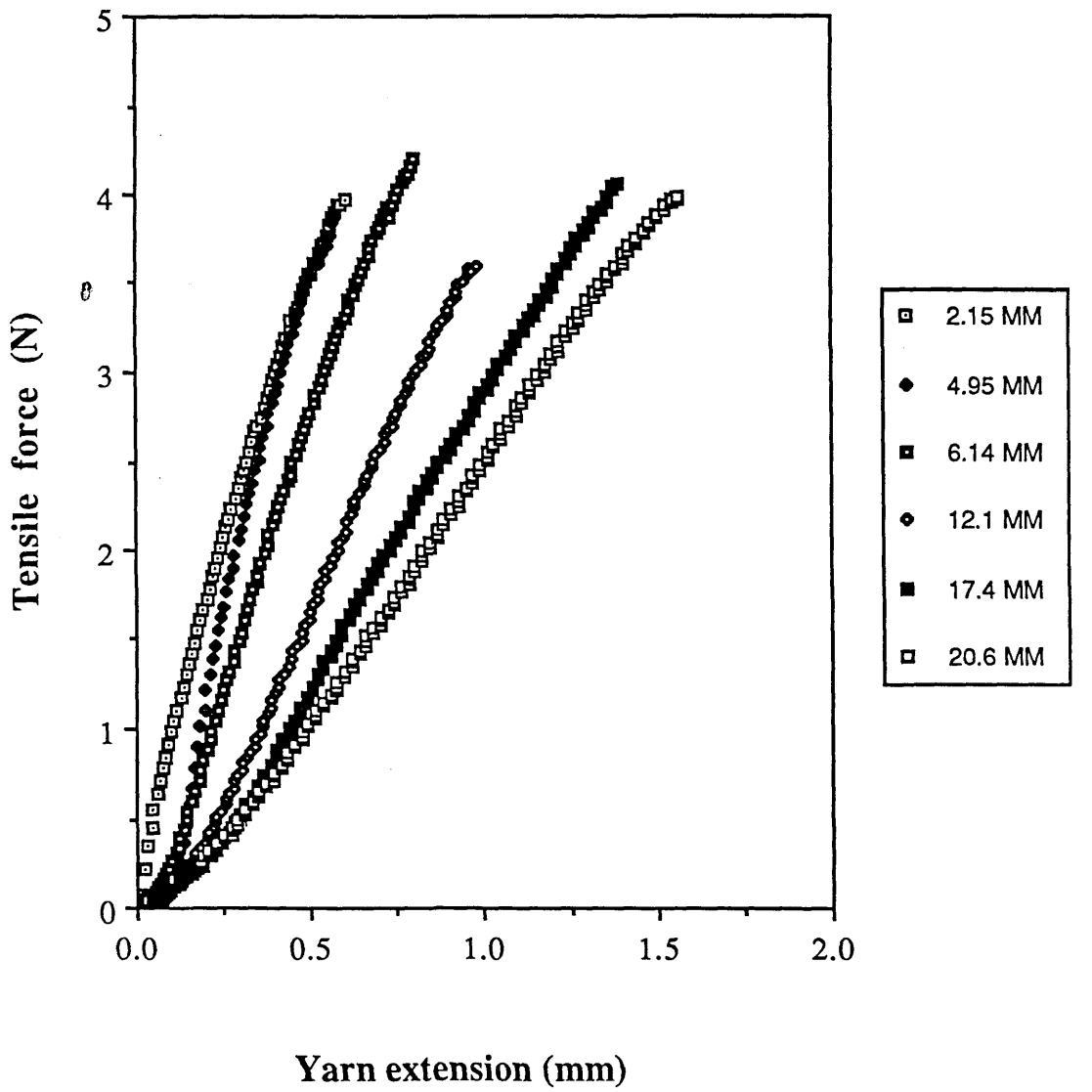

Figure 5.10 Force-extension profiles for untreated cotton yarns of varying gauge lengths. The yarns were taken to the point of rupture in the tensile experiment. Instron cross-head speed = 2 mm/min.

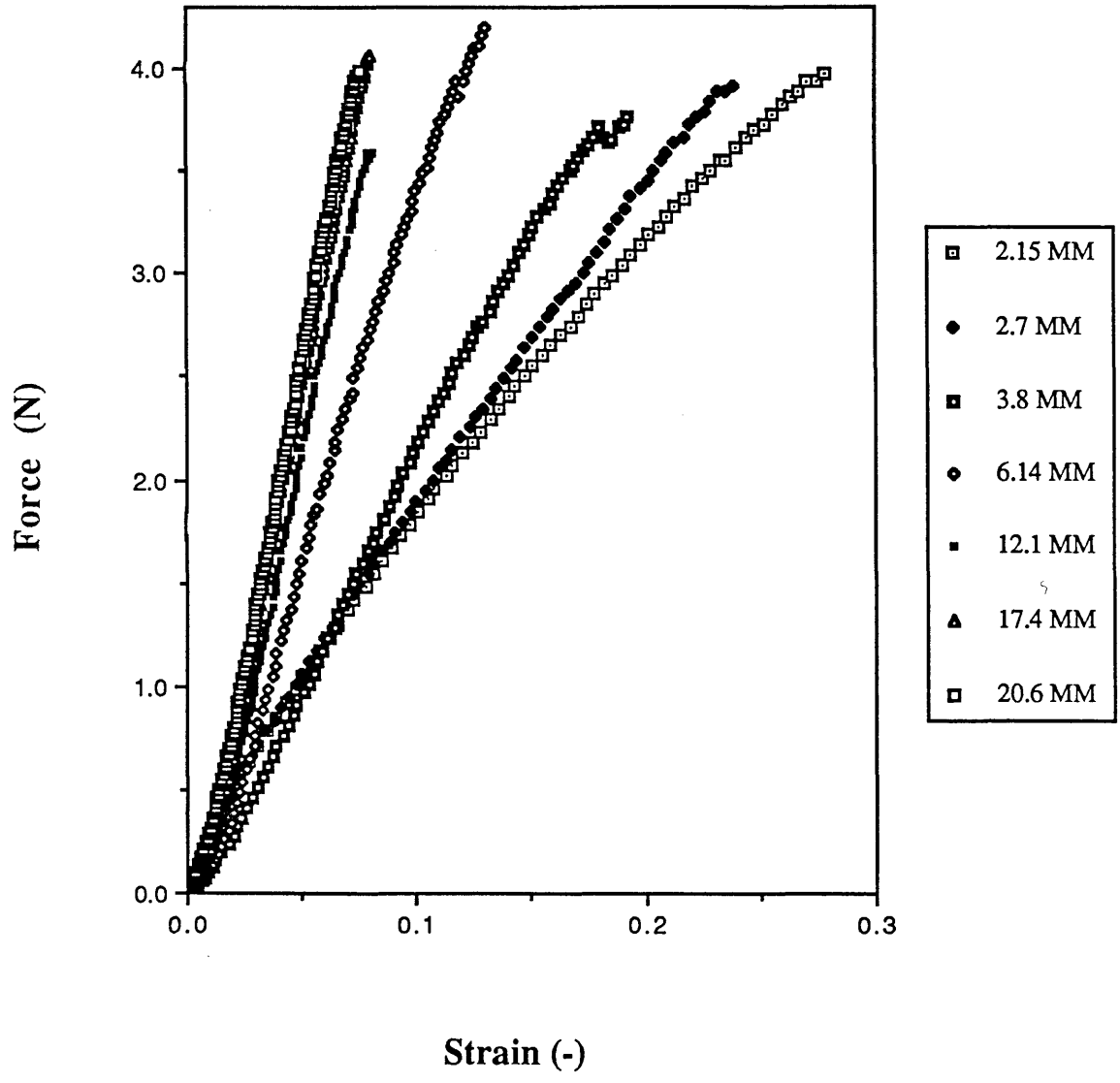

Figure 5.11 Force-strain character of untreated cotton yarns of different lengths. The extension data in Figure 5.10 was divided by the corresponding yarn length to obtain the strain. However, the position of the profiles have reversed here from that of Figure 5.10. Strain = 10% per minute.

No obvious correlation was found between breaking force and yarn length at any rate of strain. However this could be due to the relatively small numbers of samples tested. Also, with the rates of strain used, for specimens of gauge lengths 20-25 no clear trends were observed in moduli, the breaking force and the breaking extension although the literature (section 3.3.7) suggests that the breaking strength increases at higher rates of strain. The actual values obtained are given in Table 5.3 below.

TABLE 5.3 Force-strain Parameters at Different Strain Rates

Cross-head speed mm/*min*	Gradient (N)	Break force (N)	Break strain (-)
1	60	3.99	0.076
2	43.3	2.653	0.083
5	48	3.381	0.092
20	48.2	3.96	0.088

Figure 5.12 is a plot of the gradient of the force-strain curves (modulus) against the corresponding value of strain for different rates of strain. Although again there is no obvious trend between different rates of strain, the increasing trend of gradient or modulus with strain can be seen. The common feature of all the profiles is the increasing values of moduli with increasing strain towards an asymptotic value. The curves for the slower rates of strain provide similar limiting forces but these occur at lower imposed strains. These features were observed for all values of initial length and rate of strain. Another feature which can clearly be seen in Figure 5.12, for strain rates of 1 and 2 mm/min, is that values of gradient seem to decrease slightly up to strains of 0.01 and then begin to increase. The same effect also exists to a lesser extent in the curve for 5mm/min but is absent for the highest rate of extension.

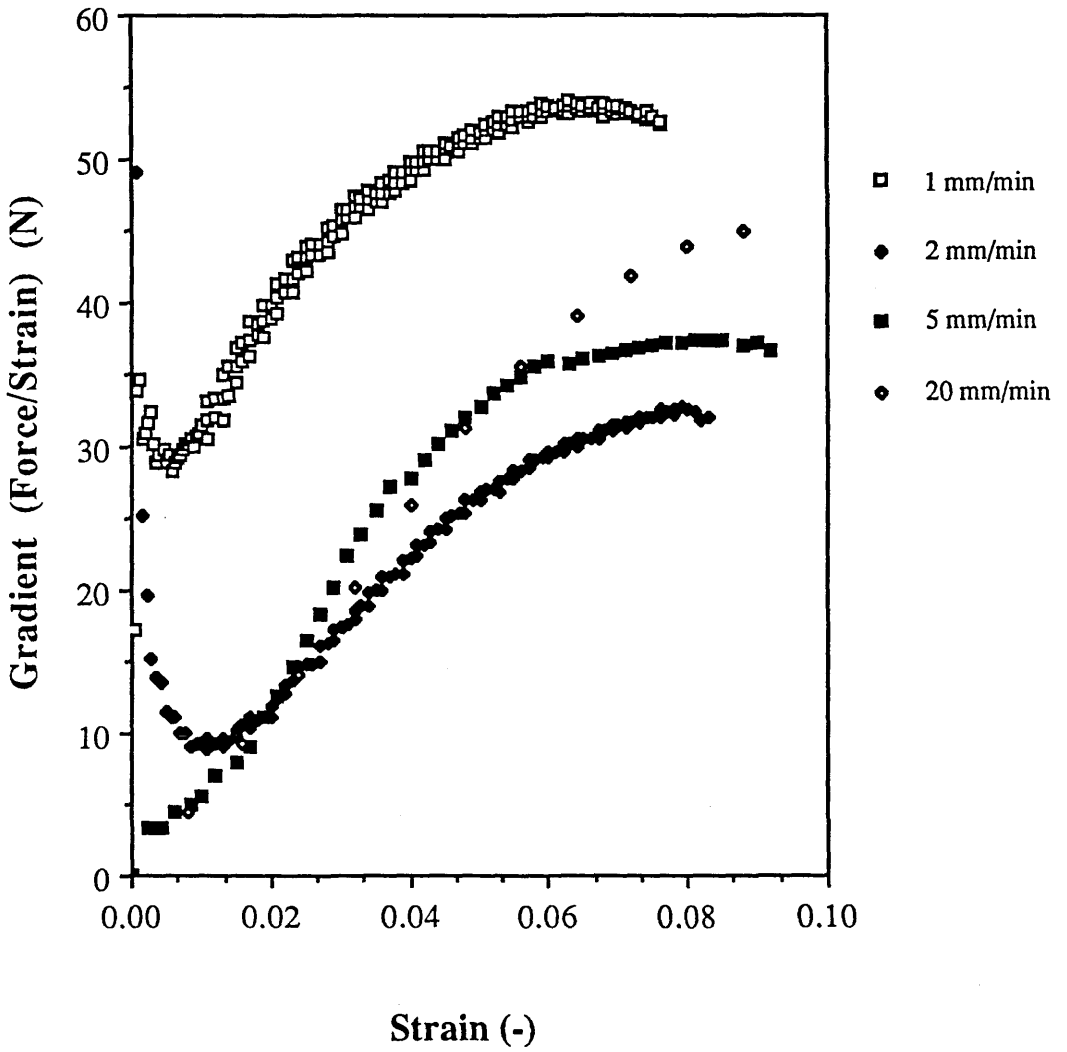

Figure 5.12 Variation of the point to point tensile modulus (force/strain) of untreated cotton yarns with strain and the rate of strain.

Figure 5.13 shows the force-strain profile of the cotton yarns treated by the methods described earlier. These profiles correspond to the averages of 3-5 experiments in each case and with gauge lengths of 20-25 mm. From these figures, the effect of the various treatments may be identified. The three most obvious variable features that may be identified are the breaking force, the breaking strain and the modulus. The averaged values of these three parameters for the different treatments are given in Table 5.4. As far as the breaking strength is concerned, all the treatments, except the wet (water) yarn, have caused the modified yarn to be weaker than the untreated yarn. The increased strength of the wet (water) cotton yarn over the untreated one is expected and was discussed in chapter 2. The constituents of the yarn, i.e. cotton fibres, exhibit increased strength when wet and this translates itself to the assembly making the yarn stronger; in this case by around 10%. The wet (water) cotton yarn has also sustained a greater strain than the untreated yarn; approx. 40%. This may be explained simply in view of the fact that the water penetrates between the fibres and lubricates the contacts. Hence the fibres can slide over each other more readily and thus the yarn is able to accommodate more strain prior to rupture. Also for the wet (water) yarn, the force required to produce a given strain, i.e. the modulus, is lower. This again can be explained in terms of the lubricating action of the water. In this case less force is required to straighten and slide fibres passed each other.

The PDMS and tetradecane treatments seemed to have had no significant effect on breaking strain, while treatment with CTAB solution has had the effect of decreasing the breaking strain by as much as 30%. Treatment with the surfactant however has decreased the breaking strength by approx. 35%, which is less than the reduction by the 1% PDMS, 5% PDMS and tetradecane treatment which have reduced the strength by 73%, 68% and 63% respectively.

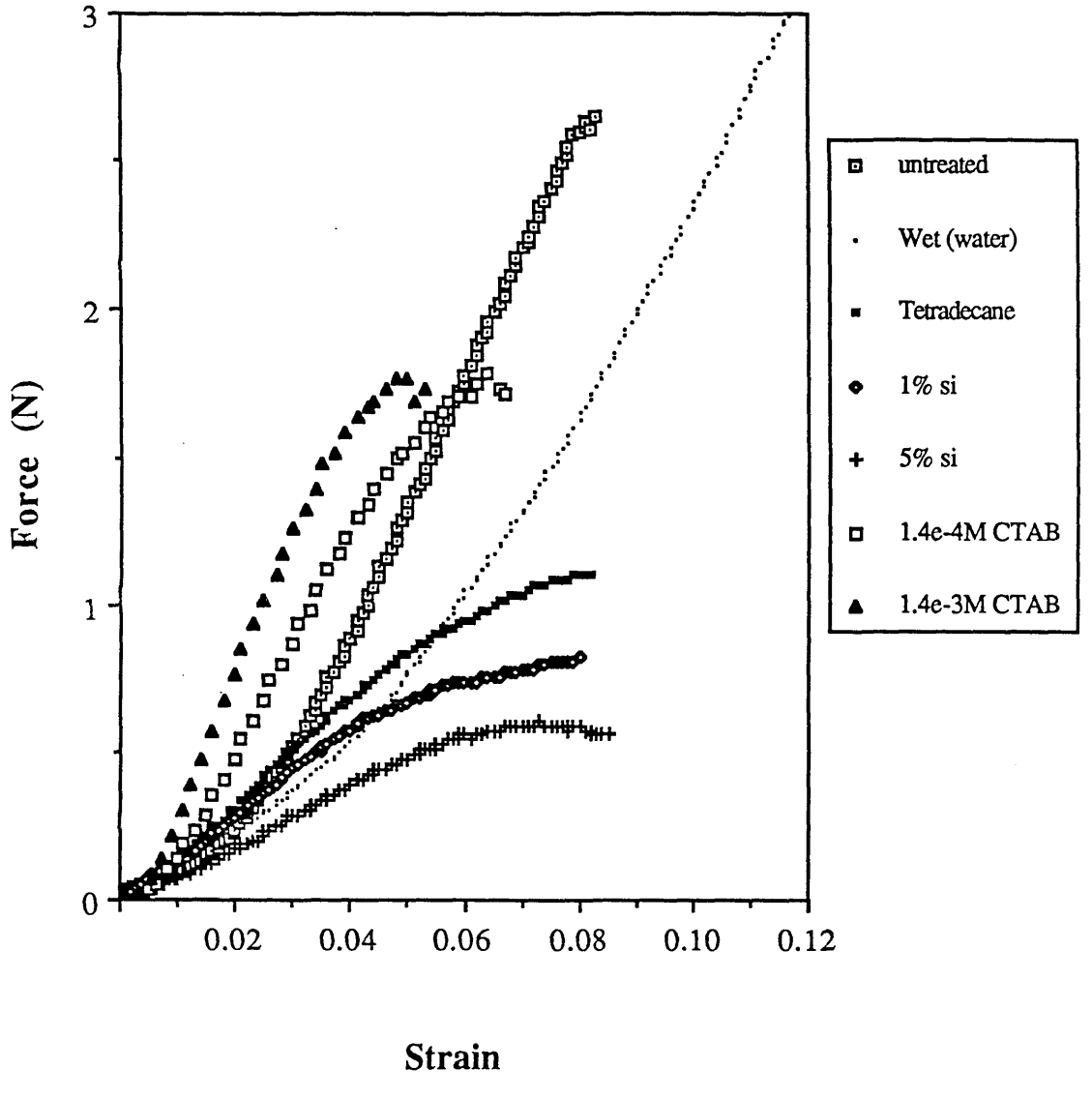

Figure 5.13 Comparison of the force-strain character of treated cotton yarns. The water and tetradecane treated yarns were wet during the experiment while the rest were dry. Average yarn length = 20± 2mm. Rate of strain

TABLE 5.4

Treatments	Modulus (N)	Break force (N)	Break strain
Untreated, dry	43.3	2.653	0.083
Water, wet	35.1	2.99	0.117
Tetradecane, wet	16.04	0.98	0.084
1% Si, dry	16.27	0.706	0.072
5% Si, dry	15.45	0.86	0.084
$1.4x10^{-4}$ M CTAB, dry	39.25	1.672	0.058
$1.4x10^{-3}$ M CTAB, dry	42.98	1.809	0.064

The tetradecane treatment reduced the modulus (for the straight portion of the curve) from that of the untreated yarn by 63%, the 1% PDMS treatment by 62% and 5% PDMS treatment by over 67%. These reductions can again be attributed to the interfibre lubrication action of these materials which results in the expenditure of less force or energy for a given strain.

In the case of the CTAB treated yarns, the modulus seems to have remained close to the untreated yarn modulus for both solution concentrations. This fact is more apparent in table 5.4.

Figure 5.14 depicts the force-strain character of the aramid 1 and 2 yarns. Aramid 1 is seen to be both stronger and stiffer, these features being represented by the breaking forces and the gradient of the force-displacement curves respectively. Table 5.5 compares the parameters associated with the force-strain curve of the three aramid 1 yarns. The unexpected result is the reduction in the modulus of the cleaned aramid 1 relative to the untreated yarn. One would expect the cleaned yarn to exhibit a higher modulus since inter filament friction is expected to have increased.

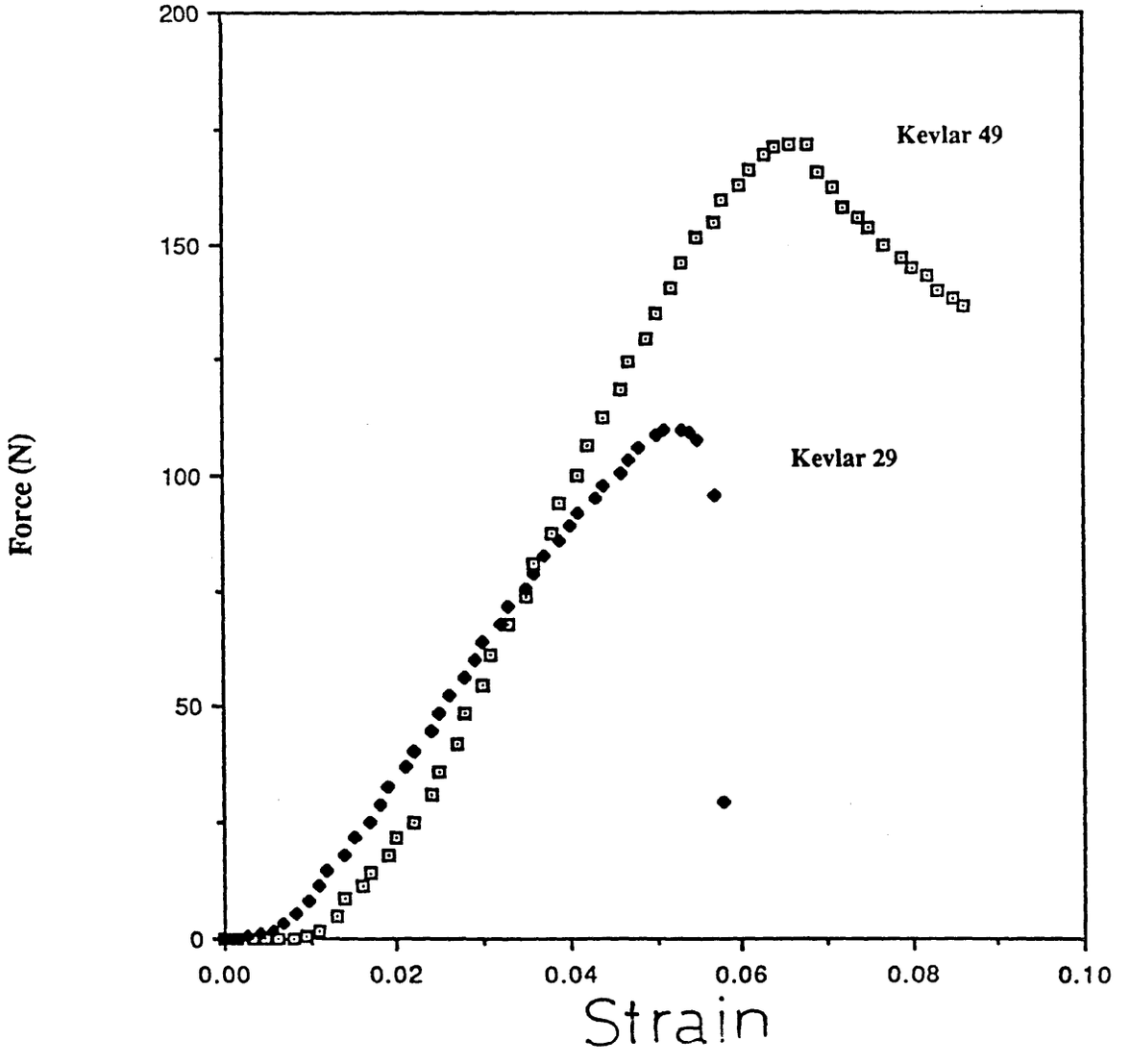

Figure 5.14 Force-strain character of as received Aramid (Kevlar 29 and 49) yarns. The experiment was taken beyond the point of failure. Yarn length = 20 ± 2mm, strain rate = 10% per minute.

TABLE 5.5

Aramid 1 yarns	Modulus (N)	Break force (N)	Break strain
As received	3112	178.8	0.07
Soxlet extracted	2329		
5% PDMS	1929		

The influence of interfilament friction on yarn tensile properties will be used more extensively in later chapters to explain some of the experimental observations.

5.5 The "hardness" Experiments

This series of experiments involved pushing an indentor into a supported fabric. The principle of this type of experiment is somewhat similar to the indentation hardness of metals and polymers, extensively investigated by many workers including Atkins & Tabor (1965) and Johnson (1985). The system of fibre assemblies investigated here are somewhat different in that it is difficult, to investigate the hardness of fabrics (hardness defined as load/area of deformation) because firstly on removal of the load, the deformation is almost totally recovered. Secondly, the deformation is almost never confined to one side of the fabric due to the very thin structure of the assembly. The whole assembly is seen to deform in the fashion of a point loaded membrane or plate.

A satisfactory means of characterising the load-deformation behaviour of fabrics is to use the stress-strain characteristics of thin plates. This is discussed in chapter 6. Here is outlined a series of experiments that were performed on woven cotton and aramid 1 fabrics (same fabrics as in the pull-out test, see later). Figure 5.15 shows a photograph of the experimental arrangement used to perform these experiments. The fabrics were held horizontally between two circular mild steel

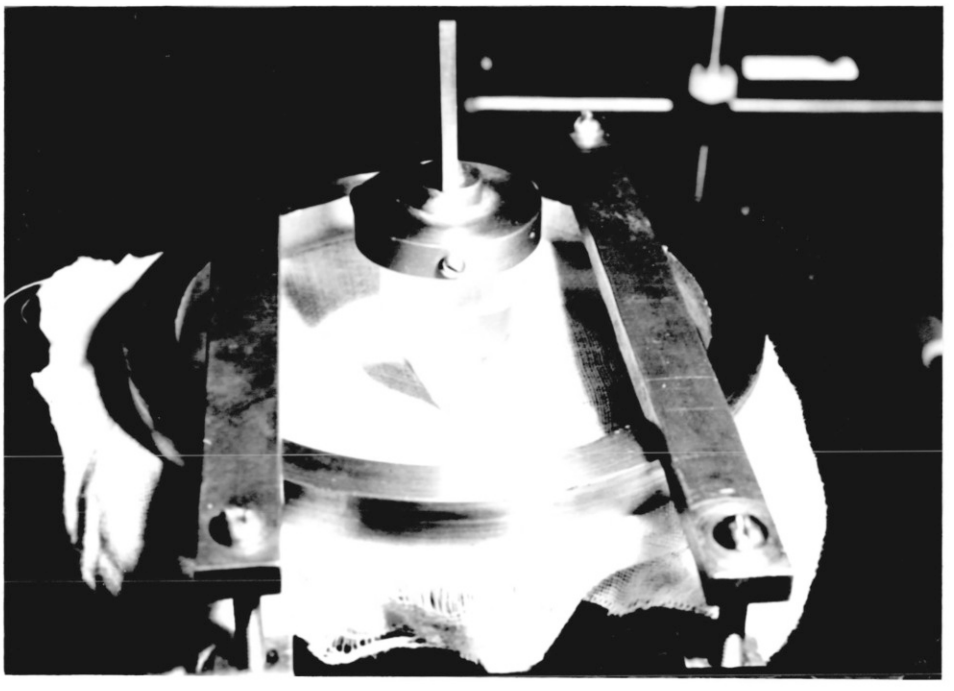

Figure 5.15 Photograph of the "hardness" experimental apparatus.

holders. The bottom holder was screwed to two metal pillars which were attached to the static bottom platen of an Instron tensiometer (Instron 1122). The tension in the weft yarns of the fabric was controlled by applying loads to one side of the fabric passing over a PTFE roller, while the other side was securely clamped. The indentors, of various sizes and shapes, were connected directly or through a special holder to the grip that was attached to the upper movable plate of the Instron. The small conical indentors used were made of stainless steel, diameter 3.2 mm and possessing the following angles, conical tips (60^{o}, 90^{o}, 120^{o}, 150^{o}included angle) and also spherical and flat tips. The large conical indentors were constructed from perspex, diameter 25.4 mm and angles 60°, 120°; spherical indentors were also used.

The experimental procedure was as follows. The indentor was brought down so that its tip just touched the surface of the fabric. The cross head speed was then set and the indentor was caused to move vertically downwards into the tightly held fabric. The force exerted and the time of travel corresponding to the vertical distance traversed were recorded by a micro computer. The force measuring and recording systems were those used in the tensile experiments described previously.

In the case of large indentors, the deformation foot print could clearly be seen on the under side of the fabric. Observations showed that the deformation zone was not circular, as one might have expected, but was similar to the type of plastic deformation that would be produced by a Knoop indentor, Tabor (1970). For the cotton fabrics the deformation was assymetric with the longer axis along the warp yarns, Figure 6.3. This meant that the contact zone (zone of contact between indentor and fabric) was not circular but took on a distorted prismatic shape. The deformation was however symmetrical for the aramid 1 fabrics. The contact cross-sectional area, necessary to calculate hardness, was measured at known indentor vertical displacements by estimating the path of contact by counting the number of cross-overs in contact in the X and Y directions. The projected areas in the plane of the weave at corresponding

vertical heights were then calculated assuming the distorted shape to be a parallelogram. The effect of cone angle on the force displacement characteristics and contact area was investigated. The effect of size of the fabric holder was also investigated using holders of internal diameters 100 and 180 mm.

Using the 100 mm ID holder, force-displacement curves were obtained for cotton fabrics treated with the following: 5% w/w solution of PDMS in petroleum spirit, solution of $1.4x10^{-4}$, $1.4x10^{-3}$ and $2.7x10^{-3}$ M CTAB in distilled water. The experiments were performed on dry fabrics after they had been treated for 2 hours in the solutions at $22 \pm 2^{o}C$. Again, cones of 60^{o} and 120^{o} were used.

The effect of side tension on the force-displacement profile and contact area of cotton fabrics was also investigated. Using the 100 mm ID holder and the 120^{o} cone, loads of 0.5,1.76, 4.12 and 6.5 N were applied to the weft yarns and the force-displacement profile and the contact areas were measured.

Small indentors were only used with cotton fabrics due to the relative sizes of the indentor and the fabric's thread spacing. In this case force-displacement profiles were recorded as well as the force required to penetrate the fabric. Also after penetration had occurred, the friction between the cylindrical body of the indentor and that of the contacting yarns was measured as a function of vertical distance or time.

The cross-head speed during all the above experiments was fixed at 5mm/min. Also all the experiments except those at various side tensions, were performed at a controlled side tension of 4.12 N and a holder of 0.1m diameter. A summary of the variables studied is given in Table 5.6.

TABLE 5.6 Operating Variables in the "hardness" Experiments

	(1) Large Cones Angle	(2) Small Cones Angle	(3) Side Tension (N)	(4) Holder dia. (ID m)
MIN value	60°	45°	0.5	0.1
MAX value	150°	180°	6.5	0.18
Standard value	60° & 120°	-	4.12	0.1

FABRICS	Variables Studied
cotton (untreated)	1, 2, 3, 4
Cotton (5% PDMS)	1
Cotton (CTAB)	1
Aramid 1 (as received)	1
Aramid 1 (Soxlet extracted)	1
Aramid 1 (5% PDMS)	1

5.6 The Ballistic impact experiments

The high speed impact experiments consisted of two separate parts; high speed photographic studies of the deformed fabric were undertaken and also measurement were made of the impact and residual velocities. These studies will be described under separate headings. The fabrics used were as received aramid 1, soxlet extracted aramid 1 and aramid 1 treated with 5% PDMS. Single layers of fabric were used. Cotton fabrics could not be used due to their relatively low ballistic strength.

5.6.1 The Measurement of Projectile Velocity

Figure 5.16 shows a photograph of the high speed impact apparatus and Figure 5.17 is a schematic representation of the experimental arrangement. The apparatus mainly consisted of two parts: a section which drove the projectile, a ball bearing, at

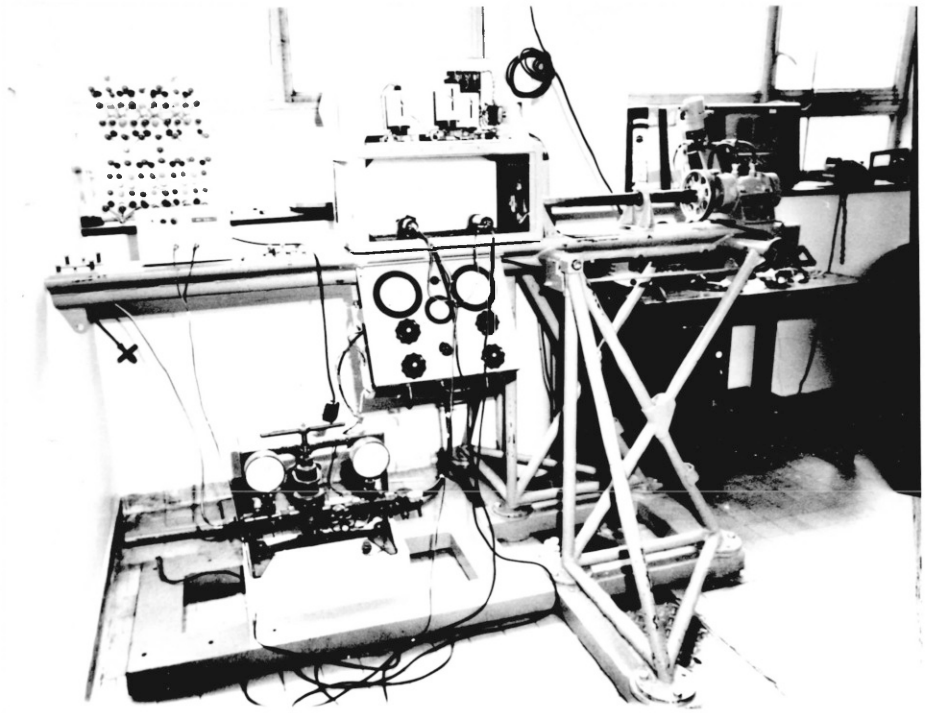

Figure 5.16 Photograph of the high speed gas gun.

Figure 5.17 Schematic diagram of the high speed impact arrangement showing the gas gun and the steel protective chamber together with the associated velocity measuring and photography equipment.

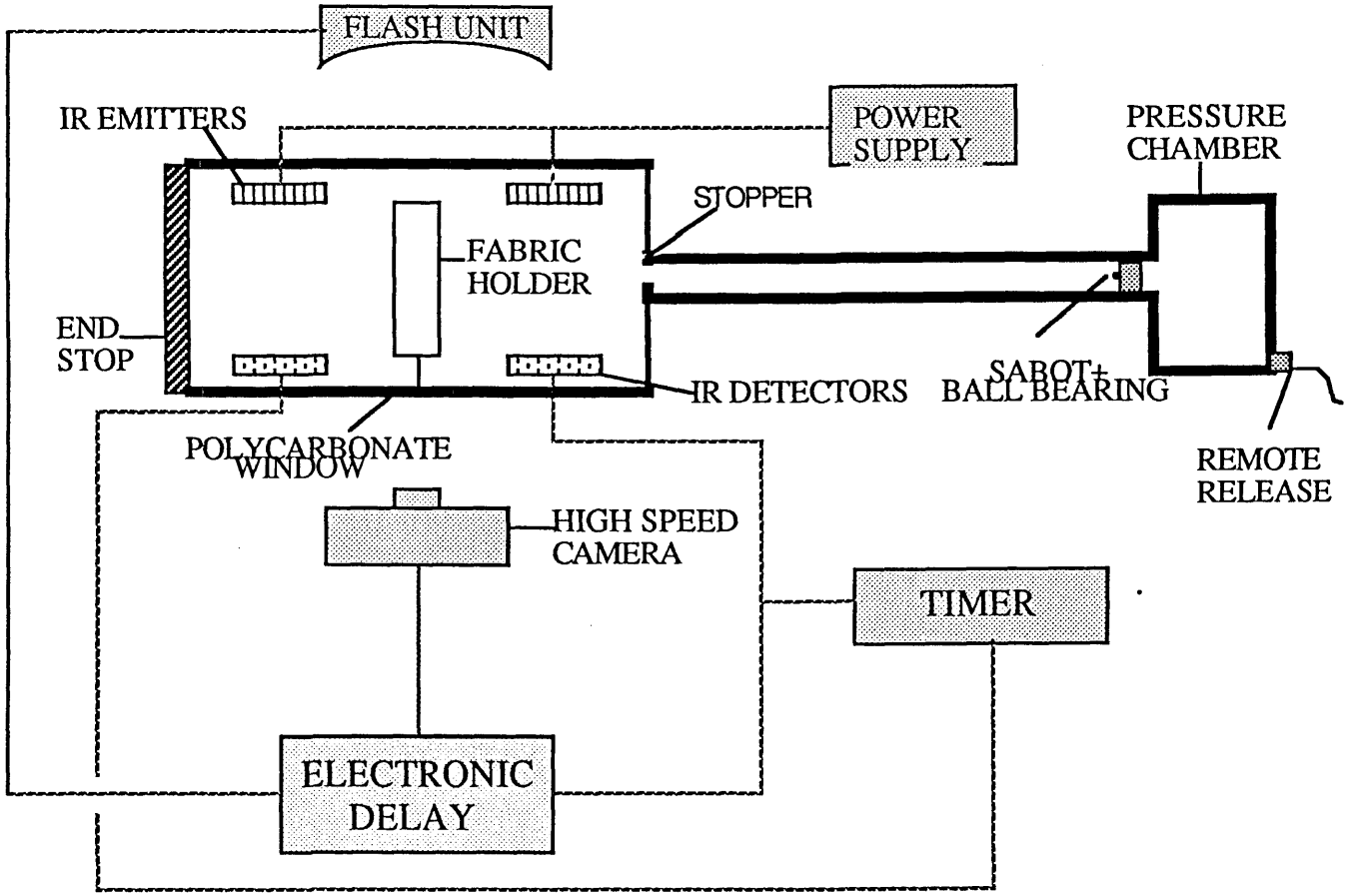

the required speed and another section which contained the fabric and the velocity measuring devices. The first part included a gas pressure chamber, a 25.4mm diameter barrel and a stopper at the end of the barrel containing a hole just under 25.4mm diameter. Figure 5.18 shows the relationship between the projectile velocity and the gas pressure in the chamber. The projectile velocities were found to be quite consistent at a particular pressure.

The second part, which was enclosed within a protective steel box with two polycarbonate windows for the purpose of photography, contained the fabric, the fabric holder and two pairs of infra red emitters and sensors. The sensors were connected to a digital storage oscilloscope (Gould OS 4000) for projectile velocity measurement. In these experiments the high speed camera and the associated flash unit and electronics were not used. The projectiles, stainless steel ball bearings (6.35mm diameter) which were cleaned with dichloroethane to remove surface grease, were placed inside a hole at one end of a 25.4mm diameter HDPE (high density polyethylene) sabot and positioned at the right hand end (figure 5.17) of the barrel nearest to the pressure chamber.

The fabric was clamped in a circular fabric holder (100mm diameter) and positioned in the middle of the two sets of sensors. The chamber was then pressurised to the desired pressure from a nitrogen cylinder (150 to 800 psi). The pressure was released remotely. The sabot travelled down the barrel where on impact with the stopper the sabot was arrested and the projectile travelled towards the fabric crossing over the circuits which triggered the CRO. The impact and exit velocities, if in fact the projectile penetrated the fabric, were then recorded. A series of experiments were conducted in this way using impact velocities ranging from 100-250 m/s.

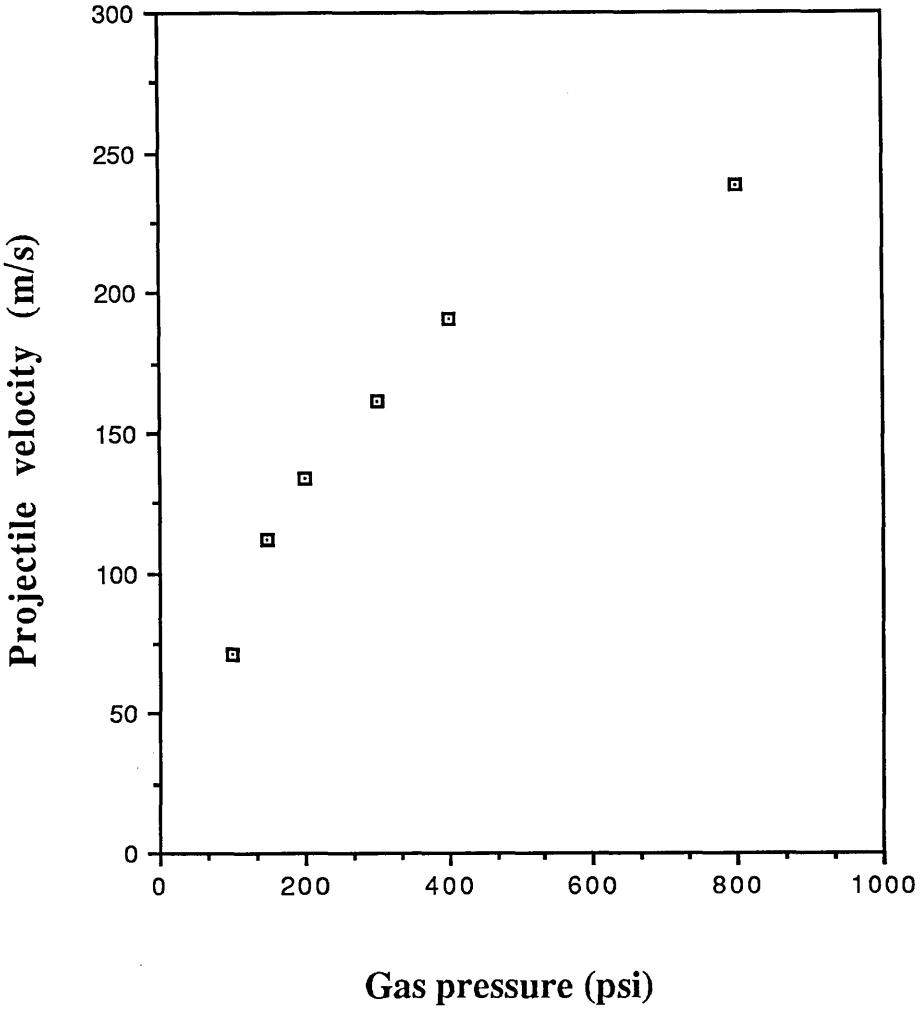

Figure 5.18 Projectile velocity in the ballistic experiments as a function of gas pressure in the gas gun.

5.6.2 The High Speed Photography of the Impact Process

Figure 5.17 shows the schematic arrangement of the camera and the associated electronics. The high speed photography was carried out using an Imecon camera (Hadland Photonics 790) in conjunction with an electronic delay and a flash unit. The camera was set at 2.5×10^4 frames per second of which about 10 frames appeared on the "Polaroid" film capturing the action at 40μs intervals. As the projectile passed over the first sensor in the first pair, the electronic delay was activated to trigger the flash and the camera. The settings on the delay were adjusted according to the projectile speed which depended on the pressure in the chamber. In this way a series of photographs of the ballistic impact of the fabrics and the deformation zone as a function of time were taken. These experiments were performed for both treated and untreated aramid fabrics and the results are presented in chapter 7.

5.7 The Yarn Pull-Out device

5.7.1 Testing the Untreated Fabrics

The yarn pull-out machine has been described previously, Sebastian *et al* (1986, 1987). The machine consisted of two parts: the force measuring device (FMD) and the optical weave deformation/displacement monitoring system. Figure 5.19 depicts a photograph of the whole arrangement and Figure 5.20 shows a photograph of the force measuring device. The FMD and the optics were enclosed in a perspex chamber where the temperature and humidity could be controlled. The temperature of the chamber during all the pull-out tests was maintained constant at $22 \pm 2^{o}C$ using a mercury bulb contact thermometer. The relative humidity of the chamber was also controlled at $45 \pm 5\%$ using a saturated solution of potassium carbonate

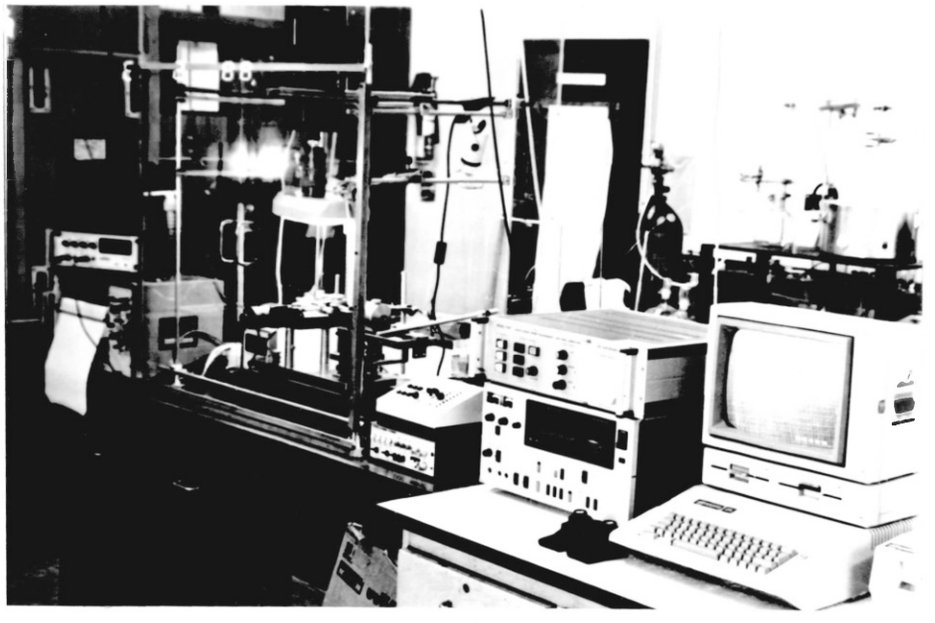

Figure 5.19 Photograph of the apparatus used in the pull-out experiments including the enclosed chamber containing the force measuring device, and the video recording measurement facilities.

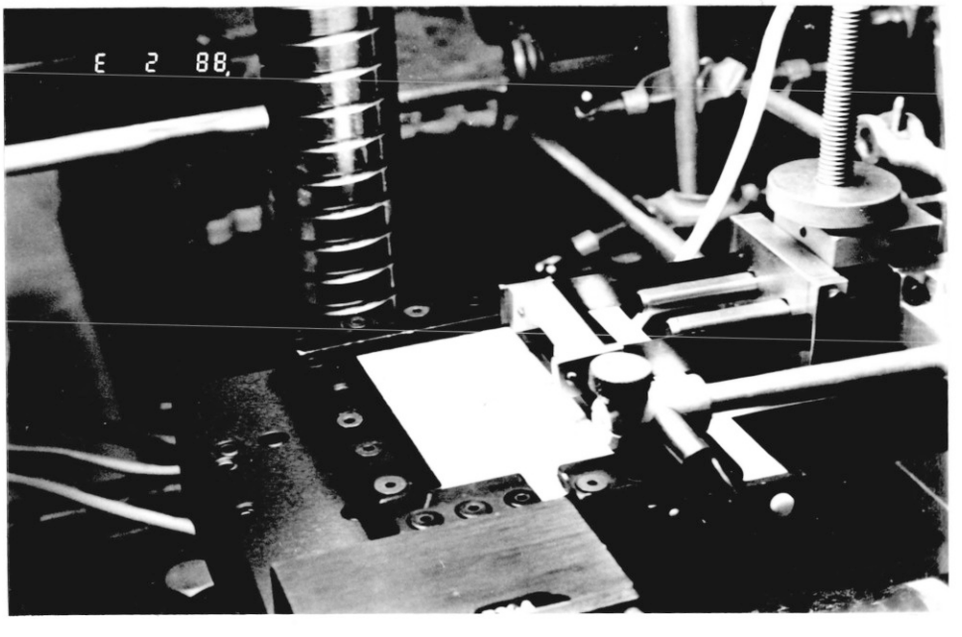

Figure 5.20 Photograph of the force measuring device showing the clamped fabric, in the movable stage, the hook, the phosphur bronze springs and the linear displacement transducer.

($K_2CO_3.2H_2O$) which yielded a relative humidity of 43% for temperatures between 20-25°C in a closed chamber.

The force measuring device consisted of a lower and an upper part. The lower part was a movable stage attached to a stepper motor (manufactured by Aerotech Inc., USA) which drove the stage horizontally. The speed of the stepper motor was adjustable. A piece of fabric was clamped horizontally onto the stage using four stiff rubber clamps.

Connected to the lower part was a simple system by which the tension of the cross-over yarn was controlled and varied. It consisted of a PTFE roller connected to the side of the stage. A fabric of size 15 x 10 cm was clamped at one end and hung over the roller at the other end. To this end was connected another clamp that extended the length of the fabric using selected weights which were attached to this clamp. The weight was applied to the cross-over yarns (weft yarns) for about 5 minutes and then the other sides of the fabric were clamped. The pull-out experiment was then performed immediately to minimise stress relaxation in the fabric. The weights or side tensions applied were varied from 0-6.5 N. The stage velocity was kept constant throughout all the experiments at 2.9 mm/min.

Figure 5.2 is a line drawing of the upper part of the force measuring device. It consisted of two thin phosphor-bronze springs (B) of equal size and thickness. The effective length and hence the flexibility or sensitivity of the springs to the applied force could be varied by positioning the slider D as required. Also, larger forces could be sensed by using thicker springs possessing smaller compliances. A typical value for the compliance of the springs, obtained by measuring the displacement of the hook (k) with a known applied force, was $5x10^{-3}$ m/N. The two springs were firmly fixed to a metal frame using the clamps (C). The ends of the springs which were free to move were attached to a metal frame (A), to which the hook (k) was connected. The

horizontal movement of the spring system was monitored by a linear displacement transducer (Sangamo Transducers) which was calibrated previously using known forces. The signal from the transducer was amplified by a signal amplifier (Sangamo, Gemini) and fed to a chart recorder.

The experimental procedure for a typical experiment was as follows. After the fabric was clamped in position, a single warp yarn from the fabric was chosen such that it was positioned directly below and in line with the hook (k). It should be noted that in all tests on cotton the warp yarn was chosen as the pull-out yarn and side tensions were applied to the weft yarns. One end of the chosen yarn was then cut and tied to the hook. The other end was also cut so as to leave a yarn of such a length that it crossed an arbitrary 20 weft yarns. 20 cross-over or junctions were arbitrarily chosen because this number produced satisfactory and easily measurable forces and deformation characteristics. The stage was then set into motion and the yarn pulled out of the weave.

Directly above the stage was placed a high resolution black and white television camera (National Panasonic WV-1800/B) fitted with a Cannon zoom lens, in such a way that the entire pull-out process could be recorded. Illumination of the fabric was achieved using a 40 W circular fluorescent tube. The output from the camera was fed to a video timer (For-A co., VIG-33F) where the lapsed time (1/10 sec increments) was superimposed onto each frame. The output from the timer was recorded on magnetic tape using a professional video recorder (Sony U-matic VO-5630). Recording the experiment enabled the subsequent freezing of the pictures for the analysis of the deformation patterns. The hardware involved for this purpose comprised of an Apple IIe computer and paddles, a TV monitor, a time base corrector and synchroniser (CEL Electronics Model P147), and an electronic programmer (Viscount 1107, Canada). The use of the timer enabled the recorded pictures to be related in real time to the force measurements on the chart recorder. Figure 5.21 shows

the schematic arrangement of this apparatus.

By employing the appropriate software it was possible to digitise the location of a cross wire onto the TV screen into X and Y coordinates. The signal from the computer and that from the video recorder were synchronised and stabilised in the time base corrector. These signals were then electronically mixed in the electronic programmer and appeared on the TV monitor.

The accuracy of the location of the cross-wire depended on the magnification of the image. However, in the case of experiments with dry cotton, the effective resolution was approximately 0.05mm. The two paddles enable the movement of the cross wire across the screen to this level of spatial precision.

The procedure described above was used on dry untreated cotton fabric and the effect of side tension was examined. The same procedure was used for dry, untreated aramid and the effect of the number of contact junctions on frictional force as well as the effect of varying the side tension were examined. Two types of weaves for the untreated aramid were examined, a simple weave of aramid 2 which was several years old and a "new" twill fabric of aramid 1. The effect of side tension was only examined on the aramid 1 fabric and the simple weave aramid 2 was only studied at nominally zero lateral or side tension.

5.7.2 The Pull-out Test on Treated Fabrics

Two different kinds of experiments are now described. Experiments were performed with the fabric totally submerged under the treating liquid. In addition, experiments were also performed on fabrics of cotton or aramid 1 that had undergone treatment and were subsequently dried. The former was only performed on cotton fabrics.

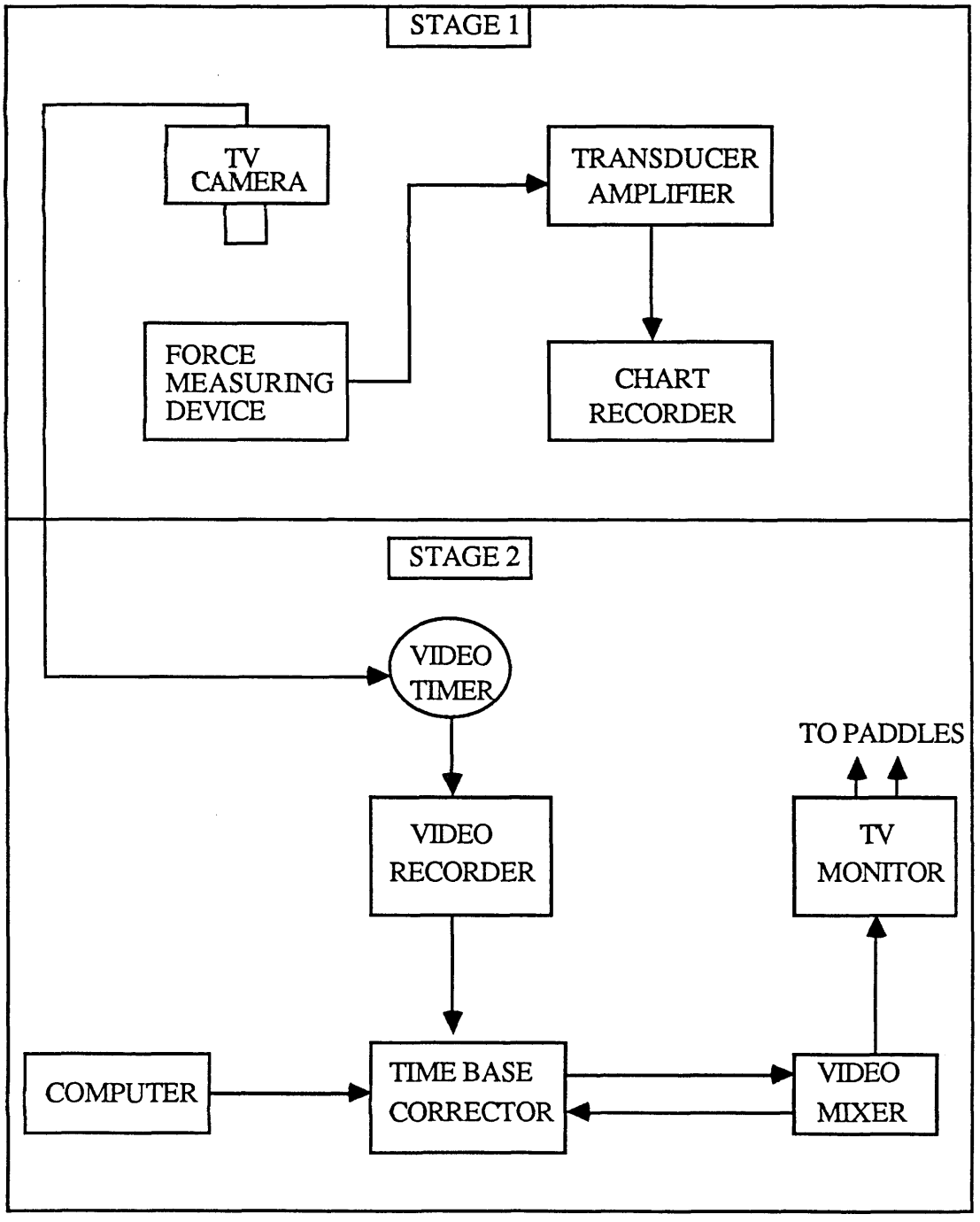

Figure 5.21 Schematic diagram of the set up used to measure the force and video record the deformation of the fabric matrix during the pull-out experiment.

5.7.2.1 The submerged fabric technique

The experimental arrangement was exactly the same as that used for the untreated dry fabrics, except the movable stage was adapted so that the pull-out test could be performed on submerged fabrics. This was achieved by using 3 slim rectangular pieces of transparent plastic (perspex) which fitted on top of each other. Two out of three had large rectangular holes in the centre. The piece without the hole (~ 3mm thick) was screwed to the movable stage. A cotton fabric of size about 10x7 cm was sandwiched between the two pieces with the holes (about 6mm and 3mm respectively) and screwed down to the first piece. In this way, a small pool was created with the fabric hanging 6mm above the bottom and 3mm below the top of the chamber. The liquid was then poured into the cavity, covering the fabric totally. Leaks were prevented by introducing thin deformable plastic sheets between the perspex pieces.

The intrinsic design of the above prevented the control of side tension as previously described. This was achieved by using a stainless steel rod of dia. 5mm and weight 56 g formed into a rectangle that fitted inside the rectangular hole of the top perspex piece and rested on the outer edges of the fabric. In this way, the same amount of constant tension was put on all yarns making them taut. The temperature in these systems were again controlled to $22 \pm 2^{o}C$.

Cotton fabrics were submerged under four different liquids or solutions under varying conditions and the results were compared with both the untreated case and each other. It should be pointed out that the experiments on the untreated fabric in the adapted system were also carried out, as standards for comparison.

Cotton fabrics were immersed under water for 0.5, 2, 5 and 23 hours prior to the pull-out experiment. The alkane n-tetradecane ($CH_3.(CH_2)_{12}.CH_3$, mol. wt. 198.39, min. assay 99%), was also used for 0.5 and 2 hours. The cotton fabrics were

also submerged under a solution of stearic acid in n-tetradecane at concentrations of 0.1 and 0.2% w/w. In this case the solution temperature had to be raised to dissolve all the stearic acid in the tetradecane. The fabrics were equilibrated in the solutions for 0.5 hour prior to experimentation. Also, a $4.5x10^{-4}$ M solution of CTAB was used for 2 hours prior to the pull-out experiment.

In this series of experiments the velocity of the stage was again 2.9mm/min. At this low velocity there was no sign of the liquid being disturbed by the movement of the stage. Also, the effect of the liquid surface tension on the hook and the transducer were minimal.

5.7.2.2. The dry treated fabric technique

This series of experiments were performed both on the cotton and the aramid fabrics. The cotton fabrics were studied in the adapted form of the yarn pull-out machine and the influence of tension was not studied. The influence of PDMS and CTAB at various solution concentrations were also studied. The cotton fabric was immersed in a solution of PDMS of viscosity 100 cp in petroleum spirit at varying concentrations of 2, 3, 5, 7, 10% w/w, for 2 hours. More information on the properties of these fluids are given by Panesar (1986). The fabric was then taken out of solution and drip-dried in air for 30 min. during which time all of the solvent evaporated. A similar procedure was adopted for the CTAB where solutions of CTAB in distilled water of molarities $1.37x10^{-4}$, $1.37x10^{-3}$ and $2.74x10^{-3}$ M were used. These treatments were performed in a closed dish and the dish was kept in a closed chamber at a temperature of $22 \pm 2^{o}C$ for the entire period of the treatment. The fabric was then drip-dried overnight in the closed chamber where temperature and humidity were controlled throughout the drying process. The unwashed aramid 1 was treated

with 5% w/w PDMS. The aramid 1 was also washed (Soxlet extracted with acetone) in order to remove the surface finishes. The washed aramid 1 was then treated with a solution of 5% PDMS in petroleum spirit and also tested.

5.8 The Vertical Micro-Discplacement Measurements

In the pull-out experiment described in the previous section, the position of the hook to which one end of the chosen yarn was tied was set approximately 4mm above the undistorted plane of the fabric. This produced a distortion in the weave that was very similar to that obtained in the "hardness" and the ballistic experiments. It was also an experimental requirement to avoid the distortion of the weave ahead of the pulled yarn fixture point. This meant that during the experiment, the yarn tied to the hook entered the weave at approx. 22° at the start of the experiment and 10° at the end when the yarn was almost totally pulled out of the matrix. A range of experiments were performed to investigate the effect of this angle on the measured force. Angles of 10, 20 and 30° were chosen and the corresponding forces measured. No significant difference in the magnitude of the force was observed. Also, the change in pull-out angle did not affect the linear displacement transducer since the transducer only sensed displacements in the horizontal direction; that is in the plane of the fabric.

As mentioned earlier, an important effect of the pull-out angle was to lift the assembly in the vicinity of the pulled yarn, i.e. the cross-over yarns, above the plane of the fabric. This displacement increased in magnitude towards the position of the hook. The phenomenon is depicted schematically in Figure 8.12. This microdiscplacement was shown to have an important bearing on the interpretation of the measured values of yarn and cross-over displacements/extensions and also on yarn migration within the assembly. A powerful microscope (Zeiss) with a movable stage

was used to study these microdisplacements. The cotton fabric (only cotton was used in these experiments) was fixed onto the stage of the microscope with tape. A chosen yarn was cut at both ends and one end was passed over a pulley and connected to an appropriate weight, i.e. 0.05, 0.10 or 0.20 N weights. The pulley was positioned such that the yarn pull-out angle was approx. 20^{o} to the fabric plane. The microscope stage was then moved, without affecting the vertical displacement of the assembly, and the microscope was focussed onto individual tensile and cross-over yarns. The points onto which the microscope was focussed were the tops of the yarns. These points alternated from the tensile to a cross-over yarn respectively. This alternation has an important bearing on the migration phenomenon discussed later. The vertical distance required to focus was measured and the heights of yarns above the unstressed plane of the fabric were measured. These experiments were performed for a constant number of cross-overs. 20, 16 and 15 cross-overs at 0.1 N and 20 cross-overs at 0.05, 0.1 and 0.2 N loads. These experiments were performed on untreated cotton fabrics at $20^{o}C$ and 40% RH.

CHAPTER SIX

INDENTATION OF TEXTILE STRUCTURES

6.1 Introduction

In this chapter the data obtained by what has been described earlier as the "hardness experiment" are presented and discussed. The experimental details are described in Chapter 5. The data in this chapter are intended to serve several purposes. First, these results provide a means of probing fibre and inter-fibre properties at relatively low strains. The pull-out test is most satisfactory for sensing high inter-fibre strains, and is described in Chapter 8. The low strain data analysis (elastic response) is complicated in the pull-out experiments by the out of plane deformations. It will be seen that this deformation produces a nearly pyramidal out of plane deformation at high forces on the pulled yarn. In this chapter similar out of plane deformations are created with an indentor. Thus, we have two reasons to pursue this type of deformation. First, the data may be compared with pull-out data and also the study offers an alternative means of obtaining these data. The latter is the second reason for the study. Finally, chapter 7 describes ballistic studies of fabrics using spherical projectiles. In that chapter the main emphasis will be upon computing the energy dissipated on impact. The hardness studies described in this chapter provide data on the quasi-static analogue and in particular a direct means of investigating the influence of fabric treatments.

The chapter is divided into several parts. The earlier parts deal with the reversible or elastic response of cotton and aramid systems. The major emphasis is upon the description of the main system variables such as fabric pretension, indentor shape and supported fabric area and the contributions of the bending and the stretching

processes to the total deformation. The general form of the force-displacement and force-geometry of deformation characteristics are described. The effects of certain fabric treatments are also presented. These data are treated in the first instance as hardness data, although it is recognised that the analogy with a hardness deformation may be potentially misleading. Also experimentally the concept is not totally applicable to fabrics since it is usually recommended that the depths of penetration should not exceed 1/10 the thickness of the specimen and similarly the diameter of the deformation should not exceed 1/10 of the diameter of the specimen. In the case of this thesis, because of the compliance of the fabrics, the penetration extended a considerable distance beyond the thickness of the fabric. Typically, the cotton fabrics were 0.06mm thick and the penetration distance were 20mm. Also, the diameter of the indentor was typically 25.4mm and that of the specimen was 100mm. However, it was considered to be interesting to see if a fabric behaved in a similar way to a solid under normal planar loading. It should be pointed out that the behaviour of the fabrics under planar loadings are treated in a different and a more realistic manner later.

This approach does however have the advantage that terminology adopted in hardness studies may be used. Also, there are apparent similarities between the current data and bulk hardness data which are subsequently explored. A later section of this chapter develops a plate deformation model which provides a remarkably good description of certain facets of the data to be presented.

The material introduced so far deals primarily with the elastic or reversible response of the chosen system. A short section also considers more extreme levels of penetration similar to those produced in the high force regimes of the pull-out experiment and also during projectile transit in the ballistic experiments.

In summary, this chapter provides a range of data which have implications in the interpretation of the pull-out data and the ballistic data to be described in later chapters.

6.2 Indentation of Untreated Fabrics

6.2.1 Introduction

This section presents the results of the indentation experiments performed on untreated cotton and aramid 1 fabrics. A range of variables have been studied including the effect of side tension, indentor shape or angle and the fabric holder size. The "hardness" values computed are described for the various parameters investigated.

6.2.2 The Response Characteristics of the Cotton Fabrics

6.2.2.1 The effect of weft yarn tension

These experiments were performed to examine whether varying the weft yarn tension had any influence on the force vs vertical displacement distance or force-contact area profile of the fabric. Here, the holder size was 100mm in diameter and the indentor was a perspex cone of angle 120°. Figures 6.1 and 6.2 illustrate the results. Figure 6.1 also shows a typical force-displacement response of a fabric in an indentation experiment. The measured force increases very slowly initially as the penetration is increased. This region is probably associated with the conical indentor penetrating into a small area in the fabric and the uncrimping of the yarns themselves. Observations show that the deformation is in fact elastic since on removal of the force the fabric returns to its original flat shape. As the displacement increases the force suddenly increases rapidly at a particular imposed displacement. At this point the area immediately adjacent to the cone is deformed more extensively. The area of contact is however not at the maximum value. The force-apparent contact area curve has a similar form.

It is observed that the shape of the deformation zone resembles that of a Knoop indentation. The deformation is highly anisotropic along the warp and weft directions with the longer axis along the warp yarns. However, the zone of actual contact

Figure 6.1 Typical force-vertical displacement profiles for untreated cotton fabrics during the "hardness" experiment. The effect of weft yarn tension is seen to be negligible; (120° conical indentor, 100 mm holder diameter).

Figure 6.2 Variation of force with area of indentation for untreated cotton fabrics. The values for different weft yarn tensions fall on the same line.

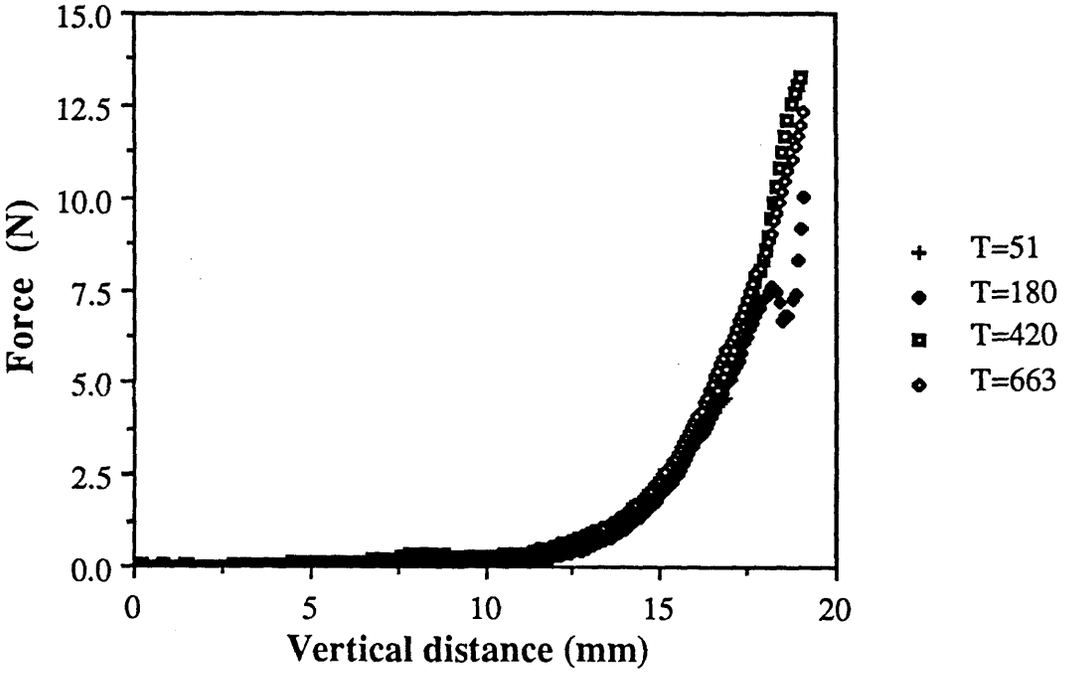
15.0
12.5
10.0
7.5
5.0
2.5
0.0
Force (N)
0
5
10
15
20
Vertical distance (mm)
T=51
T=180
T=420
T=663

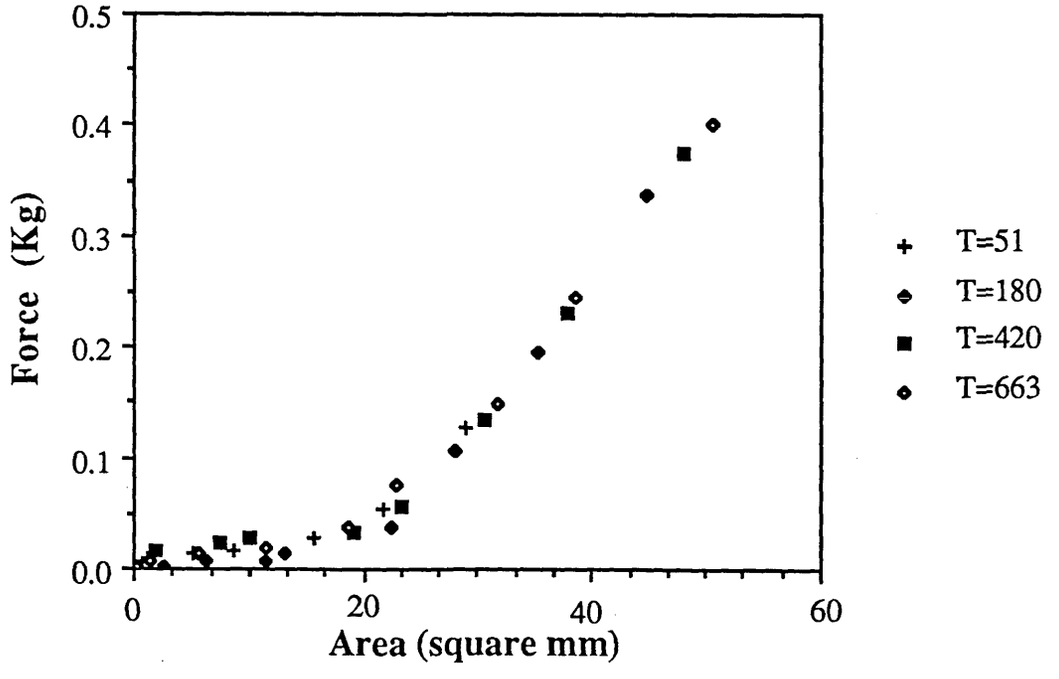
0.5
0.4
0.3
0.2
0.1
0.0
Force (Kg)
0
20
40
60
Area (square mm)
T=51
T=180
T=420
T=663

between the fabric and the cone is transverse in the sense that the fabric makes greater contact with the cone along the weft direction. Figure 6.3 shows a schematic view of this phenomenon. The reason for this anisotropy could be the fact that the fabric is less resistant to bending in the weft direction than in the warp direction. This phenomenon was not observed in the case of the aramid 1 fabric where the yarns in both the warp and weft directions possessed similar flexural rigidities and the deformation zone was symmetrical about the warp and the weft directions.

The contact area was calculated by assuming a rectangular shape deformation, measuring the distances a and b and using Equation 6.1:

$$\text{Area} = 2.a.b.\sin^2\theta \qquad (6.1)$$

where θ = half angle of cone.

The variation of the weft yarn tension was found to have very little effect, if any, on the two profiles; Figures 6.1 and 6.2. This was regarded as surprising since one would have expected the force-normal displacement profile to rise sooner and also more steeply with the increasing of the weft yarn tension. This was not the case and it indicates that the stresses introduced by the indentor are significantly greater than the variations introduced in the side tension.

6.2.2.2 The effect of indentor shape and angle

Two different shapes of indentor were used; spherical indentors and a range of conical indentors of various included angles. The indentors were 25.4mm diameter and made from Perspex. The diameter of the fabric holder was 100mm and the weft yarn tension was 4.12 N. Figure 6.4 shows the force-displacement profile of the fabrics. On the whole it can be seen that for the conical indentors the profile rises

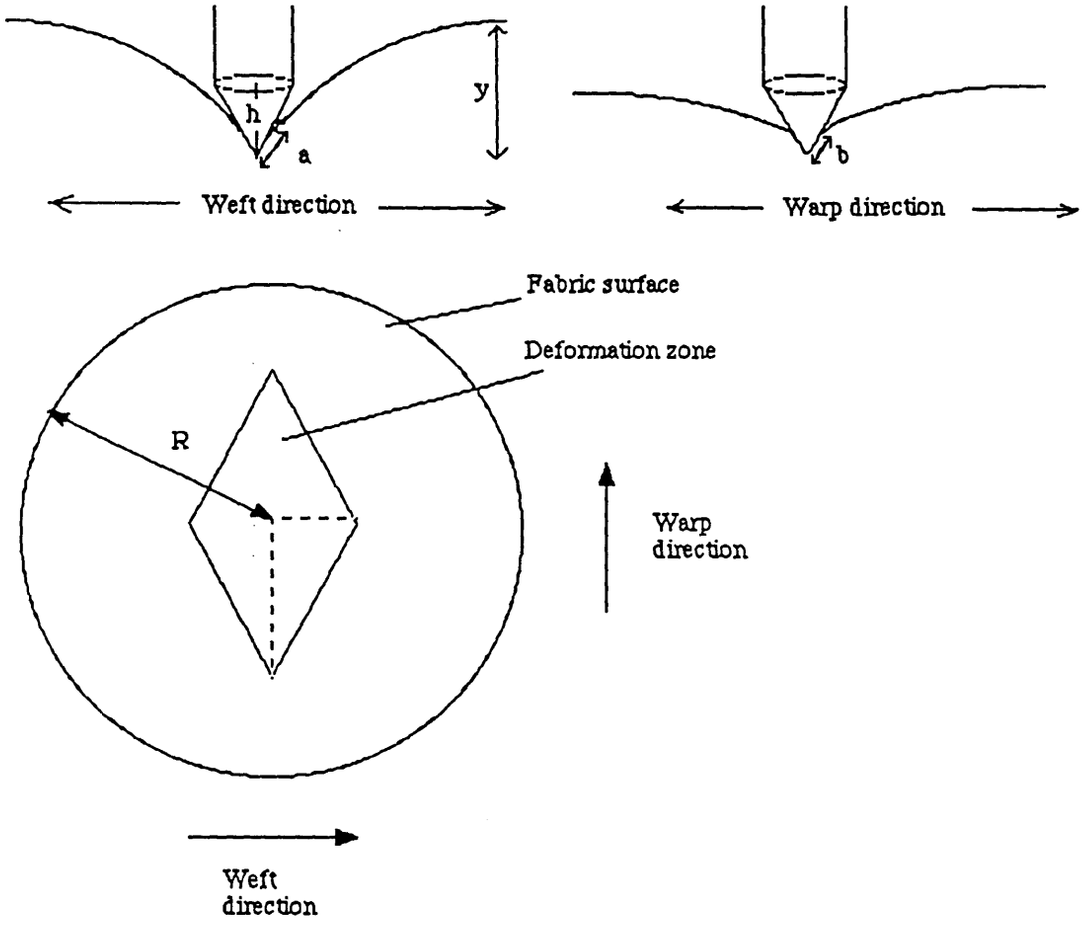

Figure 6.3 Schematic diagram of the deformations produced during fabric indentation. For cotton the deformation zone was asymmetric about the warp and weft directions, while for the Aramid fabrics the deformation zone was symmetrical.

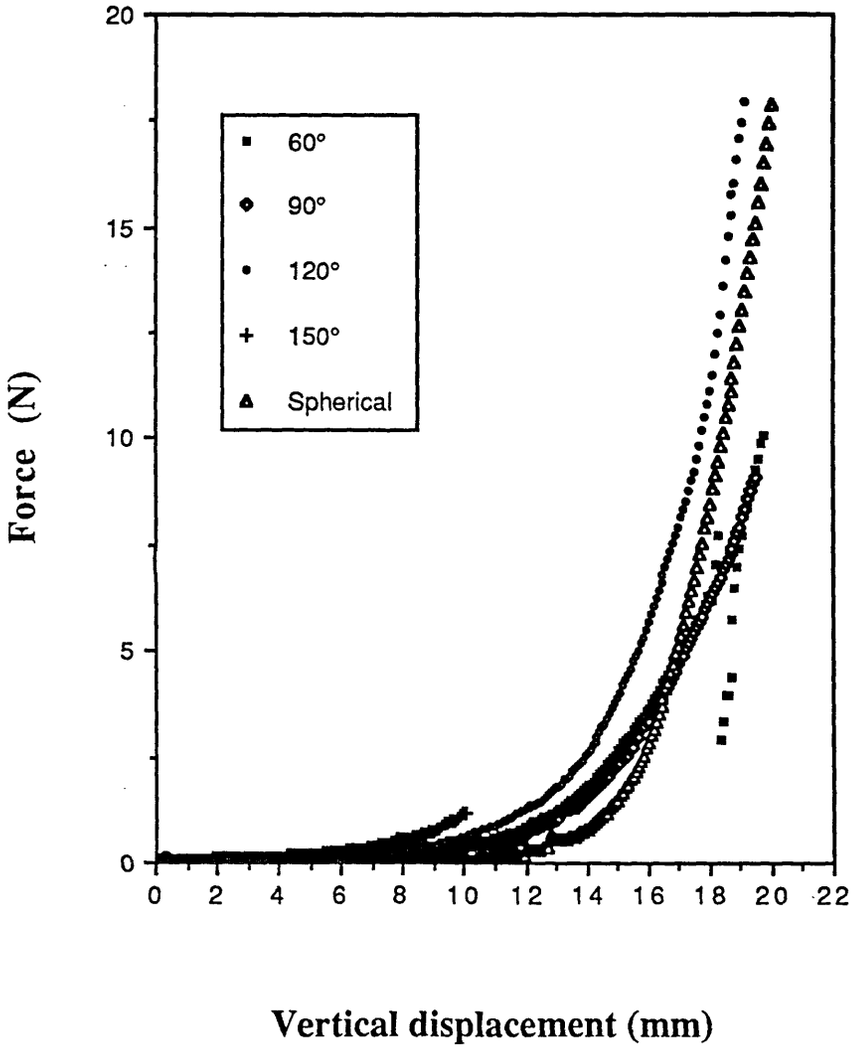

Figure 6.4 Comparison of the response of untreated cotton fabrics to indentors of differing angles in the "hardness" experiments (100 mm holder).

more steeply with the increase with cone angle. The behaviour of the fabric under a spherical indentor is also shown.

The trend in Figure 6.4 may be explained using the results presented in Figure 6.5. In this figure, force is plotted against area at the same vertical displacements. The contact area increases very rapidly with increasing cone angle for comparable applied loads. Hence, the cones with the greatest included angles produce the stiffest response. The gradient of the force against area graphs is a measure of the "hardness" of the material. This aspect of the data is discussed later.

6.2.2.3 The effect of fabric holder size

Two sizes of fabric holder were used, 100mm and 180mm in diameter. The untreated cotton fabrics were tightly clamped around the edges. The weft yarn tension in the case of the 100mm holder was 4.12 N. However, in the case of the 180mm holder, the number of yarns in the weft direction was 1.8 times that of the 100mm fabric, ca. 270 yarns. Thus, in order to maintain a similar tension in the weft yarns, the total load on the weft yarns was increased by 1.8 times to 7.35 N.

Figure 6.6 shows the force-displacement profiles of cotton fabrics using 60° and 120° cones and the 100 and 180mm holders. As before, the resisting force for the 120° cones are higher than those for the 60° cones at a similar displacement value. Also, the curves for the 100mm holder are steeper than those for the 180mm holder. The apparent contact area is much greater for the larger holder at similar force levels, as shown in Figures 6.7 and 6.8. The force-displacement and the force-area profiles are at first sight contradictory since one would expect a greater resistance to penetration of the cone as the contact area increases. This contradiction indicates that the compliance of the whole weave to normal penetration is very sensitive to the total size

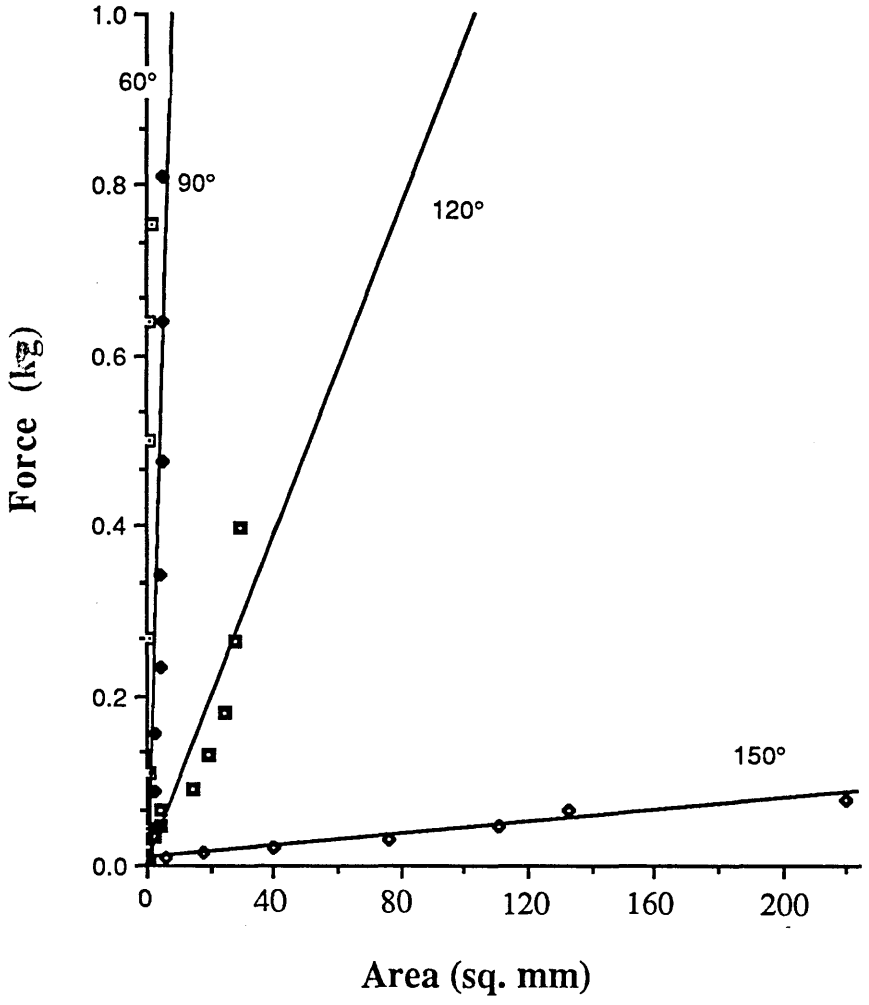

Figure 6.5 Force and area of deformation of untreated cotton fabrics as a function of the angle of the indentor.

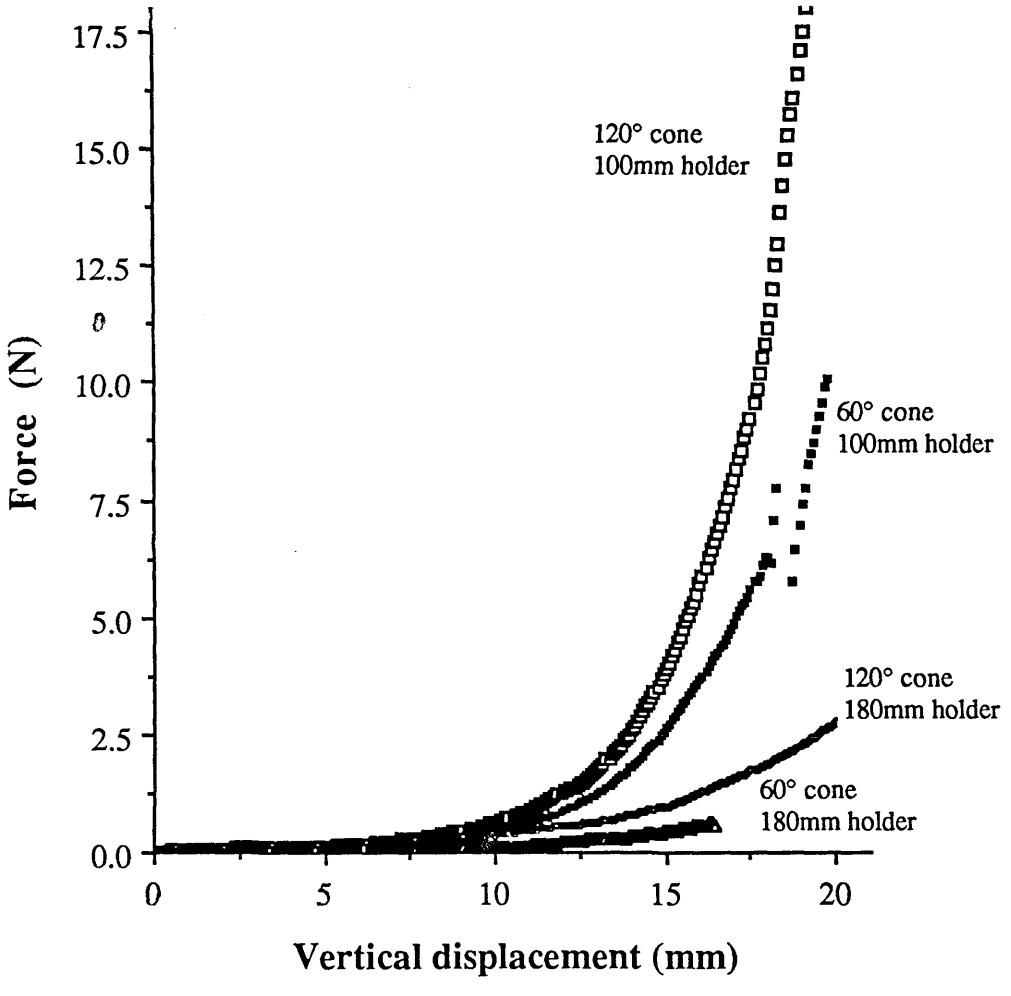

Figure 6.6 The response of untreated cotton fabrics of different diameters to indentation by 60° and 120° conical indentors. The fabric with the larger diameter is seen to be more compliant.

Figure 6.7 The effect of fabric holder diameter on the deformation zone area of untreated cotton fabrics using 60° conical indentors.

Figure 6.8 Force and area of deformation of untreated cotton fabrics as a function of fabric holder size using 120° conical indentor.

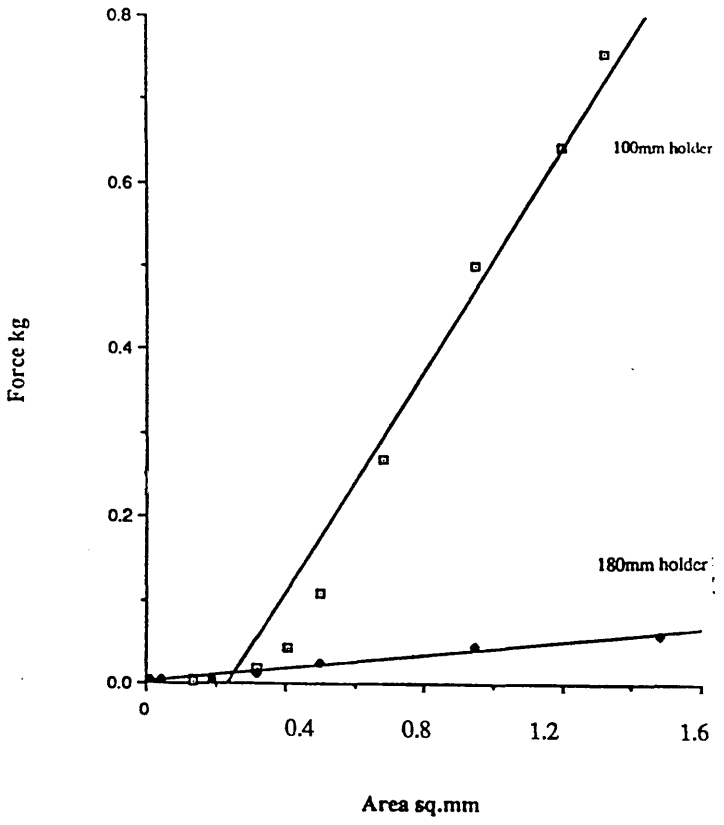
0.8
0.6
0.4
0.2
0.0
0
0.4
0.8
1.2
1.6
Force kg
100mm holder
180mm holder
Area sq.mm

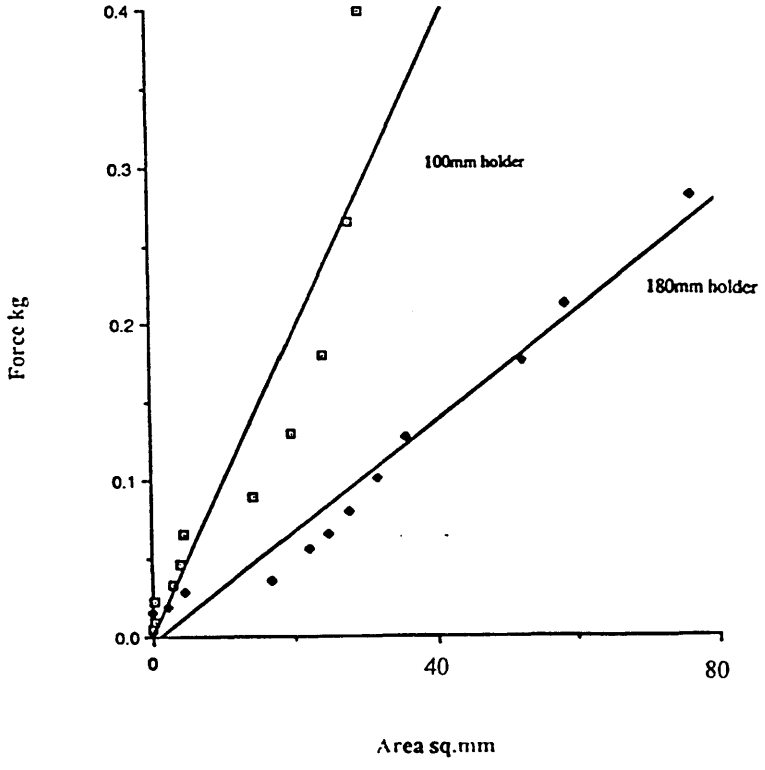
0.4
0.3
0.2
0.1
0.0
0
40
80
Force kg
100mm holder
180mm holder
Area sq.mm

of the supported weave. The weave becomes extremely compliant with increasing size despite the fact that the fabric makes a larger contact area with the cone.

6.2.2.4 Calculation of a "hardness" value

Hardness is defined as the ratio of the load applied to the projected area of deformation. This quantity is actually equal to the gradient of the force-area plot. Table 6.1 presents values of the gradients of such plots. It can be seen that the gradient decreases with increasing of both the cone angle and the supported fabric diameter.

TABLE 6.1: Hardness Values (Kg/mm^2) as a Function of Cone Angle and Fabric Size

	Holder dia. (mm)	
Cone angle θ (deg.)	100	180
60°	2.13	0.128
90°	0.204	-
120°	0.01	0.003
150°	0.0003	-

It is common to plot the hardness number as a function of tan β where $\beta = (\pi-\theta) / 2$ and θ is the cone angle, Figure 6.3. Figure 6.9 is such a plot. The shape of Figure 6.9 is very similar to the elastic region of the normalised mean pressure vs. strain plot of Figure 6.10 for the hardness of a homogeneous body, Johnson (1985).

Figure 6.9 A plot of the hardness value against $\tan \beta$ where

$$\beta = (\frac{\pi - \theta}{2}) ,$$

θ being the indentor angle.

Figure 6.10 Indentation of an elastic-plastic half space by spheres and cones. Small dashed line - elastic: A cone, B sphere. Solid line - finite elements. Chain line - cavity model: F cone, G sphere. Large dashed line - rigid-plastic. Reproduced from Johnson (1985). The fabric with the larger diameter is seen to be more compliant.

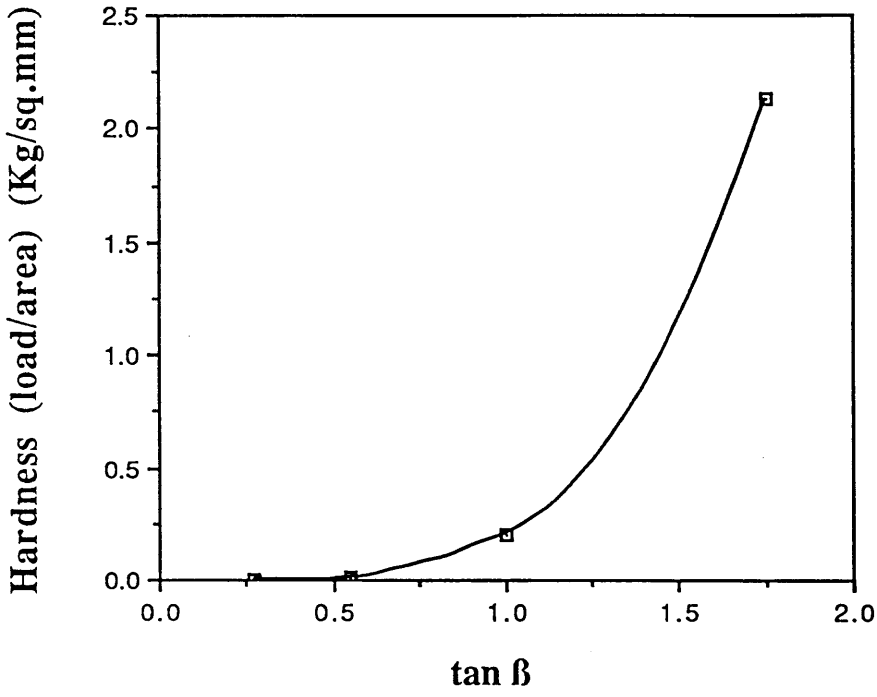
Hardness (load/area) (Kg/sq.mm)
2.5
2.0
1.5
1.0
0.5
0.0
0.0
0.5
1.0
1.5
2.0
tan ß

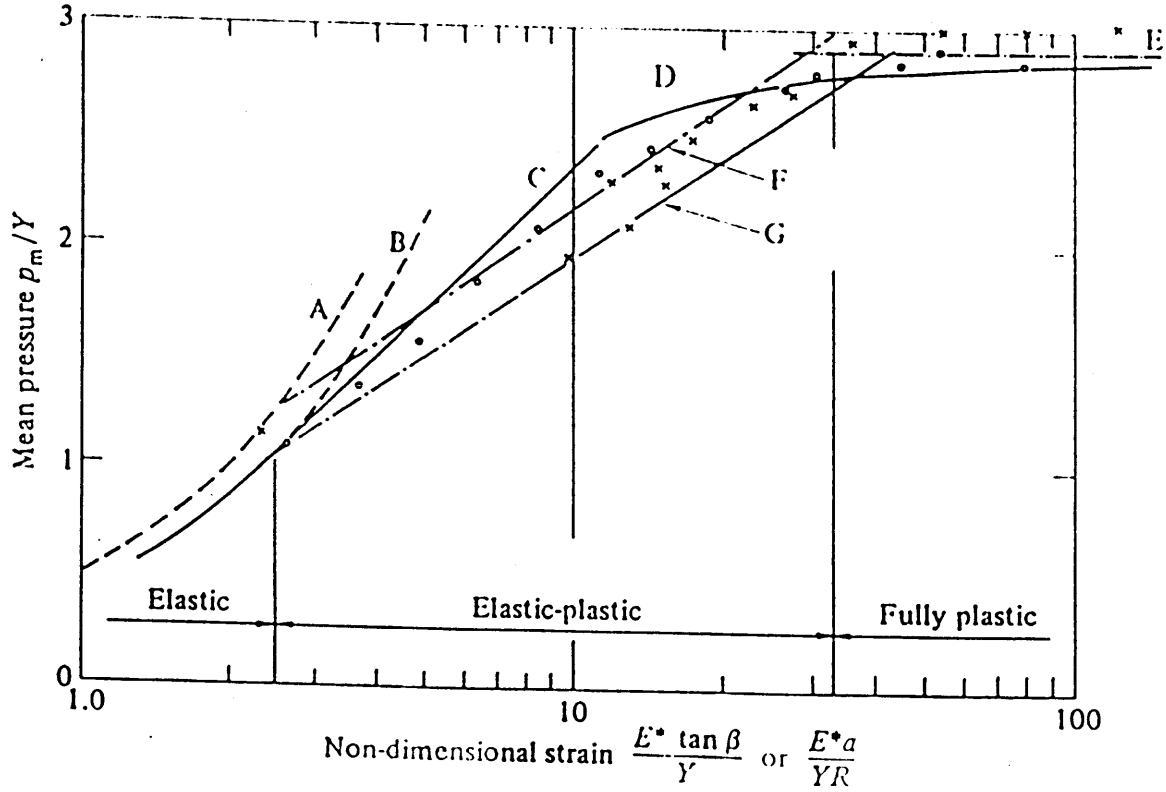
Mean pressure p_m/Y
3
2
1
0
A
B
C
D
F
G
Elastic
Elastic-plastic
Fully plastic
1.0
10
100
Non-dimensional strain $\frac{E^* \tan\beta}{Y}$ or $\frac{E^* a}{YR}$

6.2.3 The Effect of Cone Angle on the Indentation Behaviour of Untreated Aramid 1 Fabric

The procedure described above was also used for the aramid fabrics. However, no pretension was applied to the weft yarns. Figure 6.11 shows the force-displacement profile of the aramid 1 fabric for a spherical indentor and cones of angles 60° and 120°. The trend is similar to that observed for the cotton; Figure 6.4. There are however certain differences. First, the gradients are greater. Also the relative positions of the profiles for the 120° conical and the spherical indentors have reversed. However, the very high degree of reproducibility in these experiments suggests that this is a real phenomenon.

Comparing the data for the aramid to that for cotton, it can be seen that the curves for the aramid rise much more steeply, particularly at the initial stage of deformation and at corresponding values of vertical displacement. Also the values of the imposed forces are much higher for a given imposed displacement.

The initial steep rise in the response can be attributed to the very high flexural rigidity of the aramid 1 yarns resisting any initial bending of the yarns which produced the initial slow rise in the response of cotton fabrics. In aramid 1, the fabric noticeably resists deformation from the initiation of the experiment. It is thus probable that in the case of the aramid 1 fabric, the initial compliant region observed in the case of cotton fabrics and attributed to yarn bending is very small and the response is thus mainly governed by the tensile properties of the yarns themselves. This is discussed in the next section in more detail. The very high tensile modulus associated with aramid yarns explains the high values of force observed. Also, it should be pointed out that unlike cotton, a large portion of the deformations produced in the aramid 1 fabrics were irreversible.

Figure 6.11 The response of as received aramid fabric to indentation by indentors possessing different angles. Holder size=100 mm.

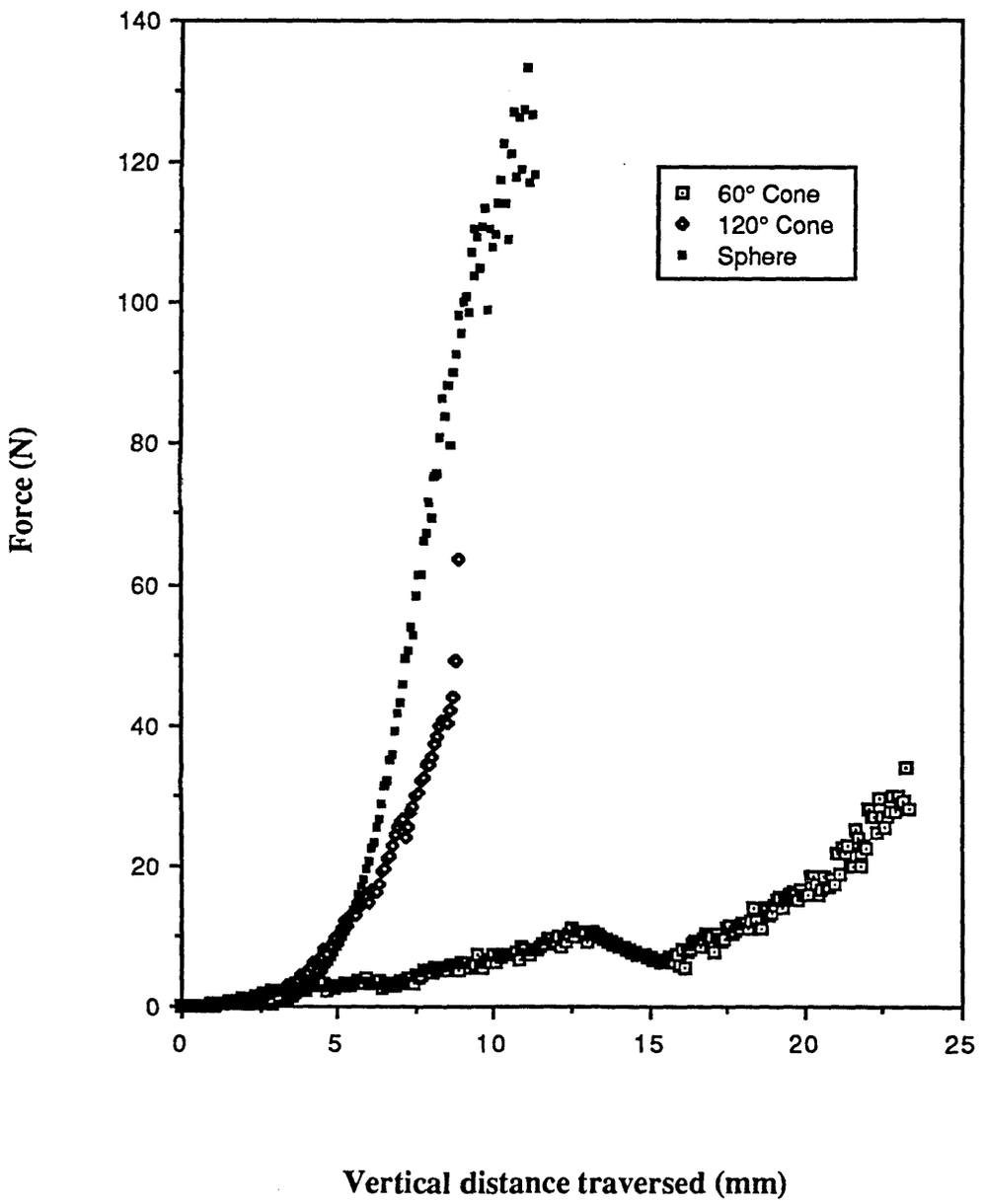

6.2.4 Bending Against Stretching in Fabric Indentation

Figure 6.3 shows schematically the shape of the deformation plate both from the side and from above. The asymmetric nature of the deformation for the cotton fabrics has been noted earlier; the longer contact axis was in the warp direction. What is also evident from figure 6.3 is that the indentation deformation produced involves elements of bending and stretching to different extents. As was discussed in the previous section observations show that initially the deformation is produced through bending of the fabric and then stretching takes over, perhaps for the majority of the vertical deformation distance. Using the measured values of the parameters a and b (figure 6.3) an attempt has been made to quantify in a fairly simple manner the relative contributions of the processes of bending and stretching involved. Because there was no clear, distinctive and measurable length which could be uniquely attributed to either the bending or the stretching phenomena, it was decided to make the assumption that large bending contributions would yield a higher value for the ratio h/y; figure 6.3. That is a larger part of the weave would be in contact with the indentor if bending contributions were significant. Figures 6.12 shows the variation of the ratio h/y with vertical displacement y. It can be seen that, on this basis, greater bending occurs with larger angle conical indentors both for the 100 and 180mm fabric holders. Also greater bending can be observed with smaller holder sizes.

The asymmetry of the deformation zone, figure 6.3, is an indication of the differences in the extents of the bending and hence the stretching in the warp and the weft directions. There is less bending and more stretching in the warp direction and *vice versa* in the weft direction. Infact, the yarns along the warp direction may be said to be more stiff in bending than those in the weft direction. It is of interest to examine where the fabrics under study lie between the extremes of the bending of very stiff and stretching of very compliant fabrics. Figures 6.13 and 6.14 show theoretical cases of very stiff and very compliant fabrics respectively together with the experimental data

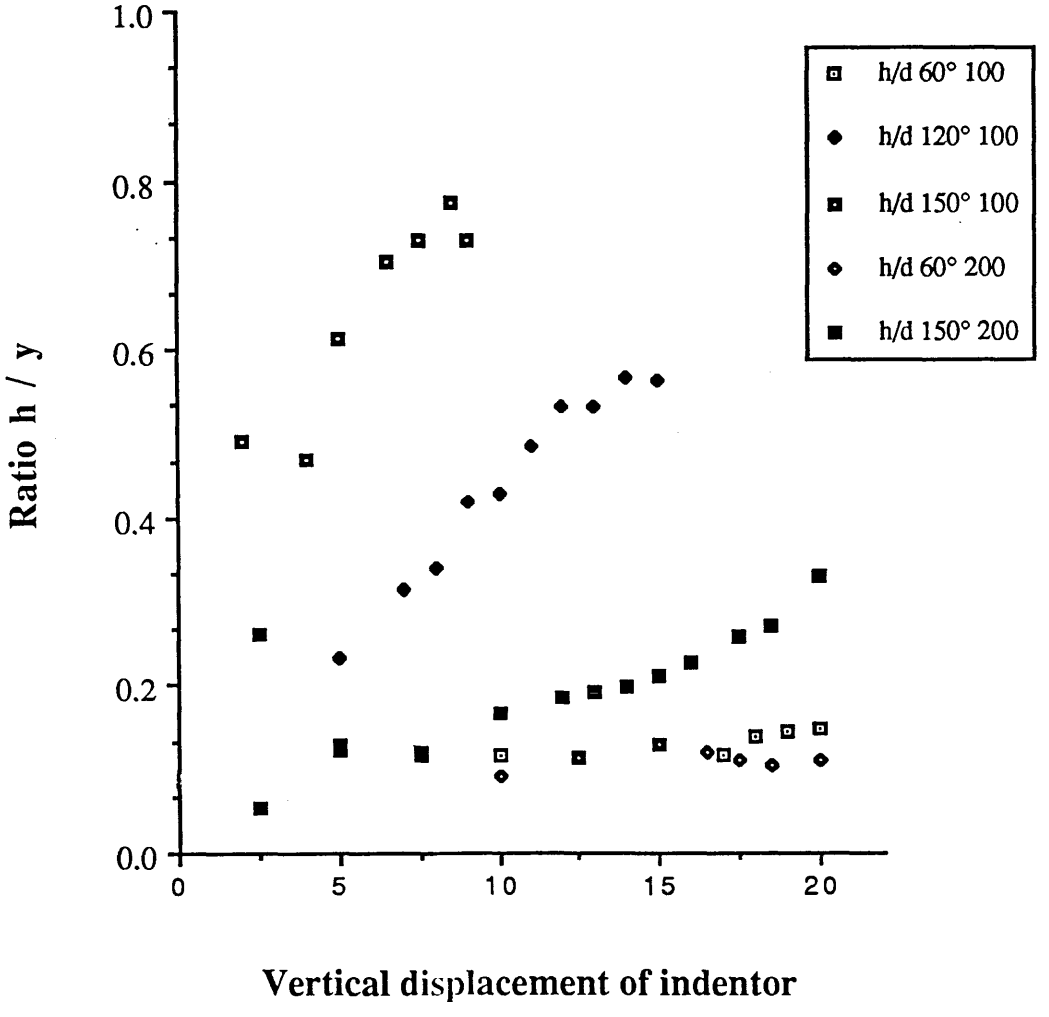

Figure 6.12 Variation of the ratio h/y with vertical displacement for different cone angles and fabric holder sizes.

Figure 6.13 The comparison of the experimental data and the ideal response of a very stiff system during fabric indentation processes.

Figure 6.14 Comparison of the "hardness" experimental data and the response of a very compliant (in bending) system to indentation for various cone angles and fabric holder sizes. The figure represents the extent to which the cotton fabric under study was bent or stretched during the indentation process.

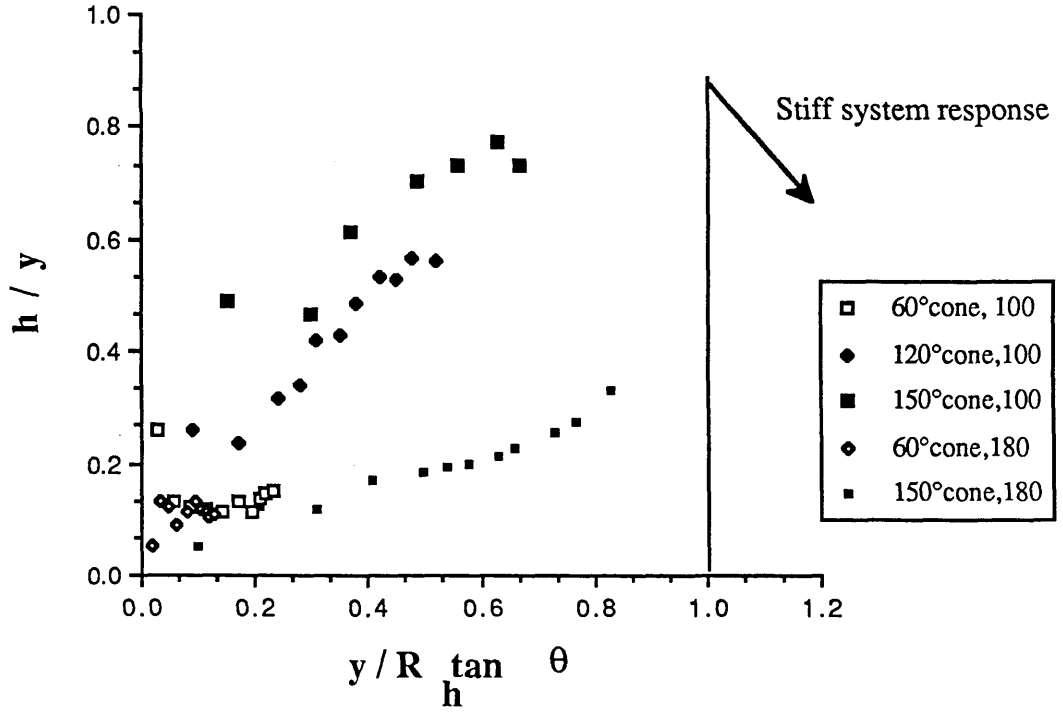
Stiff system response
60°cone, 100
120°cone,100
150°cone,100
60°cone,180
150°cone,180
h / y
y / R tan θ
h

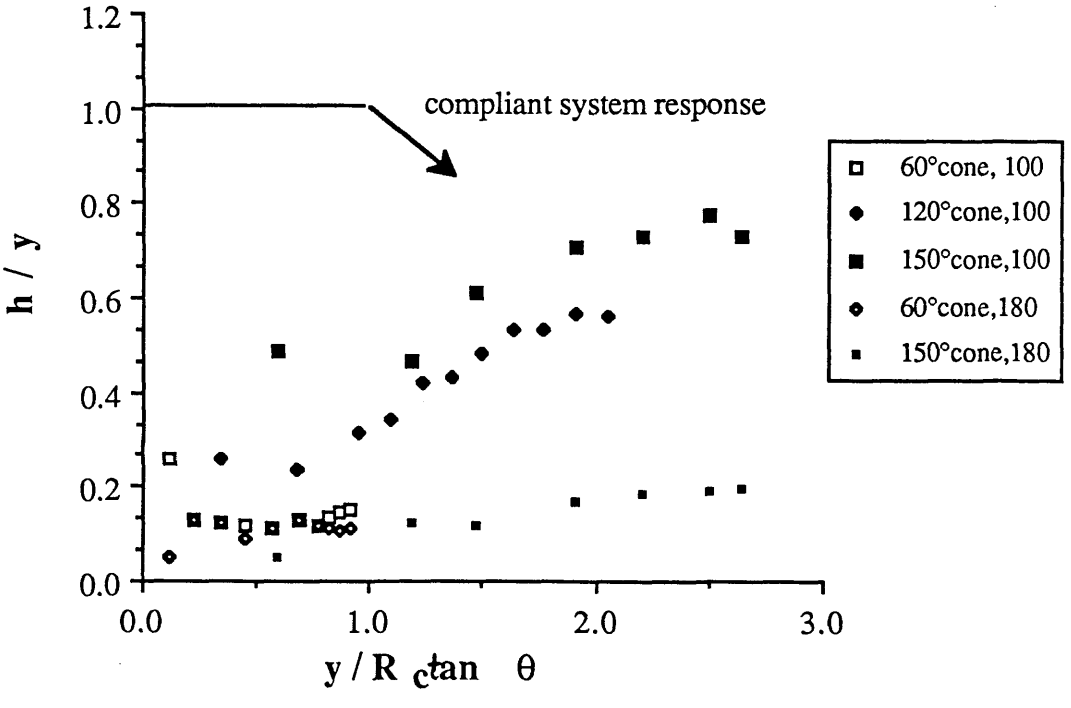
compliant system response
60°cone, 100
120°cone,100
150°cone,100
60°cone,180
150°cone,180
h / y
y / R tan θ
c

for the current system. The geometric parameter $(y/R)\tan\theta$ is chosen in each case such that it represents the response of the two extreme cases. The significance of the parameter is different in each case since h/y starts to be operative at a different value of the above parameter. In the case of the stiff system h/y is zero until the parameter $(y/R_h)\tan\theta$ reaches unity and then it increases to an unknown value of h/y before decreasing slowly. For the compliant system, h/y starts and remains at a value of one until the parameter $(y/R_c)\tan\theta$ reaches unity at which point h/y decreases slowly. What these figures show is that the current system lies somewhere between a totally stiff and a totally compliant behaviour.

6.2.5 Conclusion

The response of cotton and aramid 1 fabrics to planar loading has been examined. The variations in weft yarn tension seem to have little effect on the response. However, the shape and angle of indentors have a pronounced effect on the fabric deformation; the larger the cone angle the larger the hardness values. The size of the fabric is also seen to affect its response. The smaller the size of the supported fabric the greater the "hardness". The deformations produced were also discussed in terms of the contributions of the bending and the stretching processes. Aramid 1 fabric is seen to have a much greater hardness than the cotton both in its initial response and resistance to deformation. Also, aramid 1 exhibits a reversal in the relative positions of the profiles of the 120° cone and the spherical indentor. The reason for this reversal could be that the cotton fabric could accommodate the deformation due to the 120° conical indentor and that this was reversed in the case of the aramid 1 fabric. These differences may be explained in terms of differences in bending and tensile

characteristics of the constituent yarns of the two fabrics (Section 5.4).

6.3 Indentation of Modified Fabrics

6.3.1 Introduction

The response of untreated cotton and aramid 1 fabrics to indentation and the effect of several variables were described and discussed in Section 6.2. This section will deal with the response of modified fabrics to the same indentation processes. The modification was brought about by treating the fabrics with controlled amounts of PDMS and CTAB. These treatments were the same as those applied to the fabrics in other experiments and discussed elsewhere in the thesis. This section discusses the response of modified cotton fabrics first and then that of the modified aramid 1 fabrics.

6.3.2 The Response of Modified Cotton Fabrics

Figures 6.15 and 6.16 show the deformation response of untreated and PDMS treated cotton fabrics to 60° and 120° conical indentors. In both cases, the curve for the silicone treated fabric lies below the untreated fabric curve. A similar trend can be seen with cotton fabrics treated with various concentrations of a solution of CTAB shown in Figure 6.17. The difference between the untreated fabric and that treated with the highest concentration of CTAB is the most pronounced. The trend is explicable in terms of the changes that the PDMS and the CTAB treatments produce in the properties of the constituent yarns of the fabrics. The experimental results discussed in Section 5.4 show that these treatments reduce the tensile modulus of the individual yarns. It is possible that these treatments will also reduce the flexural rigidity or bending resistance of individual yarns. These two factors, and in particular the tensile properties of yarns, are believed to be the major contributors to the response

Figure 6.15 Comparison of the response of untreated and 5% PDMS treated cotton fabrics to the indentation process. (60° conical indentor, 100 mm holder).

Figure 6.16 Comparison of the responses of untreated and 5% PDMS treated cotton fabrics in the "hardness" experiment using 120° indentor and 100 mm holder.

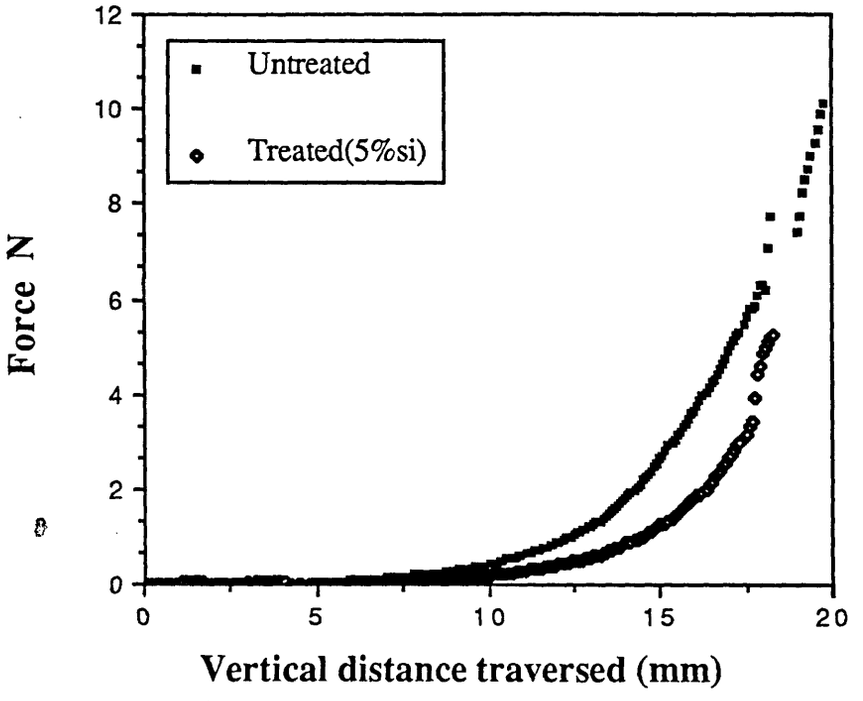
Untreated
Treated(5%si)
Force N
Vertical distance traversed (mm)
0
2
4
6
8
10
12
0
5
10
15
20

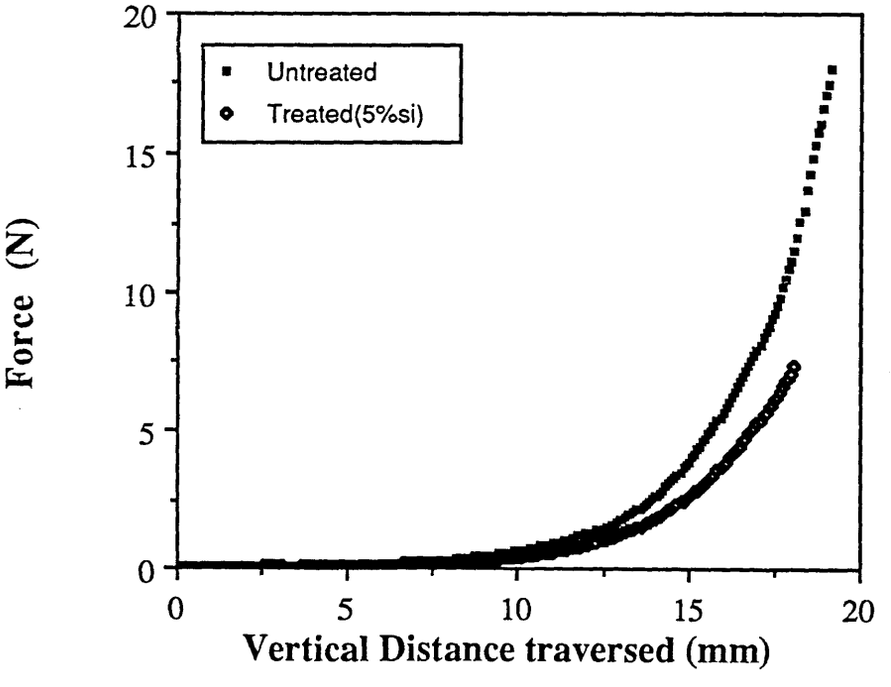
Untreated
Treated(5%si)
Force (N)
Vertical Distance traversed (mm)
0
5
10
15
20
0
5
10
15
20

of the fabrics in indentation.

The area under each curve is a measure of the work of deformation up to a particular deformation or to penetration. Table 6.2 presents the values of the work done in deformation for the treated cotton fabrics and compares them with the untreated case.

TABLE 6.2 : Work Done in Deformation up to 17mm Vertical Displacement

Cone Angle	Treatment	Work done (Nmm)
60	Untreated	14.5
60	5% PDMS	7.15
120	Untreated	21.7
120	5% PDMS	17.8
120	1.4×10^{-4} M CTAB	22.9
120	1.4×10^{-3} M CTAB	22.2
120	2.7×10^{-3} M CTAB	12.4

In the case of the 60° indentor, PDMS has reduced the work done by over 50% and for the 120° indentor by 32%. Low concentrations of CTAB have actually increased the work done very slightly. This is because at low displacements the curves for these two cases lie above the untreated curve while it is *vice versa* at higher displacements. On the whole, it can be said that at these low concentrations of CTAB the treatment has not affected the response significantly and in fact this is reflected in the results of the tensile tests where low concentrations of CTAB did not affect the modulus of the yarn. However, at fairly high concentrations, 2.7×10^{-3} M, the work done is reduced by 73%.

6.3.3 The Response of Modified Aramid 1 Fabrics

The aramid 1 fabric was Soxlet extracted in acetone to remove the unknown finishes that had been applied to it during processing. Some of the clean fabric was then treated in a solution of 5% silicone fluid (poly dimethyl siloxane, viscosity 100cp) in petroleum spirit. The indentation experiments were carried out using a 120° conical indentor and a 100mm diameter fabric holder. Figure 6.18 depicts the results of the "hardness" experiments on the treated aramid fabrics. The results show a very clear trend in the response of the three systems. The cleaned fabric shows the stiffest response. Table 6.3 compares the values of the work done (represented by the area under the curves) to produce a deformation 9mm deep for the three cases. Again, the trend is obvious with the least work done in the case of the PDMS treated fabrics and the most work being dissipated for the cleaned fabrics. The value differ by almost a factor of three.

TABLE 6.3 : Work Done in Deformation up to 9mm Vertical Displacement

Aramid 1 Fabrics	Work done (Nmm)
Untreated	118.2
Soxlet extracted	194.8
Treated (5% PDMS)	46.4

6.3.4 Conclusion

The response of treated cotton and aramid 1 fabrics has been examined. In the case of the cotton, both the PDMS and the CTAB treatments have decreased the hardness or stiffness of the assembly. Also, the work done in deforming the structure has been reduced in the treated cases with the 5% silicone treatment requiring a similar deformation work done to that of the 2.7×10^{-3} M CTAB.

Figure 6.17 Comparison of the response of untreated cotton fabric to that treated with different concentrations of CTAB solution using 120° indentor and 100 mm holder.

Figure 6.18 Comparison of the response of Aramid (Kevlar 49) fabrics possessing different surface characteristics (clean [soxlet extracted], as received and 5% PDMS treated) to the indentation process. (120° indentor, 100 mm holder).

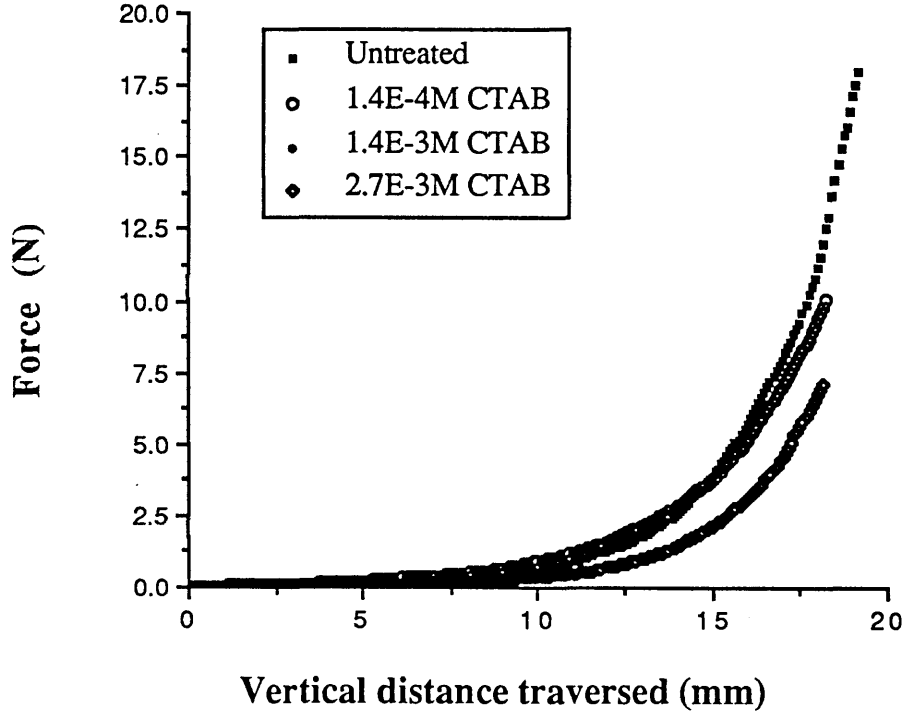
Untreated
1.4E-4M CTAB
1.4E-3M CTAB
2.7E-3M CTAB
Force (N)
Vertical distance traversed (mm)

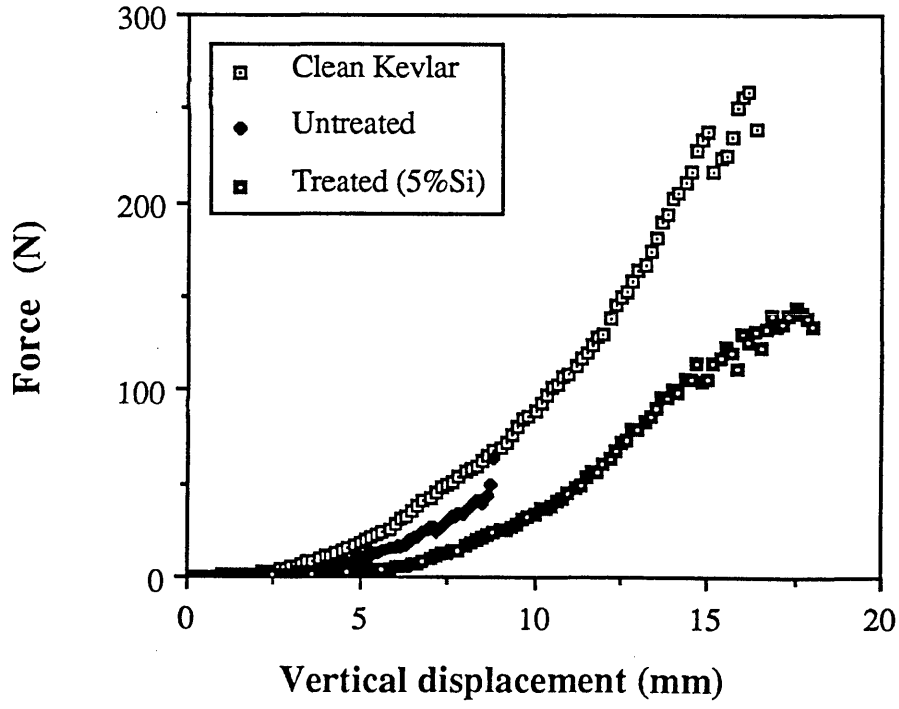
Clean Kevlar
Untreated
Treated (5%Si)
Force (N)
Vertical displacement (mm)

These changes can be attributed to the lubricating effect of the treatments whereby the extensile and bending moduli of the yarns and the assembly has been reduced through reductions in inter-fibre and inter-yarn friction.

In the case of the aramid 1 fabric, removal of the process aids increased the stiffness of the assembly through increasing the inter-fibre friction, while treatment with PDMS had the reverse effect.

6.4 The Thin Plate Model

In this section a "hardness" model based on the deformation of thin plates will be presented. In this model, it is assumed that the fabric is in fact a thin coherent homogeneous solid plate. Standard formulae exist for the deformation of thin plates in various configurations. These relationships are included and summarised in text books by Griffel (1968) and Roark and Young (1986). For a circular plate of uniform thickness, of homogeneous isotropic material and nowhere stressed beyond the elastic limit where the outer edges are fixed and a uniform load is applied over a concentric area of radius r_0, the maximum deflection at the centre is given by:

$$\text{Max } y = \frac{3q(1-\upsilon^2)}{16\pi Et^3}\left(4r^2 - 4r_0^2 \log\frac{r}{r_0} - 3r_0^2\right) \qquad (6.2)$$

where y = vertical deflection of plate from original position, q = unit applied load (lb/in^2), υ = Poisson's ratio, E = modulus of elasticity, t = plate thickness and r = radius of plate. However equation 6.2 only applies if the maximum deflection is not more than about one-half the thickness of the plate. In this case, the load is mostly carried through bending stresses at the surface of the plate while the middle surface remains unstressed. Clearly this is a different situation to the one under study here,

since the deflection of the fabric or the plate is much greater than one-half of the plate thickness. This situation is dealt with by the thin plate theory where the middle surface becomes appreciably strained (as is the case here) and the stress in it cannot be ignored. This stress, called the diaphragm stress, enables the plate to carry part of the load as a diaphragm in direct tension. If the edges are held, this tension is balanced by radial tension at the edges. At large deflections, the plate is stiffer than indicated by the ordinary theory of stress-strain and the load-deflection and load-stress relations are non-linear. Roark and Young (1986) propose the following equation for a circular plate under a uniform load where the edges are fixed and held:

$$q = [k_1 \frac{y}{t} + k_2 (\frac{y}{t})^3] \frac{Et^4}{r^4} * 4.44 \qquad \text{.....(6.3)}$$

$$\text{where } k_1 = \frac{5.33}{1-\upsilon^2} \text{ and } k_2 = \frac{2.6}{1-\upsilon^2}$$

The factor 4.44 enters the equation when converting lb/in^2 to N/m^2. Taking the Poisson ratio υ of the fabric as zero and $F = q*\pi r^2$, the force-maximum deflection profile of such a plate is thus:

$$F = [5.33 \frac{y}{t} + 2.6 (\frac{y}{t})^3] \, 13.98 \frac{Et^4}{r^4} \qquad \text{.....(6.4)}$$

However equations 6.3 and 6.4 are for a uniform load distributed over the whole of the surface area of the plate. Roark (1965) proposed equation 6.5 for a square plate with a concentrated centre load when the edges are fixed;

$$P = \frac{Et^3 y}{12(1-\upsilon^2) r^2} (192 + 36 (\frac{y}{t}) \qquad (6.5)$$

where P = concentrated centre load. Equations 6.3 and 6.5 may be reduced to the equations 6.6 and 6.7 respectively. The latter two equations are of similar forms and the only difference is associated with the equation constants.

$$q = \frac{At^3 y}{r^4}\left[B + C\left(\frac{y}{t}\right)^2\right] \qquad (6.6)$$

$$P = \frac{A't^3 y}{r^2}\left[B' + C'\left(\frac{y}{t}\right)^2\right] \qquad (6.7)$$

The general form of the load-deflection equation may thus be written as;

$$\text{load} = \frac{At^3 y}{r^n}\left[B + C\left(\frac{y}{t}\right)^2\right] \qquad (6.8)$$

where depending on the area over which the load is applied, n takes the values between 2 and 4.

The shape of the deformation produced by uniformly loading a fixed circular plate resembles the schematic drawing below, which is not very far from the shape obtained in the planar loading experiments here.

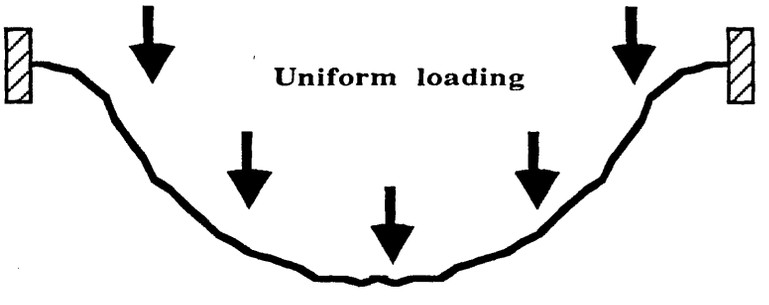

The diameter of the area under the load is a quarter of the diameter of the plate. However the actual form of the loading distribution using cones is rather uncertain and

probably non-uniform. An exact solution for a fixed circular plate with a concentrated load is not available in the literature. Equation 6.4 is used in later analyses. This formula will be used in chapter 10 to model the force-displacement response of the fabrics under planar loading. It will be recognised that this relationship contains three disposable material parameters, E, υ and t. The excercise of setting $\upsilon = 0$ is a convenience and the values of E and t which result will be apparent or effective values computed on this basis. More is said on this later.

6.5 The Response of Fabrics to Small Indentors

6.5.1 Introduction

Sections 6.2 to 6.4 discussed the results and observations of indentation experiments using 25.4mm diameter, i.e. relatively large indentors. This section will present observations and results on experiments performed using 3.2mm diameter indentors, i.e. small indentors. The purpose of these experiments was to simulate ballistic penetration of smaller diameter objects into fabrics more closely than that discussed in Sections 6.2 to 6.4. The diameter of the indentors were such that it was not possible to perform any experiments on the aramid fabrics. Untreated cotton fabrics were used in conjunction with the 100mm diameter fabric holder.

6.5.2 The Effect of the Shape of the Indentor tip on Fabric Response

Unlike Sections 6.2 to 6.4 where the important features were the shape of the response profile and its gradient, here we were more concerned with the penetration force or energy. The shape or angle of the tip of the indentors are not as strong a determining factor in the gradient of the profile as in the case of the large indentors

which occupied a relatively large area on the surface of the fabric. The small indentors only occupy a space of about 10 yarn diameters. Table 6.4 presents data obtained from the above experiments.

TABLE 6.4 The effect of indentor shape on "hardness" character of fabrics

Indentor	Gradient (N/mm)	Penetration Force (N)	Energy (Nmm)
45° Conical	0.8	4.7	11.3
90° Conical	1.7	8.6	30.1
120° Conical	1.6	9.7	32.7
Spherical	1.64	6.5	17.1
Flat	1.9	10.2	46.5

On the whole one may say that the gradient increases as the angle of the conical indentor increases if the flat tip indentor is regarded as a 180° conical indentor. This can be explained in a similar manner to the large indentors. With larger angles a larger number of yarns are initially involved in the deformation process and their tensile resistances become effective earlier and to a greater degree than for smaller included angle indentors. Figure 6.19 shows typical data obtained. The penetration force can be seen to increase with increasing cone angle with the exception of the spherical indentor value which falls between 45° and 90° values. This is as expected since sharper indentors penetrate objects more easily because the load is concentrated onto a relatively small area producing large pressures.

During penetration two processes occurred simultaneously; one was that some of the yarns were torn under the pressure while the rest were "pushed aside" to make way for the indentor. It was observed that on the whole the number of torn yarns increased with increasing cone angle in a similar way to the penetration force. For the flat indentor the number of torn yarns was about 7. The area under each curve in Figure 6.19 represents the work done in penetrating the fabric. These values also

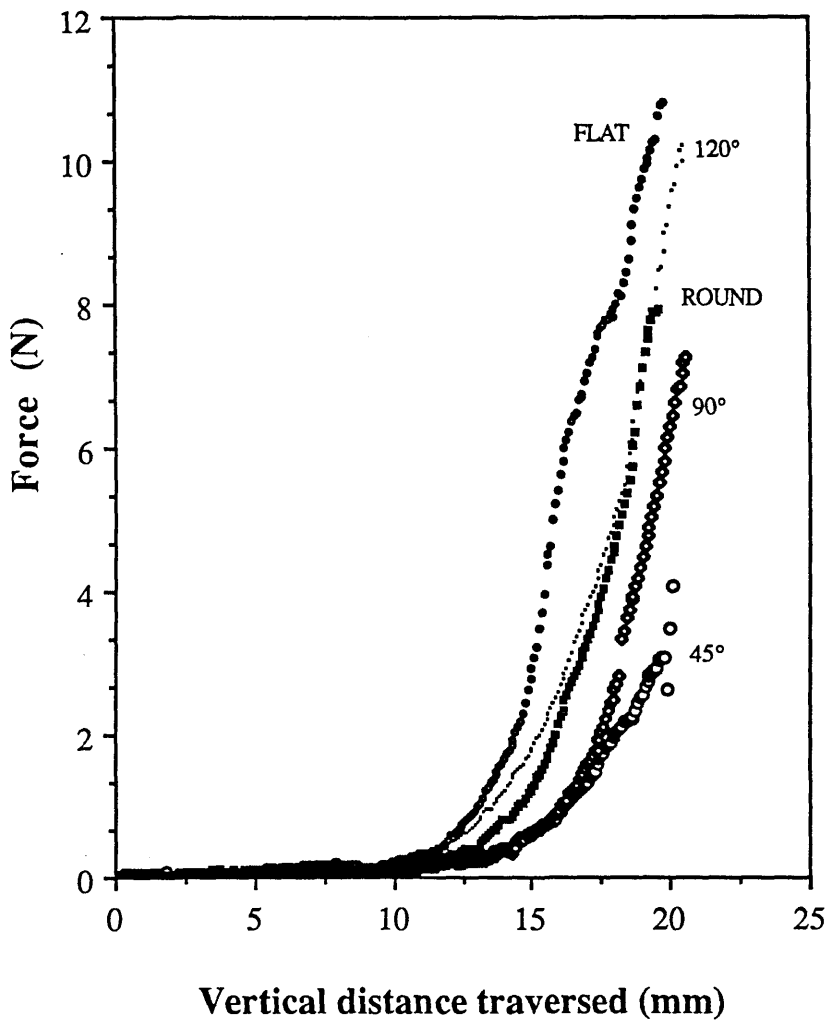

Figure 6.19 The response of untreated cotton fabrics to small diameter indentors as a function of the indntor angle (100mm holder).

appear in Table 6.4. Again these values increase with cone angle, the exception being the spherical indentor. The difference between the values for the spherical indentor and the rest cannot be solely due to experimental error since the values presented in Table 6.4 are averages of at least 5 tests. It is more probable that the inherent shape of the spherical indentor acts in a manner similar to a cone of some angle between 45° and 90°.

6.6 Conclusion

The indentation characteristics of cotton and aramid 1 fabrics have been discussed in terms of the bending and tensile properties of the constituent yarns. The effect of weft yarn tension on fabric response was surprisingly found to be negligible. However, in the case of large indentors, the size of the fabric and the shape and angle of the cone affected the indentation response of fabrics greatly. Treating the fabrics with lubricants such as PDMS and CTAB reduced the penetration resistance of the fabrics. This was argued to be due to a reduction in the tensile and bending moduli of the yarns brought about by a reduction in interyarn and interfibre friction.

Using small indentors, the penetration character of different indentors were examined. It was found that the work done in penetration was reduced for sharper indentors.

These results will be used in a later chapter to facilitate the modelling of some of the observations and the results of the ballistic experiments of fabrics involving very high rates of strain in the yarns.

CHAPTER SEVEN

THE TRANSVERSE BALLISTIC IMPACT OF FABRICS

7.1 Introduction

This chapter presents the data obtained from the ballistic impact experiments on single layers of aramid 1 fabrics. The experimental details were described in Section 5.6. In Chapter 6 the data for the "hardness experiments" were presented which represented deformation at relatively low strains, the deformations being nearly pyramidal. In this chapter, similar out of plane deformations are created but at much higher rates of strain. The "hardness experiments" can be thought of as a simulation of the ballistic impact experiments in the sense that the conical distortion by the ballistic shock waves may be produced statically in a "hardness experiment". Similar distortions are also obtained in the pull-out experiments to be described later. The aim of the ballistic impact experiments was to investigate the deformation of fabrics in transverse impact, using steel balls as the projectiles. The experiments also evaluate the energy absorption and penetration characteristics of the fabrics. The influence of surface treatments on the above characteristics are also examined and will be described in this chapter.

The chapter is divided into three parts. The first part presents the information obtained in the form of high speed photographic images. The main emphasis here will be on the nature or evolving shape of the deformation produced. The second section describes the wave propagation velocities of the aramid fabrics measured using the high speed photographic images. The third part of the chapter deals with the projectile velocity measurements both before and after penetration and the computation of the energy dissipated which occurs during the impact.

7.2 The Deformation Character of Fabrics Impacted Transversely

The main emphasis in this section will be on the examination of the qualitative nature of the deformation produced on impact. Figures 7.1, 7.2 and 7.3 present high speed photographs representing cleaned, untreated and treated (5% PDMS) aramid 1 fabrics. Each photograph contains 10 frames at 40μs intervals, tracing the process from just before impact, on the right, to total penetration, on the left. The impact velocity in the three cases was ca. 113 m/s. The conical shape of the deformation zone is apparent and resembles that obtained in the "hardness experiments" described in the previous chapter. It also closely resembles the out of plane deformation obtained during the pull-out experiments to be described in the next chapter. The shock waves progressively develops in the early stages of the impulse and it can be seen that the diameter of the deformation zone in the viewing plane increases with increasing depth of penetration. In fact, when the two dimensions are measured on the photograph, it was found that there was a direct relationship between the two measurements. There was a nearly constant propagation angle θ, figure 10.16. Separate studies also indicated that the deformation was to a good approximation axially symmetrical about the impact axis. The photographs also show a considerable amount of fibre pull-out during the penetration process. This may or may not be accompanied by fibre rupture. The extent of both the deformation and the fibre pull-out are related to the surface treatments and will be discussed later. After penetration the cone and the adjacent distortion collapses and the fabric largely recovers its original planar shape.

Finally, using these photographs, it was possible to evaluate the residual velocity of the projectile after impact and compare it with the values obtained using the infrared detectors. They were found to agree well.

Comparing the three different treated aramid fabrics, it can be seen that in the case of the PDMS treated fabric the transverse deformation before appreciable deformation has occurred is less than the other two cases. This has an important

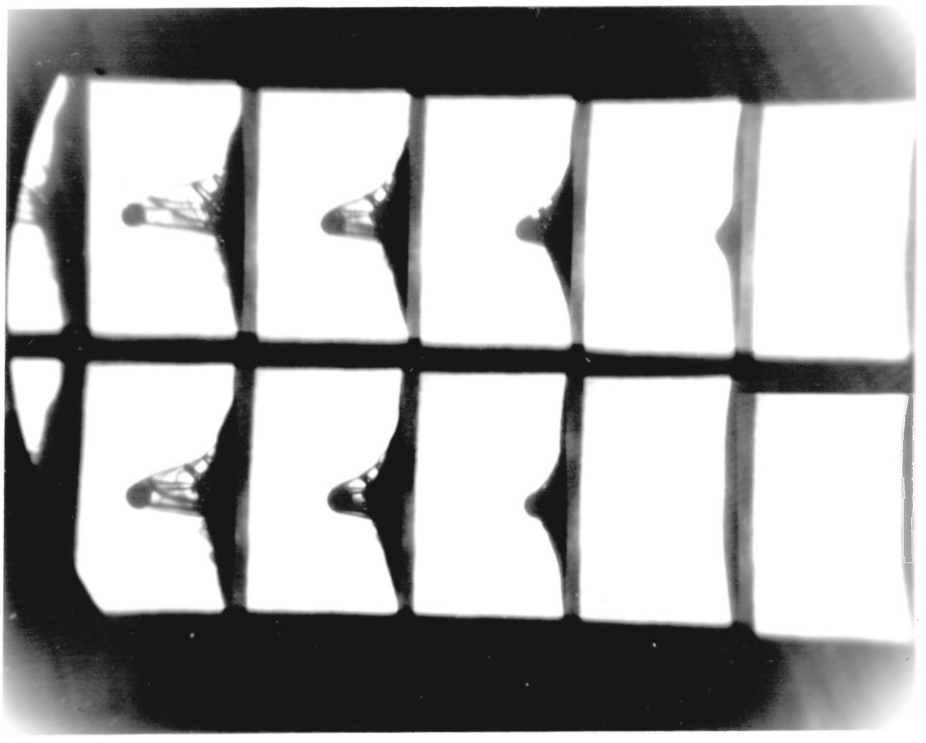

Figure 7.1 High speed photograph of the impact process. Projectile velocity=113 m/s, as received aramid 1 fabric, time interval between frames=40 μs.

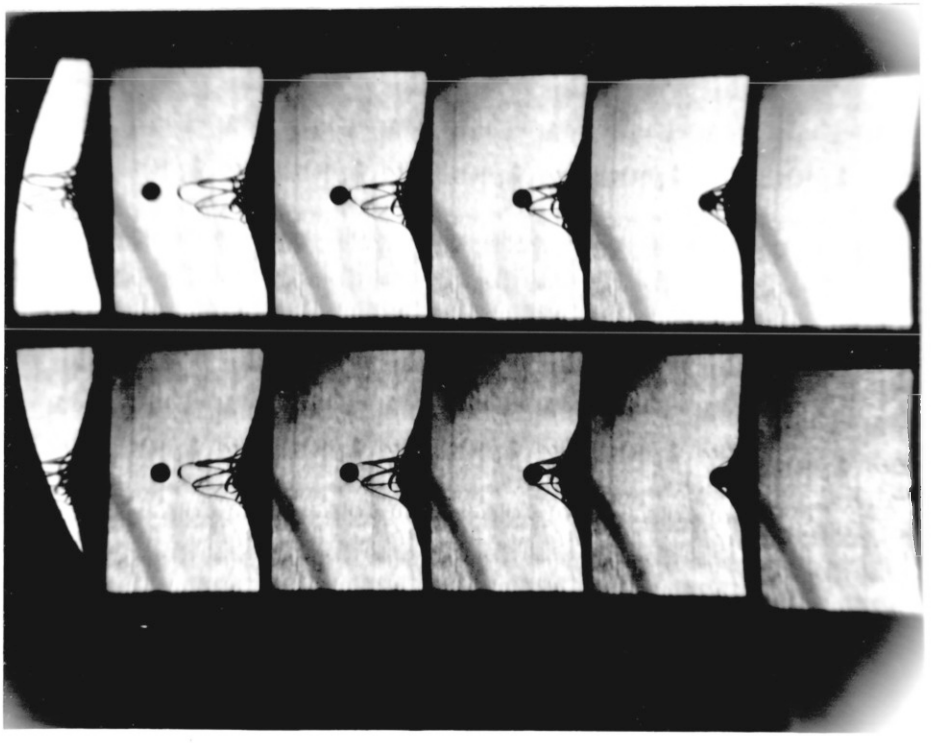

Figure 7.2 Same as figure 7.1 for the 5% PDMS treated aramid 1 fabric.

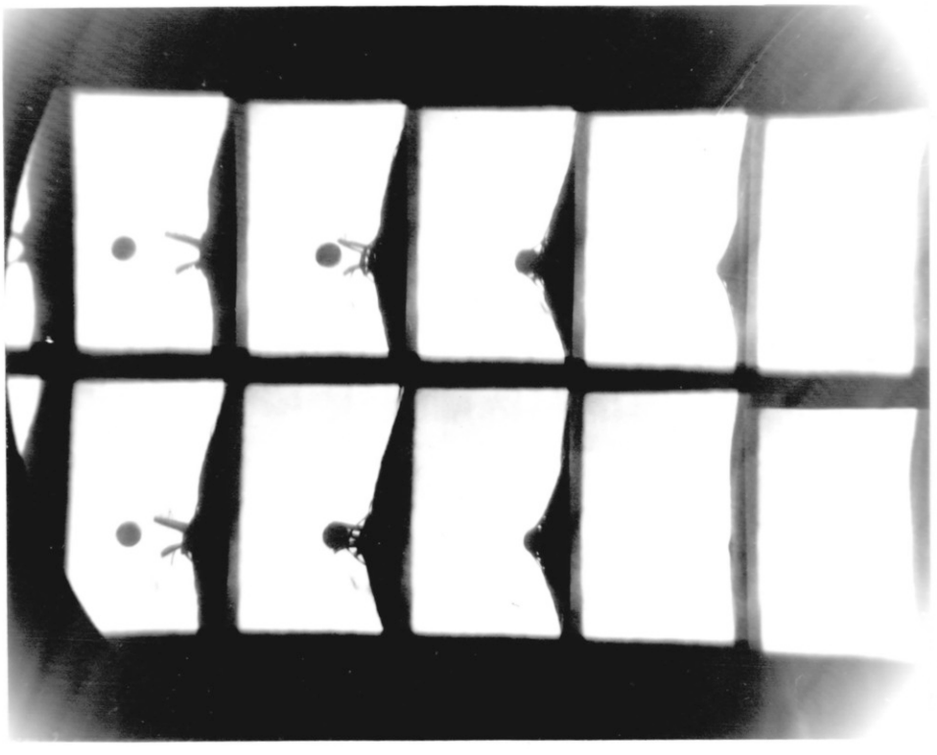

Figure 7.3 Same as figure 7.1 for the soxlet extracted aramid 1 fabric.

bearing on the shock wave propagation velocity in the fabric. This is discussed in the next section. Also, penetration in the cleaned fibre only is accompanied by fibre rupture and very little fibre pull-out has occurred. In the other two cases appreciable fibre or yarn pull-out can be clearly observed.

7.3 Transverse wave propagation through fabrics

The ballistic capture efficiency of a fabric in a transverse impact situation depends to a great extent on it's ability to propagate the stresses and the strains through the fabric. The faster these stresses are transmitted through the fabric before the strains reach rupture point, the better are the ballistic capture properties of that fabric. This point was already made in the review section 4.7. This section deals mainly with the transverse wave propagation velocity of the aramid fabrics under investigation. This velocity is the same as the velocity at which the hinge in the high speed photographic images move away from the impact point. The wave propagation velocity was obtained, for the three aramid fabrics, from figures 7.1, 7.2 and 7.3 by measuring the movement of the hinge with time before penetration occurred. Table 7.1 tabulates these values. The measurements are susceptible to a degree of error mainly because of the limited accuracy of the measuring technique and the uncertainty in the exact position of the hinge at any particular time.

Table 7.1 Wave propagation velocities through the aramid 1 fabrics.

Aramid 1 fabric	velocity (m/s)
As received	98 ± 20
PDMS treated	102 ± 20
Soxlet extracted	170 ± 20

It can be seen that the values for the PDMS treated and the as received fabrics are very similar and significantly less than that of the cleaned fabric. The results of the tensile experiments, section 5.4.2, and the values of the residual velocities (see later) and the energy dissipation characteristics of the aramid fabrics indicates that the as received fabric should probably possess a higher wave propagation velocity than the treated fabric. The as received fabric contained an unknown proprietory lubricant. The soxlet extracted fabric clearly possesses a high value in line with it's superior ballistic properties, as outlined in the next section.

7.4 The Energy Dissipation Character of Fabrics during impulse loading.

This section deals with the energy absorption characteristics of the fabrics, particularly in relation to the surface treatments used. This was carried out by monitoring the impact and exit or residual velocities of the projectile as described in Section 5.6. Figure 5.18 shows the projectile velocities increasing with gas pressure. The velocities were found to be quite consistent at a particular pressure.

Table 7.2, in conjunction with Figure 7.4, presents the values of residual velocities obtained at various impact velocities for the fabrics as a function of different surface treatments. It can be seen that for all the impact velocities there is an increasing trend in the magnitude of the residual velocity from cleaned to untreated to PDMS treated fabrics, as well as the more obvious trend of increasing residual velocity with impact velocity.

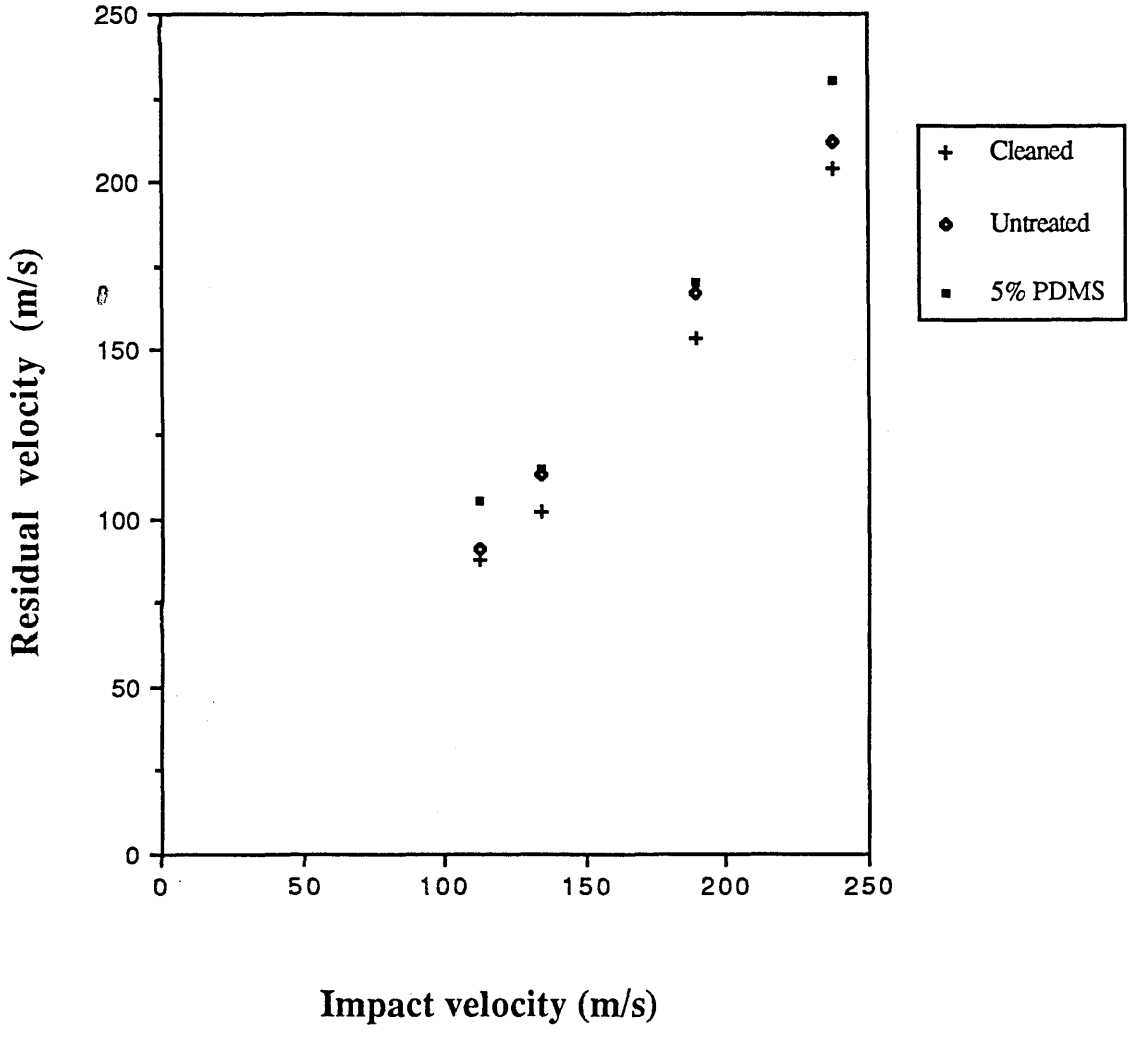

Figure 7.4 The effect of impact velocity and surface treatment of Aramid (kevlar 49) fabrics as the projectile residual velocity.

Table 7.2 : Impact and Residual Velocities as a Function of Surface Treatments

	Residual Velocity (m/s)		
Impact velocity(m/s)	Cleaned	Untreated	5% PDMS treated
112	87.5	90.7	105
134	102	113	115
189	153.3	167	170
238	207	212.3	230

The energy dissipated through the fabric E_d, was evaluated using the equation for the kinetic energy as in Equation 7.1;

$$E_d = \frac{1}{2} m (v_i^2 - v_r^2) \qquad (7.1)$$

where m is the mass of the projectile measured as 1.03g and v_i and v_r are impact and residual velocities. Table 7.3, in conjunction with Figure 7.5, presents the values of the absorbed energies calculated using Equation 7.1. It is clear that on the whole the energy absorbed increases with impact velocity and decreases with the addition of surface treatments.

TABLE 7.3 : The Effect of Surface Treatments on Energy Absorption Character of Aramid 1 Fabrics

	Energy absorbed by fabric (J)		
Impact velocity(m/s)	Cleaned	As received	5% PDMS treated
112	5.03	4.45	1.56
134	7.78	5.34	4.87
189	12.59	8.07	7.03
238	15.48	11.92	3.86

7.4 Conclusion

The high speed photographs clearly show the kind of deformation and damage that the transverse impact of a high speed projectile induces in the fabric. The deformation takes place in three processes. First, there is elastic deformation of the fabric which is accompanied by the generation of tensile strains in the fibres and yarns. Then, there is yarn displacements and pull-out and, finally, there may be yarn rupture. To a first approximation, the first part depends on the elastic modulus of the yarns, the second on the surface properties and friction between contacting yarns and the third on yarn strength. However, the energy dissipated also depends on the speed with which the shock waves travel away from the point of impact and spread the load through the fabric. This point will be dealt with in more detail later. An interesting observation that can be made from the high speed photographs is that as the projectile progresses through the fabric prior to penetration, the angle of the deformation cone remains almost constant while the diameter of the deformation zone increases. However this propagation angle is apparently a function of the surface treatments since the transverse wave propagation velocities are found to be different, with the cleaned fabric expected

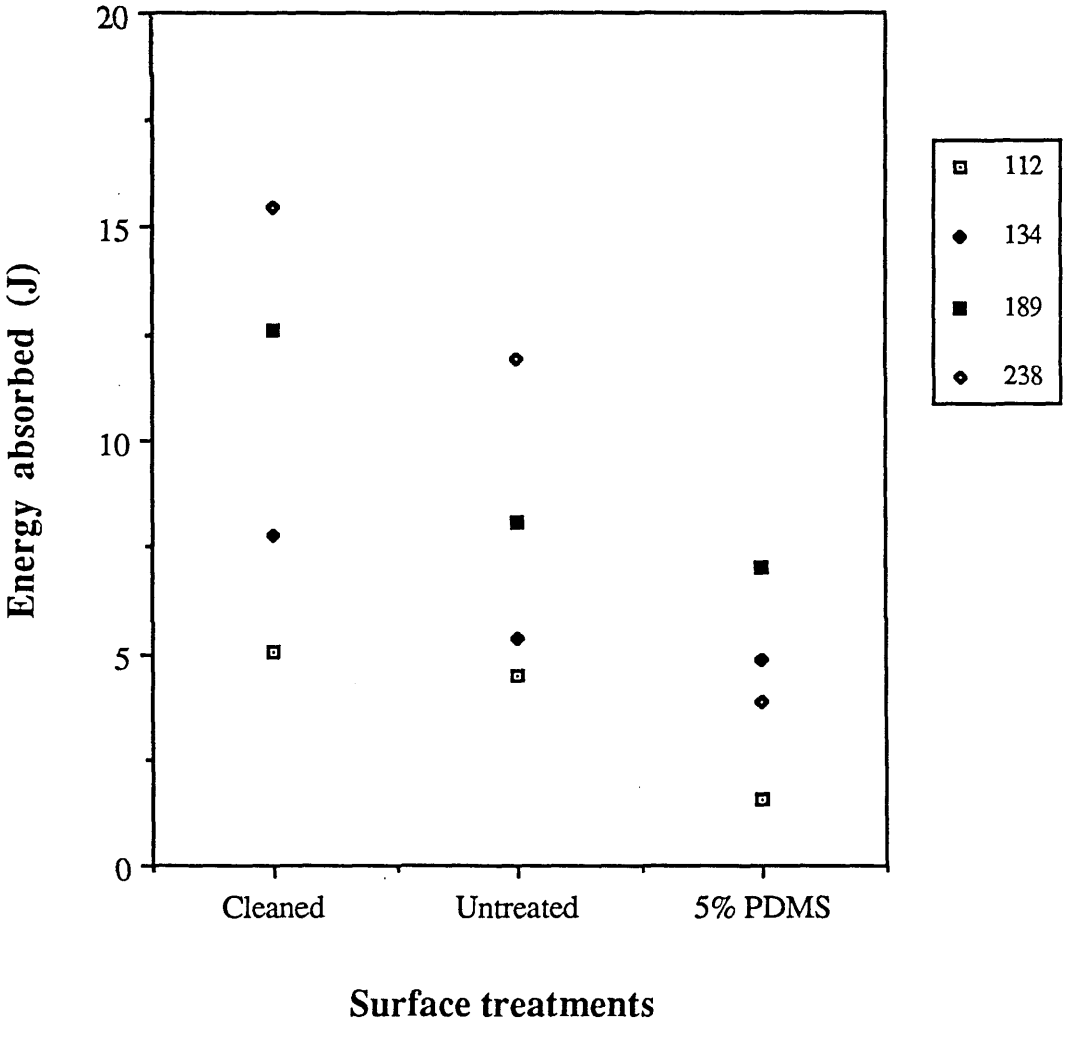

Figure 7.5 The effect of surface treatment on the energy absorbing efficiency of aramid (Kevlar 49) fabrics at different impact velocities.

to possess the largest angle.

Also, the photographs show differences in the extent of deformation prior to penetration for different surface treatments. These differences were more obvious in the measured impact and residual velocities and the calculated values of the energies dissipated. The values show that the most energy was dissipated by the cleaned fabric and least by the fabric treated with 5% PDMS. The reasons for such variations brought about by the surface treatments will be discussed in terms of changes in the yarn modulus or density in a later chapter.

CHAPTER EIGHT

THE YARN PULL-OUT PROCESS

8.1 Introduction

This chapter presents the results of the experimental methods described in Sections 5.7.1 and 5.8. The yarn pull-out process possesses several features which are important. First, the pull-out involves yarn-yarn friction accompanied by the making and the breaking of the inter yarn junctions. Hence, it provides a way of studying the frictional interaction of yarns within a weave. It is also an alternative method of quantifying the friction when used in conjunction with appropriate geometric models (see later). These data are compared with the classical methods of investigating friction phenomena (described in Chapter 3) in a later section. Intrinsic in the pull-out process are the local deformations of the pulled yarn and the adjacent weave which can be useful in the study of the mechanics of fabrics and the effect of fabric modifiers on these properties. Another important feature of the pull-out process and associated deformations is their similar geometric character to those observed in the "hardness" and the ballistic experiments described in the previous chapters. Both the latter processes also involve yarn pull-out and, as will be seen in this chapter, the shapes of the deformation in the pull-out experiments are similar to those obtained in the "hardness" and the ballistic experiments.

This chapter is divided into three main sections. The first deals with the general features of the pull-out experiment on untreated cotton fabrics and the effect of variable parameters upon these features. The second part deals with the geometry of the deformation and, in particular, the vertical deformation of the cotton weave referred to as vertical microdisplacements. The third section presents the results of the pull-out

experiments on aramid 1 and 2 fabrics. The results provided in this chapter are mostly presented in graphical form and the major portion of the analysis are reserved for a subsequent chapter.

8.2 Yarn Pull-Out of Cotton Fabrics

8.2.1 General Force-Displacement Behaviour

The general force-displacement profile of the chosen pulled yarn is shown in Figure 8.1. It has four basic features or regions of response: I/ uncrimping of the loose yarn, II/ the elastic deformation of the tensile or pulled yarn and the adjacent weave, III/ a critical junction rupture force when all the junctions break (the junction rupture point), and IV/ a progressive withdrawal of the pulled yarn which is controlled by the dynamic frictional force. The uncrimping part of the profile has a variable and relatively small slope. Also, because the extent of the crimp in different yarns varies, data obtained in this region is not very reproducible. These type of data are not considered further.

The second region prior to junction or yarn-yarn rupture, is characterised by the nearly elastic extension of the yarn and the deformation of the cross-over yarns parallel and in contact with the pulled yarn. After this point, there is a substantial reduction in the magnitude of the restraining force. The yarn and matrix then undergo fluctuating deformations where the pulled yarn clears a few cross-over yarns in a single "slip" phase. The fourth and final region is characterised by a fairly uniform stick-slip motion where the pulled yarn undergoes small microslips before clearing each cross-over in a single slip.

Figure 8.2 shows typical force-imposed displacement profiles obtained at three lateral tensions of 0, 1.4 and 3.8 N. The experimental details were described in section 5.7. The measurable parameters that are of interest in the force-displacement profiles

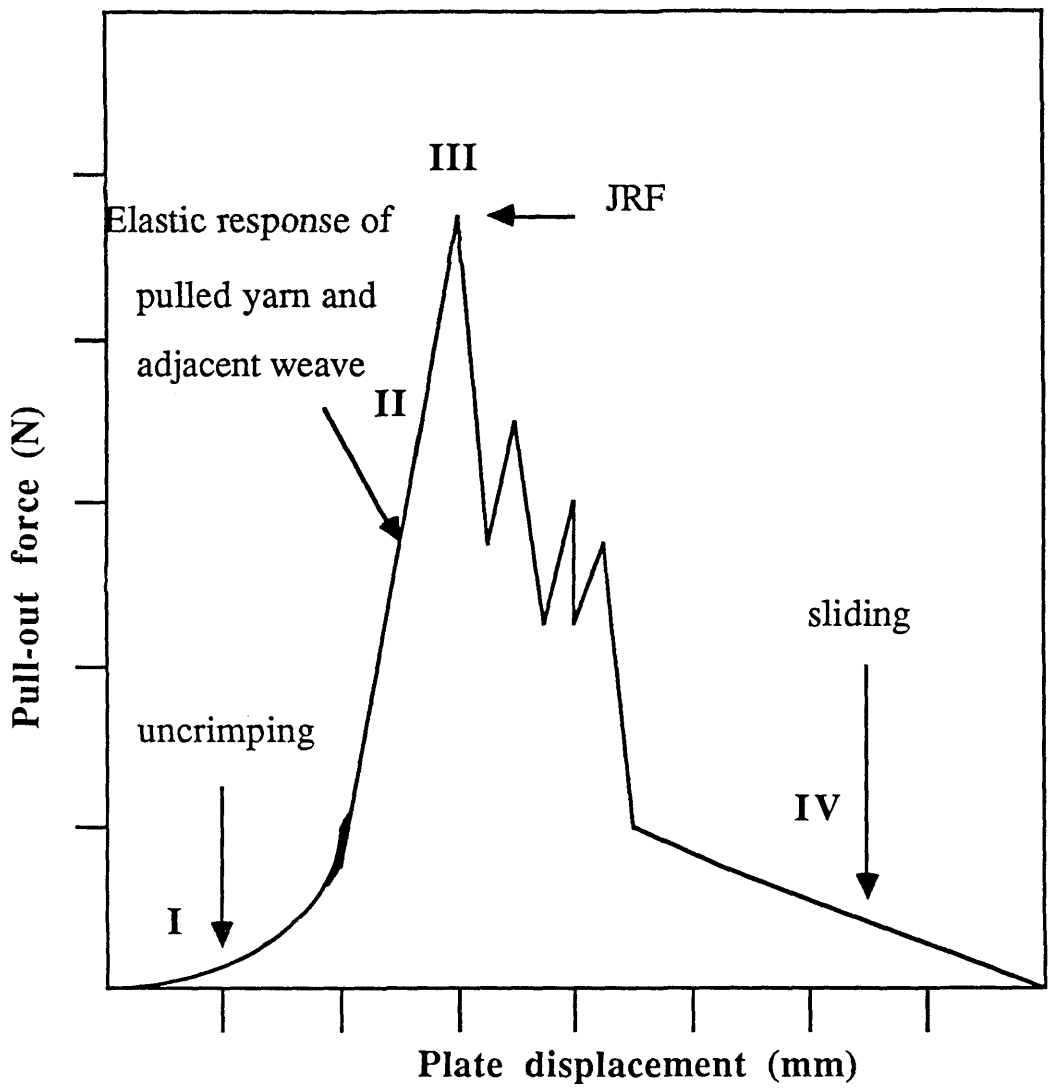

Figure 8.1 General form of the force-displacement profile obtained in the yarn pull-out process showing the four regions of response.

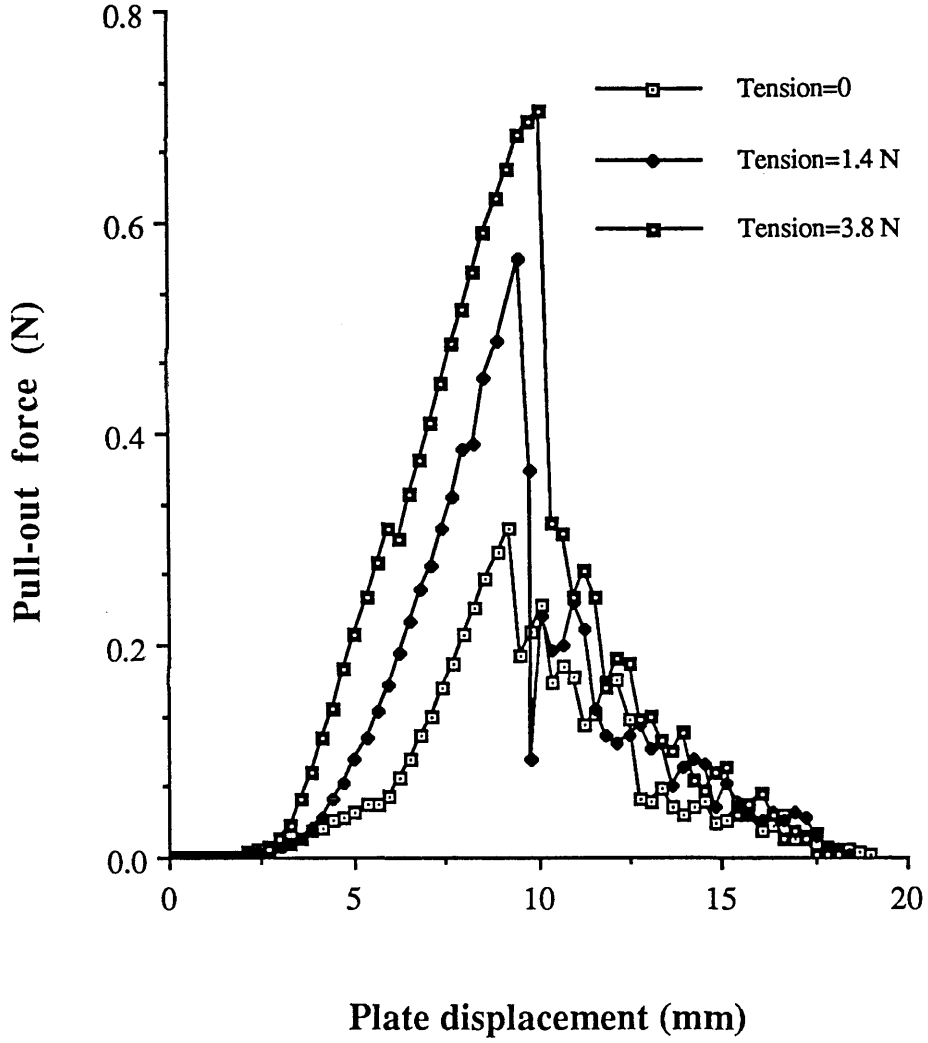

Figure 8.2 Variation of the pull-out profile and the associated parameters of untreated cotton fabric with imposed side tension.

are: (a) the gradient of the elastic part of the profile, (b) the maximum value of junction rupture force (JRF), and (c) the gradient of the kinetic friction portion of the profile. The mean gradient of the elastic region II may be calculated simply by dividing the force by the distance traversed by the supporting frame after accounting for the compliance of the transducer. This quantity is denoted as G(N/mm). Figure 8.3 is a plot of the quantity G as a function of the imposed side tension. The correlation between the two quantities is a positive one. G increases with the increasing of the side tension, although the rate of increase is very slow. The gradient and the intercept of the least squares fits for various data are presented in Table 8.1. The quantity G is in part controlled by the shear compliance of the weave, that is the resistance of the cross-over yarns to the applied load. This point is discussed in relation to the moduli of the cross-over yarns later. However, it seems that with the increasing of the side tension on the cross-over yarns the compliance of the system has decreased.

Figure 8.4 shows the variation of the maximum static frictional force (JRF) with side tension. Again, with the increasing of the side tension the JRF increases in magnitude. The figure also indicates the variability in the measured force at nominally the same values of the side tension. This variability is intrinsic to the system and is not due to experimental error. It is attributable mainly to the heterogeneous nature of the yarns and the weave. The pulled yarn is chosen randomly from the weave. The yarns within the weave vary significantly in diameter and spacing and the diametric variation may be as high as 30% (see Section 5.2).

Figure 8.5 shows the dynamic friction force per cross-over against the imposed lateral tension. The ordinate is calculated from a plot of dynamic friction force against the number of cleared cross-overs, Figure 8.6. As can be seen from this figure, the dynamic frictional force is an increasing function of the number of cross-overs or contacts, each contact contributing to the total friction. However, this relationship only becomes reasonably linear after the pulled yarn has cleared approximately six

Figure 8.3 The gradient of elastic part of the pull-out profile (Region II) G, as a function of side tension for untreated cotton fabrics.

Figure 8.4 Junction rupture force (JRF) as a function of imposed side tension for untreated cotton.

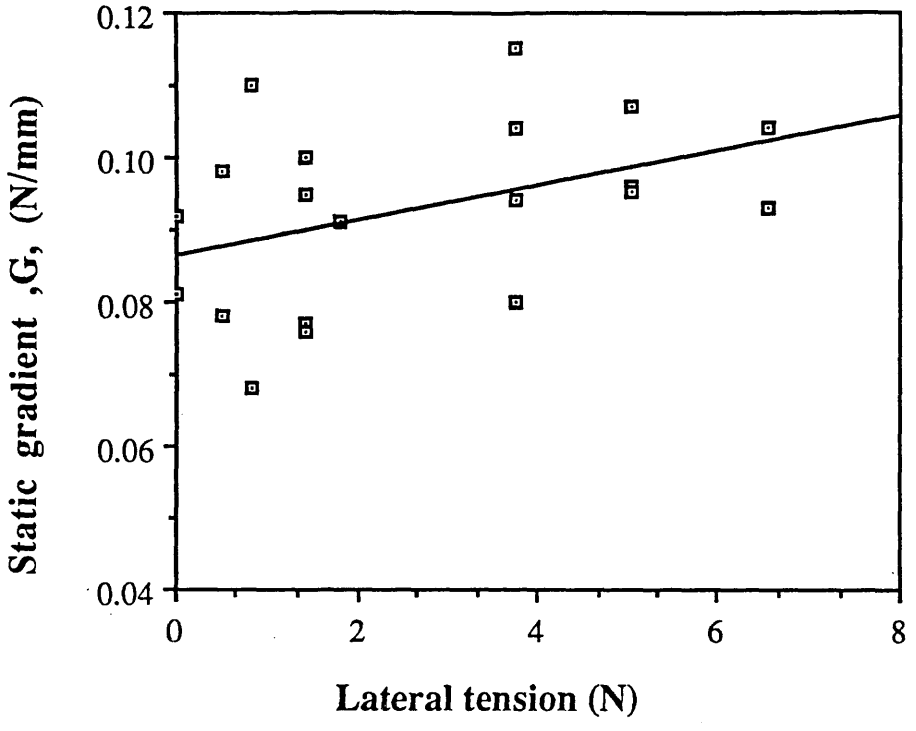
Static gradient ,G, (N/mm)
0.12
0.10
0.08
0.06
0.04
0
2
4
6
8
Lateral tension (N)

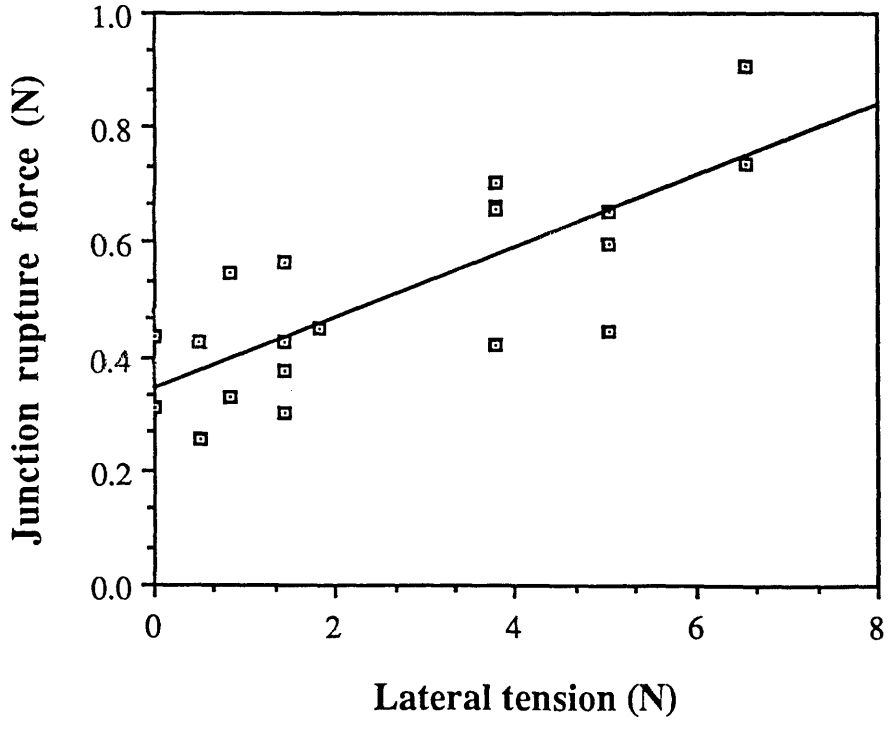
Junction rupture force (N)
1.0
0.8
0.6
0.4
0.2
0.0
0
2
4
6
8
Lateral tension (N)

Figure 8.5 Sliding friction force per cross-over (Region IV) as a function of side tension for untreated cotton fabrics.

Figure 8.6 Measured pull-out force (Region IV) as a function of the number of cross-overs remaining for untreated cotton fabric under zero side tension.

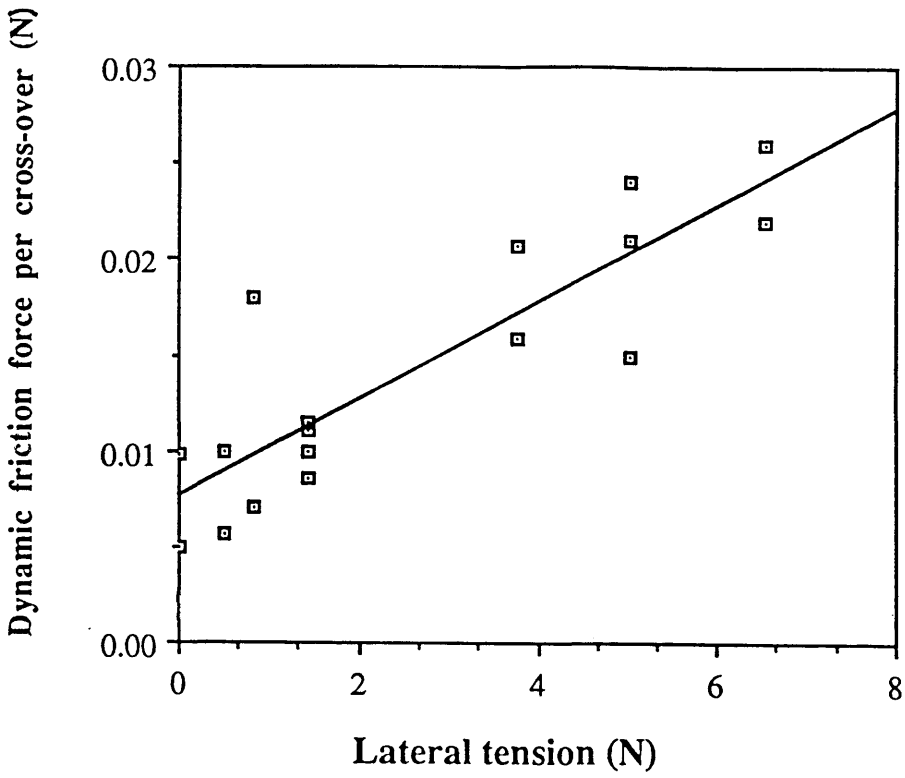
Dynamic friction force per cross-over (N)
0.03
0.02
0.01
0.00
0
2
4
6
8
Lateral tension (N)

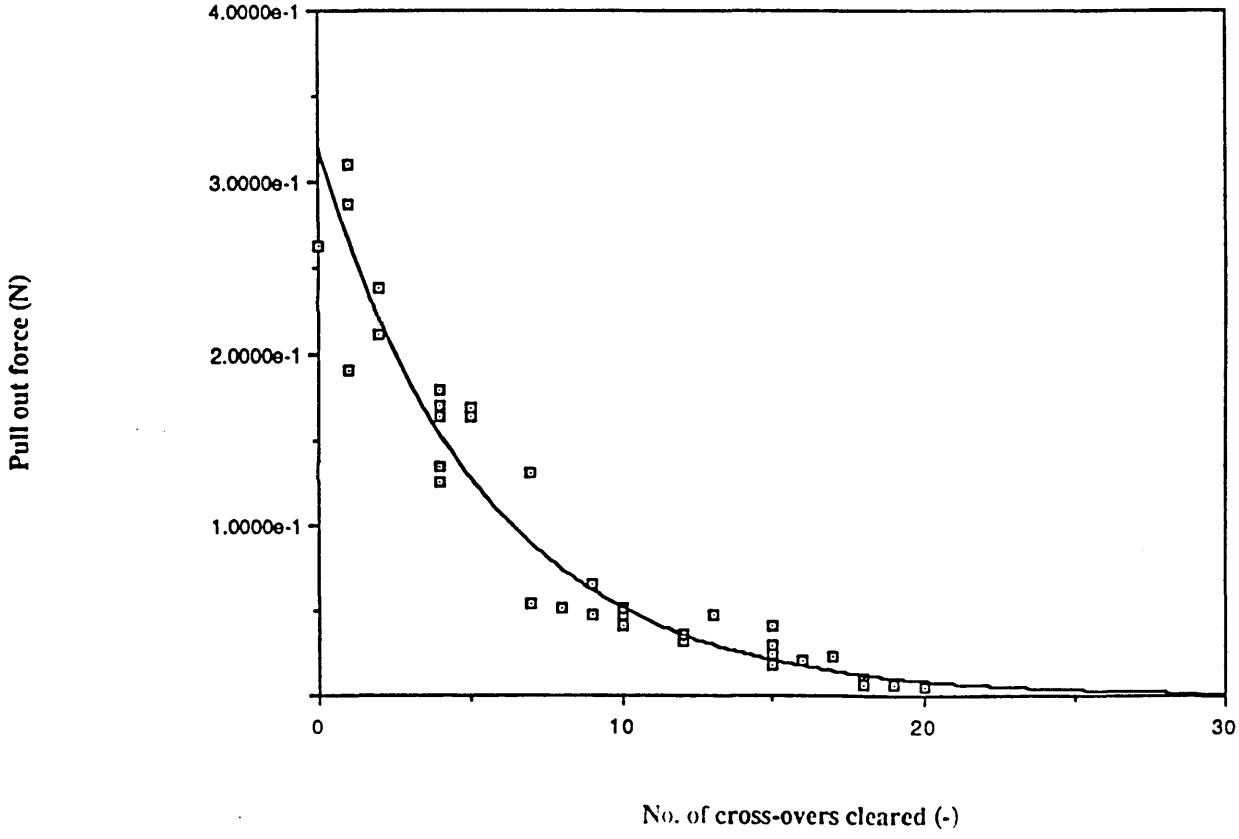
Pull out force (N)
4.0000e-1
3.0000e-1
2.0000e-1
1.0000e-1
0
10
20
30
No. of cross-overs cleared (-)

cross-overs. The ordinate of Figure 8.5 is the gradient of the linear part of Figure 8.6.

The variation of the JRF and the kinetic frictional force per junction with side tension is most simply explained by assuming that both quantities are a function of the normal load at the cross-overs and that the side tension provides a component of this load. A geometric model developed to relate the side tension to the orthogonal resolved component of the normal load, to the friction experienced at the junctions is described later. Table 8.1 lists the parameters obtained from a linear regression in terms of the units employed.

TABLE 8.1

Plot	Gradient	Intercept	Corr. Coefft.
G vs. side tension	0.002 mm^{-1}	0.086 N/mm	
JRF vs. side tension	0.062	0.344 N	0.78
Kinetic friction vs. side tension	0.003	0.008 N	0.87

It is clear that the variation of the parameters with the side tension is quite different. The data presented in Table 8.1 will be used in chapter 10 in conjunction with a number of simple geometric models to evaluate the overall coefficient of friction in the pull-out process. Figure 8.7 shows that the ratio of G/JRF is a decreasing function of side tension. These data provide a series of relationships between the pull-out force and the imposed displacement which are utilised in a later chapter. The modelling of these forces in terms of single fibre properties requires an identification of the micro strains developed in the fabric. This aspect of the study is dealt with in the next section.

8.2.2 Micro-displacement Response in the Plane of Deformation

Figure 8.8 shows a set of typical data for the pull-out force and the extension of the pulled yarn against the distance traversed by the plate, that is the imposed displacement. The extension shown is that of the whole yarn from the hook to the loose end (20 cross-over elements). Using this plot, it is possible to relate the measured extensions to the force- displacement profile. The extension noted in the region from A to B, figure 8.8 relates to the portion of the force profile which is produced at relatively small forces and is the part where the free yarn (that part between the hook and the entry point into the weave) undergoes decrimping. The elastic extension of the pulled yarn is probably very small in the region A-B. In contrast, region B-C is almost wholly dominated by the elastic extension of the yarn relating to the elastic response part of the force profile up to JRF. The region B-C comprises the extension of the part of the yarn that is inside the weave, as well as that outside it in the adjacent weave. The JRF represents the maximum extension sustainable by the system. After junction rupture, as the force decreases, so does the total yarn extension and it then oscillates with the stick-slip motion of the yarn. At zero imposed force, the yarn contracts significantly and is close to its original length. Figure 8.9 depicts the measured force as a function of the extension of those portions of the yarn which are within the weave, i.e. the pulled yarn between cross-over numbers 1 and 20. Both Figures 8.8 and 8.9 refer to an experiment carried out at initially zero side tension. Figure 8.9 is similar to the force-extension curve obtained from a tensile experiment (see Chapter 3). It can be seen that the contribution of the part of the yarn inside the weave to the total pulled yarn extension of 3.7 mm from it's initial position was approximately 0.55 mm and this part is mostly recovered as the tensile force is slowly reduced.

The extension of the yarn at the maximum force (JRF) within the weave was calculated by subtracting the measured displacement of cross-over 20 from that of

Figure 8.7 Ratio G/JRF as a function of side tension showing JRF to be a stronger function of tension.

Figure 8.8 Extension of the pull-out yarn against plate displacement at particular values of the pull-out force. The diagram compares each portion of the extension profiles to a particular region in the pull-out profile.

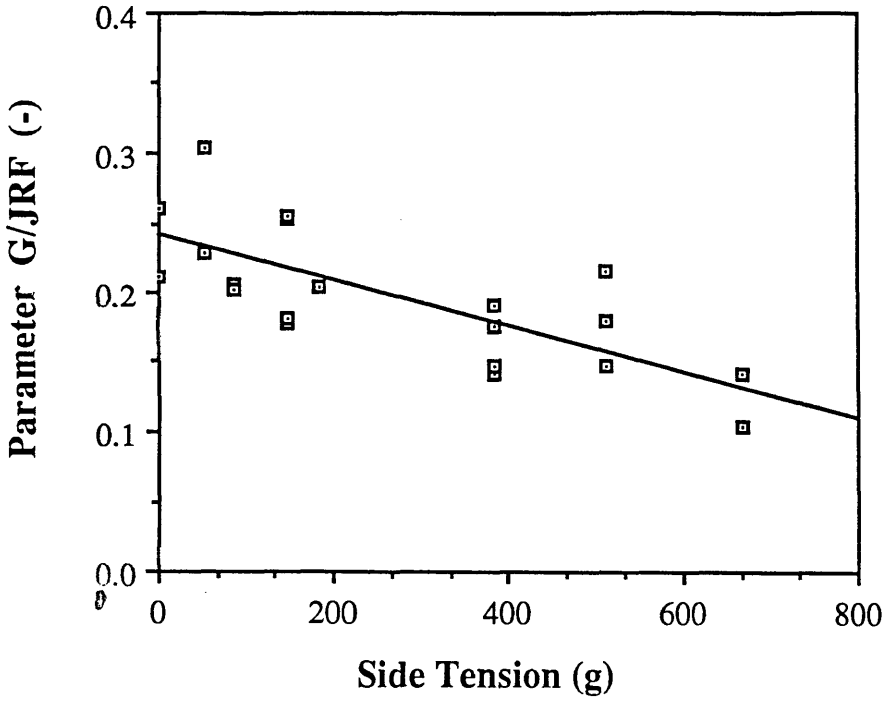
Parameter G/JRF (-)
0.4
0.3
0.2
0.1
0.0
0
200
400
600
800
Side Tension (g)

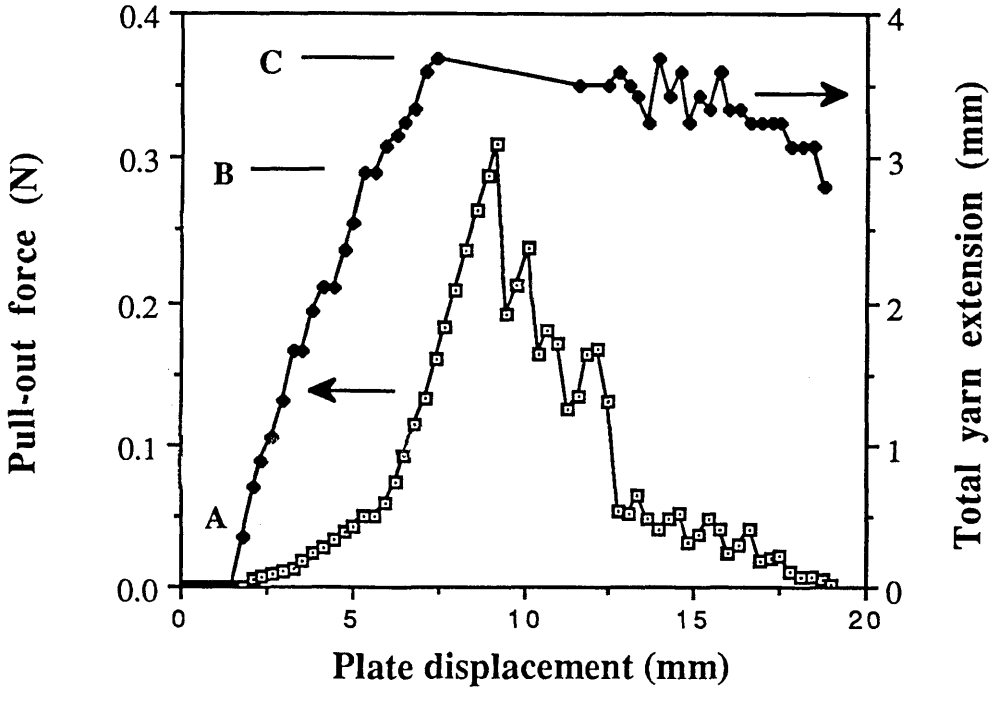
Pull-out force (N)
0.4
0.3
0.2
0.1
0.0
C
B
A
0
5
10
15
20
Plate displacement (mm)
4
3
2
1
0
Total yarn extension (mm)

cross-over 1. The displacement of cross-overs were measured on the TV monitor using a crosswire (chapter 5). A cross-over displacement d was calculated as:

$$d = D - \left[\frac{x_2 - x_1}{a}\right] \qquad (8.1)$$

$$D = \frac{2.97}{60} * \text{time (t)} \quad \text{(mm)} \qquad (8.2)$$

where D = displacement of stage

x_2 = digitised position of cross-over at time = t

x_1 = digitised position of cross-over at time = 0

a = number of digitised positions/mm

The parameter a was related to the magnification used on the zoom lens. For most experiments this was kept constant at approximately 11.2 units/mm.

A typical trend observed in the measured cross-over displacements with cross-over number is shown later, Figure 8.16. Subtracting consecutive cross-over displacements produces values for the incremental extensions of the pulled yarn itself inside the weave at the point just before gross slip occurs. An example is given in Figure 8.10. These data were obtained from the corrected curve given in Figure 8.16. The correction and its importance is discussed later in conjunction with micro-displacements of the yarn and the matrix.

In summary, what has been observed is that the extension of the pulled yarn within the weave does not vary with side tension, although the measured values of cross-over displacements increases with increasing side tension. This is shown in Figure 8.11 where the displacements of cross-over numbers 1 and 20 are plotted against lateral tension. The least square fit for the two are also drawn showing how they increase with lateral tension. However, the distance between the two least square

Figure 8.9 Measured force before JRF (Region II), as a function of the extension of the portion of the pull-out yarn between cross-overs 1-20.

Figure 8.10 Tensile extension of discrete elements of the pulled yarn between cross-overs corrected for the out of plane displacements as a function of cross-over number. The averaged increasing trend is depicted by the solid line.

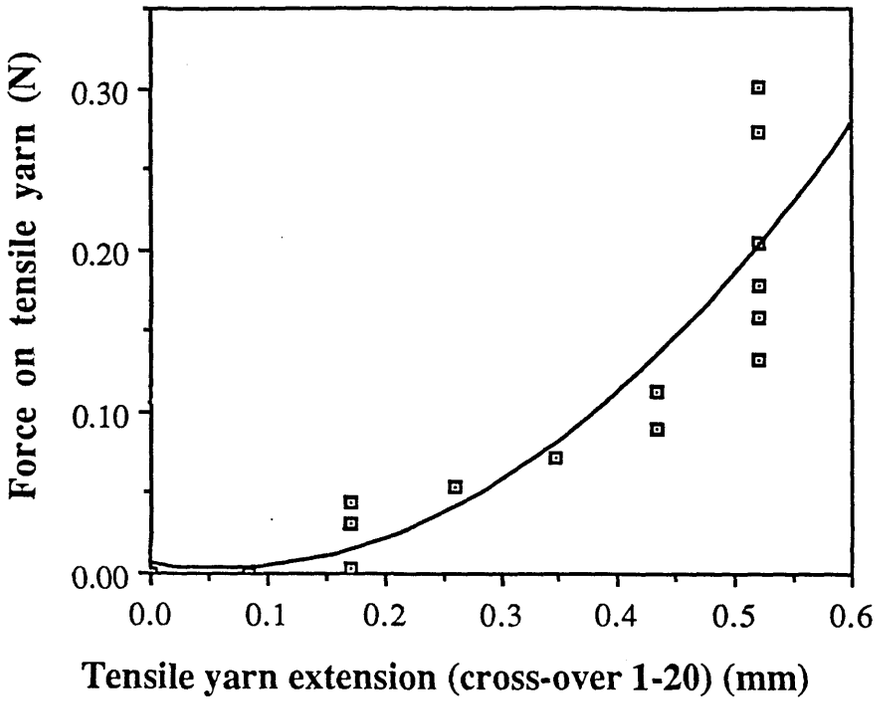
Force on tensile yarn (N)
0.30
0.20
0.10
0.00
0.0
0.1
0.2
0.3
0.4
0.5
0.6
Tensile yarn extension (cross-over 1-20) (mm)

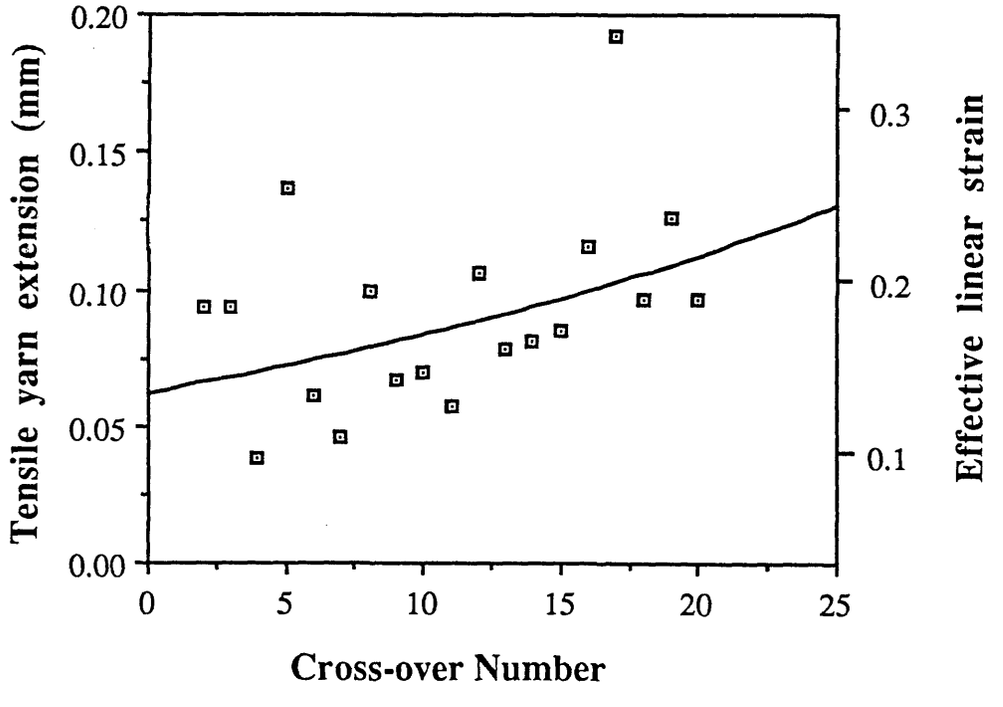
Tensile yarn extension (mm)
0.20
0.15
0.10
0.05
0.00
0
5
10
15
20
25
Cross-over Number
Effective linear strain
0.3
0.2
0.1

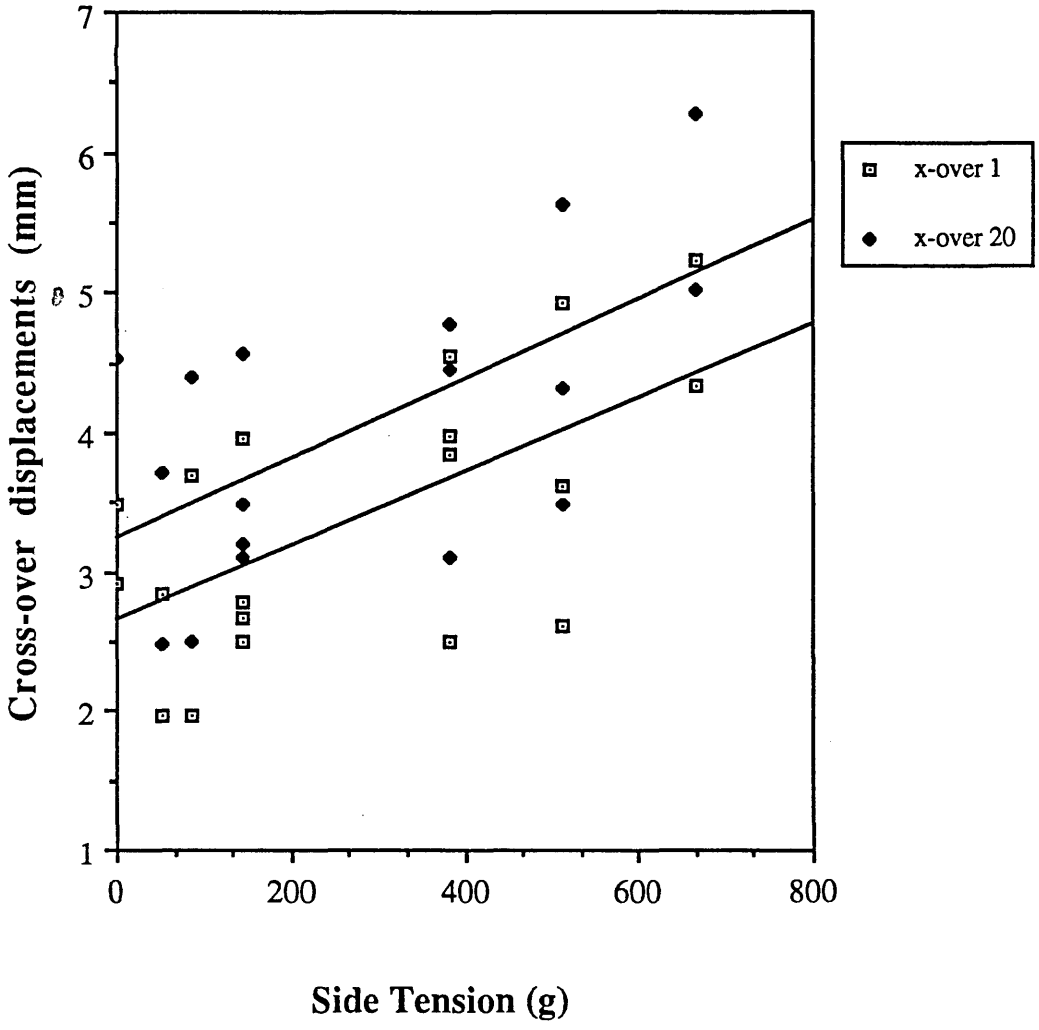

Figure 8.11 Displacement of cross-overs 1 and 20 with side tension. The solid lines represent the least square fits to the data.

fits, representing the total extension of the yarn between cross-overs 1-20 remains surprisingly constant. Careful investigation shows that this effect is due to the out-of-plane displacement of the yarn and matrix. It is not a real matrix property and the origin of the effect is discussed in the next section.

8.3 Micro-Displacements of the Weave

8.3.1 Yarn Displacement above the weave plane

This section presents the results of the experiments described in Section 5.8. The form of the micro-displacements are depicted pictorially in Figure 8.12. The kind of deformation produced can clearly be seen with the vertical displacements increasing as the cross-overs approach the hook. This effect is illustrated in Figure 8.13. The pull-out arrangement adopted introduces the vertical displacements since the yarns were pulled in such a way that they made an angle of approximately 20° with the plane of the fabric. In fact, this was found to be the correct procedure for the pull-out experiment. This facet of the experiment is discussed later. Also, these experiments showed that slight variations of ±10° in the pull-out angle had an insignificant effect the measured parameters discussed earlier (Table 8.1).

The displacements depicted in Figure 8.12 and in particular that in the side view resemble those obtained in the "hardness" and the ballistic experiments described in the previous chapters. The "tent" or cone shaped deformation obtained in the pull-out test also occurs in both of the latter experiments mentioned except that in the case of the ballistics experiments the imposed rates of strain are much higher. The rate of strain in the pull-out experiments was not greater than $3*10^{-3}$ s^{-1}.

Returning to Figure 8.13, it can be seen that the results accurately fit an exponential relationship and are positively correlated with the force on the pulled yarn.

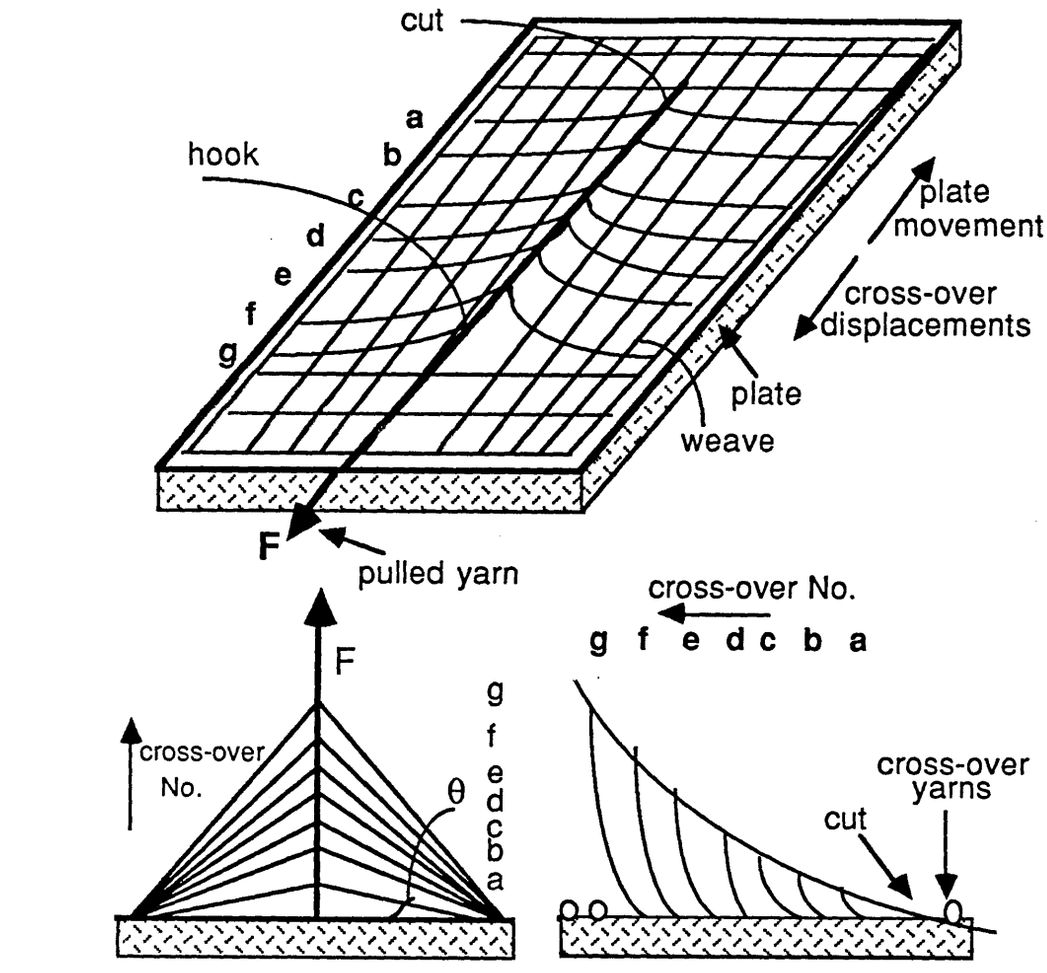
cut
a
b
c
d
e
f
g
hook
plate movement
cross-over displacements
plate
weave
F
pulled yarn
cross-over No.
g f e d c b a
F
g
f
e
d
c
b
a
cross-over No.
θ
cross-over yarns
cut
ELEVATION
SIDE VIEW

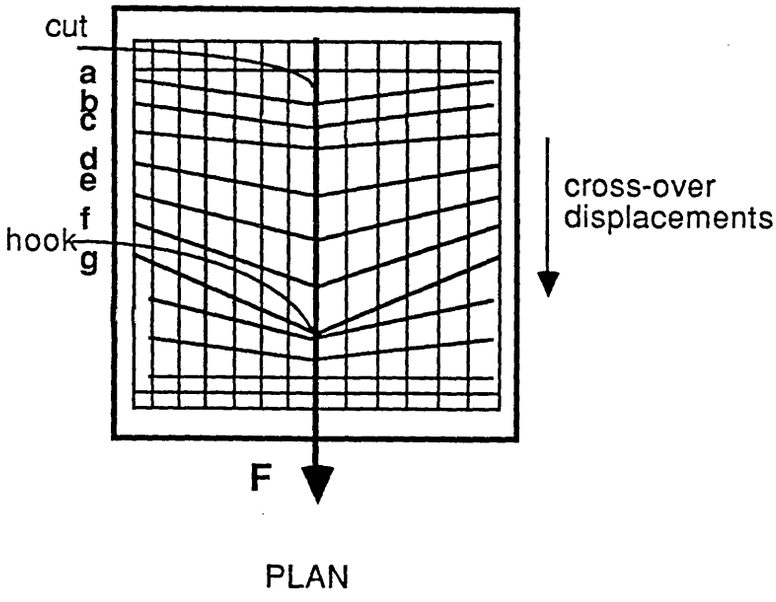
cut
a
b
c
d
e
f
g
hook
cross-over displacements
F
PLAN

The variation of vertical displacements between cross-over numbers 1 and 20 can be as high as 150%. Figure 8.14 shows the vertical displacements at a force of 0.1N on the pulled yarn. The data resemble those obtained for imposed forces close to the JRF values.

The vertical displacements increase with the decrease in the cross- over number. This is simply because the load has to be accommodated by a lower number of junctions resulting in greater deformation per cross-over.

The video camera system views the weave in a vertical axis which is normal to the plane of the undeformed weave (Section 8.2.1) and thus measurements of extensions and displacements refer to these deformations in this plane. The vertical displacements mentioned above necessitate an important correction to the measured values of the extensions and the displacements described in Section 8.2.1. The data given in Figure 8.10 were corrected for these vertical displacements. The correction was performed as follows. The vertically displaced pulled yarn is represented by an exponential equation based on those representing the fits to the data of Figure 8.13. Figure 8.15 shows a section of the pulled yarn with three cross-over points at O, A and B. The initial measured extension of the section AB was d_o and the new and actual extension is $d_c = \sqrt{d_o^2+L^2}$. L is found by calculating the vertical displacement of point B using the exponential equation and subtracting from the vertical displacement of A. In this way, the corrected extensions of the different yarn sections were found and the displacement of cross-overs were thus corrected (Figure 8.16).

Apart from providing a significant correction term, these data, Figure 8.13, indicate that the forces which exist at the contact points are also generated in rather different contact geometries down the length of the pulled yarn.

Figure 8.13 Out of plane micro displacements for the weave as a function of cross-over number for three different force levels on the pulled yarn.

Figure 8.14 The effect of the number of cross-over points at the same force level (0.1 N) on the vertical displacements of the weave.

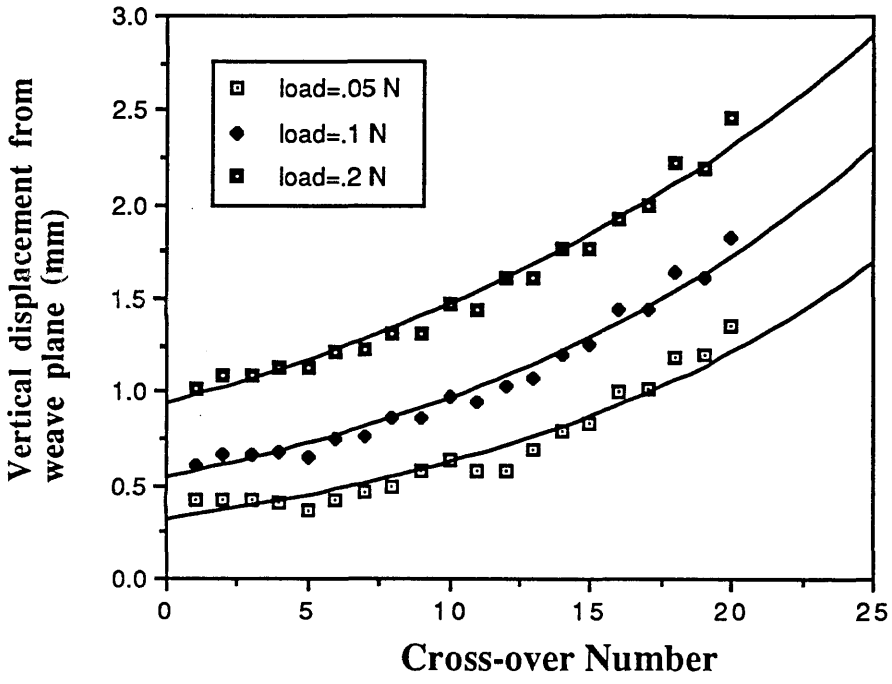
load=.05 N
load=.1 N
load=.2 N
Vertical displacement from weave plane (mm)
3.0
2.5
2.0
1.5
1.0
0.5
0.0
0
5
10
15
20
25
Cross-over Number

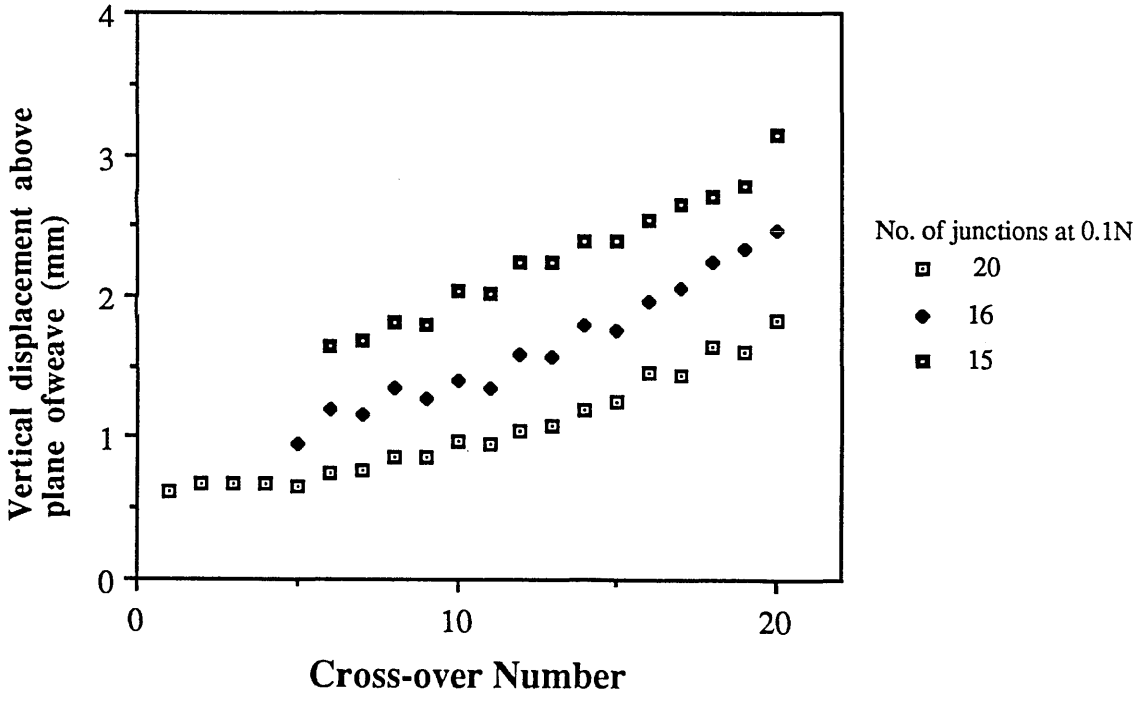
Vertical displacement above plane ofweave (mm)
4
3
2
1
0
0
10
20
Cross-over Number
No. of junctions at 0.1N
20
16
15

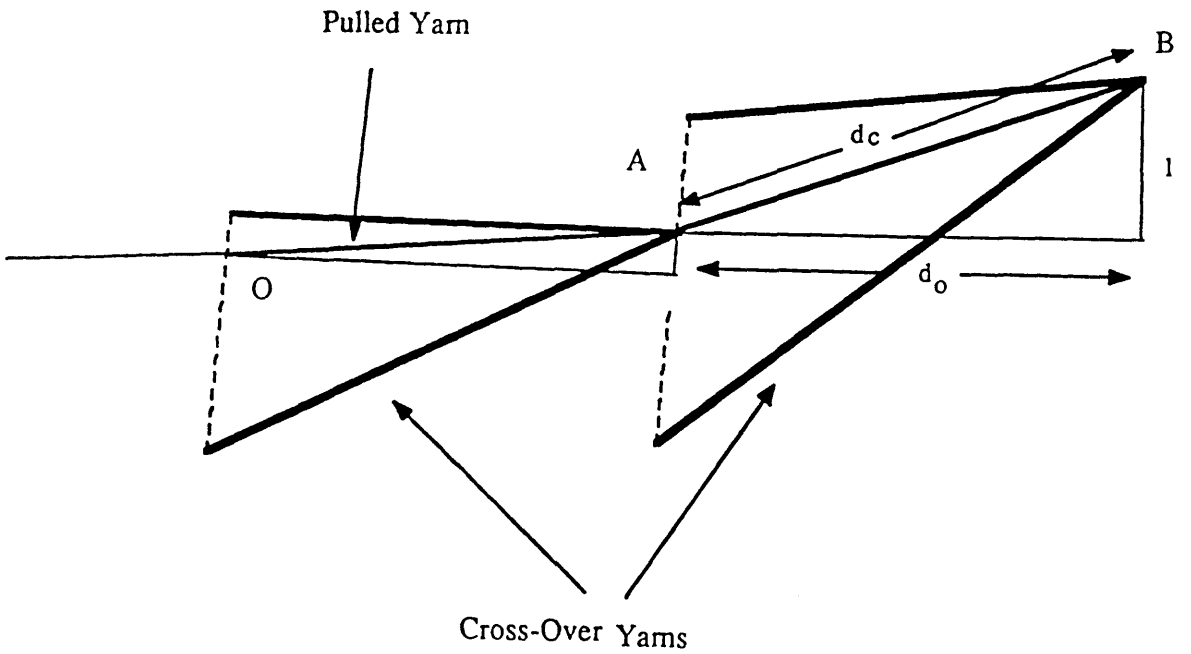

Figure 8.15 Schematic diagram of the vertical micro displacement of a section of the weave, used to correct the displacement of the cross-overs and the extension of the elements of the pulled yarn.

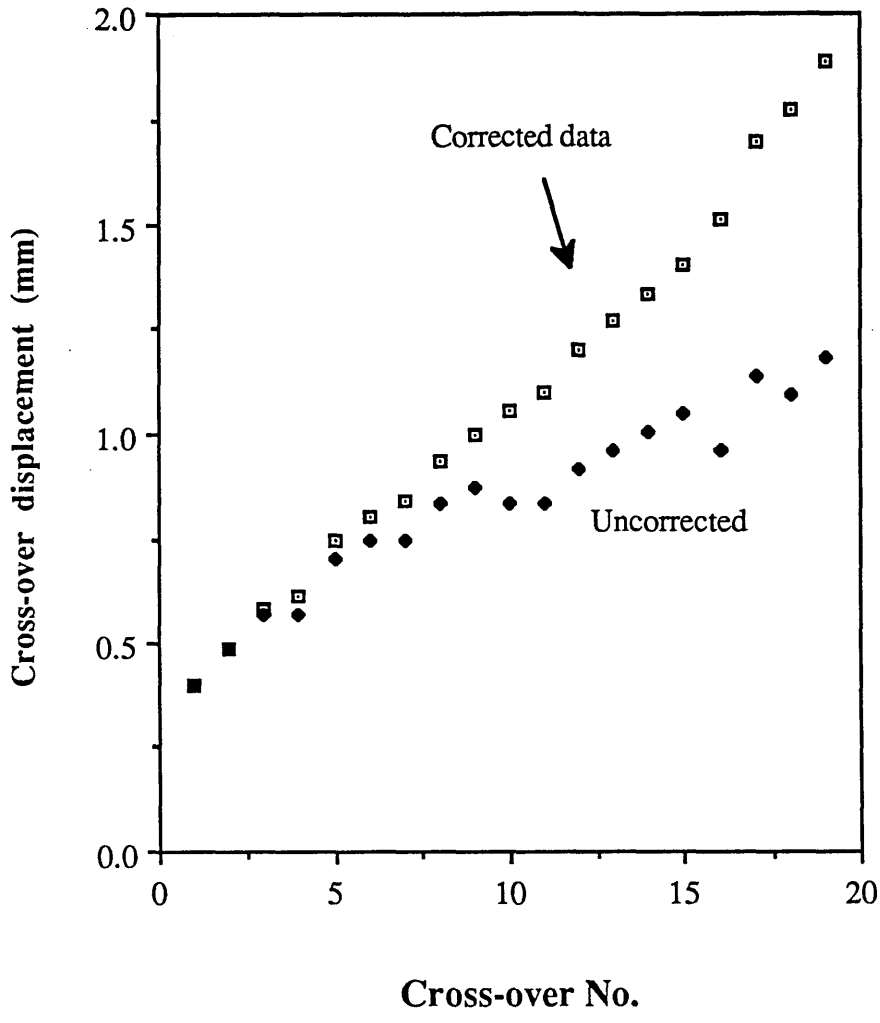

Figure 8.16 Experimental values of the cross-over displacements for untreated cotton fabric at zero side tension as a function of cross-over number. Both the corrected and the uncorrected data are shown, the correction becoming more significant at higher cross-over numbers.

8.3.2 The concept of hardness applied to the pull-out process

As mentioned in the introduction to this chapter, the micro-displacements of the yarn above the plane of the fabric (described in the previous section) are very similar in shape to the pyramidal deformations observed in the hardness experiments. There (chapter 6), the deformation was quantified in terms of a hardness value H_V (section 6.2.2.4) where H_V = applied normal load / area of deformation. This concept can also be applied to the pull-out experiments using appropriate simplifying assumptions. The deformation is depicted in figure 8.12. If it is assumed that the projected deformation area is a rectangle of width equal to two yarn diameters (since the deformation is fairly localised in the cross-over directions) and a length equivalent to the distance between the centres of 20 yarns (see section 5.2), then the projected area would be:

$$(20 * 0.58) * 0.6 = 6.96 \text{ mm}^2$$

The force or normal load on the deformation zone (taken as being a component of JRF) was seen to vary for different values of imposed side tension, figure 8.4. The actual normal load on the fabric is:

$$\text{normal load} = \text{JRF} * \sin 20°$$

since the yarn was pulled at an angle equivalent to the weave angle of approximately 20°. Taking the extreme JRF values of 0.3 and 0.9 N produce hardness values of 0.004 and 0.013 Kg/mm^2. Inspection of table 6.1 reveals that these values lie between the H_V values for the 100 mm holder and included cone angles of 90° and 150°. It is worth noting however that the shape of the actual area of contact was linear in the case of the hardness experiments while for the pull-out experiments the shape was exponential.

8.3.3 Yarn Migration in the Weave Plane

It will be plain that the deformations produced in this apparently simple experiment are most complex. So far the investigation has dealt with the in and the out of plane deformations assuming that the fabric is a rigid sheet. This is not the case and important relative yarn migrations were found to occur within the section of the fabric. For example, Figure 8.17 describes the vertical distance between the tops of the pulled yarn and cross-over yarns as measured by microscopy, chapter 5. The curve marked "difference" represents the difference in vertical distance between consecutive cross-over and tensile yarn positions in the deformed weave. This indicates that with increasing cross-over number (which corresponds with the increase in the force acting at the cross-over) the yarns have migrated such that the yarns crossing over the pulled yarn have been "pushed up". Those crossing under the pulled yarn have been "pushed down". Figure 8.18 also quantifies this phenomenon for the two forces of 0.05 and 0.2N. The observed migration is greater for the higher forces as indicated by the fits to the points.

8.4 Yarn Pull-out Test on Untreated Aramid Fabrics

8.4.1 The Observed General Response

Two kinds of aramid fabrics were investigated: a simple weave of a aramid 2 fabric and a twill aramid 1 fabric. The response of the two to the pull-out test were significantly different. It should be noted that in both cases the number of cross-overs investigated was 20. The force-displacement profiles for aramid 1 and aramid 2 fabrics at zero side tension are given in Figure 8.19. The general shape of the profiles are similar to that of the cotton, see Figure 8.1. There are however certain differences. In the profile for the aramids, the region representing the uncrimping of the yarn is not present. This is to be expected since the aramid yarns possessed very little crimp. The

Figure 8.17 Experimental values of the distance between the top of the cross-over or pulled yarn and the surface of the weave with increasing junction number. The yarns orthogonal and crossing over the pulled yarn were displaced upward more than the adjacent portions of the pulled yarn and this is depicted in the line named "difference".

Figure 8.18 The "difference" line in Figure 8.17 depicted for two different force levels. The figure shows the influence of the force on the pulled yarn on the level of yarn migrations.

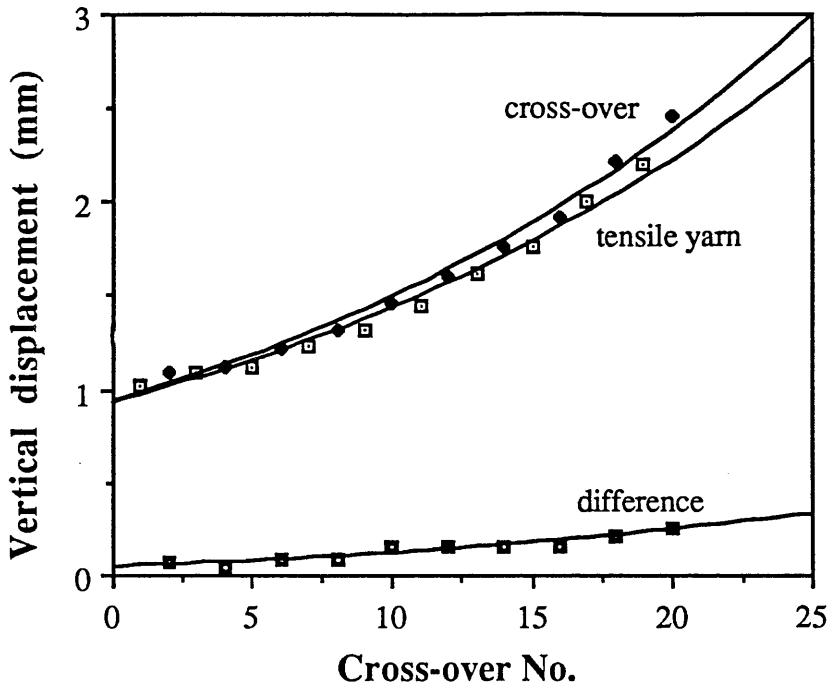
Vertical displacement (mm)
3
2
1
0
cross-over
tensile yarn
difference
0
5
10
15
20
25
Cross-over No.

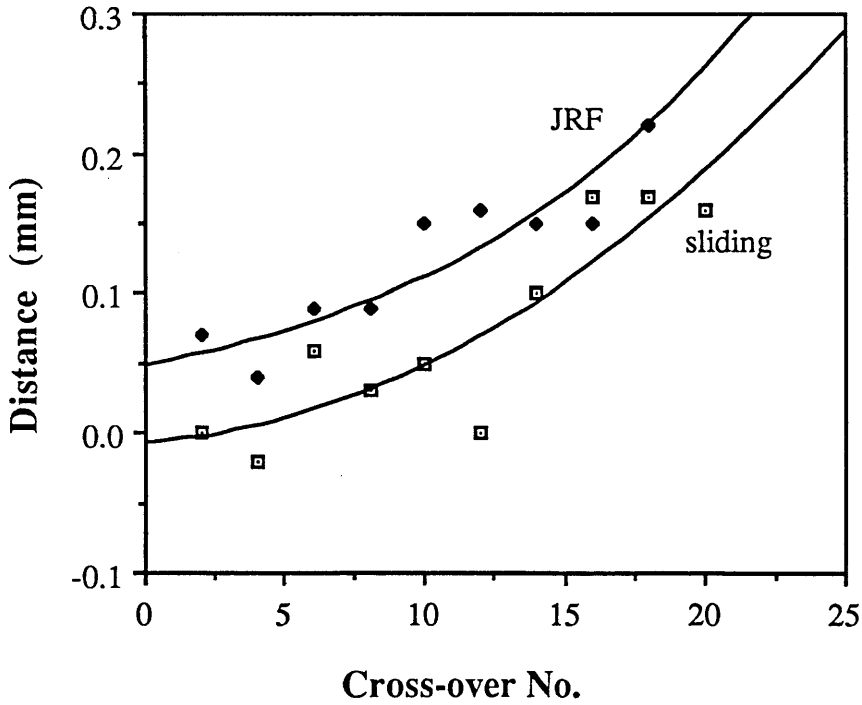
Distance (mm)
0.3
0.2
0.1
0.0
-0.1
JRF
sliding
0
5
10
15
20
25
Cross-over No.

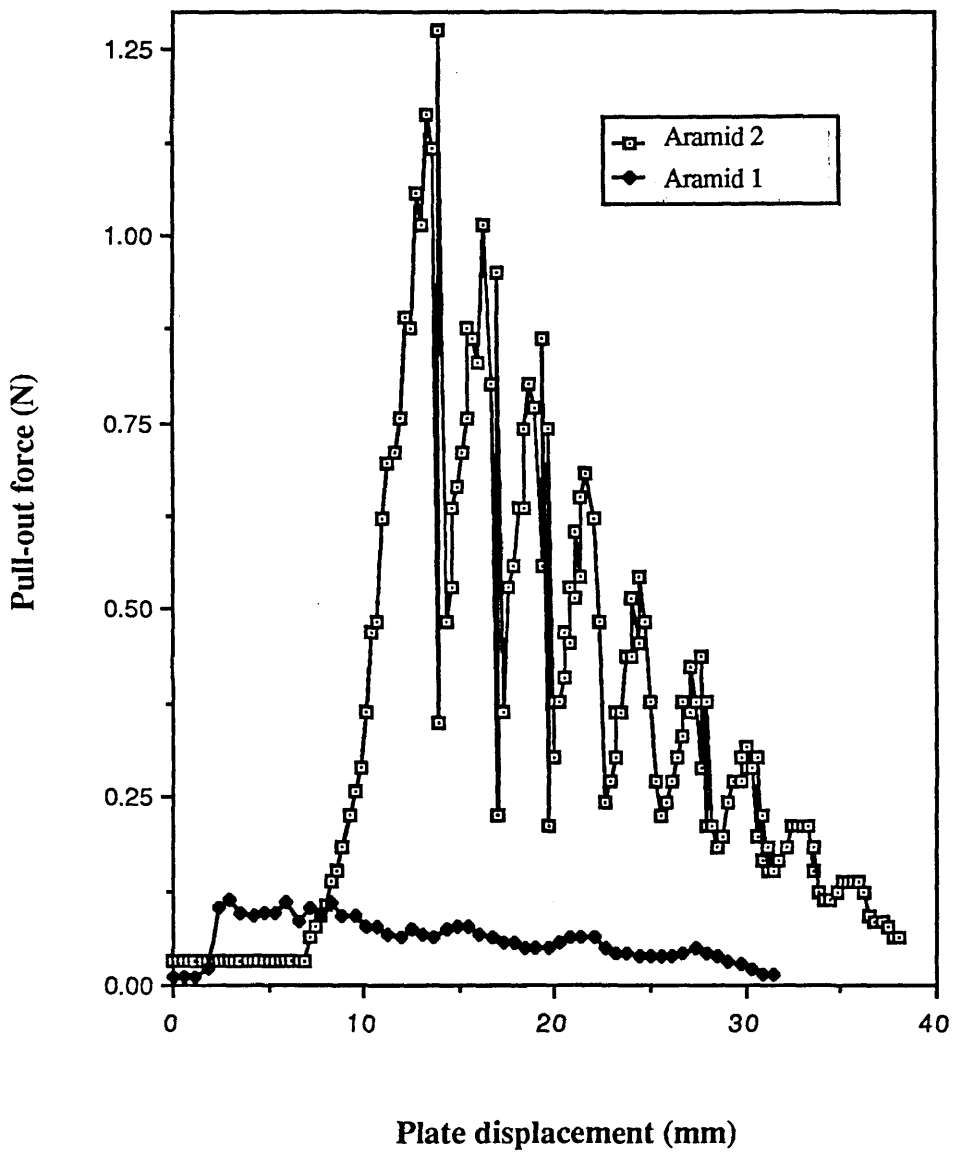

Figure 8.19 The pull-out profiles for two untreated Aramid (kevlar 29 and 49) fabrics. Side tension = 0.

amount of crimp was, however, greater in the aramid 2 fabric. This fabric exhibited sharp stick-slip peaks and troughs. Another difference which is most pronounced in aramid 1 is that immediately after JRF, the frictional forces are not reduced to a fraction of JRF and, what is more, the weave does not produce a pronounced unsteady state region of stick-slip. Also, unlike cotton, immediately after JRF the pulled yarn does not clear several cross-overs in one slip. Rather, it clears the cross-overs one by one until all have been cleared. The stick-slip and the dynamic friction regions are similar to cotton except that the aramid fibre pulled yarn undergoes a much greater number of slippages to clear a cross-over than the cotton.

8.4.2 The Effect of Weft Yarn Tension

The differences between aramid 1 and 2 fabrics are clearly seen from figure 8.19. Table 8.2 lists the characteristic values of the parameters of the force-displacement profiles for the two fabrics. First of all, the reduction of the number of cross-overs in the aramid 2 fabric has the expected result of reducing all the parameters accordingly. Also, increasing the side tension on the aramid 1 fabric has the same effect as that observed with cotton, i.e. increasing the measurable parameters of the profile. Figures 8.20 and 8.21 depicts the variation of average values of the JRF and the dynamic gradient with lateral tension in the same way as Figure 8.4 and 8.5 for cotton.

Figure 8.20 Variation of JRF with side tension for the Aramid 1 (kevlar 49) fabric.

Figure 8.21 Variation of the sliding friction force per junction (Region IV) with imposed side tension for untreated aramid 1 fabrics.

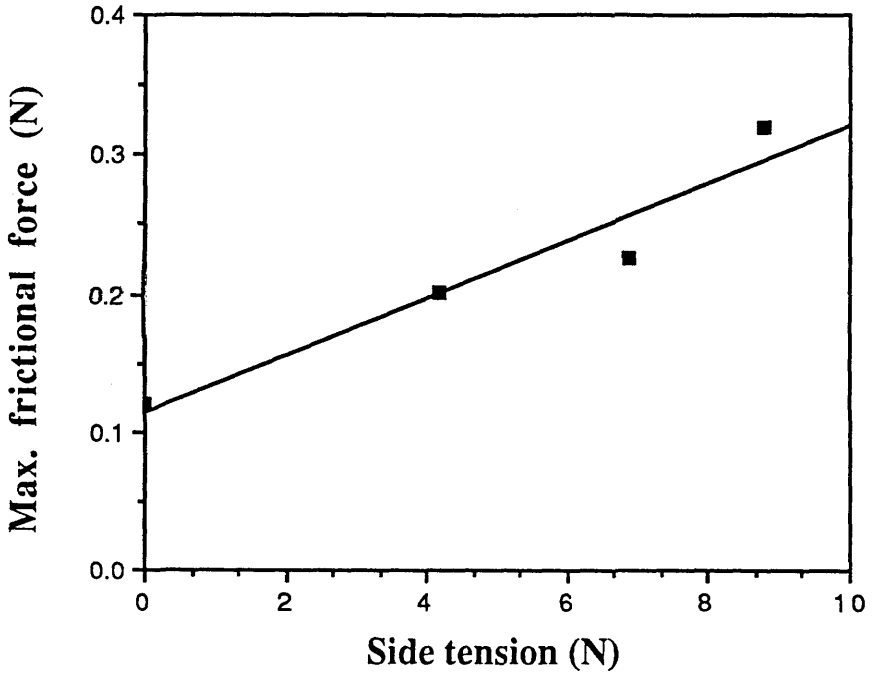
Max. frictional force (N)
0.4
0.3
0.2
0.1
0.0
0
2
4
6
8
10
Side tension (N)

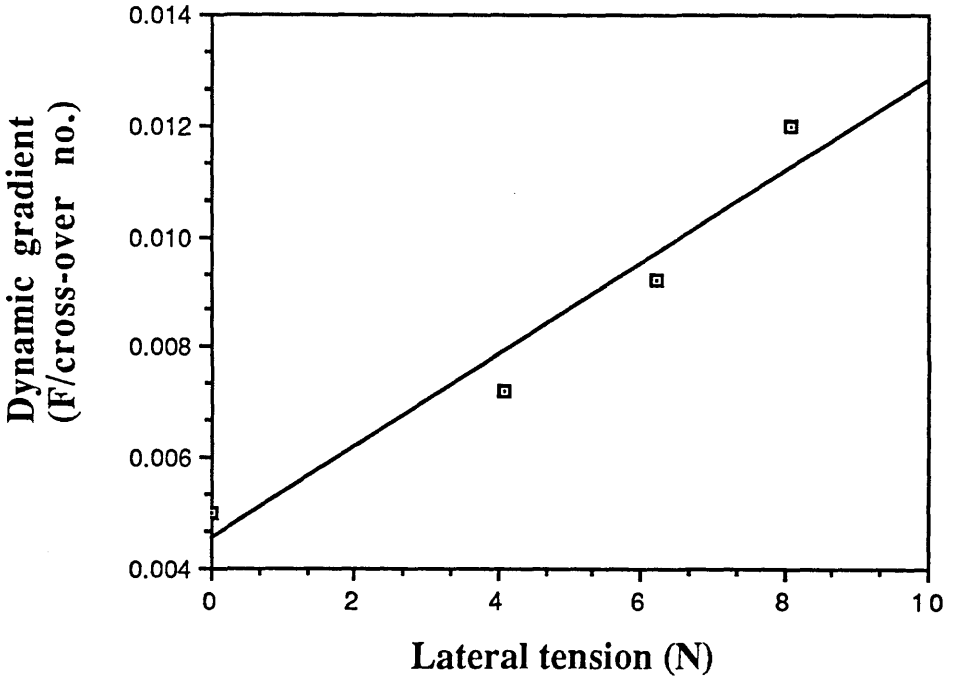
Dynamic gradient
(F/cross-over no.)
0.014
0.012
0.010
0.008
0.006
0.004
0
2
4
6
8
10
Lateral tension (N)

TABLE 8.2

Fabric	Side Tension (N)	No. of X-overs	G (N/mm)	JRF (N)	Dyn.Grad. (N)
Aramid 1	0	20		0.12	0.005
	4.12	20		0.2	0.0075
	6.55	20		0.225	0.0095
	8.23	20		0.32	0.012
Aramid 2	0	30	0.274	2.54	0.065
	0	20	0.234	1.48	0.073
	0	10	0.15	0.47	0.034
	0	5	0.14	0.27	0.03

Table 8.3 lists the values obtained from a linear regression to the data presented in figures 8.20 and 8.21 in terms of the units employed. As before, it is supposed that the variations apparent in Figures 8.20 and 8.21 are again simply due to the side tension providing a component of the normal load at the cross-overs.

TABLE 8.3

Plot	Gradient	Intercept	Corr.Coefft.
JRF vs. lateral tension	0.022	0.108 N	0.97
Dyn.grad. vs. lateral tension	8.4×10^{-4}	0.005 N	0.99

It is notable, however, that the absolute values of the JRF and the dynamic frictional force for aramid 1 are several factors smaller than those for aramid 2. This may be due to several factors. One is that the yarns in the aramid 2 fabric possessed some crimp while those of aramid 1 had no apparent crimp. Another reason could be that the structure and the tightness of the weave modifies the response. The simple and relatively tighter weave of aramid 2 suggests that there may be greater pressure at

the cross-over junctions than there was for the aramid 1 weave. The ages of the fabrics may also be a contributing factor, with the older fabric possessing an increased adhesion at the junctions. Surface roughness may be excluded as a factor here since no significant difference in the roughness of the aramid yarns were observed.

In the case of the aramid fabrics, it was not possible to measure the displacements of cross-overs or extensions of yarns because of the intrinsic stiffness of the yarns. The weave did not produce measurable deformations at the force levels employed.

8.5 Conclusion

The friction and the deformation of the pulled yarn and the adjacent matrix is found to play important parts in the pull-out process. Increasing the tension on the orthogonal yarns increases the identifiable parameters associated with the pull-out experiment and in particular the friction. This was attributed to an increase in normal load (as a component of side tension) at the contacts.

The extension of the pulled yarn increments between cross-overs was found to increase with cross-over number. This was particularly so when the extension measurements were corrected for the out-of-plane micro-displacements. These vertical micro-displacements, which were imposed by the experimental arrangement, were also found to increase both with cross-over number and initial force on the pulled yarn.

The migration in the orthogonal yarns were observed and measured and it was found that the yarns lying underneath the pulled yarn were "pushed down" while those lying above it were "pushed up". Migration was found to increase with both the cross-over number and the force on the pulled yarn. Finally, the shape of the matrix deformation component in the pull-out process was found to resemble the shape of the deformed fabrics in the "hardness" and the ballistic experiments.

CHAPTER NINE

THE PULL-OUT EXPERIMENTS ON TREATED FABRICS

9.1 Introduction

The finishing of textiles involves the deposition or the reaction of various chemical substances with a particular fabric to yield a material with the "desired" characteristics. These substances may be lubricants, cross-linking agents such as dimethyl silicones, cationic, anionic or non-ionic surfactants such as fabric softeners. These treatments may produce modifications to both the surface and/or the bulk. In the case of a yarn, for example, the treating agent, depending on its molecular size and charge, may either deposit itself on the surface of the yarn or penetrate the yarn and deposit on the surface of the fibres. In the case of cotton, it may also modify the fibril surface. Finally, of course, the substance may sorb into the fibril or monofilament itself. The identification of the level of surface modification and the specification of the extent of bulk sorption are generally not resolved in practice. This study has rather assumed that the fabric treatments introduced have been surface specific, although no evidence is available to confirm this belief.

The results of the yarn pull-out experiment on treated cotton and aramid 1 (Kevlar 49) fabrics (described in Section 5.7.2) are presented in this chapter. The results are divided into two sections: (1) the studies on submerged treated fabrics and (2) the investigations carried out on dry treated fabrics. As well as discussing the parameters associated with the pull-out profile, the values of cross-over moduli (as denoted by E_m) which are calculated using the spring model (described later in Chapter 10) are also presented.

9.2 Deformation and Pull-out Experiments Carried out on Submerged Fabrics

In these experiments, the cotton fabric was totally submerged in the solution of the treating agent. Only cotton fabrics were used in this study. The procedure for these experiments was described in Section 5.7.2.1. The treating agents used were distilled water (various immersion times), pure tetradecane (0.5 and 2 hours immersion), solutions of 1% and 2% w/w stearic acid in tetradecane and a solution of 1% w/w CTAB in distilled water. Untreated and dry cotton fabrics were also examined in this configuration as a standard for comparison purposes. These solutions were chosen as typical of the two generic classes of solution based fabric treatments. The aqueous systems represent a simple common fabric treatment system. The surfactant introduces a charge surface layer which may be considered as a very effective electrical double layer lubricant. The apolar system was chosen to explore the role of classical boundary lubricant action in these systems.

The parameters associated with the force-displacement profiles were introduced in Chapter 8. Figure 9.1 shows a typical force-displacement profile for an untreated cotton fabric and also for one submerged under water for 30 minutes. The shapes of the profiles are similar in that they both exhibit the four response regions described previously (Chapter 8). The profile for the submerged fabric is consistent with lower values of G, JRF and the dynamic friction (see Chapter 8). Table 9.1 lists the values of these parameters and values for the cross-over moduli of the treated fabrics. The table also provides data for various immersion times in water as well as the data produced for the CTAB solution (2 hours immersion) and the various apolar solutions.

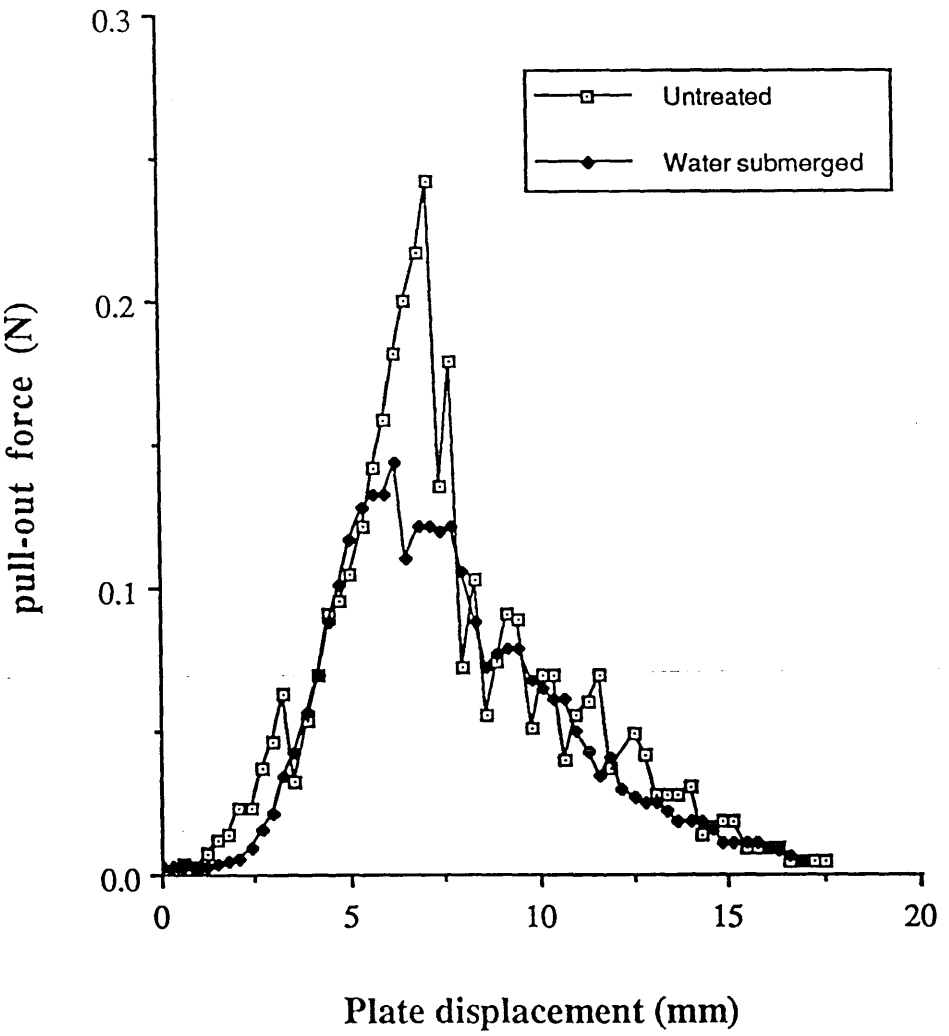

Figure 9.1 Comparison of the pull-out profiles of dry untreated cotton fabric with that of a cotton fabric submerged under water for 30 minutes prior to pull-out. Side tension = 0.

TABLE 9.1

Treatment	G(N/mm)	JRF(N)	Dyn.grad. ($x10^{-3}$)(N)	Modulus (N/m)
Untreated (dry)	0.063	0.2414	6.26	94
Water (1/2 hr)	0.038	0.125	5.1	78
Water (2 hr)	0.035	0.095	2.6	67
Water (5 hr)	0.015	0.08	1.7	42
Water (23 hr)	0.022	0.075	2.88	37
Tetradecane (1/2 hr)	0.064	0.186	6.96	127
Tetradecane (2 hrs)	0.088	0.2437	6.18	140
0.1% w/w stearic in C_{14} (1/2 hr)	0.064	0.25	8	54
0.2% w/w stearic in C_{14} (1/2 hr)	0.07	0.3	8	65
CTAB ($4.5x10^{-4}$M soln.) (2 hrs)	0.039	0.104	3	113

Figures 9.2, 9.3 and 9.4 summarise the parameters G, JRF and dynamic gradient as a function of immersion time for cotton fabrics submerged under water. All the parameters decrease quite significantly with time. These results indicate that the interyarn friction at the junctions has decreased both relative to the friction at the dry contacts and also with increasing immersion time. It is well known that the friction of cotton fibres increases with increased relative humidity or "wetness" (Viswanathan,1973). These data apparently contradict these findings. However, the trend obtained here can be explained in the light of the fact that water penetrates between the contacts, lubricating them and reducing the friction and this lubrication increases with increased submerged time. However, after about five hours, the trends seem to have ceased and in fact increased submerged times of up to 23 hours produced higher values of G and the dynamic gradient. This may result from the swelling of the cotton after long immersion times which in some way undermines the lubricating

Figure 9.2 The effect of the time of submergence on the value of the gradient G of the linear portion of the pull-out profile (Region II).

Figure 9.3 Values of junction rupture force (JRF) for submerged cotton fabrics as a function of the time submerged.

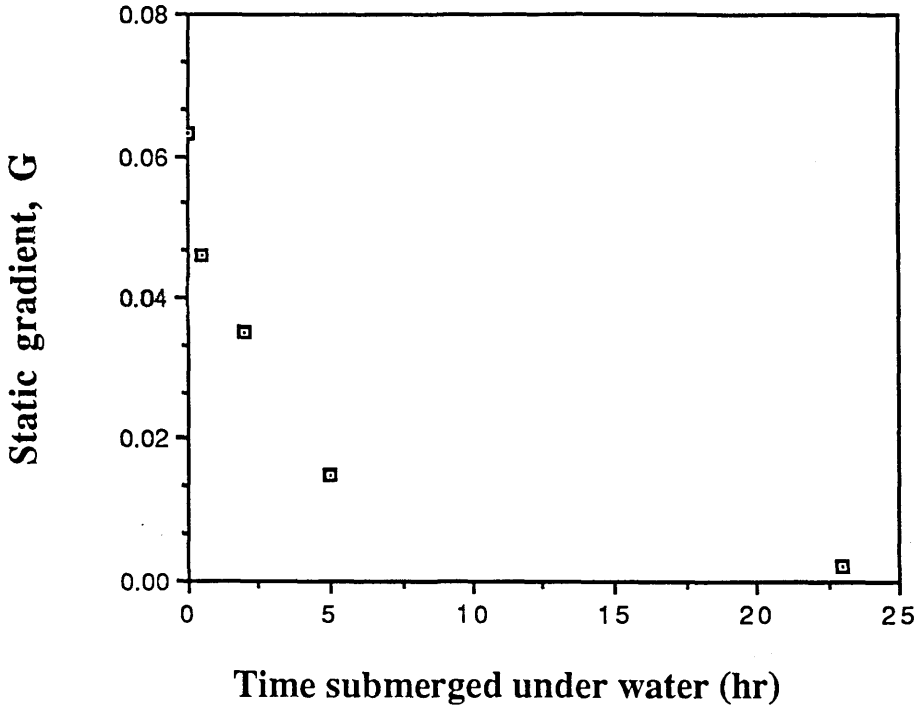
Static gradient, G
0.08
0.06
0.04
0.02
0.00
0
5
10
15
20
25
Time submerged under water (hr)

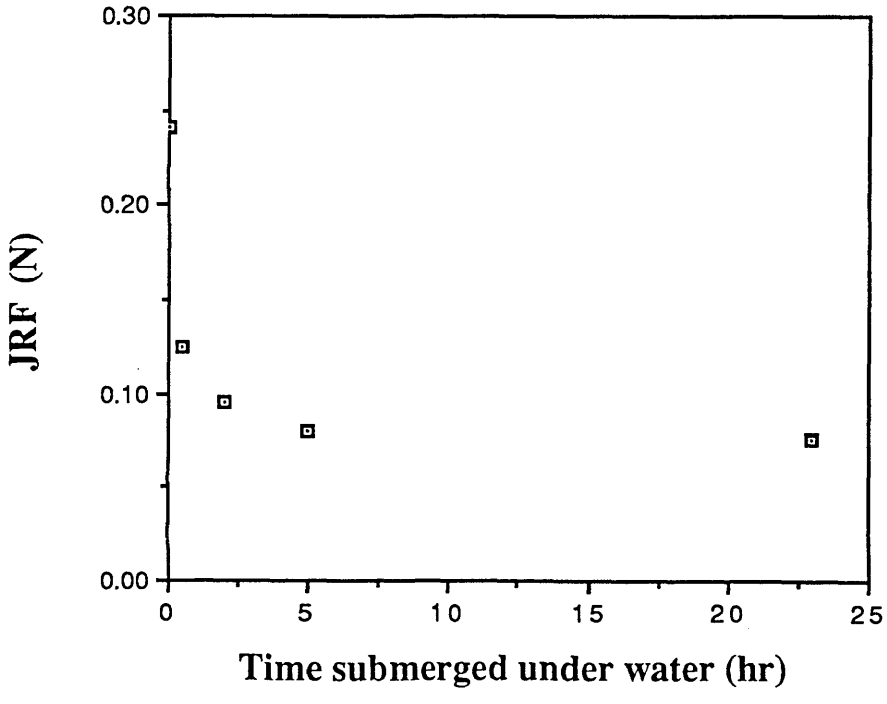
JRF (N)
0.30
0.20
0.10
0.00
0
5
10
15
20
25
Time submerged under water (hr)

action of the water.

In the case of pure tetradecane, the parameters directly associated with the interyarn friction processes, i.e. the JRF and the dynamic gradient, have not been affected significantly. However, the parameters that control the compliance or stiffness of the weave or pulled yarn, i.e. G and cross-over modulus, have increased indicating a decrease in the weave compliance. Stearic acid solution in tetradecane has decreased this effect to some extent but the friction parameters have still scarcely been affected. Stearic acid is known to be a fairly efficient boundary lubricant. However, it must be present at the interface before it can impart any lubricity to the fibre system. Apparently both the amount and the application method used here were such that this condition was not satisfied. For the cotton fabric submerged in a solution of CTAB in water (below the CMC) the data may be compared with the results for the cotton submerged in pure water for 2 hours. The parameters G, JRF and dynamic gradient are hardly altered. The cross-over modulus has, however, increased by ca. 40%. Although the absolute values of these parameters are subject to some error, the trends are quite obvious. It is anticipated that the positively charged CTAB molecules will attach themselves to the negatively charged cotton and produce reductions both to the friction and the modulus through their lubrication and plasticisation properties. The absence of these changes may be due to the low concentration of the CTAB in solution.

9.3 Pull-out Studies on Dry Treated Fabrics

These data divide into two categories, treated cotton and treated aramid 1 fabrics. The procedures for these experiments were described in detail in Section 5.7.2.2. For the cotton, experiments were performed on fabrics treated with solutions of PDMS (poly dimethyl siloxane) at concentrations of 2, 3, 5, 7, 10% w/w and three

different concentrations of CTAB solution in water. The CTAB concentrations were chosen to fall on both sides of the CMC, which for CTAB is ca. 10^{-3} M. These lubricant systems are fairly typical of those used in practice but it is ofcourse not practical to lubricate aramid fibre systems for ballistic purposes. The PDMS systems are, however, obvious fluid lubricants and the CTAB material is an effective fabric conditioner. The Aramid fabric was washed with acetone (soxlet extracted). The clean fabric was then treated with a solution of 5% PDMS in petroleum spirit.

The results for the cotton fabrics are presented first. Figures 9.5, 9.6 and 9.7 depict the way in which the main parameters of a force-displacement profile, i.e. G. JRF and dynamic gradient change with the increasing solution concentrations of PDMS for the cotton fabrics. All three parameters are seen to decrease with the increasing of the silicone fluid concentration. Table 9.2 presents computed values for these parameters. The calculated moduli of the cross-over yarns does not follow the same trend. The decrease in the friction parameters may be interpreted as arising from the lubricating properties of silicone fluids. Apparently, the effectiveness of the PDMS has also increased with the increase in bulk concentration of the treating solution. However, the fact that the weave compliance parameters and especially the modulus have not decreased is perhaps because the silicone did not penetrate into the yarn structures in order to reduce the inter-fibre friction.

Figure 9.4 The effect of increasing submerged times on the dynamic friction force per junction of cotton fabrics during pull-out (Region IV).

Figure 9.5 The effect of PDMS solution concentration on the gradient G of the linear region of the pull-out profile. The fabric (cotton) was submerged under the PDMS solution for 2 hours and subsequently dried prior to the experiment.

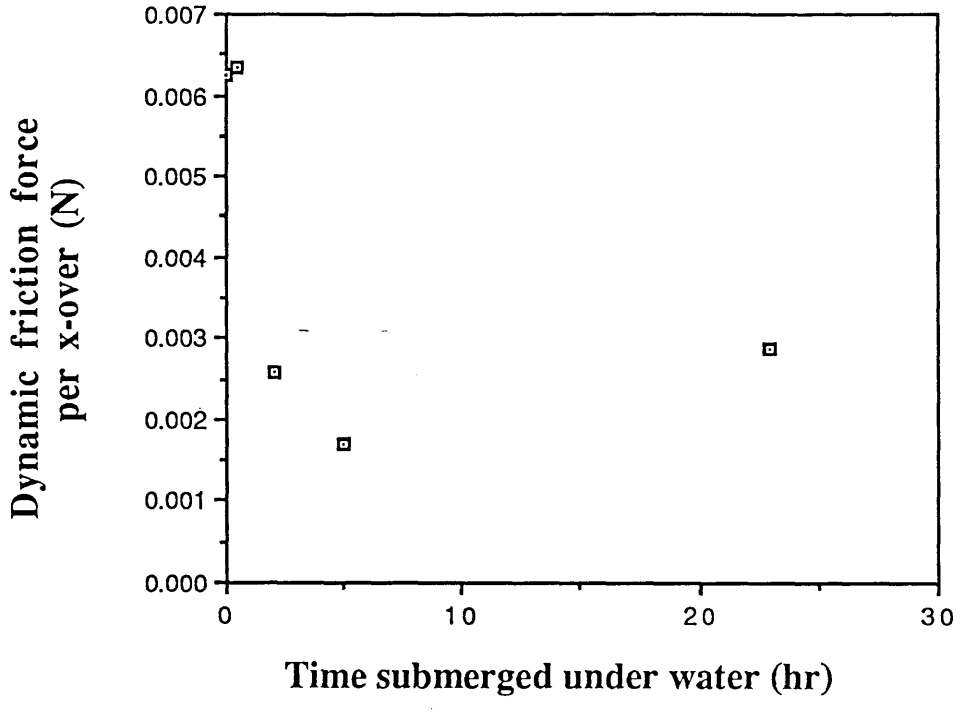
Dynamic friction force per x-over (N)
0.007
0.006
0.005
0.004
0.003
0.002
0.001
0.000
0
10
20
30
Time submerged under water (hr)

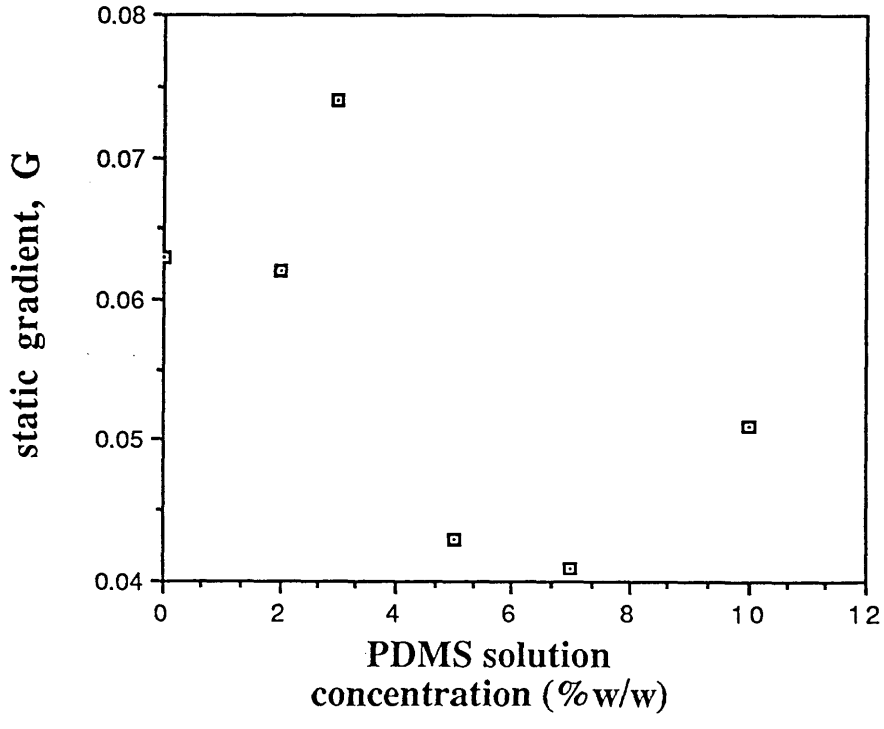
static gradient, G
0.08
0.07
0.06
0.05
0.04
0
2
4
6
8
10
12
PDMS solution concentration (%w/w)

Figure 9.6 Variation of JRF with increased concentration of PDMS in the treatment solution.

Figure 9.7 The effect of PDMS treatment solution concentration on the dynamic friction force per junction of cotton fabrics.

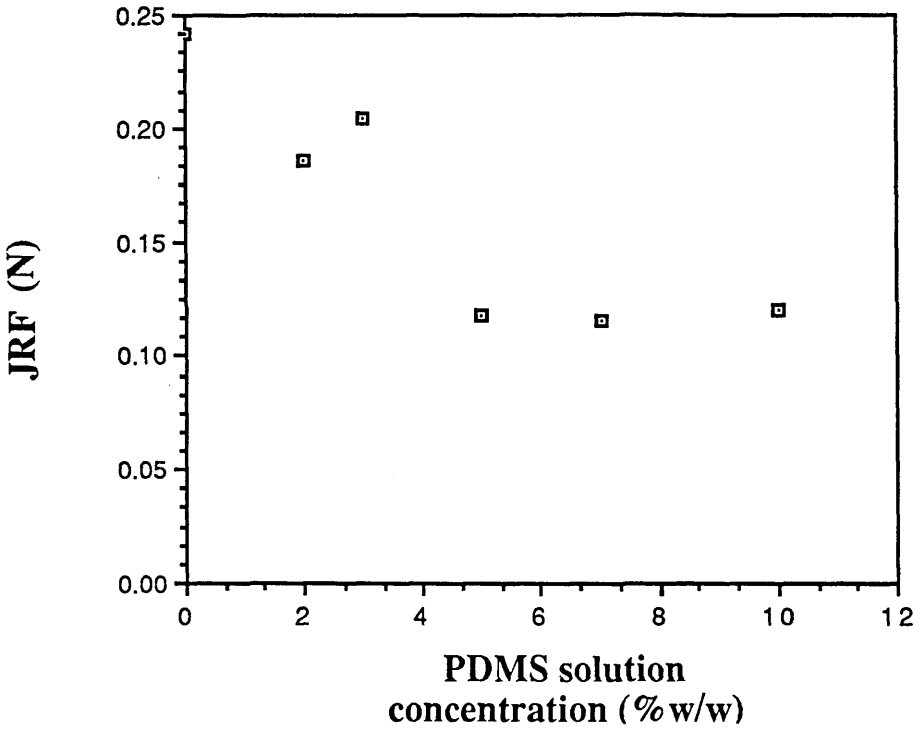
JRF (N)
0.25
0.20
0.15
0.10
0.05
0.00
0
2
4
6
8
10
12
PDMS solution
concentration (%w/w)

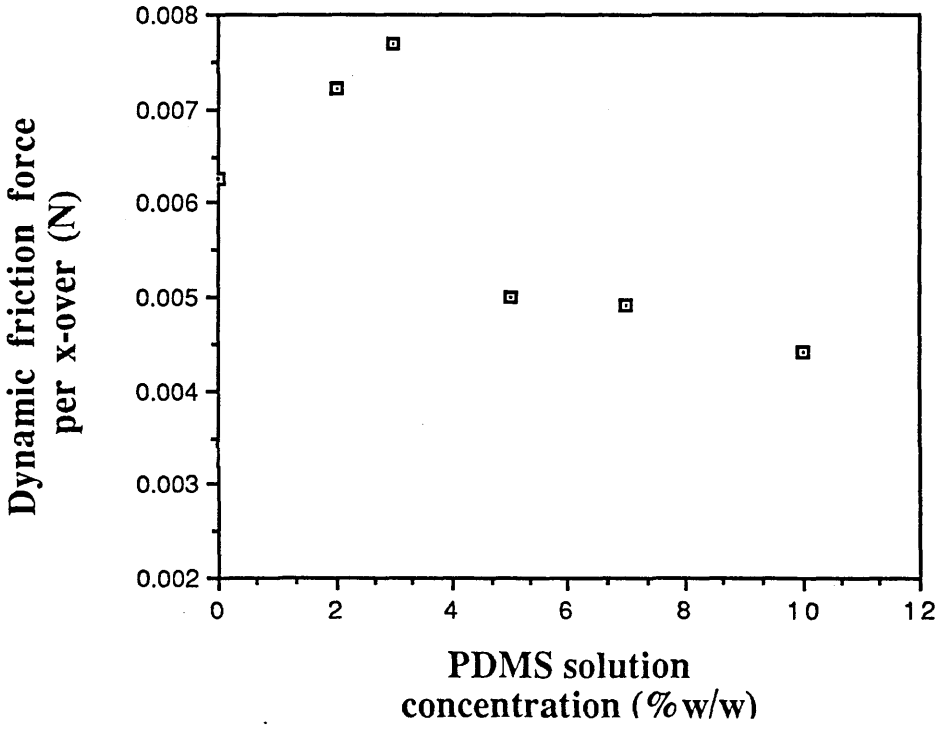
Dynamic friction force
per x-over (N)
0.008
0.007
0.006
0.005
0.004
0.003
0.002
0
2
4
6
8
10
12
PDMS solution
concentration (%w/w)

TABLE 9.2 The Effect of Various Treatments on the Pull-out Parameters of Cotton

Treatment	G(N/mm)	JRF(N)	Dyn.Grad. $x10^{-3}$(N)	Modulus (N/m)
PDMS				
2%	0.062	0.186	7.22	57
3%	0.074	0.204	7.77	62
5%	0.043	0.118	5	63
7%	0.052	0.116	4.92	110
10%	0.051	0.12	4.4	73
CTAB				
$1.37x10^{-4}$M	0.071	0.1844	5	179
$1.37x10^{-3}$M	0.070	0.168	3.48	100
$2.74x10^{-3}$M	0.053	0.145	3.34	41
CTAB+$1.37x10^{-4}$M Marlophen 825	0.069	0.168	3.49	119

The results for the CTAB solution shown in Table 9.2 indicate that with the increasing of the solution concentration, both the friction and compliance parameters have decreased. Also the CTAB solution containing the Marlophen 825 non-ionic surface active agent shows a decrease in these parameters compared to the solution with no Marlophen 825 added. Cationic surface active agents are well known for their softening properties. Increased softness, as discussed in chapter 4, is usually accompanied by a decreased friction and stiffness. The data for CTAB is consistent with this hypothesis. The tensile moduli of the fabric treated with CTAB, Figure 5.13 is also consistent with this argument. The addition of the Marlophen 825 has not affected the values of G or JRF, but the dynamic gradient and the modulus have been significantly reduced. The way in which these reductions are brought about are not known.

Comparing the results of Table 9.2 with the results for the untreated fabric given in Table 9.1 indicates that in the case of PDMS treated cotton, almost all the parameters are reduced when silicone fluids are introduced onto the cotton fabric. The

same trend was observed in the case of the tensile and the "hardness" studies (Figures 5.13 and 6.13). The case of CTAB is rather different. The lower concentrations of CTAB, i.e. $1.37x10^{-4}M$ and $1.37x10^{-3}M$ have not reduced the parameters significantly when compared to the untreated case. The same result was obtained for the cotton treated with the same concentrations in the tensile experiments (Figure 5.13) and the "hardness" experiments (Figure 6.14). However, the $2.7x10^{-3}M$ solution of CTAB seems to have reduced the JRF, the dynamic gradient and the modulus values by as much as 50%. This reduction is not as substantial as was observed for the tensile and the "hardness" tests. Thus, it seems that a reduction in the friction and tensile properties of the yarns by CTAB is only brought about at relatively high concentrations above the CMC of the surfactant.

Table 9.3 lists the data for the pull-out experiments with cleaned and 5% PDMS treated aramid fabrics. It can be seen that removing the surface finishes, through cleaning the fabric with acetone, has increased both the JRF and the dynamic friction parameters. The treatment with a lubricant, the silicone fluid, has reduced these parameters significantly. As with the cotton, the changes observed in the case of the aramid fabric may be explained through the changes that are brought about in the interyarn friction.

TABLE 9.3 The Effect of Treatment on the Pull-out Parameters of Aramid 1 Fabric

Treatment	JRF(N)	Dyn.Grad.(N)
Untreated	0.12	0.005
Cleaned	0.18	0.009
5% PDMS	0.07	0.003

9.4 Summary

The response of treated cotton and aramid 1 fabrics to the pull out of a single yarn from the fabric matrix has been described. These responses were quantified in terms of two processes, the interyarn friction, being represented by JRF and the dynamic gradient, and the weave compliance represented by the parameter G and the modulus. In most cases treatment with the chosen surface agents was seen to be accompanied by a reduction in these parameters and in particular in the friction. This was seen to be more pronounced when the lubricant or the surface active agent was deposited at the interface as in the dry treated studies rather than when it was present in solution as in the submerged experiments. In the case of PDMS and CTAB treatments, increased concentration of the treating agents were found to have a positive effect on the extent of the lubrication.

CHAPTER TEN

ANALYSIS AND DISCUSSION

10.1 Introduction

In previous chapters the various experimental data obtained in this study were presented without substantial comment or analysis. This chapter will seek to explain and evaluate these data in more detail and also in the light of some of the information described in Chapters 2, 3 and 4.

The chapter is loosely divided into several sections each dealing with the analysis and discussion of a particular set of experiments. However, the important notion which should be pointed out is that the "hardness", the ballistics and the pull-out processes all involve similar fabric distortions. That is a pyramidal or a partially pyramidal deformation the shape of which may be represented fairly well by an exponential relationship, figure 8.13. Both the "hardness" and the ballistic experiments involve yarn pull-out, matrix shear and yarn extension processes of varying degrees. This was particularly so in the case of the ballistic impact of lubricated aramid fabrics. Thus the three experiments are closely related, except that the microscopic deformation and migration processes which occur during the quasi-static indentation and the ballistic processes are more amenable to investigation in the pull-out experiments.

A local displacement model is presented first which describes the matrix shear during the pull-out experiment. The variation of JRF and kinetic friction with load on the weft yarns is then discussed in conjunction with a fairly simple geometric representation of the matrix. Next, the result of applying the diaphragm model (thin plate model) to the "hardness" experiments is discussed. Finally, the application of the

thin plate model to the ballistic deformation experiments is described and the results discussed.

10.2 Matrix Shear during the "Pull-out" Experiment

10.2.1. Introduction

The results and observations relating to the pull-out experiments were mostly discussed in chapter 8 under separate headings. These included the general results and observations of the pull-out experiments and their relation to side force and the in plane and out of plane micro-displacement of the weave. This section outlines a model that will attempt to predict the form of the elastic part of the force-displacement profiles, of which Figure 8.1 is a typical example. The model is based upon the behaviour of a series of springs depicted in Figure 10.1. Several cases are examined. The way in which the imposed force, F, produces the localised extensions which propagate along the length of the tensile yarn has been dealt with by Sebastian *et al* (1986). In that model, Figure 10.1(b), two assumptions were made. First, the tensile (pulled) yarn modulus, E_y, was taken as a constant. Second, the force experienced by the weave which acts at the individual cross-overs was also assumed to be constant and thus independent of the local displacements. This model is effective in so far as it fits the form of the experimental data but it has many obvious weaknesses. A model is offered here which is based on the previous model but allows the tensile yarn modulus, E_y, to be a function of strain, ε. It also, in contrast, considers that the elasticity of the matrix arises from the resolved tensile forces, fc, in the adjacent weave. Hence the cross-over restraining forces vary with the local strain developed in the cross-overs.

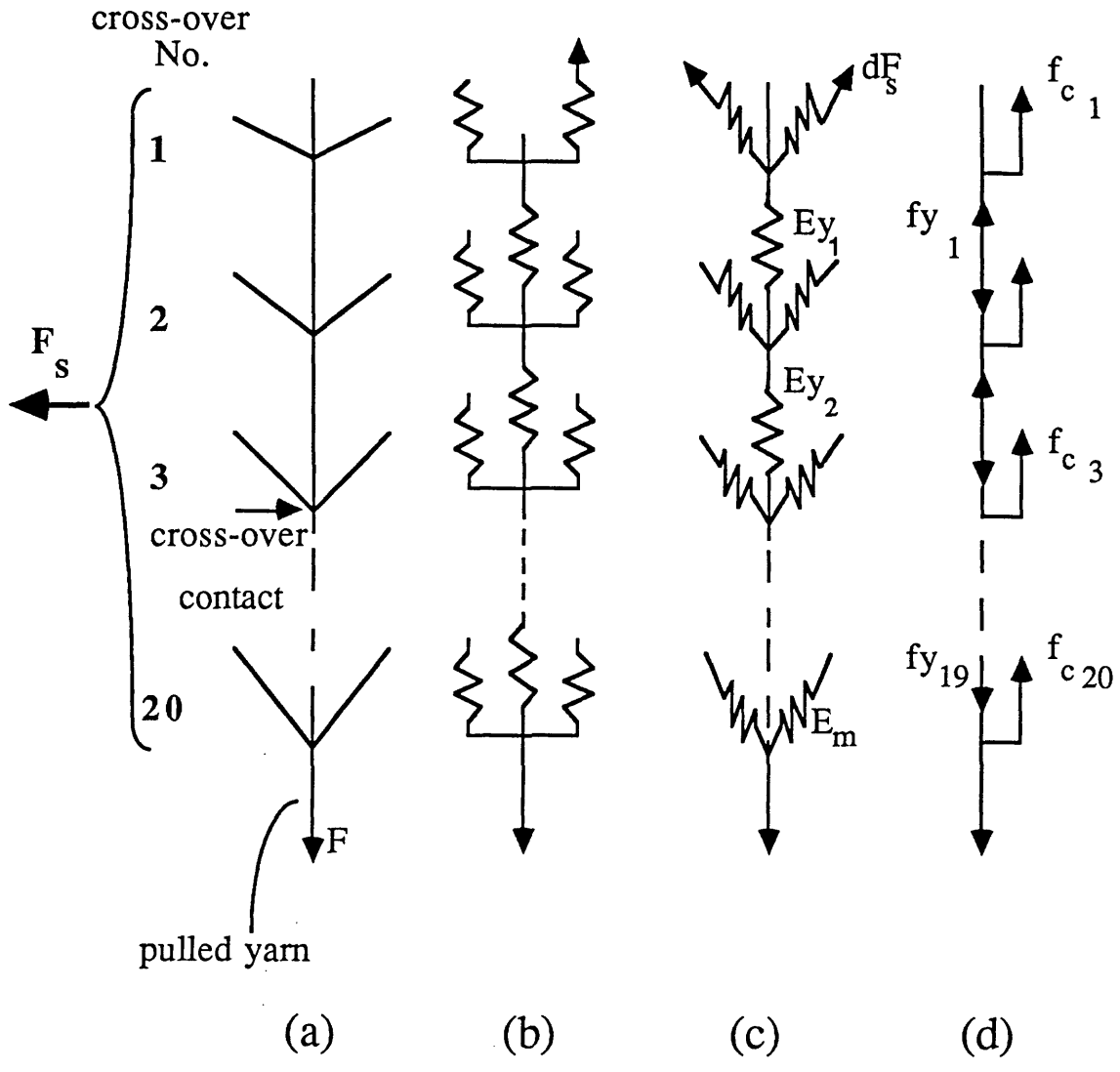

Figure 10.1 A schematic representation of the model adopted to predict the form of the elastic part of the force-displacement profile.

10.2.2 Theoretical Representation of the Model

Figure 10.1(b) depicts the original model adopted by Sebastian *et al* (1986). As was mentioned earlier, it assumed the tensile yarn modulus to be independent of strain and took the forces in the cross-over yarns to act in the same direction as the tensile yarn. Although this model effectively described a number of trends in their data, it is clear that the simplified assumptions mentioned undermine its credibility. Figures 10.1(c) and 10.1(d) depict the model to be described in this section. This model, whilst still first order, does avoid some of the major weaknesses of the original approach. It, for example, considers the forces on the cross-over yarns to act, not along the direction of the tensile yarn, but at an angle to it; Figure 10.1(d) illustrates the action of these forces. Another facet of the current model is that it assumes a common stress-strain curve for all the tensile elements, that is for both the pulled yarn and the cross-over yarns. It actually turns out that it is sufficient in the system to be described to assume that the cross-over yarn modulus, E_m, is independent of the strain and is thus constant.

The basic elements of the model are now described. Reference to Figure 8.10 shows that the extensions of the tensile yarn elements between adjacent cross-overs increased with increasing cross-over number. (N=20 at the hook where the force is applied). These individual extensions, ε_N, can be adequately related to the cross- over number, N, by the equation:

$$\varepsilon_N = a.\exp(b.N) \qquad (10.1)$$

where a and b are constants. The experimental values of ε as a function of N were shown in Figure 8.10. The values were calculated by subtracting the displacements of adjacent cross-over positions. The relation between the cross-over displacements, d_N,

and ε_N may be written as:

$$d_N = \Sigma \varepsilon_N \qquad (10.2)$$

d_N as defined in Figure 10.2.

In order to calculate the magnitude of d_N, one can either use the experimental values of ε or those incorporated in Equation (10.1) with appropriate fitting parameters. In the subsequent analysis, the actual experimental values of ε_N were used.

Figure 10.2 shows the definitions of geometrical parameters associated with a single cross-over region. d_0 is the half width of the fabric transverse to the pulled yarn; fc_N is the force on an element of the tensile yarn acting in the cross-over direction. θ_N is the weave angle. In the model it is assumed that during the pull-out, the cross-over displacements, d_N, are solely brought about by the tensile extension of the cross-over yarns. The yarns are therefore assumed to be perfectly flexible. There will also be a contribution from the extension of the local element of the tensile pulled yarn. In addition, these extensions are regarded as acting through the weave to the edge of the fabric where it was clamped. If the half extension of the cross-over yarns is represented by δ_N (Figure 10.1(c)) then:

$$\delta_N = \sqrt{d_o^2 + d_N^2} - d_0 \qquad (10.3)$$

The model assumes that a global spring modulus, E_m, operates on the cross-over yarns which is independent of strain and is thus a constant. It also assumes

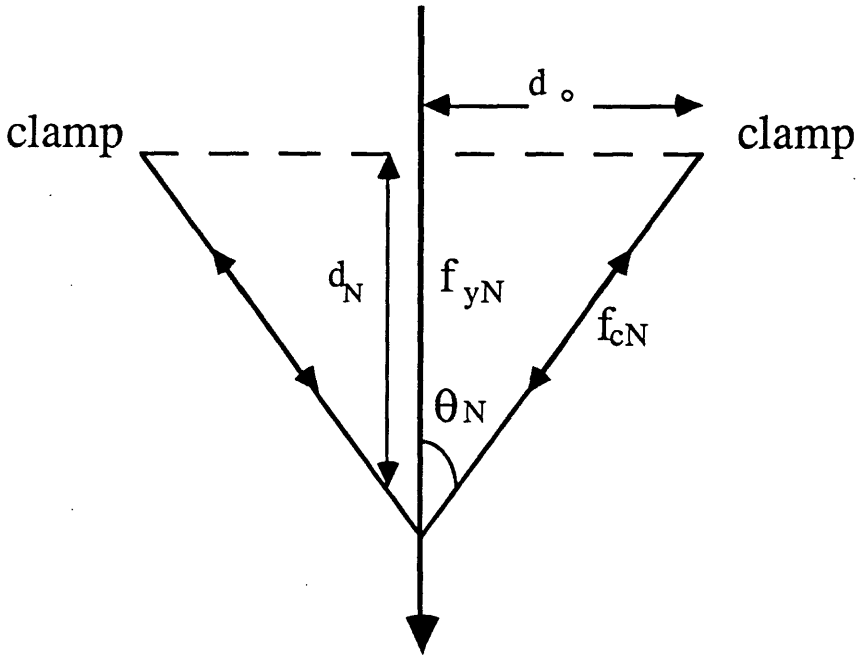

Figure 10.2 A schematic representation of a single cross-over region.

that the extension of the cross-over yarns, both singly and as a whole (i.e. the addition of all cross-over extensions) is proportional to the forces acting on them. That is, fc_N in the case of a single cross-over and the JRF in the case of the whole matrix. Thus one can write the appropriate relationships for E_m and fc_N as:

$$E_m = JRF/\sum_{1}^{N} 2\,\delta \cos \theta_N \qquad (10.4)$$

and $$fc_N = E_m \,.\, \delta_N \qquad (10.5)$$

The factor 2 in Equation (10.4) arises from the fact that there are two force components generated by the cross-over yarns. Hence, a knowledge of the values of ε and JRF yields a value for E_m (Equations (10.1) to (10.4) inclusive) and this enables fc_N to be calculated.

The force fy_N on a particular element of the tensile yarn can be thought of as being made up of the combination of the force on the element before it, fy_{N-1}, and a component of the force on the adjoining cross-over yarn, fc_N. The relationship can be written as:

$$fy_N = fy_{N-1} + 2\,fc_N \cos \theta \qquad (10.6)$$

This argument is then applied throughout the weave back to the first cross-over where the yarn is cut (furthest from the hook) where:

$$fy_1 = fc_1 \quad \text{since } fy_o = 0$$

Hence one appreciates that the forces on the tensile yarn elements are expended through extending the cross-over yarns and the tensile yarn elements only act as springs to transmit the force down the line of the pulled yarn. Thus:

$$fy_N = \Sigma\, 2\, fc_N \cos\theta \qquad (10.7)$$

The important experimental variable, as mentioned in Chapter 8, Figure 8.2, was the imposed side tension. fc_N can also be thought of as arising from the combination of a component of fy_N in the direction of the cross-over yarn and the initial tension imposed on the cross-over yarn, f_s. Equation (10.8) represents this relationship and provides a means of examining the effect of f_s on fc_N.

$$fc_N = fy_N \sin\theta + f_s \qquad (10.8)$$

Finally, a tensile yarn element spring constant, Ey_N, can be calculated using the calculated values of fy_N and the experimental values of ε_N, since by definition:

$$fy_N = Ey_N \cdot \varepsilon_N \qquad (10.9)$$

In summary, the experimental observations, together with the model and Equations (10.1) to (10.9) inclusive, have enabled the calculation of (a) a global cross-over modulus, E_m, (b) the forces acting on individual cross-over and tensile yarn elements and (c) spring moduli for discrete elements of the tensile (pulled) yarn. The calculation of these values provides useful information when comparing the effect of different mechanical and chemical modifications on the deformation behaviour of weaves.

10.2.3 The Application of the Model

Figure 10.3 shows the variation of the computed cross-over yarn modulus E_m with lateral tension. E_m seems to increase very slightly with F_s. In effect, increasing F_s does not seem to effect E_m but enables one to operate at different overall fc ranges of 0.004 to 0.1 N.

Figure 10.4 depicts the variation of the computed values of fy and E_y with cross-over number. The yarn tensile force increases in magnitude in the direction of the hook. E_y also increases markedly with the tensile force on the tensile elements. The force-strain curves for the yarns, Figure 5.8, indicate that the extent of this increase is not unreasonable. Figure 10.5 shows the modulus of the pulled yarn as a function of cross-over number for cotton submerged under water for varying lengths of time. It is seen that as time increases the modulus of the yarn decreases. It is interesting to compare the values of E_y for the treated cotton with those for untreated cotton, Figure 10.4. The values have decreased significantly due to the treatment. A similar change is seen in the force-strain profiles of the untreated and water treated cottons; Figure 5.10 and Table 5.2. There again, the modulus has decreased in line with the observations.

The reduction in modulus with time can be attributed to the fact that the lubrication effect imparted by the water molecules involves the migration of water between filaments and into filaments. The fact that the curves for the 5 and 23 hour cases are so close can be an indication that there is no extra lubrication to be gained after 5 hours of the cotton fabric being immersed in the water.

The elastic part of Figure 8.1 has two interacting components; one due to the tensile yarn and the other due to the adjacent weave. An intermediate result of this interaction is depicted in Figure 10.6 where the total extension of the tensile yarn in the

Figure 10.3 The effect of side tension on the cross-over yarn spring constant, E_m.

Figure 10.4 Variation of the forces and the tensile yarn moduli E_y associated with discrete elements of the pulled yarn.

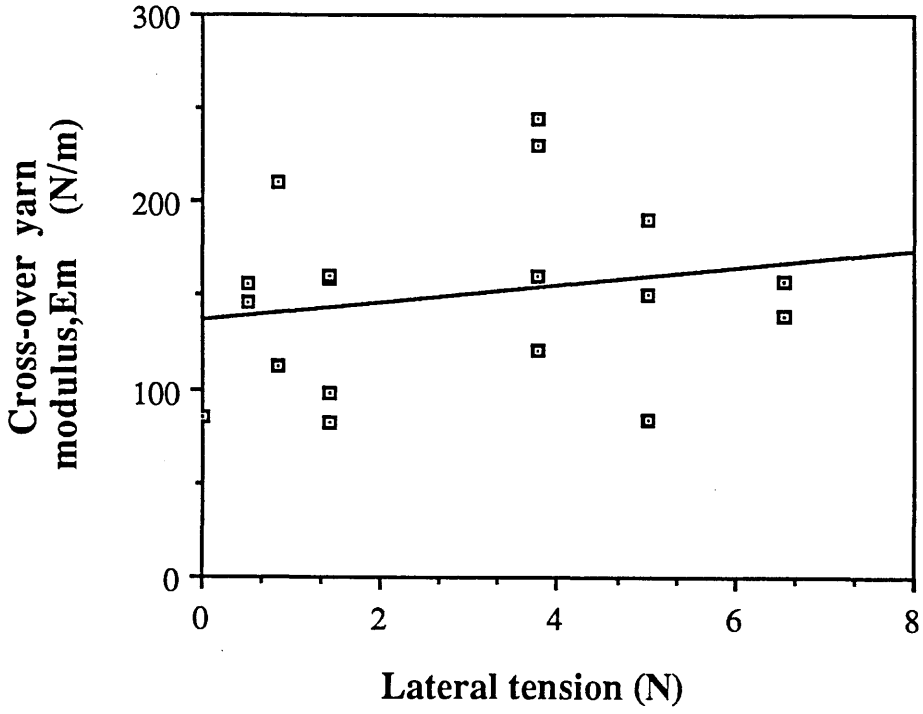
Cross-over yarn modulus,Em (N/m)
300
200
100
0
0
2
4
6
8
Lateral tension (N)

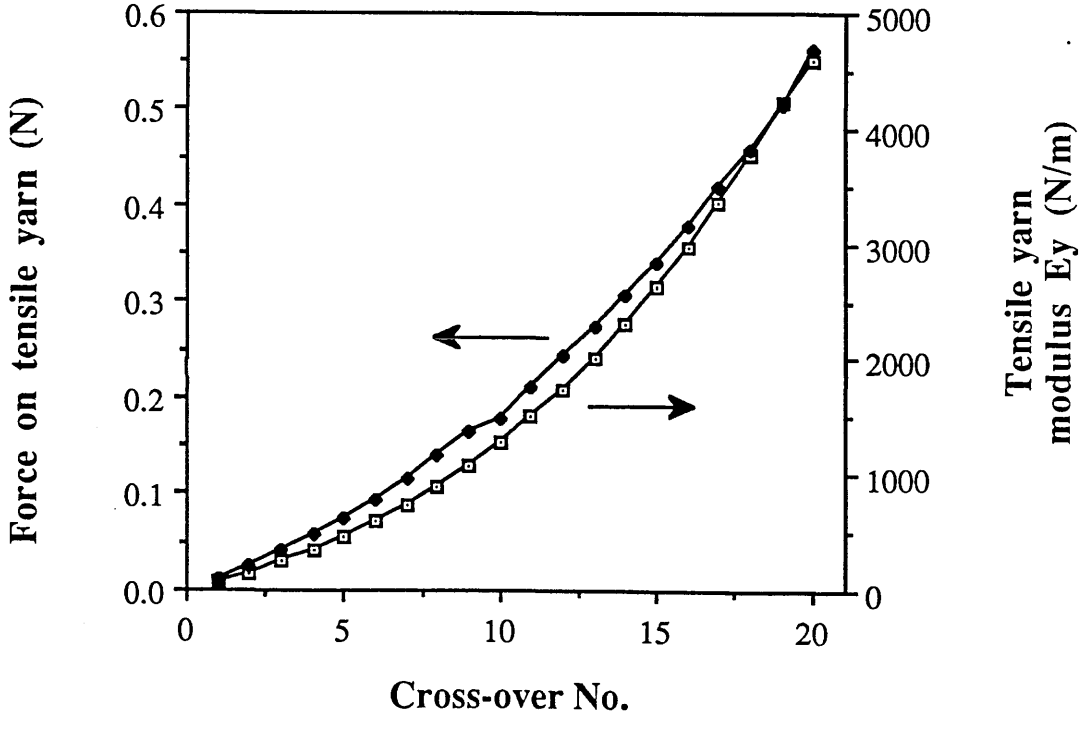
Force on tensile yarn (N)
0.6
0.5
0.4
0.3
0.2
0.1
0.0
5000
4000
3000
2000
1000
0
0
5
10
15
20
Cross-over No.
Tensile yarn modulus Ey (N/m)

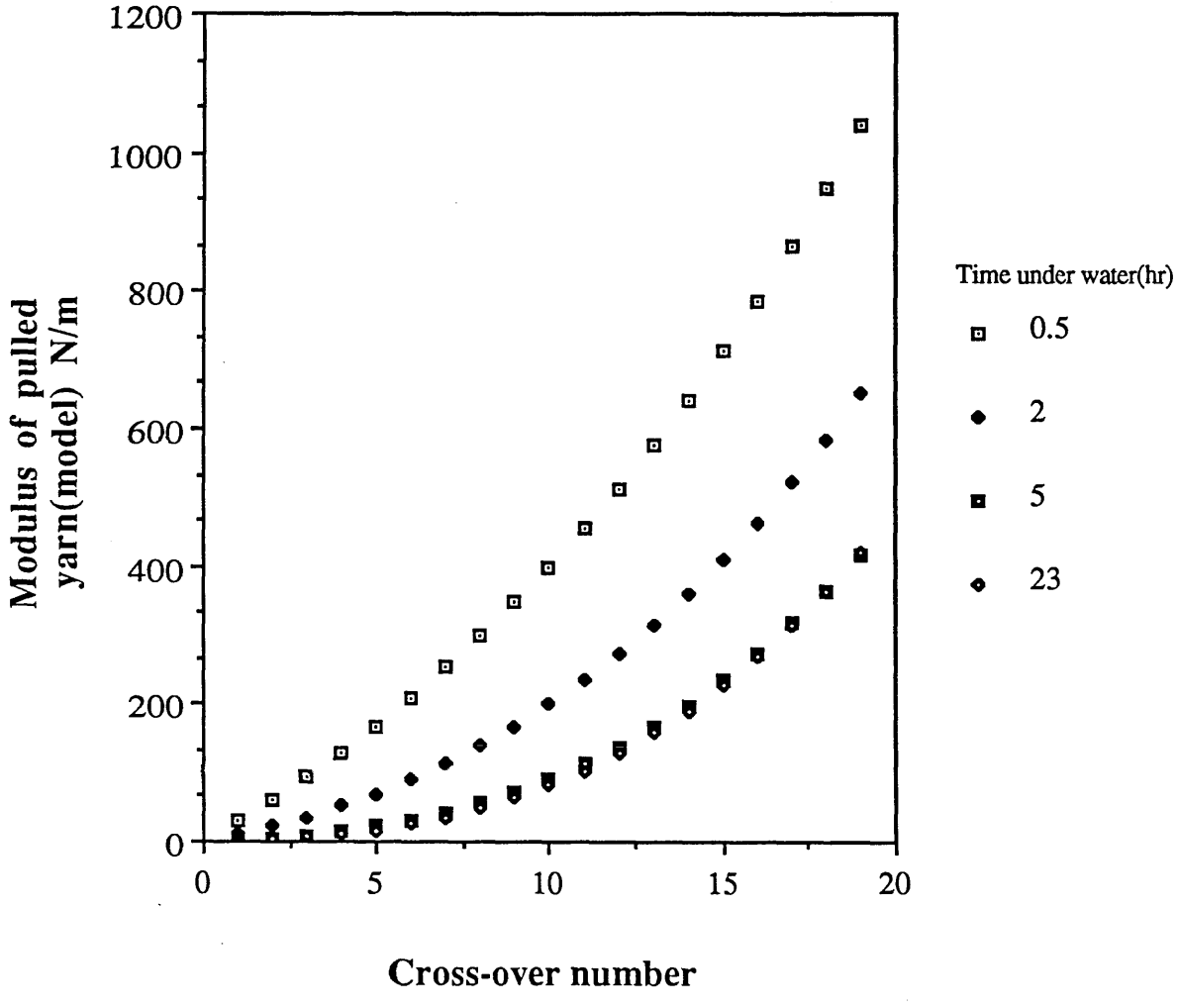

Figure 10.5 Values of the moduli of discrete elements of the pulled yarn as a function of cross-over number for cotton fabrics submerged under water for variouslengths of time.

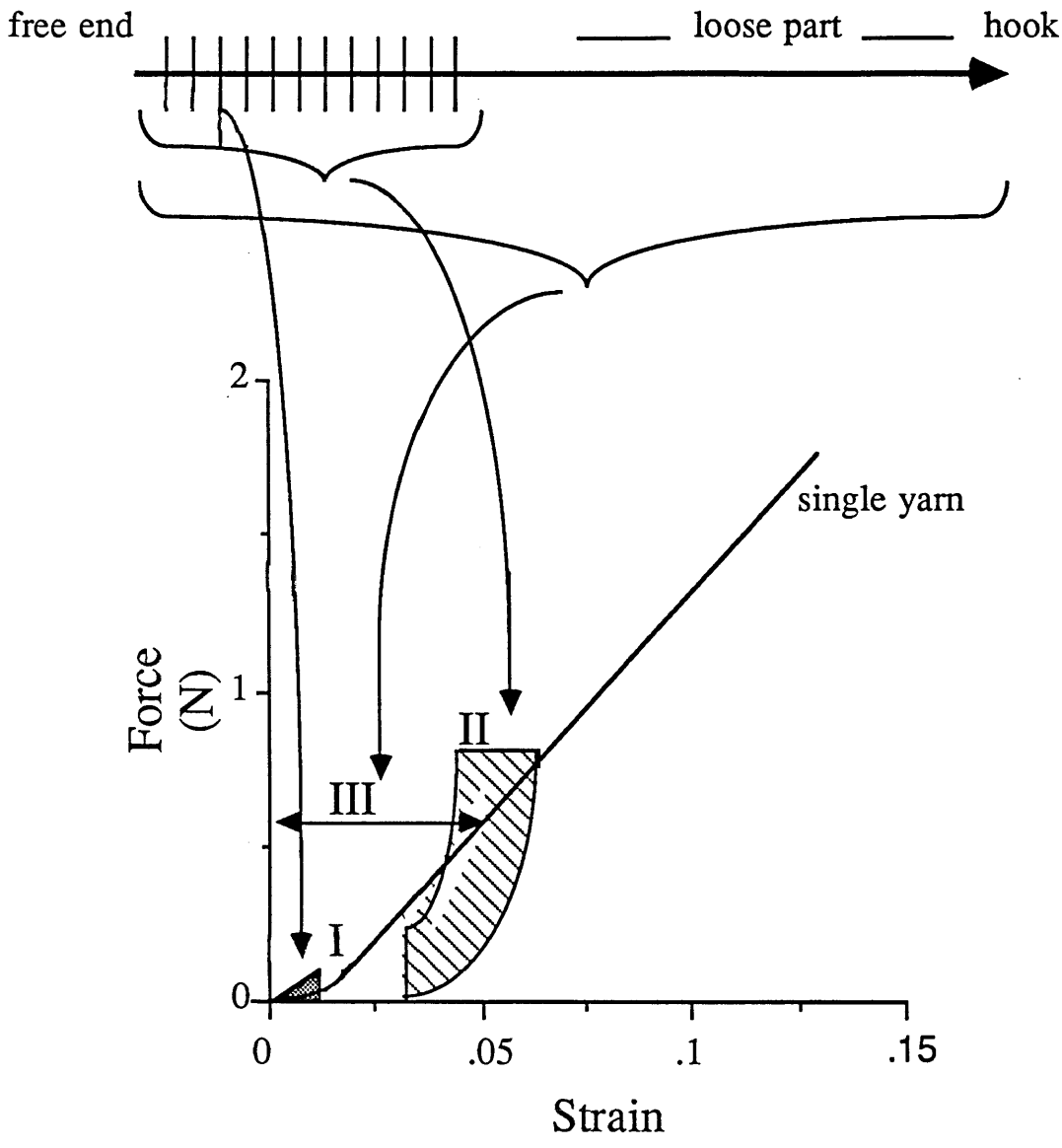

Figure 10.6 The common force-strain profile associated with different parts of the distorted cotton weave. The shaded areas represent the boundaries within which the force-strain profiles of the tensile yarn and the cross-over yarns would fall. The single yarn characteristics is also seen to fall within these boundaries. The profiles were calculated using the spring model, figure 10.1.

weave is described as a force-strain relation (a common force-strain profile). The curve is highly non-linear. Also shown in Figure 10.6 is the corresponding experimental curve for a free yarn, Figure 5.8. The force-strain profile is obtained using the model described. The significance of the common force-strain curves of Figure 10.6 is that the pulled yarn tensile part is associated with high forces, while the adjacent weave characteristics are associated with relatively low forces. Part (I) represents the cross-over (matrix) only characteristics; Part (II) the combined characteristics of the cross-overs and the yarns between them and Part (III) the matrix and the yarn between cross-overs as well as the loose part of the tensile yarn. The free yarn tensile characteristics is seen to represent the interaction between matrix and pulled yarn responses fairly well.

The ultimate requirement of the model is the prediction of the form of the elastic part of the force-displacement profile, Figure 8.1. This is done by using the Equations 10.2 to 10.9 and the reverse procedure to that used in the model. Here, experimental tensile moduli of single yarns together with chosen values of force are used in Equations 10.4 to 10.9 to calculate δ. Then using this value of δ and d_o, a value for d_N and hence ε is calculated. By increasing the value for the force from a small number up to the experimental JRF, the force-displacement characteristics of cross-over number 20 is calculated. Figure 10.7 shows the experimental force-displacement profile (also see Figure 8.2), together with the calculated curve. The forces generated in the model ranged from 0.01 to 0.4 N and the values of the tensile moduli adopted ranged from 100 to 400 N/m. At the relatively low force levels that the pull-out test operates at, the moduli are realistic; Figure 5.7. It is seen that at comparative values of force, the model predicts the displacements to be approximately half the experimental value. This indicates that the tensile moduli used are about

Figure 10.7 Comparison of the experimental force-displacement profile (elastic region II) with data obtained using the spring model.

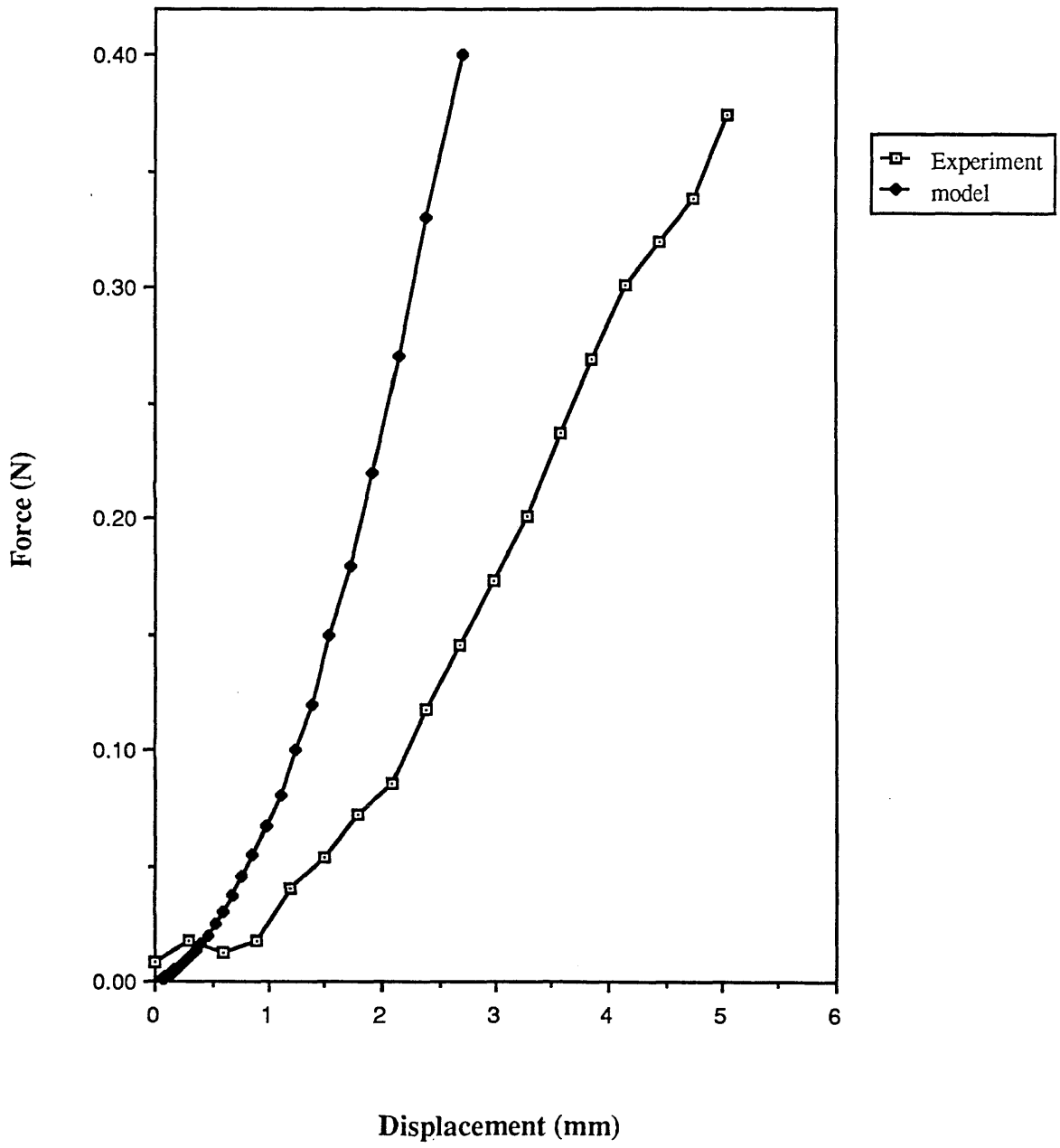

double the values of the modulus operating in the system. In fact, when comparing the moduli obtained from the model, Figure 10.3, and those obtained from single yarn experiments, it can be seen that the values for the matrix ranged from 100 to 200 N/m, while those for a free yarn ranged from 100 to 400. If a value of 100 to 200 is used in the latter calculations, the "model" curve of Figure 10.7 would lie much closer to the experimental curve. Thus the model provides a satisfactory description of these data.

10.2.4 Variation of JRF and Kinetic Friction with Side Load

The variation of side tension in a fibre pull-out experiment produces significant and systematic changes in the force-imposed displacement profile and the associated migration of cross-over points in the weave. Figure 10.8 illustrates the confined environment of the yarns in the weave as well as the displacements of the pulled yarn and the cross-over yarns in contact with it and the direction of cross-over yarn migration. Figure 10.9 is a force diagram showing the resolved components of the forces acting upon the cross-overs. The experimentally determined angles α and ϕ of this figure are plotted in Figure 10.10. It can be seen that towards the hook, α decreases significantly while ϕ increases to a lesser extent. Also evident is that if no tension is applied to the pulled yarn, $\alpha = \phi = 20$ and this is the weave angle θ since the fabric weave is orthogonally symmetrical.

A rather complicated analysis of the force components acting at the cross-overs has been carried out which will be presented later. The derivation of the formulae are given in Appendix 2. First, a simplified treatment will be followed, which brings out the main points in a more direct way. It is assumed that the side force F_S acts uniformly throughout the fabric. There are approximately 150 cross-over yarns in the

Figure 10.8 Schematic representation of the tensile and the cross-over yarns inside the cotton weave showing the associated angles.

Figure 10.9 A diagram of the forces acting at a cross-over junction.

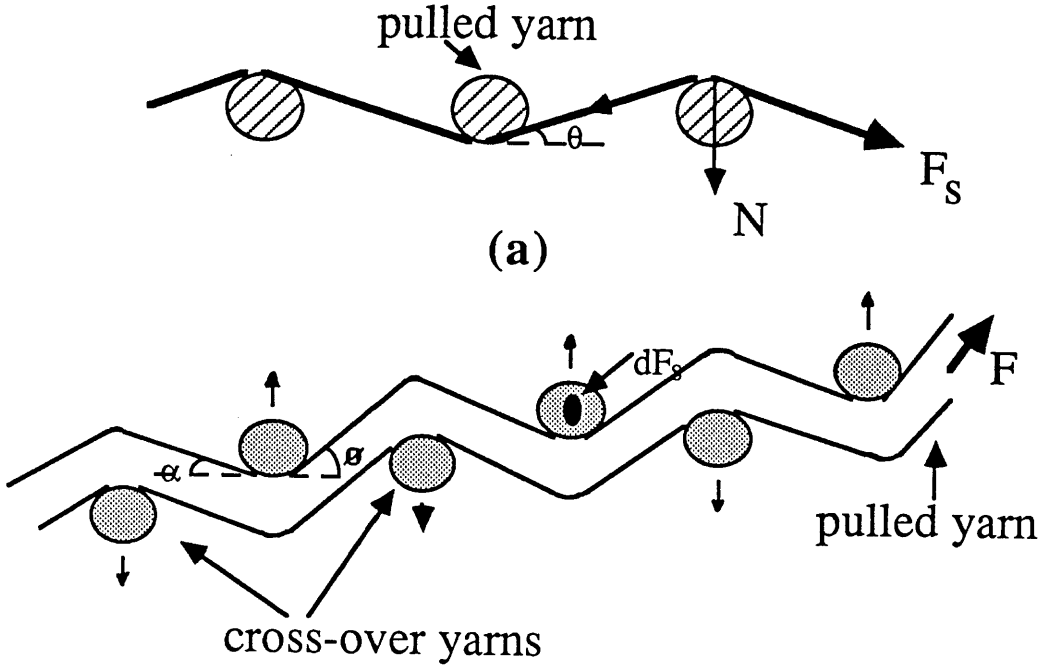
pulled yarn
θ
N
F_s
(a)
dF_s
F
α
β
pulled yarn
cross-over yarns
(b)

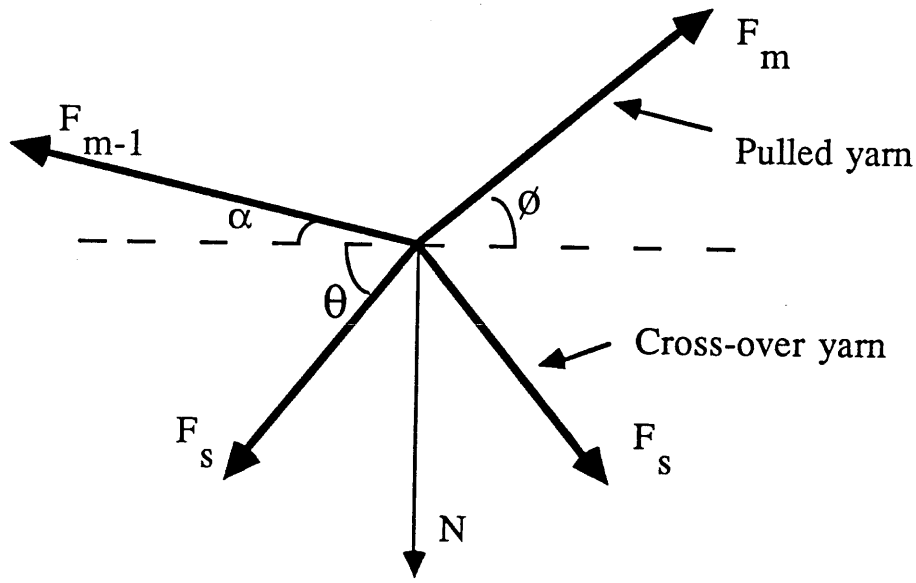
F_m
F_{m-1}
Pulled yarn
α
Ø
θ
Cross-over yarn
F_s
F_s
N

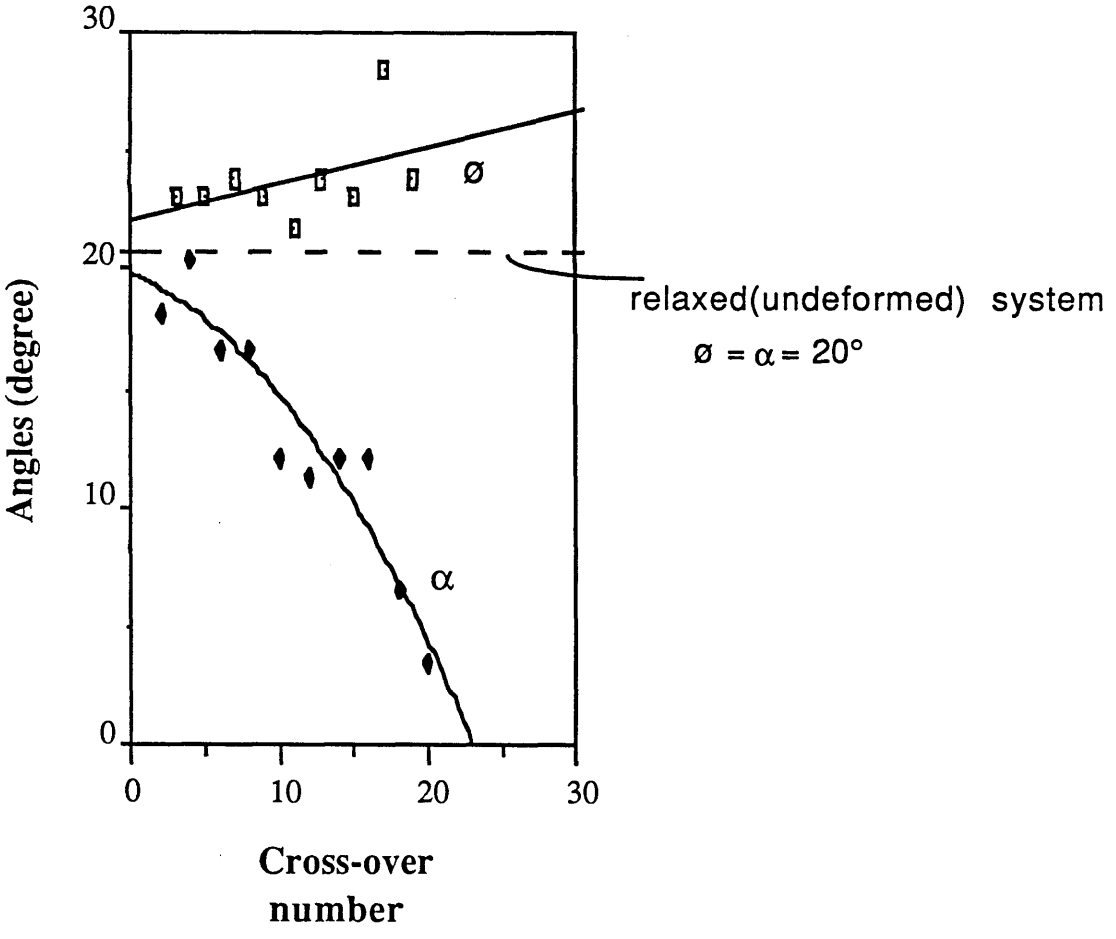

Figure 10.10 Experimental values of the angles α and Ø inside the cotton weave at various cross-over numbers.

cotton fabric specimen studied so that the side force f_s in each cross-over yarn is ca. $F_s/150$. For the fabric as shown in Figure 10.8, if all other distortions are neglected, the vertical component p of f_s is:

$$p = 2 f_s \sin \theta \qquad (10.10)$$

If we assume that this contributes a frictional resistance of μp (assuming a constant coefficient of friction), the additional friction force at each cross-over will be:

$$\mu p = \mu\, 2 f_s \sin \theta \qquad (10.11)$$

$$= \mu f_s \times 0.7 \qquad \text{since } \theta \approx 20°$$

$$= \mu \cdot \frac{Fs}{150} \cdot 0.7 = \mu \cdot 4.7\ 10^{-3} F_s$$

From frictional measurements of single yarns, Figure 5.4, it would be reasonable to take $\mu \approx 0.65$.

Hence $\mu p = 3 \times 10^{-3} F_s$.

In this simple analysis the influence of angles α and ϕ on the measured force are not considered. The more complex analysis is given in Appendix 2. Then the observed dynamic friction force per cross-over will be:

$$f = f_o + 3 \times 10^{-3} F_s \qquad (10.12)$$

where f_o is the intrinsic frictional force when F_s is zero. The observed results of Figure 8.5 for orthogonal free pairs gave:

$$f = 0.008 + 3 \times 10^{-3} F_s$$

suggesting that the fabric weave itself produces a normal force between yarns of the order of 0.012N since 0.012 x 0.65 = 0.008. The simple model thus agrees very well with the observed influence of F_s on the dynamic friction. A detailed analysis

assuming that the friction at each cross over includes a "capstan" type contribution gives very poor agreement and will not be given here (see Appendix 2). One cannot expect such a simple model to cope with the influence of F_s on the junction rupture force (JRF) or provide sensible friction coefficients for the initiation of junction rupture since this process is apparently not a simple frictional process. The side load sensitivity shown in Figure 8.4 may be a reflection of the geometric changes which occur in the cross-over zones rather than a reflection of the load dependent strength of the junctions. Thus, unlike the sliding friction, it is not so readily amenable to a simple modelling of force resolution in the cross-over regions. However, if we assume that the additional frictional force at each cross-over as calculated above acts on the twenty cross-overs when junction rupture occurs, we obtain:

$$JRF = F_o + 20 \times 3\times10^{-3} F_s \qquad (10.13)$$

$$= F_o + 6\times10^{-2} F_s \quad \text{in Newtons}$$

Surprisingly, the experimental results of Figure 8.4 (see Table 8.1) gave:

$$JRF = 0.34 + 6\times10^{-2} F_s.$$

This good agreement is probably largely fortuitous. A more complex model which has been used to calculate values for the coefficients of friction and determine the relationship between the measured force and normal load on a junction is outlined in Appendix 2. It assumes that JRF and kinetic friction are a function of normal load, through an angle θ which is supposed to include the contribution of the side tension to normal load, Figure 10.9. Table 10.1 presents values of the dynamic coefficient of friction μ_d as a function of $\omega = \alpha+\phi$ and θ, Figure 10.9, using the point contact model $F = \mu P$, Equation A.1, where F = friction force and P = normal load.

Table 10.1 ($F=\mu P$)

θ \ ω	30	32	34	36	38	40
12	0.1					
13	0.15	0.15				
14	0.22	0.18	0.15	0.1		
15	0.3	0.25	0.21	0.17	0.1	
16	0.37	0.33	0.28	0.23	0.18	0.13
17	0.45	0.4	0.35	0.3	0.27	0.22
18	0.5	0.45	0.43	0.4	0.35	0.3
19	0.55	0.53	0.5	0.45	0.43	0.38
20	**0.6**	0.57	0.55	0.52	0.5	0.45
21	**0.65**	**0.63**	**0.6**	0.57	0.55	0.53
22	0.7	**0.66**	**0.65**	**0.63**	0.6	0.58
23	0.73	0.7	**0.68**	**0.66**	**0.65**	**0.63**
24	0.75	0.74	0.73	0.7	0.7	**0.67**
25	0.77	0.76	0.75	0.74	0.73	0.72

Table 10.2 presents a similar set of results to Table 10.1 using an alternative point contact model; $F = F_o + \mu P$.

Table 10.2 ($F=F_o + \mu P$)

θ \ ω	30	32	34	36	38	40
13	0.15	0.15	0.1			
14	0.3	0.27	0.18	0.13	0.1	
15	0.35	0.33	0.3	0.27	0.2	0.15
16	0.45	0.4	0.37	0.35	0.33	0.3
17	0.48	0.45	0.45	0.43	0.43	0.4
18	0.53	0.51	0.5	0.5	0.5	0.47
19	0.57	0.55	0.55	0.54	0.54	0.53
20	0.6	0.6	0.57	0.58	0.58	0.57
21	**0.63**	**0.63**	**0.63**	0.62	0.62	0.62
22	**0.65**	**0.65**	**0.65**	**0.65**	**0.65**	**0.65**
23	**0.67**	**0.67**	**0.67**	**0.67**	**0.67**	**0.67**
24	0.7	0.7	0.7	0.7	0.7	**0.69**
25	0.73	0.73	0.73	0.73	0.73	0.73

Finally, Table 10.3 presents the results of applying a capstan model of contact; $F = F_o \exp(\mu\omega)$.

Table 10.3 ($F=F_o * e^{\mu\omega}$)

θ \ ω	30	31	32	33	34	35	36	37	38	39	40
11	0.45	0.35									
12	0.9	0.8	**0.65**	0.5	0.35						
13	1.2	1.1	1.0	0.9	0.8	**0.7**	**0.55**	0.4			
14	1.5	1.4	1.3	1.25	1.1	1.05	0.95	0.85	0.75	**0.65**	0.45
15		1.7	1.6	1.5	1.45	1.35	1.25	1.2	1.1	1.0	0.95
16						1.7	1.6	1.5	1.4	1.35	1.25
17									1.7		1.6

None of the above models was capable of producing a realistic static coefficient of friction and hence the tables only present the dynamic values. The angle ω in the tables is representative of the values believed to occur at the cross-overs. The included angle decreases with increasing cross-over number, Figure 10.10. There does not seem to be a great deal of difference between the two descriptions of μ in the point contact models while the capstan results are different to those obtained from the point contact models. Also, the influence of θ on μ is seen to be greater than that of ω. For an average $\mu \sim 0.65$, for the point contact models, θ ranges from 20 to 25 degrees. In the capstan model θ ranges from 11 to 14 degrees. Figure 10.11 shows the values of μ given in Tables 10.1 to 10.3 for $\omega = 30$ degrees. It seems that the values for the two point contact models are very similar, while the capstan predicts higher coefficients of friction.

10.2.5 Summary

Two models, one to describe the matrix shear of the weave during the pull-out process and the other to provide a means of examining the effect of the side load and

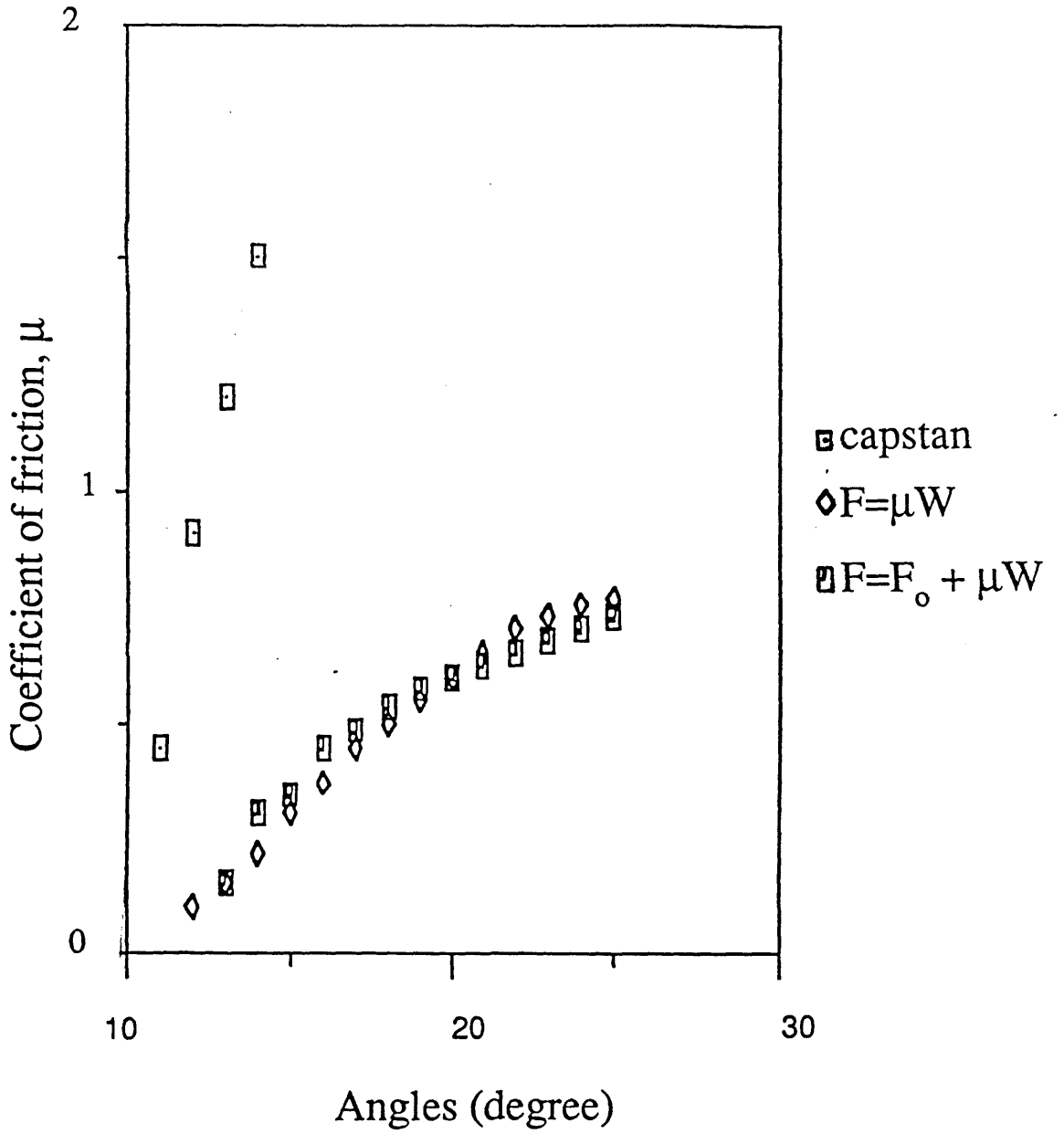

Figure 10.11 Coefficient of friction as a function of the weave angle θ for the three friction models examined.

the weave angles on the measurable force values, JRF and kinetic friction, were presented. The models were found to describe the data, presented mainly in chapter 8 satisfactorily. By virtue of the pull-out process, a out of plane deformation was obtained and studied in detail (see section 8.3) which was very similar to the deformations observed in the so called "hardness" and the ballistic experiments. It is believed that similar processes, that is yarn pull-out and weave distortions occur in the latter two experiments (discussed in the later sections of this chapter). However it was possible to examine these effects more closely in the pull-out experiments.

10.3 Indentation of Textile Structures

10.3.1 Introduction

The general features of the "hardness" or the indentation experiments were described in chapter 6. It was observed that regardless of the size or shape of the indentors, the deformation was a pyramidal one, resembling that obtained in the pull-out experiments. It was also found that lubrication caused the fabrics to be less stiff and more amenable to deformation, in a similar manner to the deformation and force values obtained in the pull-out process.

Although the deformation of the fabrics in the "hardness" experiments are modelled using plate deformation equations (presented in the next section), the deformations actually arises from the tensile extension and distortions of the yarns and the cross-over points similar to that in the pull-out experiments. In fact the origins of the elasticity of the indentation plate deformation may be considered to come from the elasticity of the pull-out process. In this respect the moduli calculated for the pull-out process may be assumed to be operating in the "hardness" experiments as well, since the rates of deformation are of similar orders of magnitude.

10.3.2 Diaphragm Strains (Thin Plate Model)

The general description of the model adopted for membrane strains was outlined in Section 6.4, where an equation for the force-max deflection profile of a thin plate, held at the edges and loaded uniformly, was presented, Figure 10.16. That equation was:

$$F = [5.33(\frac{y}{t}) + (\frac{y}{t})^3] \frac{13.98\ E\ t^4}{r^2} \qquad (10.14)$$

Using this equation and appropriate values for Young's modulus, E, and membrane thickness, t, the forces, F, were calculated for increasing vertical displacements. It was noted earlier that the Poisson's ratio υ was set to zero and indeed the selection of E and t values is quite arbitrary. Figures 10.12 and 10.13 for cotton, are replicates of Figure 6.6 for the 120° cone with the 100mm and 180mm holders respectively. Figures 10.12 and 10.13 also show the calculated curves using Equation (10.14). In both cases t was chosen as 0.3mm, the same as a yarn diameter. Figures 10.14 and 10.15 for aramid 1 are the same as the untreated and 5% PDMS treated curves in Figure 6.16. In both cases t was taken as 0.15mm, and equal to the yarn thickness. Table 10.4 presents the values of the Young's modulus E, that were incorporated into Equation (10.14) in order to fit the experimental curves. (Recall $\upsilon = 0$ and t was set at a nominal thickness of the plate equal to the fibre diameter)

Figure 10.12 Comparison of the experimental fabric indentation force-displacement profile with that produced using the plate model. The data are for cotton fabric with 120° conical indentor and 100 mm fabric holder.

Figure 10.13 Experimental against plate model data for the indentation of cotton fabrics with a 120° conical indentor, fabric holder size=180mm.

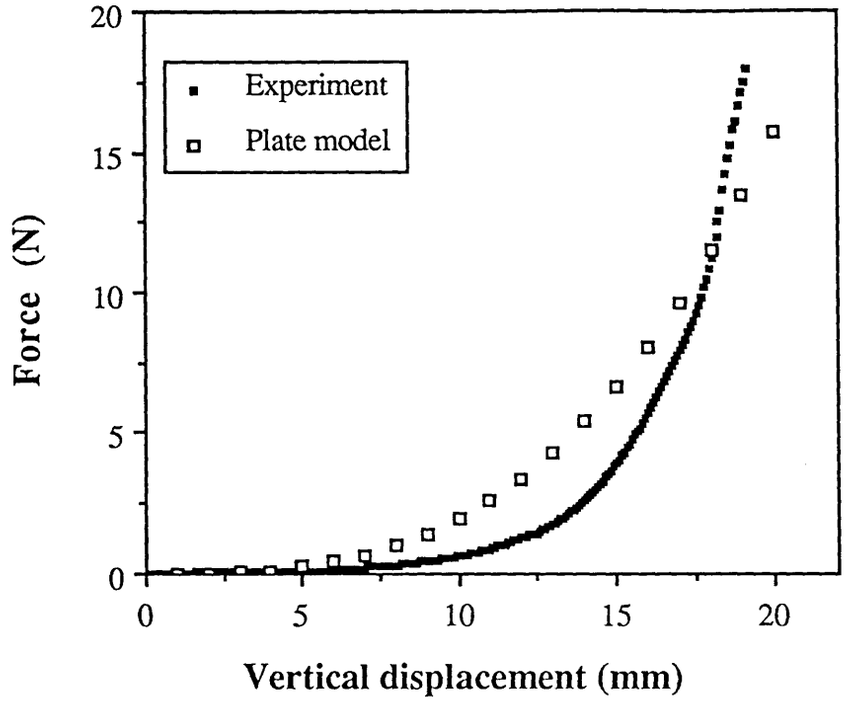
Experiment
Plate model
Force (N)
Vertical displacement (mm)
0
5
10
15
20

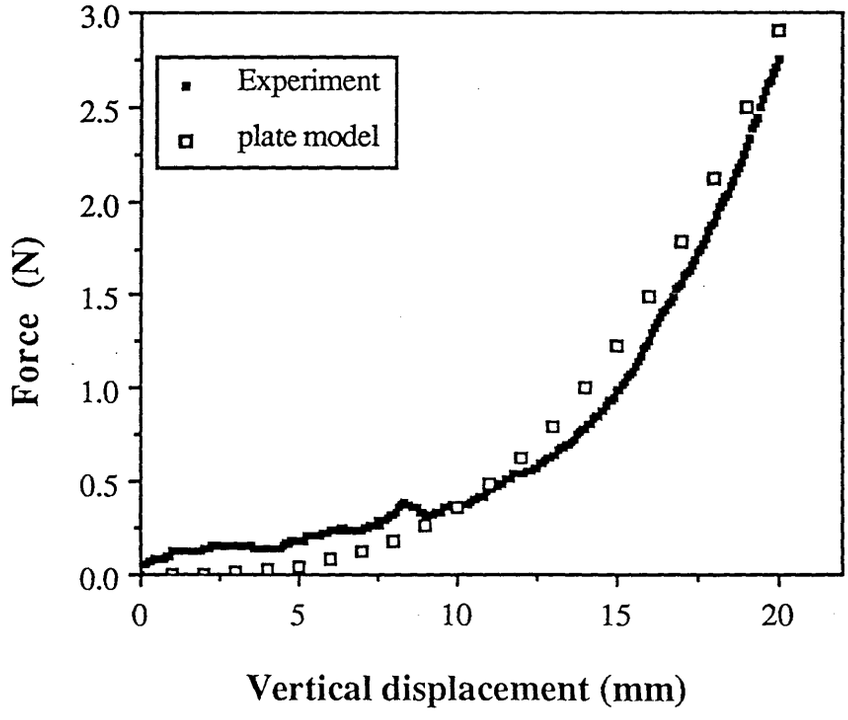
Experiment
plate model
Force (N)
Vertical displacement (mm)
0.0
0.5
1.0
1.5
2.0
2.5
3.0
0
5
10
15
20

Figure 10.14 Experimental vs. plate model profiles for the indentation of untreated (as received) aramid 1 fabric using 120° cone and 100 mm fabric holder.

Figure 10.15 Same as figure 10.14 for 5% PDMS treated aramid 1 fabric.

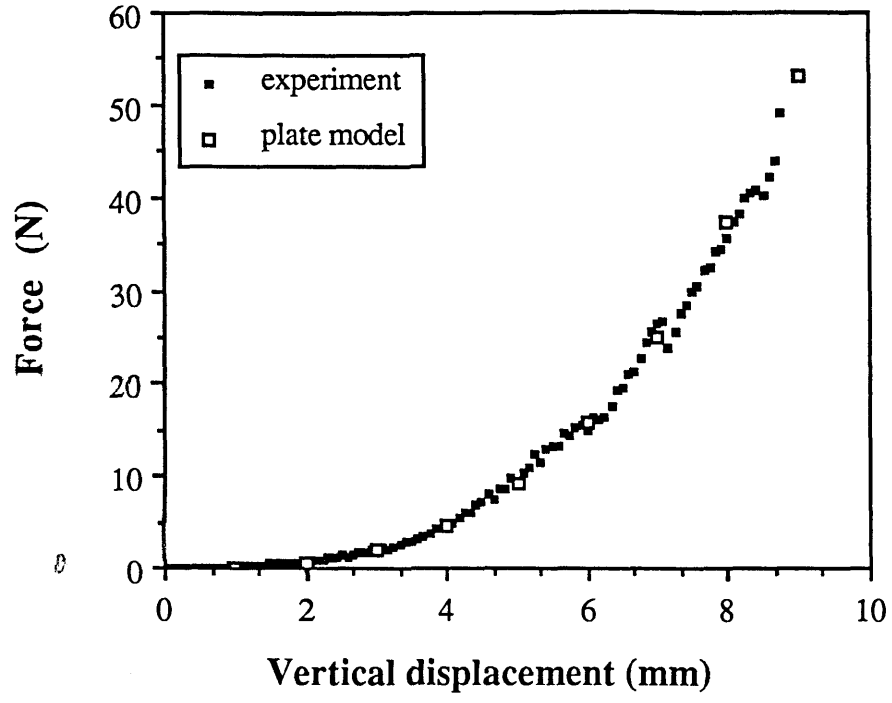
experiment
plate model
Force (N)
Vertical displacement (mm)
0
10
20
30
40
50
60
0
2
4
6
8
10

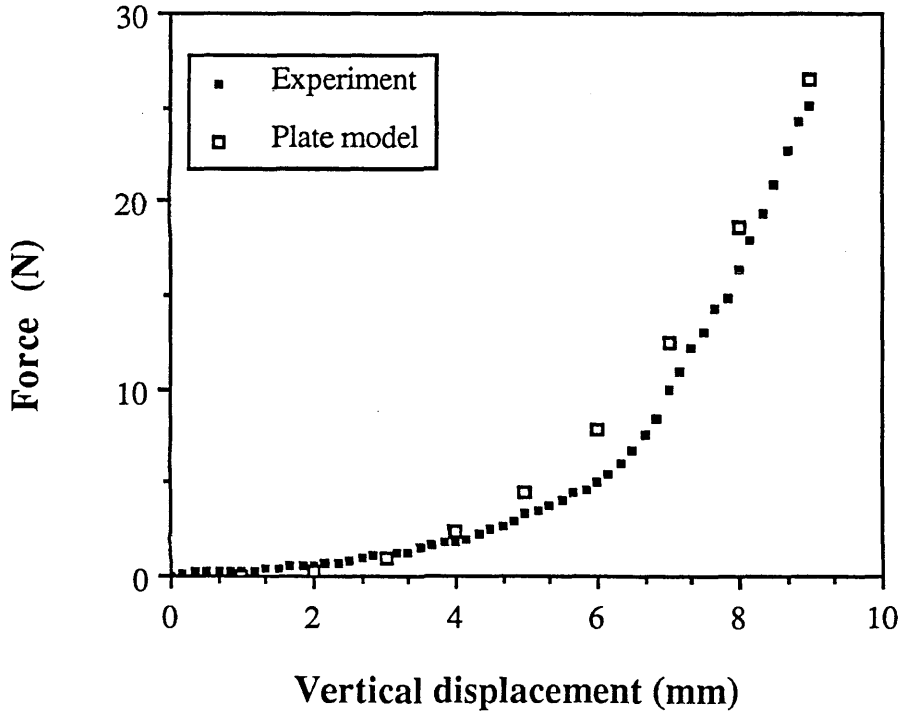
Experiment
Plate model
Force (N)
Vertical displacement (mm)
0
10
20
30
0
2
4
6
8
10

TABLE 10.4

Fabric	Plate diameter (mm)	Cone angle (degrees)	Young's Modulus E (MPa)
cotton (untreated)	100	120	2.0
cotton (untreated)	180	120	1.2
cotton (untreated)	100	60	1.8
cotton (5% PDMS)	100	120	1.5
Aramid 1 (untreated)	100	120	200
Aramid 1 (soxlet extracted)	100	120	300
Aramid 1 (5%PDMS)	100	120	100

Figures 10.12 to 10.15 show that the response of the fabrics to a conical indentor pushing into them can be represented quite well using a membrane deflection model such as the one presented and the fabric behaves as if it were a coherent solid thin plate possessing the mentioned values of thickness and equivalent plate Young's modulus. From Table 10.4 it can be seen that the value of E is more sensitive to a change in plate radius than a change in the cone angle. Also, treatment with a lubricant such as PDMS has reduced the modulus for both the cotton and the aramid fabrics. Table 10.4 also shows that the aramid fabric produces a plate which is ca. 10^2 times stiffer than the cottons.

The transverse ballistic impact of fabrics and it's relation to the pull-out and indentation processes are discussed in the next section. In that respect the indentation experiments are a satisfactory simulation of the ballistic deformation processes. This simulation is even better when using small diameter indentors of similar size to the ballistic projectile. The response of cotton fabrics to small indentors were discussed in section 6.5. However a similar experiment could not be performed with the aramid fabrics because the relative sizes of the indentor, the weave and the time scales involved allowed the indentor to penetrate the weave before appreciable deformation had occurred.

10.3.3 The effect of friction on the "hardness" experiments

The influence of friction processes were examined in fine detail for the case of the pull-out experiments in chapter 8 and section 10.2. In the case of the "hardness" experiments frictional effects were not investigated in detail although it was recognised that friction played a part in the indentation process, similar to that in the pull-out experiments. The pyramidal deformation involved extensions and to some extent bending of yarns together with a degree of cross-over junction rupture. Because, unlike the pull-out experiments, the yarns were constrained in all directions within the weave, the extent of fibre pull-out is uncertain in the hardness experiments, however, the deformation certainly involved orthogonal fibre slippages and cross-over deformations similar to the matrix deformations obtained in the pull-out experiments. In this respect one would expect that frictional effects would be similar in both indentation and pull-out processes and that the results of the analyses on the friction and migration of yarns (the elastic part of the analysis only since post JRF processes and fibre pull-out is not thought to occur in the hardness experiments), section 10.2.3 and 8.2 would apply to the hardness experiments. This aspect was not pursued in this study.

10.4 A Quasi-Static Model of the Transverse Ballistic Impact of Aramid Weaves

10.4.1 Introduction

Previous sections in this chapter have dealt with the analysis and discussion of the pull-out and the "hardness" experiments. This section deals with the transverse ballistic impact process of the fabrics under study here. It has become clear from previous chapters that all three experiments produce similar out of plane deformations in the fabrics involving a significant amount of fibre or yarn pull-out, yarn extension and matrix shear. The importance of friction and lubrication effects are also important

in the ballistic experiments. Admittedly the rates of deformation are similar in the pull-out and the "hardness" experiments, but very different to the ballistic case. However it is believed that despite differences in the rate of deformation, the ballistic processes may still be simulated, explored and analysed using quasi-static experimentation and modelling.

In Sections 6.4 and 10.3 a model was presented which assumed an elastic energy dissipation involving a loaded membrane analysis. The model effectively described the experimental data. This section describes a first attempt to interpret the transverse energy absorbing characteristics of three aramid fabrics (see earlier) using that static model. In this way the relative energy absorbing characteristics of the three fabrics may be predicted.

The general appearance of a fabric during progressive deformation in a transverse ballistic impact was shown in Figures 7.1 to 7.3. The main points of note have been frequently reported but one feature is important in the context of the current section. That is to a first order the stress wave propagation angle θ_w, Figure 10.16 remains relatively constant throughout the history of the impact. This is a consequence of an essentially constant longitudinal shock wave velocity in the assembly.

The photographic evidence is thus for a strain energy absorbing process incorporating extension and bending in a relatively simple deformation geometry which is geometrically similar throughout the impact. The scale of the deformation is controlled by the wave velocity in the fabric. In this section, the value of a first order model of the impact process based upon a static model where the geometry of deformation is controlled not by the wave velocity but by the geometry of the support is explored.

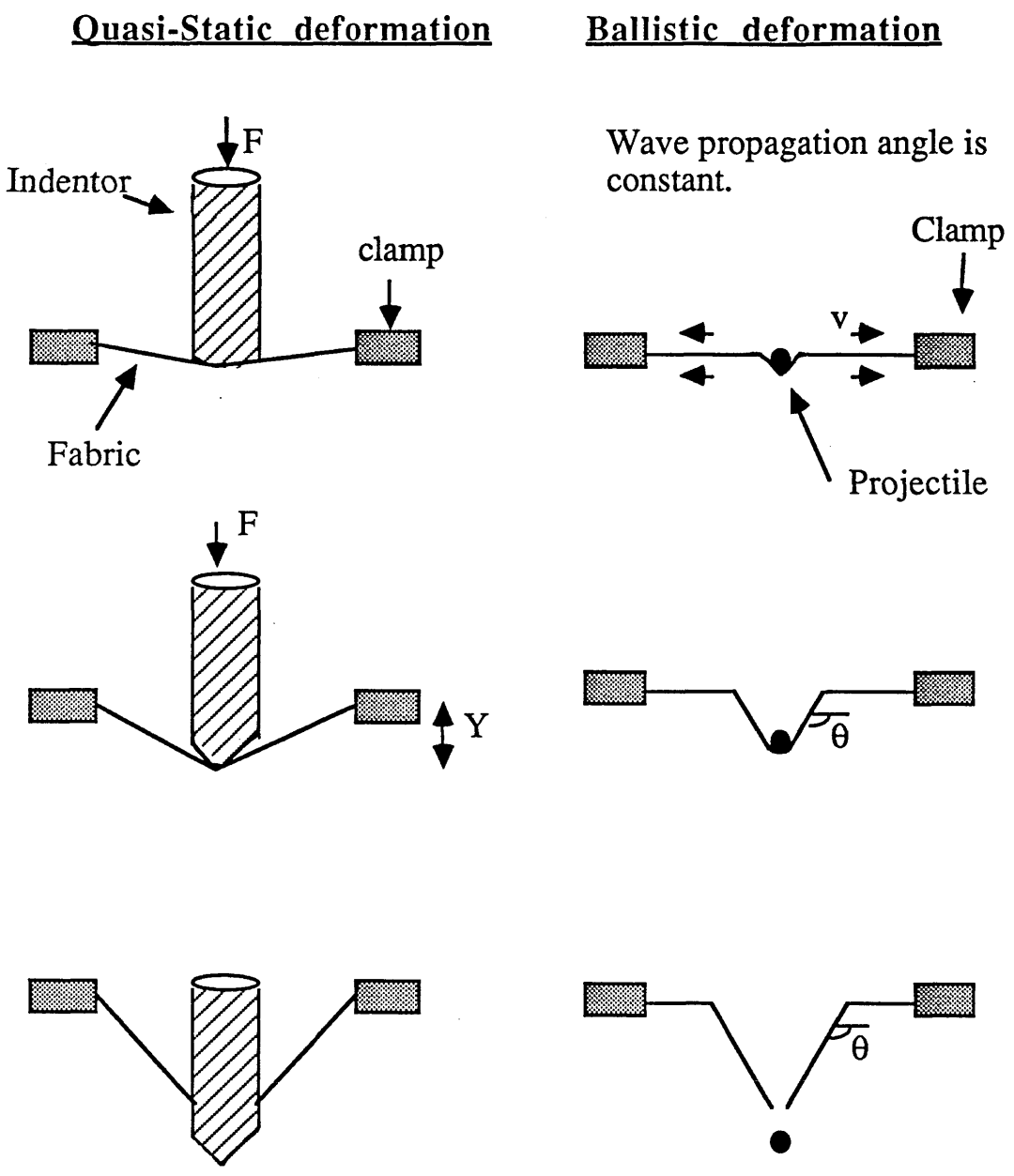

Figure 10.16 A schematic representation of the indentation and the ballistic processes showing their respective deformation patterns. In the quasi-static case, the hinge is at the clamp while for the ballistic case it is variable.

10.4.2 A Quasi-Static Model of the Ballistic Capture Efficiencies of Aramid Fabrics

From Figures 7.1 to 7.3 the wave propagation velocities in the fabrics were measured and table 7.1 presented the values. These values were obtained by measuring the increase in the diameter of the deformation at each time interval. Using the sonic velocity equation (section 4.7.2):

$$v = \sqrt{\frac{E}{\rho}} \qquad (10.15)$$

and taking the fibre density $\rho = 1440\ kgm^{-3}$ (Kevlar 49 Data Manual, E.I.du Pont Co.), the values of E are thus calculated as $1.4*10^7$ Pa for the as received fabric, $1.5*10^7$ Pa for the PDMS treated and $4.16*10^7$ Pa for the soxlet extracted aramid fabric. Roylance (1977) suggests a sonic velocity for Kevlar 29 yarns of 570 m/s. (E is then of the order of $5x10^8$ Pa). The modulus for the Kevlar 29 yarn is quite close to effective values computed for the static plate deformation obtained using the plate model for the aramid fabrics, table 10.4. Recall however that for the plate υ was set to zero and the plate thickness was equivalent to the yarn thickness. Inspection of equation 10.14 shows that the force F scales, for a given displacement, with Et^4. In the static experiments one might suppose that t ought to be less than the yarn diameter. Hence a suitable value of E to obtain a good fit of these data would require a significantly greater value of E for the effective plate in the ballistic experiments.

The target images shown in Figures 7.1 to 7.3 show subtle differences between the various fabric treatments. The geometries of the deformation are noticeably different and indeed this leads to different shock wave velocities, as discussed in

section 7.3. As mentioned previously, the shock wave propagation angle θ_w, has been assumed to be a constant. The subsequent analysis has not used the sonic modulus but the static modulus computed for the three fabric systems.

It must also be noted that the strains to failure in the three cases are rather similar. Failure in this context is the point when very significant penetration is observed. The equivalent homogeneous tensile strain value was computed from the photographic images at penetration. It is approximated here as $\cosh \theta_c - 1$ where θ_c is the propagation angle at penetration. It is also clear from the three images that the post penetration processes are rather different in each case (see Section 7.2).

From Figure 7.5 it can be seen that the ballistic energy absorbed decreases with decreasing impact velocity. More importantly, the energy absorbed decreases when PDMS is introduced and increases when the fabric is cleaned.

In order to calculate the integral work done W_I during impact, Equation (10.14) was integrated twice with respect to y giving:

$$W_I = [5.33 \frac{y^3}{6t} + 2.6 \frac{y^5}{20t^3}] \frac{13.98 E t^4}{r^2} \qquad (10.16)$$

Figure 10.17 is a block diagram showing the path taken to calculate the integral work done in the ballistic experiments. The modulus used in Equation (10.14) to describe the static deformation profile was used in Equation (10.16) to calculate W_I. However, in the static case, the plate radius was taken as constant at r = 50 mm while for the ballistic case, the plate radius was changing with depth of penetration, y, as: r = 2y, measured on the photographs. This variation was incorporated in Equation (10.16) when calculating W_I. Figure 10.18 shows the integral work done as a function of

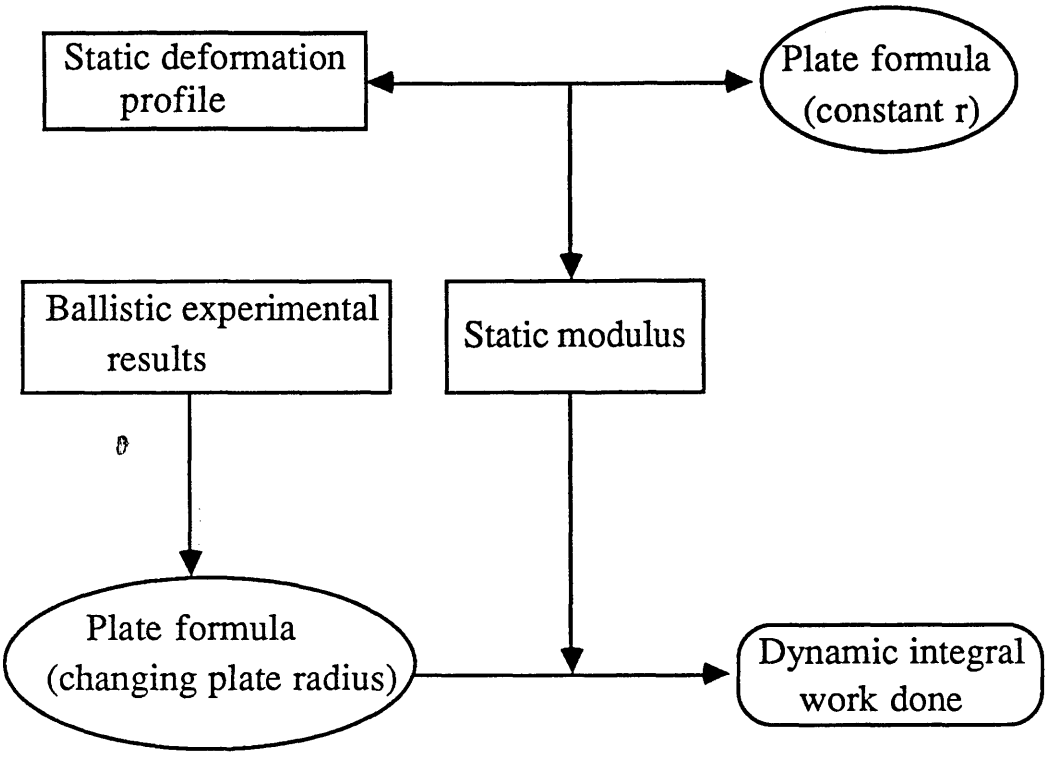

Figure 10.17 A block diagram showing the path taken to calculate the integral work done W_I in the ballistic process from information produced in the quasi-static analyses.

displacement for the three fabrics. The trends observed with surface treatment are similar to those in the ballistic case. Figure 10.19 quantifies these comparisons. The data have been normalised to the energy adsorbing characteristics of the PDMS modified system. The static prediction of the elastic energy dissipated has been taken from Figure 10.18 assuming a ballistic failure strain of 15%. Recall that this figure was computed using a static modulus and assumed a fixed propagation angle. The computed static based energy adsorbing capacities scale was 3:2:1 (cleaned: untreated: PDMS). The ballistic capture performance as measured by the kinetic energy lost in translation through the fabric is a function of the input kinetic energy. Figure 10.19 shows clearly that the trends are correct but in no case amongst the three input velocities do we reproduce the same scaling as was predicted in the static model. The static model does not contain a basis to explain this variation with impulse velocity.

The reasons for the lack of quantitative correlation may be extremely various. We have neglected the kinetic energy imported to the fabric for example. In the immediate context of the static model, effective plate moduli were used for a relaxed state with an homogeneous strain. In addition, a fixed propagation angle and a constant apparent failure strain were assumed. At this time it has not been possible to precisely define the importance of these factors on the static model as applied to the ballistic case. However, these considerations apart, one can deduce that, to a first order, the ballistic behaviour of weaves is controlled to some extent by the processes which are responsible for the same weave's static stiffness. Pragmatically this may simply provide a means of assessing the likely effects of surface finishes on ballistic performance. At a more fundamental level these studies indicate that appreciable interfibre and interyarn slip or migration occurs in ballistic impact. These processes are more amenable to experimental investigation in static experiments and the present work suggests that such studies may provide a qualitative means of interpreting the influence of surface treatments on the ballistic characteristics of fabrics.

Figure 10.18 Quasi-statically based values of integral work done for the ballistic impact process at increasing transverse fabric displacements (depths).

Figure 10.19 Normalised absorbed energy as a function of the fabric surface characteristics. Energies were calculated at 15% nominal strain.

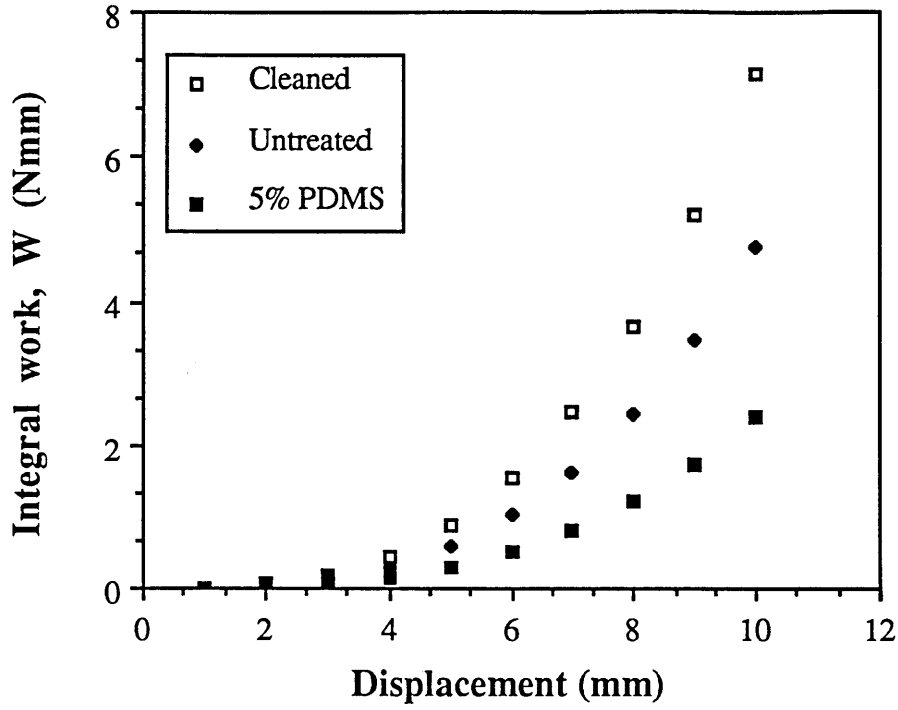
Integral work, W (Nmm)
Displacement (mm)
Cleaned
Untreated
5% PDMS
0
2
4
6
8
10
12

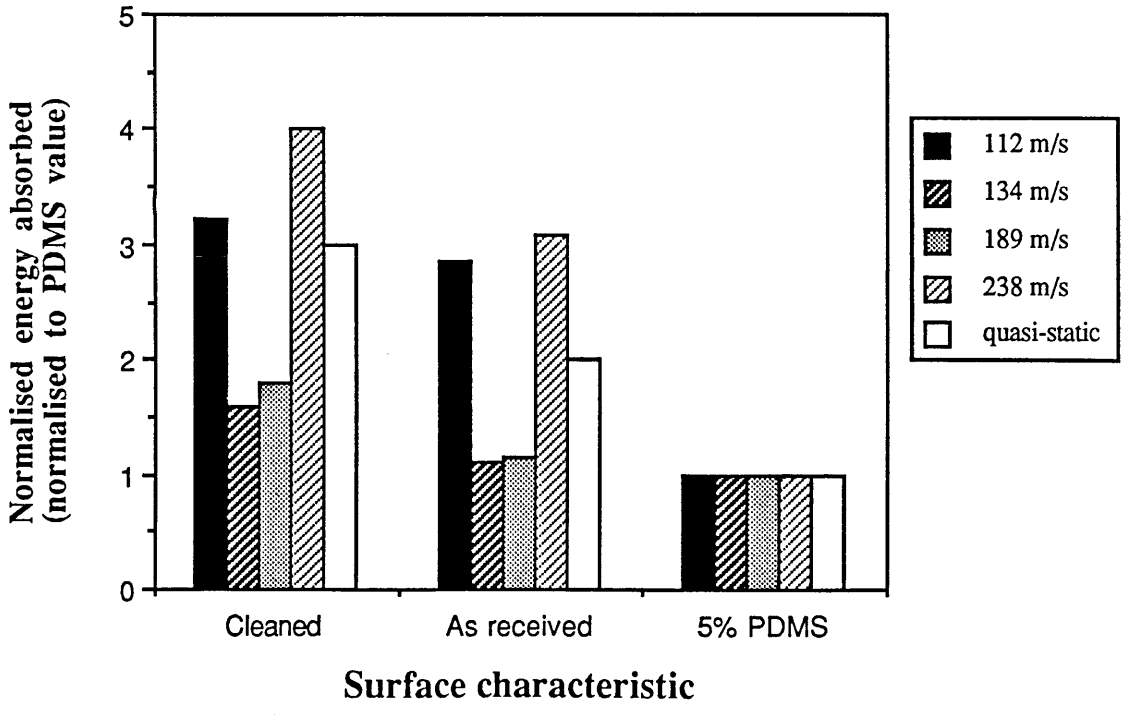
Normalised energy absorbed (normalised to PDMS value)
Surface characteristic
Cleaned
As received
5% PDMS
112 m/s
134 m/s
189 m/s
238 m/s
quasi-static
0
1
2
3
4
5

10.4.3 The Effect of Friction on the Ballistic Performance of Fabrics

As already mentioned in the introduction to this chapter, the three main experiments undertaken in this study were intrinsically similar in their deformation processes and the origins of the elasticity of their respective matrices. Frictional processes also operate in a similar manner in these experiments although friction was not studied in detail in the "hardness" and the ballistic experiments. The ballistic deformation involves a significant amount of fibre slip and pull-out. The studies by Roylance (1980) described in section 7.4.3 elude to the fact that increased friction at cross-over junctions would result in a better "spreading" of the propagation wave and hence a higher ballistic capture efficiency. The current study (figures 7.1 to 7.3) also showed that increased lubrication leads to increased fibre pull-out accompanied by a decrease in the ballistic capture performance of the fabric.

It was not possible to study in detail (as was done for the pull-out experiments) the effect of friction in the ballistic experiments simply because of the experimental time scales involved. However, it is envisaged that due to the intrinsic similarities of the deformations and the trends in energies with lubrication, the analyses used in the pull-out experiments, both for the elastic part of the deformation (figure 8.1) and after junction rupture and the onset of steady fibre pull-out, will probably apply in the ballistic case.

10.5 Conclusion

The deformation characteristics of the fabric weaves during fibre pull-out and indentation were described accurately using two different models producing nominal values for the elasticity of the weave. A quasi-static model was also used for the ballistic impact experiments and was found to satisfactorily describe the trends of the capture efficiency of the three aramid fabrics with respect to their surface

modifications. However during the course of this study, there were certain anomolies which should be pointed out. Although it was recognised that the elasticity of the matrix in the "hardness" experiments originated from the elasticity of the weave in the pull-out process, side tension was seen to influence the two processes in rather different ways. Side tension was observed to affect almost all the parameters associated with the pull-out of a yarn from the weave, but not the parameters of the "hardness" experiments. The applicability of a uniformly loaded plate model to the indentation experiments can also be questioned since obviously the system was loaded in a central area using a cone with an uncertain loading pattern. The analysis used in modelling the ballistic capture rankings using quasi-static equations also contained several anomalies. The first and the most obvious is the large difference in the respective rates of deformation in the "hardness" and the ballistic experiments. Also important is the fact that the assumptions regarding constant propagation angle θ_w and constant apparent failure strain for the three aramid fabrics may not be fully justified. The other anomaly which may not be so obvious is the assumption of homogeneous strain. It is envisaged that due to the reflections that occur at the cross-over junctions as the strain wave propagates (see section 4.7.2), the strain along any particular fibre or yarn would infact not be homogeneous.

Despite these anomalies in both the analyses and the experimental techniques, it may be concluded that friction and migration of yarns do play a major part in the ballistic and indentation processes, but more importantly, the response of these systems is seen to be controlled to a small extent by bending and to a much greater extent by the extensile properties of the constituent fibres and yarns.

CHAPTER ELEVEN

CONCLUSIONS

This thesis has considered various aspects of the out of plane deformation of constrained fabrics. The experimental parts have been divided into three sections. A major section has dealt with what is called the pull-out experiment where essentially a semi-pyramidal displacement has been produced by withdrawing one yarn from a constrained weave. This experiment has sought to elucidate in fine detail the origin of the elastic response of simple fabric systems. The major work has been carried out on cotton fabrics with complimentary work using aramid fabrics. In these studies the main occupation has been to obtain correlations and interrelationships between micro-displacements and the force balances created within the system. By this means it has been possible to develop a reasonably good predictive model to describe the behaviour of a fabric system in this type of deformation. The data has been largely analysed assuming that the major response of the system arises almost entirely from extensile and not bending deformations. This experiment has three features. The important part has dealt with the origin of the apparent elasticity of the fabric during this type of deformation. The two subsidiary parts have dealt with the way in which a pulled yarn may be progressively withdrawn from the system. These studies have been complemented by separate investigations of the friction and the tensile properties of single yarns. A major feature of this particular part of the study has been the role played by lubricants or fabric conditioners in defining the behaviour of the system in it's three important modes of response. The major conclusion of this particular study is that it is possible using simple models and the assumptions described above and detailed elsewhere in the thesis to generate realistic models for the deformation of

fabrics on the basis of the operation of tensile forces only. Surface modifications by the use of various fluids and agents is believed to modify the tensile properties of the yarns by interfilament lubrication and the behaviour of cross-overs by cross-over contact lubrication. The friction data have been quantified for effects of lubrication for yarn systems but not for filament systems. These studies produce a self consistent picture of the origins of the plate deformation or semi-plate deformation of yarn systems.

These studies have then been taken forward in a less precise microscopic way to investigate the behaviour of a fabric during apparent plate deformation. Again the data strongly indicate that the major mode of force transmission is extension rather than bending and an attempt has been made to quantify this effect. The use of a standard, but arguably not totally appropriate, constrained plate deformation model which incorporates substantial membrane forces allows a very good prediction of the force-displacement characteristics of this system and hence a measure of the hardness or the out of plane deformation of the fabric. This type of deformation closely resembles that observed in part in the fibre pull-out experiments. The hardness experiments have been extended to look at the nominal hardness, that is the area of contact produced by cones of various diameters and included angles. The overall conclusion of this work is that the behaviour of the system can be reasonably interpreted in terms of an effective Young's modulus and by inference a modulus which arises largely through the propagation and the interaction of mostly tensile forces and hence the operation of a tensile rather than a bending modulus. In these studies the effects of lubricants and surface modifications are in keeping with those observed in the fibre pull-out experiments and we can therefore conclude that lubrication influences the effective modulus of the plate in certain ways as were speculated in the fibre pull-out experiments. The "hardness" work has been extended to compute, in a first order way, the work done rather than the deformation introduced

into the fabric as displacements imposed on the system and data have been produced for a variety of surface treatments not only for cotton fabrics but also for aramid systems.

The third experimental part of the thesis has sought to use the plate deformation theory to interpret the ballistic capture performance of aramid weaves. As a matter of experiment it was not possible to pursue these types of investigations with cotton systems because they were not sufficiently durable to withstand the impact phenomenon. It turns out that the ballistic experiments actually show the three key features that were described in the pull-out experiments and also eluded into the "hardness" experiments above. There is an elastic deformation, a junction rupture of cross-overs and finally the pulling out of the yarns from the constrained weaves. The elastic parts of the system are very adequately described by an extension of the "hardness" model based upon the work done argument with a modification to the geometry of the deformation system assuming a relatively constant wave propagation angle. The influence of surface modifications is in keeping with that observed in the hardness experiments and largely predicted from the behaviour of the system in the pull-out experiments. The agreement here is quite satisfactory in view of the fact that the ballistic experiment is not quasi-static in a way which is the case for the two previous experiments, that is the pull-out and the "hardness" experiments. It was not possible to examine in detail in a quantitative way the pull-out phenomena associated with the ballistic experiments (and indeed in the hardness experiments described previously) simply because it was not possible to identify in an explicit way the extent of the pull-out in these systems. However it was very apparent that when lubricants were introduced into the ballistic system then the extent of fibre pull-out was significantly greater. The more effective the lubricant as quantified in the fibre pull-out experiments and inferred from the hardness experiments confirmed the general trends of the ballistic experiments.

The main overall conclusion of this study is that the out of plane deformation of these fabrics is well described by models which suppose that the forces are mainly transmitted by tensile forces in the yarns. Lubrication influences the stress fields in the yarns by modifying filament-filament interactions and also the way in which forces are transmitted between yarns into the fabric as a whole. These intra and inter yarn friction effects are manifest in the whole spectrum of the force-extension behaviour of the system. For small stress and extension lubricants reduce the elastic effective modulus of the systems. The lubricants also reduce the effective pull stress of the system (they reduce the JRF in the pull-out experiment for example) and also promote yarn "flow" or yarn pull-out processes. In the broader definition of the term, the lubricant action is one of plasticisation al beit at a macroscopic level at filament-filament and yarn-yarn interfaces. We cannot however exclude "true" plasticisation of microscopic interactions with the filaments themselves although there is no experimental evidence that this occurs for the present systems.

APPENDIX 1

SEM Photographs of the Cotton and the Aramid 1 Yarns

Cotton yarn

Magnification=100

Aramid1 yarn

Magnification=100

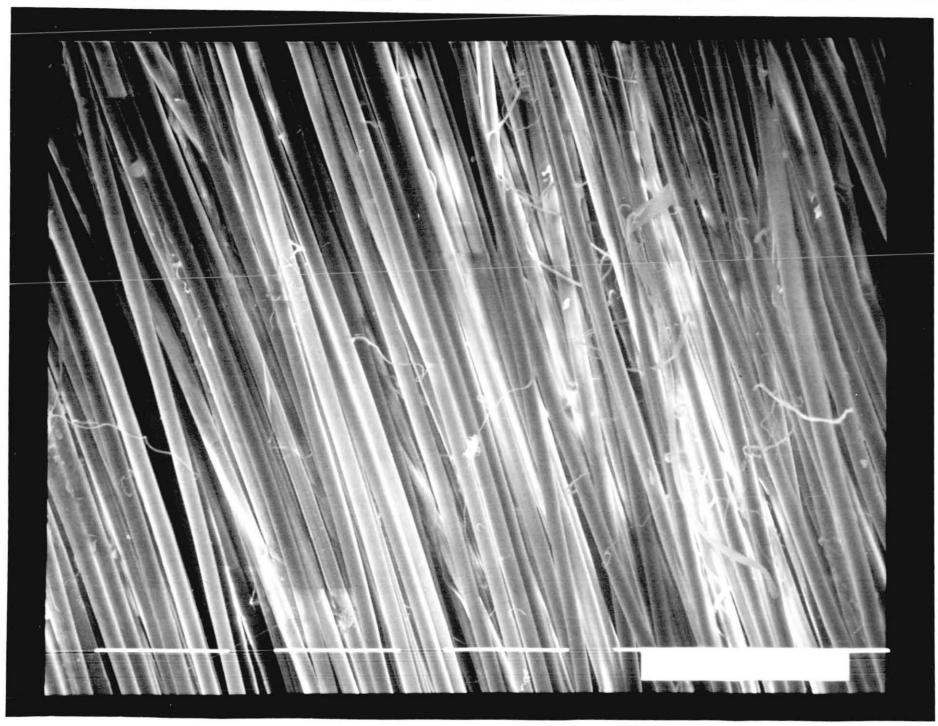

APPENDIX 2

A Geometric Model for the Analysis of Friction in the Pull-out Experiments

A mainly geometric model is outlined below which enables the calculation of the values of the coefficient of friction μ and determines the relationship between the measured force and the normal load on a junction. The model considers one junction only and hence the forces obtained from plots of JRF vs. lateral tension, Figure 8.4, and kinetic friction vs. tension, Figure 8.3, are per cross-over, Figure 10.9. It assumes that JRF and kinetic friction are a function of normal load through an angle θ which is supposed to include the contribution of the side tension to the normal load. The process is considered at the point of slip.

$$P = F_S * \sin\theta$$

where P = normal load, $\omega = \phi + \alpha$, F_S = lateral tension and F_m = measured force.

For the simplest geometry, a point contact model; when $F = \mu P$

$F_m - F_{m-1} = \mu P$.

If $F_m/F_S = k$ then we have:

$$\frac{k^2}{\sin^2\theta} - \frac{k^2\cos\omega}{\sin^2\theta} + \frac{k\mu\cos\omega}{\sin\theta} - \frac{\mu^2}{2} - \frac{k\mu}{\sin\theta} = \frac{1}{2} \qquad \text{(A.1)}$$

From Figures 8.4 and 8.5:

$$\text{For static friction I : } k = \frac{(0.82\text{-}0.35)}{(800*0.0098/150)} = 9$$

$$\text{For dynamic friction II: } k = \frac{(0.018\text{-}0.005)}{400*0.0098/150)} = 0.38$$

Table 10.1 presents values of the dynamic coefficient of friction μ as a function of ω and θ, using the point contact model, equation (A.1).

However, if $F = F_o + \mu P$, one gets $F_m - F_{m-1} = \mu P + F_o$.

If $F_m/F_s = k$ and $F_o/F_s = k_1$ then:

$$\frac{2k^2}{\sin^2\theta} - \frac{2k^2\cos\omega}{\sin^2\theta} + \frac{2k\mu\cos\omega}{\sin\theta} + \frac{2kk_1\cos\omega}{\sin^2\theta} - \frac{2k\mu}{\sin^2\theta} - \frac{2kk_1}{\sin^2\theta} + \mu^2 + \frac{2k_2\mu}{\sin\theta} + \frac{k_2^2}{\sin^2\theta} = 1 \qquad \text{(A.2)}$$

The results for dynamic coefficient of friction are shown in Table 10.2.

Alternatively a capstan model can be used where $F_m = F_{m-1} \exp(\mu\omega)$ giving:

$$\frac{k^2}{\sin^2\theta} - \frac{2k^2\cos\omega}{\exp(\mu\omega)} * \sin^2\theta + \frac{k^2*\cos^2\omega}{\exp(2\mu\omega} * \sin^2\theta + \frac{k^2*\sin^2\omega}{\exp(2\mu\omega)} * \sin^2\theta = 1$$

The results for the capstan type model are presented in Table 10.3.

REFERENCES

Atkins, A.G. and Tabor, D.; *J. Mech. Phys. solids*, **13**, 149 (1965)

Abbott, C.M., Grosberg, P., Leaf, G.A.V., *Text. Res. J.*, **41**, 4, 345 (1971).

Abbott, C.M., Grosberg, P., Leaf, G.A.V., *J. Text. Inst.*, **42**, 346 (1972).

Archard, J.F., *Nature*, **172**, 918 (1951).

Backer, S., Private Communication (1987).

Balasubramanian, P. and Salhotra, K.R., *Text. Tes. J.*, **55**, 1, 74 (1985).

Balls, W.L., "Studies of Quality in Cotton", Macmillan, London (1928).

Basu, S.N., Hamza & Sikorski, J., *J. Text. Inst.*, **2/3**, 68 (1978).

Besler & Taylor, 1st Symp. Int. de la Recherde, Paris (1969).

Beste, L.F. and Hoffman, R.M., *Text. Res. J.*, **20**, 441 (1950).

Berkeley, E.E. and Woodward, I.; *Text. Res. J.*, **18**, 71 (1948)

Binns, H.A., *Text. Res. J.*, **25**, 157 (1934).

Bowden F.P. & Tabor, D., "Friction and Lubrication of Solids", Parts I and II, Clarendon Press, Oxford (1950).

Briscoe, B.J., Scruton, B. and Willies, F.R., *Proc. Roy. Soc.*, **A333**, 99 (1973).

Briscoe, B.J. in "Adhesion 5", Ed. K.W. Allen, Elsevier, London (1981).

Briscoe, B.J., Adams, M.J. and Kremnitzer, S.L., *Proc. 34th Intl. Conf. Societe de Chemie Physique*, Microscopic aspects of adhesion and lubrication, ed. J.M.Georges, 405-419 (1982)

Briscoe, B.J., Winkler, A. and Adams, M.J., *J. Phys. D: Appl. Phys.*, **18**, 2143 (1985).

Brown, T.D. and Onions, W.J., *J. Text. Inst.*, **52**, T101 (1961).

Buckley, G.H., "Mechanics of Flexible Fibre Assemblies" , Sijthoff & Noordhoff publishers, Netherlands (1979).

Cameron, A., "Basic Lubrication Theory", Longmans (1971).

Chapman, B.M., *Text. Res. J.*, (1971).

Chapman, B.M., *J. Text. Inst.*, (1973).

Clayton, F.H. and Peirce F.T., *J. Text. Inst.*, **20**, T315 (1929).

Collins J.D. and Chaikin, M., *Text. Res. J.*, **39**, 121 (1969).

Coplan, M.J. and Bloch, M.G., *Text. Res. J.*, **25**, 902 (1955).

Cork, C.R., "Aspects of ballistic impact onto woven textile fabrics", Ph.D. thesis, UMIST (1983)

Dawes, V. and Owen, J.D., J. *Text. Inst.*, **62**, 233 (1971).

Dent, R.W. and Hearle, J.W.S., *Text. Res. J.*, **30**, 805 (1960).

Dobb, M.G., Johnson, D.J. and Saville, B., *Phil. Trans. R. Soc. London*, **A294**, 483 (1979).

Dowson, D., "History of Tribology", Longmans (1979).

Dubrow, P.L. and Linfield, W.M., *Soap and Sanitary Rep.*, **46**, 2, 41 (1957).

Duckett, K.E., in "Surface Characteristics of Fibres & Textiles", Ed. M.J. Schick, Marcel Dekker, NY (1975).

El-behery, H.M., *Text. Res. J.*, **38**, 321 (1968).

Elder, H.M., 'Textile Finishing', Textile Inst., U.K. (1978).

Elder, H.M., Fisher, S. and Armstrong K., 'Book of Papers', Index 81 Congress (EDNA), Amsterdam (1981).

Elder, H.M., Fisher, S., Armstrong, K. and Hutchinson, G., *J. Text. Inst.*, 1, **37** (1984).

Evans, W.P., *Chemistry & Industry*, July, 893 (1969)

Eyring, H., Glassstone, S., and Laider, K.J., "The theory of rate processes", McGraw Hill, NY (1941)

Farrow, B., *J. Text. Inst.*, **47**, T58 (1956)

Figucia, F., "Energy absorption of Kevlar fabrics under ballistic impact", US Army Natick Research and Development Command, Natick, MA (1980)

Flesher, D.J., US Patent 3,541,843 (1970).

Fort, T. and Olsen, J.S., *Text. Res. J.*, **52**, 12, 1007 (1961)

Fowkes, F.M., *J. Phys. Chem.*, **57**, 98 (1953)

Galuszynski, S. and Ellis, S., *Text. Res. J.*, **53**, 7, 462 (1983)

Galuszynski, S., SAWTRI Texchnical Report No. 554 (1984)

Gibson, V.L. and Postle, R., *Text. Res. I.*, **48**, 1, 14 (1978)

Gillespie, *J. Coll. Sci.*, **13**, 32, 50 (1958)

Ginn, M.E., Schemach, T.A. and Jungerman, E., *J. Am. Oil. Chem. Soc.*, **42**, 1084 (1965)

Gralen, N., *Proc. Roy. Soc.*, **A212,** 491 (1952)

Greenwood, J.A. and Tabor, D., *Proc. Phys. Soc.*, **71**, 989 (1958)

Gregory, J., *J. Text. Inst.*, **44**, T515 (1953)

Griffel, W., "Plate Formulas", Frederick Ungar Publishing Co., NY (1968)

Grosberg, P., *Text. Res. J.*, **36**, 3, 205 (1966)

Grosberg, P. and Kedia S., *Text. Res. J.*, **36**, 71 (1966)

Grosberg, P. and Swani, N.M., *Text. Res. J.*, **36**, 4, 332 (1966)

Grosberg, P., "Surface Characteristics of Fibres and Textiles", Ch. 15 (1977)

Guthrie, J.C., *J. Text. Inst.* (1954)

Hailwood, A.J. and Horrobin, S., *Trans. Faraday Soc.*, **42B**, 84 (1946)

Halling J., "Introduction to Tribology", Wykeham (1976)

Hamilton, J.B., *J. Text. Inst.*, **49**, T411 (1958)

Hansen, W.W. and Tabor, D., *Text. Res. J.*, **27**, 300 (1957).

Hardy, W.B., "Collected Works", Cambridge Univ. Press (1936).

Hayes, D., Textile Month, July, 38 (1972).

Hearle, J.W.S., El-behery, H.M.A.E. and Thakur, V.M., *J. Text. Inst.*, **51**, T299 (1960).

Hearle, J.W.S., El-behery, H.M.A.E. and Thakur, V.M., *J. Text. Inst.*, **52,** 5, T197 (1961).

Hearle, J.W.S. and Merchant, V.B., *J. Test. Inst.*, **53**, T537 (1962).

Hearle, J.W.S. and Peters, R.H., "Fibre Structure", Butterworths (1963).

Hearle, J.W.S. and Bose, O.N., *Text. Res. J.*, **35**, 693 (1965).

Hearle, J.W.S., Gupta, B.S. and Merchant, V.B., *Text. Res. J.*, **35**, 329 (1965).

Hearle, J.W.S., *J. Polymer Sci.*, **20**, 215 (1967).

Hearle, J.W.S., Grosberg, P. and Backer, S., "Structural Mechanics of Fibres, Yarns and Fabrics" (1969).

Hearle, J.W.S. and Green, R., *J. Text. Inst.*, **61**, 415 (1970).

Hearle, J.W.S. and Sparrow, *Text. Res. J.*, **41**, 9, 736 (1971).

Hearle, J.W.S. and Sakai, T., *J. Text. Mach. Soc. Jap.*, **31**, T136 (1978).

Hepworth, I. and Sikorski, J., Proc. 3rd Leeds-Lyon Symp. on Tribology (1976).

Hickie, T.S. and Chaikin, M.J., *J. Text. Inst.*, **51**, T1120 (1960).

Hoffman, R.M., *Text. Res. J.*, **35**, 428 (1965).

Holdaway, H.W., *J. Text. Inst.*, **47**, T586 (1956).

Hollies, N., Kaessinger, M. and Bogaty, H., *Text. Res. J.*, **26**, 829 (1956).

Honold, E. and Grant, J.N., *Text. Res. J.*, **31**, 7, 643 (1961).

Howell, H.G., *J. Text. Inst.*, **45**, T575 (1954).

Howell, H.G., Tabor, D. and Mieszkis, K.W., "Friction in Textiles" (1959).

Hughes, C.K. and Koch, S.D., *Soap & Chem. Specialities*, Dec., 109 (1965).

Iyengar, R.L.N. and Gupta, A.K., *Text. Res. J.*, **49**, 489 (1974).

Johnson, K.L.; "Contact Mechanics", Cambridge publishers (1985)

Kakiaga, S., *J. Text. Mach. Soc. Jap.*, **4**, 49 (1958).

Kawabata, S., "Mechanics of Flexible Fibre Assemblies", Ed. Hearle, Thwaites, J.J. and Amirbayat, J., Proc. NATO Adv. Study Int., Greece (1979).

Kawabata, S., "Objective Evaluation of Apparel Fabrics", Ed. Postle, R., Kawabata, S. and Niwa, N., *Text. Mach. Soc. Jap.*, Osaka (1983).

Kawase, T., Sekoghuchi, S., Fujii, T. and Minngowa, M., *Text. Res. J.*, **56**, 7, 409 (1986).

Kilby, W.F., *J. Text. Inst.*, **54**, T9 (1963).

Kim, C.J. and Vaughn, E.V., *J. Text. Mach. Soc. Jap.*, **32**, 6, T47 (1979).

Kis a, E., *J. Coll. Int. Sci.*, **83**, 265 (1981).

Komori, T., Makishima, K. and Itoh, M., *Text. Res. J.*, **50**, 548 (1980).

Koza, W.M., *Text. Res. J.*, **66**, 9, 639 (1975).

Kramer, A., Kaban, G., Cooper, D., and Papavasiliou, A., *Chem. Senses and Flavour* , **1**, 1, 121 (1974).

Kremnitzer, S.L., "The Adhesion, Friction and Lubrication of PET Fibres", PhD Thesis, University of Cambridge (1978).

Kruger, R., Polymers in Defence, International Conf., Bristol, 20/1 (1987)

Langmuir, E., *J. Amer. Soc.*, **40**, 1361 (1918).

Leaf, G.A.V., in "Mechanics of Flexible Fibre Assemblies" Ed. Hearle, Thwaites and Amirbayat, (1979).

Leaf, G.A.V. and Anandjiwala, R.D.; *Text. Res. J.*, **55**, 2 (1985)

Lundgren, H.P., *Text. Chem. Coll.*, **1**, 35 (1969).

Lyne, D.G., *J. Text. Inst.*, **46**, 112 (1955).

Lyons, W.J., "Impact phenomena in textiles", M.I.T. press, Cambridge, MA, 72-75 (1963)

Mallinson, P., *J. Soc. Dyers & Col.*, ., **90**, 67 (1974).

Mercer, E.H. and Makinson, K.R., *J. Text. Inst.*, **38**, T227 (1947).

Meredith R., *J. Text. Inst.*, **41**, T199 (1950).

Meredith R., *J. Text. Inst.*, **42**, T291 (1951).

Meredith R., in "Fibre Science", Ed. J.M. Preston, The Text. Inst. (1953).

Meredith R., *J. Text. Inst.*, **45**, T489 (1954).

Meredith, R., *J. Text. Inst.*, **36**, T107 (1975).

Minor, F.W., Schwartz, A.M., Wulkow, E.A. and Buckler, L.C., *Text. Res. J.*, **29**, 931 (1959).

Mogat, E.E., *Phil. Trans. Roy. Soc. Lond.*, **A294**, 763 (1980).

Montgomery, T.G., Grady, P.L. and Tomasino, C., *Text. Res. J.*, **7**, 442 (1982)

Mooney, W., Textile Month, Oct. 32 (1980).

Morlier, O.W., Orr, R.S. and Grant, J.N., *Text. Res. J.*, **21**, 6 (1951).

Morrow, J.A., *J. Text. Inst.*, **22**, T425 (1931).

Morton, W.E. and Yen, K.C., *J. Text. Inst.*, **22**, 60 (1952).

Morton, W.E., *Text. Res. J.*, **26**, 325 (1956).

Morton, W.E. and Hearle, J.W.S., "Physical Properties of Textile Fibres", Published in conjunction with the textile institute (1975).

Nachane, R.P. and Iyer, K.R., *Text. Res. J.*, **50**, 639 (1980).

Northolt, M..G., *Polymer*, **21**, Oct. 1199 (1980).

Olofsson, B., *Text. Res. J.*, **20**, 6, 476 (1950).

Olofsson, B., *J. Text. Inst.*, **55**, T541 (1964).

Olsen, J.S., *Text. Res. J.*, **39**, 31 (1969).

Onions, W.J., Toshniwal, R.L. and Townend, A.A., *J. Text. Inst.*, **51**, T73 (1960).

Owen, J.D., *J. Text. Inst.*, **56**, (1965).

Owen, J.D., *J. Text. Inst.*, **59**, 313 (1968).

Oxley, A.E., *J. Text. Inst.*, **13**, 54 (1922).

Panesar, S.S., "Mould Release Layers for Poly-urethanes", PhD Thesis, Imperial College (1986).

Pascoe, M.W. and Tabor, D., *Research*, **8**, S15 (1955).

Peirce, F.T., *J. Text. Inst.*, **14**, T1 (1923).

Peirce, F.T., *J. Text. Inst.*, **17**, T342 (1926).

Peirce, F.T., *J. Text. Inst.*, **21**, T377 (1930).

Peirce, F.T., *J. Text. Inst.*, **28**, T45 (1937).

Peirce, F.T., *Text. Res. J.*, **17**, 123 (1947).

Penn, L. and Larson, F., *J. Appl. Polym. Sci.*, **23**, 59 (1979).

Pietikainen, I., "Effect of some treatments on the properties of cotton and rayon fibres", PhD Thesis (1973).

Platt, M.M., *Text. Res. J.*, **20**, 10, 665 (1950).

Plummer, C.H., US Patent 3, 151,483 (1964).

Prosser, R.A., *Text. Res. J.*, 58, **2**, 61 (1988)

Pruneda, C.O., Steele, W.J., Kershaw, R.P. and Morgon, R.J., 182nd National Meeting of the Amer. Chem. Soc. Polym. Chem. Div., N.Y., Aug. (1981).

Riding, G.J., *J. Text. Inst.*, **55**, T9 (1964).

Roark, R.J. and Young, W.C., "Formulas for Stress and Strain", McGraw Hill (1986).

Roder, H.L., *J. Text. Inst.*, **44**, T247 (1953).

Roylance, D. and Wilde, A., Army symp. on solid mechanics, Ocean city, Maryland, 232-240 (1972)

Roylance, D., *Text. Res. J.*, 679 (1977)

Roylance, D., *Fibre Science and Technology*, **13**, 385 (1980)

Rudolph, *Textil-u-Faserstofftech.*, **5**, 293 (1955).

Rusca and Sands (1968).

Schick, M.J., "Surface Characteristics of Fibres and Textiles", Fibre Science Series, Chapter 1 (1975).

Schwartz, E.R., *Am. Dyestuff Rep.*, **28**, 138 (1939).

Schwartz, E.R., *Am. J. Phys. D.*, **20**, 130 (1987).

Schwartz, M.A., US Patent 2,718,142 (1955).

Sebastian, S.A.R.D., Bailey, A.I., Briscoe, B.J. and Tabor, D., *Text. Res. J.*, **56**, 10 (1986).

Sebastian, S.A.R.D., Bailey, A.I., Briscoe, B.J. & Tabor, D. ; *J. Phys. D: Appl. Phys.*, **20**, 130 (1987)

Seshan, K.N., *J. Text. Inst.*, **69**, 214 (1978).

Sexsmith, F.H. and White, H.J., *J. Coll. Sci.*, **14**, 598 (1959).

Shiloh. M. and Litav, *Text. Res. J.*, **35**, 159 (1965).

Simmens, S.C., and Hearle, J.W.S., *J. Polym. Sci., Polym. Phys. Ed.*, **18**, 871 (1980).

Skau, E.L., Honold, E. and Bondreau, W.A., *Text. Res. J.*, **28**, 3, 206 (1958).

Smith, J.C., McCrackin, F.L. and Schiefer, H.F., *Text. Res. J.*, **28**, 4, 288 (1958)

Sollenberger, W.S., *Am. Dyestuff Rep.*, **46**, 2, 41 (1957).

Speel, H.C. and Schwartz, E.W.K., "Textile Chemicals and Auxiliaries" Rainhold Publishing Co., N.Y., 2nd Ed. (1957).

Spencer-Smith, J.L., *J. Text. Inst.*, **36**, T35 (1947).

Syed, I.A., "Chemical Modification of Fabric Handle", PhD Thesis, University of Strathclyde (1982).

Tabor, D., Ch. 3 of "Friction in Textiles" by Howell, H.G., Tabor, D. and Mieszkis, K.W., 54 (1959).

Tabor, D., "Friction, Lubrication and Wear", *Surface and Coll. Sci.*, **5**, 245 (1972).

Taylor, E., US Patent 3,683,681 (1972).

Treloar, L.R.G. and Riding, G., *J. Text. Inst.*, **54**, 4, T156 (1963).

Treloar, L.R.G., *J. Text. Inst.*, **56**, 7, T359 (1965).

Treloar, L.R.G. and Riding, G., *J. Text. Inst.*, **56**, 7, T381 (1965).

Turner, A.J., *J. Text. Inst.*, **20**, T233 (1929).

Valko, I.E., *Am. Dyestuff Rep.*, Jan., **33** (1966).

Vaughn, E.A. and Kim, C.J., International Non-wovens and Disposables Assocn. Technical Symp., Washington (1973).

Viswanathan, A., *J. Text. Inst..*, **64**, 553 (1973).